FLUID MECHANICS OF HIGH SPEED DEFORMABLE ROLL COATING

An experimental and theoretical study of film thickness and stability in high speed deformable roll coating flow with Newtonian and non-Newtonian liquids

Sreedhara SARMA (B.Tech, MSc, GradIMMM)

Submitted for the degree of

Doctor of Philosophy

Faculty of Engineering and Informatics

University of Bradford

2015

ABSTRACT

Name: Sreedhara Sarma

Title: Fluid Mechanics of High Speed Deformable Roll coating

Keywords: Deformable Roll coating, Coil Coating, Rheology, High Speed, Film Thickness, Ribbing, Misting

High operation speeds and thin coating films are desirable in many industrial applications. But the quality of the product, which is primarily determined by an optimum process window, is affected by non-uniformities and instabilities originating at higher operation speeds.

Unlike other academic works, because of associated industrial relevance, particular attention was given towards the use of industrially relevant coating systems or generation of model fluids, which replicate the real coating solutions. One of the novelties of the research proposed lie in an integrated approach, utilising a range of comparative rheometrical techniques, with a focus on measurement of: (i) high strain rate shear viscosity [η], (ii) high strain rate uniaxial extensional viscosity [η_E] (iii) high strain rate elasticity (N1).

Deformable roll coating, in terms of classification, is the ultimate metered coating flow. The flow is controlled by the combination of hydrodynamic force and elastic deformation effect, which could be complicated by the presence of non-Newtonian fluid. This study necessitated the design and construction of a sophisticated deformable coating rig with the ability to operate over a wide range of conditions. Although the irregularities and instabilities associated with the roller coating process

has been studied previously, the concerned speeds of operation in this study is around three times higher.

The main objectives of this study was to carry out a comprehensive experimental programme establishing relationship exist between film thickness, film quality and operating parameters. Main identified operating parameters are roll speeds, roll gaps or applied load between the rolls, the elasticity with thickness of elastomeric layer and different rheological properties of the coating fluids. Surface instabilities and air entrainment are identified as the major limitations to being able to coat at higher speeds.

DECLARATION

No portion of this work referred to in this thesis has been submitted in support of an application for another degree or qualification of this or any other university, or other institute of learning.

Sreedhara Sarma

ACKNOWLEDGEMENTS

I wish to express deepest gratitude to my supervisor, Prof. Hadj Benkreira of Bradford University for his invaluable advices and timely guidance in my study period. His expert opinions and comments with full of encouragement have always inspired me throughout the duration of my research in the department.

I am deeply indebted to my sponsors Tata Steel Europe for giving me the opportunity to undertake this research. I wish to thank specially my Industrial Supervisor Dr. Siva Bohm, Principal Scientist at Tata Steel R&D, for his presence in my work from day one to the last. I take the privilege to place on record my deep sense of gratitude to Dr. Raj Patel and Mr David Steele of Bradford University for their keen interest and critical evaluation of my work. My special thanks to Prof Rob English of Edinburgh Napier University for his guidance during my studies. I would also like to thank my colleagues in The Netherlands, Dr Eelco Van Vliet and Margot Klassen for their help during the theoretical work.

Last but not the least, I would like to thank and dedicate this work to my family especially to my dearest wife. Their love, blessings and encouragement gave me the courage to go through tough periods of my life.

To Sid…….

…….My life

CONTENTS

Chapter 1 : INTRODUCTION 1
1.1 Introduction 1
1.2 Coating and its application 2
1.3 Coating flows: definition, limitations and classification 4
1.3.1 Classification of coating flows 5
1.4 Background to the steel coil-coating industrial process 9
1.5 Roller coating: product and process interaction 11
1.6 Challenges in coating flows 17
1.7 Aim and objectives of the research 18
Chapter 2 : LITERATURE REVIEW 21
2.1 Introduction 21
2.2 Coating flows: definition & features 22
2.3 Classification of coating flows 24
2.3.1 Free coating flow 25
2.3.2 Metered coating flow 27
2.3.3 Exact or pre-metered coating flow 31
2.3.4 Gravure or print coating flow 36
2.4 Forward roll coating flows: film thickness 38
2.4.1 Introduction 38
2.4.2 Rigid roll coating 40
2.4.3 Deformable roll coating 44
2.5 Forward roll coating flow: surface instabilities 53
2.5.1 Introduction 53
2.5.2 Rigid roll coating 53
2.5.3 Deformable roll coating 58
2.6 Forward roll coating flows: air entrainment & misting 60
2.6.1 Introduction 60
2.6.2 Rigid roll coating 61
2.6.3 Deformable roll coating 62
2.7 Research challenges in deformable roll coating 66
2.8 Conclusions 67
Chapter 3 : EXPERIMENTAL METHOD & EQUIPMENT 69
3.1 Introduction 69

3.2 Deformable roll coater rig design 69
3.3 Feeding and related problems 74
3.3.1 Different feeding methods for high speed operation 77
3.4 Wet film thickness measurement 83
3.4.1 Contact wet film thickness measurement 83
3.4.2 Non contact wet film thickness measurement 85
3.5 High speed visualisation of coating flow 89
3.6 Industrial coating full rheological characterisation 94
3.6.1 Significance of rheological measurements 95
3.7 Rheological techniques 97
3.7.1 Rotational rheometer 97
3.7.2 Capillary rheometry background 98
3.7.3 CaBER test background 101
3.8 Measurement of wetting property 102
3.9 Generation of model fluids 104
3.10 Rubber cover physical and mechanical characterisation 104
3.10.1 Dynamic mechanical analysis (DMA) experiments 105
3.10.2 Measurement of elastic modulus by coating rig 109
3.11 Deformation of rubber roll cover during roll coating process 112
3.11.1 Maximum strain 112
3.11.2 Frequency and strain rate 116
3.12 Conclusions 122
Chapter 4 : THEORETICAL STUDIES 124
4.1 Introduction 124
4.2 Rigid roll coating of Newtonian fluids 124
4.3 Lubrication modelling of deformable roll coating flow 140
4.4 Simulation on forward roll coating with a positive gap 147
4.4.1 Introduction 147
4.4.2 Setup of the simulation 148
4.4.3 Results: variation of viscosity 151
4.4.4 Results: variation of roll speed 156
Chapter 5 : EXPERIMENTAL RESULTS AND DISCUSSION 165
5.1 Introduction 165
5.2 Coatings used & their characterisation 166
5.2.1 Industrial coatings 166
5.2.2 Model fluid generation 177
5.3 Coatings used & their film thicknesses 184

5.3.1 Pick up roller feed film 184
5.3.2 Film thickness at equal roll speeds 186
5.3.3 Film thicknesses at unequal roll speeds 207
5.4 Coatings used & their flow stability 218
5.4.1 Ribbing instabilities 218
5.4.2 Misting instabilities 229
5.5 Pilot line trial 233
5.5.1 Description of the pilot line 233
5.5.2 Trials with PET and aluminium substrates 235
5.5.3 Trials with steel substrate 236
5.6 Conclusions 242
Chapter 6 : CONCLUSIONS & RECOMMENDATION 244
6.1 Introduction 244
6.2 Future work 248
REFERENCE 250
Appendix 1 264
Operating procedure for deformable roller coater rig 264
Risk assessment for deformable roller coater rig 267
Appendix II 267
Wet film thickness gauge- Performing a calibration test 267
Performing a calibration test for wet film thickness IR guage 268
Roll speed calibration 273
Load cell calibration 276
Roller speed calibration 277
Linear transducer calibration 278
Appendix III 279
Modifications for real industrial fluid trial 279
Experimental rig study with EB paint 279
Experimental procedure 282
Appendix IV 283
Derivation of basic differential equation of fluid mechanics: 283
Conservation of mass 283
Alternative approach – Study of linear flow rates 302
Film thickness measured- Raw data from the rig study 306
Appendix V Diagrams of Techma pilot lines 332

LIST OF FIGURES

Figure 1-1 Simplified schematic diagram of industrial coating process 2
Figure 1-2 Various coating processes [2] 5
Figure 1-3 Dip coating process (a free coating flow) 6
Figure 1-4 Roll coating process (a self metering flow) 7
Figure 1-5 Curtain coating process (Pre-metering flow) 8
Figure 1-6 Gravure coating process 8
Figure 1-7 Cross section of precoated steel [7] 9
Figure 1-8 Typical coil coating line [7] 10
Figure 1-9 Some of the possible 2 and 3 roll configurations for coil coating [8] 13
Figure 1-10 (a & b) Different rheological behaviour types 14
Figure 1-11 Time scale and typical values of process parameters in coil coating [9] 16
Figure 1-12 Ribbing phenomenon in forward mode [9] 16
Figure 2-1 Coating flow with liquid sheet falling under gravity to coat a thin layer film 22
Figure 2-2 Dip coating a) with a flat substrate b) with a roller 25
Figure 2-3 Metered coating flow- blade coating 27
Figure 2-4 Metered coating flow- forward rigid roll coating 28
Figure 2-5 Metered coating flow- deformable forward roll coating 28
Figure 2-6 Metered coating flow- reverse roll coating 29
Figure 2-7 Curtain coating flow [20] 32
Figure 2-8 Slot die coating onto a roller [22] 33
Figure 2-9 Tensioned web slot die coating (Lin et.al [27] arrangement) 34
Figure 2-10 Slide coating system [33] 35
Figure 2-11 Direct gravure coating flow 37
Figure 2-12 a, b, & c, Common cell patterns used for gravure rolls [35] 38
Figure 2-13 Forward roll coating film splitting flow 39
Figure 2-14 Flow rate and film split location predicted by Coyle et.al 40
Figure 2-15 Measured pressures along the main flow direction in forward roll coating [46] 42
Figure 2-16 Effect of shear thinning on film thickness ratio [16] 43
Figure 2-17 Deformable roll coating flow 45
Figure 2-18 Computed pressure and gap profiles as a function of load and speed parameters [52] 48
Figure 2-19 a) Elastic modulus as function of angular frequency b) Effect of thin cover on coating thickness [64] 49
Figure 2-20 Comparison of theoretical predictions and experimental measurements [53] 51
Figure 2-21 Ribbing instabilities in forward roll coating (74) 53
Figure 2-22 Film splitting meniscus and ribbing mechanism in forward roll coating [40] 55
Figure 2-23 Experimental results of critical capillary number for two-roll coater and roll wall systems [81] 57
Figure 2-24 Side view of the experimental set up [85] 58
Figure 2-25 Effect of gap on film thickness and critical capillary number [87] 59

Figure 2-26 Critical capillary number as a function of the dimensionless positive gap (Chong et.al [87]) 59
Figure 2-27 Experimental apparatus used for air entrainment studies [93] 62
Figure 2-28 Images from the nip (μ = 0.63, W = 4 kNm^{-1}) a) 500m/min b) 800m/min c) 1100m/min [98] 63
Figure 2-29 Cavitation and misting in roll coating [100] 64
Figure 2-30 Sequence of side view images of a septum of deformable configuration [102] 65
Figure 2-31 Drop count increase at 74 (□), 230 (◊), 282 (○) and 460 (Δ) mPa.s oils [102] 65
Figure 3-1 Schematic diagram [120] and photo (front view) of lab roller coater rig 71
Figure 3-2 The experimental rig, feed & deformation control (gap & load) [120] 71
Figure 3-3 Schematic arrangement of different possible two roll deformable coater set up in coil coating line 73
Figure 3-4 Open pan for feeding 75
Figure 3-5 Splash guard fitted onto the roller coater rig 76
Figure 3-6 Air entrainment in open pan for feeding 77
Figure 3-7 a) Feeding straight into nip b) Feeding from die onto roller 78
Figure 3-8 Example for industrial die feeding set up in roller coating 78
Figure 3-9 Die feeding set up for roller coater rig 79
Figure 3-10 (a & b) Die design specifications 79
Figure 3-11 Die fitted onto the roll from a front view 80
Figure 3-12 (a & b) Pressure vessel set up & die feeding inlet 81
Figure 3-13 Mechanism of pressurised pan feeding 82
Figure 3-14 Schematic of pressurised pan feeding system 82
Figure 3-15 Scraper blade and holder dimensions and location in the rig [120] 83
Figure 3-16 Non uniform scrapping with aluminium scrapper 84
Figure 3-17 Contact angle of polyester topcoat drop with different scrapper substrates 84
Figure 3-18 Capacitor probe arrangement 86
Figure 3-19 Non contact wet film thickness (WFT) instrument in coating rig 87
Figure 3-20 Schematic IR gauge sensor head and mounting [121] 88
Figure 3-21 Electronic control unit (ECU) for Infrared gauge 89
Figure 3-22 Single high speed camera set up 90
Figure 3-23 Experimental lab visualisation techniques 91
Figure 3-24 Photograph of the rib pattern from the model fluid rig trial (Conditions: -0.5mm gap/ 60 m/min roll speed) 92
Figure 3-25 Schematic misting phenomena and measurement method 93
Figure 3-26 Integrated rheological measurement for roller coating 95
Figure 3-27 Paint map approach for an industrial coating feasibility with roller coater 96
Figure 3-28 a) Rotational rheometer b) Cone and plate measuring system [113] 97
Figure 3-29 Mechanism of capillary rheometer 99
Figure 3-30 Mechanism of capillary break up rheometer [112] 101
Figure 3-31 Flow mechanism during CaBER test [116] 102
Figure 3-32 Principle of contact angle measurement 103
Figure 3-33 Pendent drop contact angle measurement technique 103

Figure 3-34 Q800 Dynamic mechanical analysis instrument 105
Figure 3-35 Dual cantilever clamps in DMA test machine 106
Figure 3-36 Schematic diagram of DMA test piece 107
Figure 3-37 DMA test pieces of the rubbers 108
Figure 3-38 Roller coater arrangement for measuring elastic modulus [64] 110
Figure 3-39 Static load variation with gap 111
Figure 3-40 Deformation of rubber during roll coating process 113
Figure 3-41 Strain versus gap distance 116
Figure 3-42 Strain of roll cover versus operating time 117
Figure 3-43 Triangle of gap condition of rolls 118
Figure 3-44 Relationship between gap distance and 'α' 119
Figure 3-45 Strain rate versus gap distance 121
Figure 3-46 Storage modulus measured with DMA at 2 mm amplitude 122
Figure 4-1 Fluid element between parallel plates 125
Figure 4-2 Roll coating flow geometry 128
Figure 4-3 Flow field and co-ordinates system 141
Figure 4-4 Overall view of the rigid roll coating process 148
Figure 4-5 Overview of the boundary conditions 149
Figure 4-6 Global overview of a flow field (150 mPa.s, 2rpm) 151
Figure 4-7 Position of the meniscus with increasing viscosity 152
Figure 4-8 Comparison of the situation just before the meniscus. Top: viscosity=50 mPa.s bottom: viscosity =200 mPa.s 153
Figure 4-9 Velocity profiles just before and after the gap 154
Figure 4-10 Pressure distribution and velocity across the x-axis (y=0m) 155
Figure 4-11 Determination of the film thickness 156
Figure 4-12 Position of the meniscus 157
Figure 4-13 Velocity field just before the meniscus, 2 rpm top, 5 rpm middle, 20 rpm bottom 158
Figure 4-14 Velocity profiles just before and after the gap 159
Figure 4-15 Pressure distribution and velocity across the x-axis (y=0m) 160
Figure 4-16 Thickness of the film on the top roll 161
Figure 4-17 Position of the meniscus in relation to the capillary number 162
Figure 4-18 Normalised flow rate in relation to the capillary number 163
Figure 5-1 Flow curve for pre-treatment primer (WBPP) at 20°C 167
Figure 5-2 Flow curve for EB topcoat coating 168
Figure 5-3 Temp ramp for EB topcoat 169
Figure 5-4 Image of CaBER experiment with EB coating 169
Figure 5-5 Stretch profiles used in CaBER experiments 170
Figure 5-6 Mid-filament diameter for EB coating (from CaBER results) 171
Figure 5-7 Limiting extensional viscosity for EB paint 171
Figure 5-8 EBR coating temperature ramp results from CaBER 172
Figure 5-9 Relaxation time from CaBER experiments 173
Figure 5-10 Trouton Ratio's of EB paint 174
Figure 5-11 Capillary rheometer measurement for EBR coating 175
Figure 5-12 Flow curve for capillary rheometry 175
Figure 5-13 Extensional viscosity for EB coating 176
Figure 5-14 Coating map for EB coating 177

Figure 5-15 Coating fluids against available process information 178
Figure 5-16 Trend lines for shear viscosity for 50 mPa.s base with corresponding higher molecular weight addition blends 179
Figure 5-17 Measured apparent extensional viscosity (CaBER) against higher mole. wt PDMS addition (wt% in 50 mPa.s base solution) 180
Figure 5-18 Measured Trouton ratio against shear viscosity for different PDMS blends 180
Figure 5-19 PIB-Kerosene blending to achieve specific high shear viscosity 181
Figure 5-20 Apparent extensional against shear viscosity for PIB-Kerosene blends 182
Figure 5-21 Normal axial force (N1) measured against increasing shear rate 183
Figure 5-22 Rheologies of different non-Newtonian model fluids 183
Figure 5-23 Single roll pick up film thickness at different immersion depths 185
Figure 5-24 Film thickness with increase in pick up roll speed 186
Figure 5-25 Deformable roll coating: Operating variables 187
Figure 5-26 Film Thickness variation (Carvalho equation) with speed at various gaps and for viscosity 14 mPa.s 191
Figure 5-27 Film thickness variation with speed at various viscosities and for gap 192
Figure 5-28 Predicted Film thickness variation with speed in previous analytical studies (0.014 Pa.s, 55 Shore A, -0.25mm gap) 192
Figure 5-29 Comparison with previous experimental (low speed) roller coating studies 195
Figure 5-30 Influence of the external load on the coating thickness (thick rubber cover regime) 195
Figure 5-31 Film thickness measured at lower speed and extrapolation to higher speed 196
Figure 5-32 Measured film thickness data with model fluid (0.04 Pa.s, 45 Shore A) 197
Figure 5-33 Shear viscosity Vs Temperature for EB topcoat paint at constant shear rate (500 s^{-1}) 197
Figure 5-34 Measured film thickness data with extrapolated data from lower roll speed (0.04 Pa.s, 45 Shore A) 201
Figure 5-35 Film thickness comparisons with Carvalho's theoretical equation [19] 201
Figure 5-36 Film thickness comparisons with previous theoretical and experimental studies done at lower roll speeds [44, 19, 61, 63] 202
Figure 5-37 Comparison of our results with O.Cohu and A.Magnin [64] study 203
Figure 5-38 Low mole wt PDMS film thickness results 205
Figure 5-39 Medium mole wt PDMS film thickness results 205
Figure 5-40 High mole wt PDMS film thickness results 206
Figure 5-41 PDMS model fluid similar shear viscosities 206
Figure 5-42 Dimensionless total flux relation with varying average roll speed under different negative gap condition (0.19 Pa.s, 55 Shore A) 209
Figure 5-43 Total flux Vs speed ratio, 0.19 Pa.s, b = 15mm, 55 Shore A Hardness . 210
Figure 5-44 Thickness ratio with speed ratio for average speed 0f 0.67 m/s and different viscosities (-0.2 mm gap) 211

Figure 5-45 Thickness ratio with speed ratio for different average speeds and different viscosities (Shore A 55) 211
Figure 5-46 Flux ratio with speed ratio with average speed of 0.67m/s (Shore A 70) 212
Figure 5-47 Flux ratio with speed ratio for different average roll speeds 213
Figure 5-48 Flux ratio with gap number for different speed ratios 213
Figure 5-49 Flux ratio with elasticity number for different negative gaps (Gent [119]) calculation modulus used 214
Figure 5-50 Measured and calculated elastic modulus of rubber with different methods 215
Figure 5-51 Hypothetical model for roll coating flux distribution 216
Figure 5-52 Diverging flow after film splitting creates ribbing 218
Figure 5-53 Ribbing on steel substrate Figure 5-54 Ribbing lines observed in... 219
Figure 5-55 Flow curve for WBPP 219
Figure 5-56 Oscillatory study for WBPP 220
Figure 5-57 Pendent drop measurement system 221
Figure 5-58 Contact angle measurement (~ 41°) 222
Figure 5-59 Rib formation in roll coating 222
Figure 5-60 Experimental set up for rib measurement 223
Figure 5-61 Film thicknesses against roll speed for WBPP solution 224
Figure 5-62 Ribbing frequency vs. WFT for smooth roll configuration 225
Figure 5-63 Masking effect of ribbing phenomena 226
Figure 5-64 Groove geometry dimensional details 226
Figure 5-65 Photograph of coated surface with new geometry roll 227
Figure 5-66 Rib wavelength measured for low mole wt: PDMS 227
Figure 5-67 Rib wavelength measured for medium mole wt: PDMS 228
Figure 5-68 Rib wavelength measured for high mole wt: PDMS 228
Figure 5-69 Mechanism of ribbing wavelength reduction 229
Figure 5-70 Misting phenomena in roller coating [71] 230
Figure 5-71 Onset of misting with mole wt system 231
Figure 5-72 Onset of misting with roll speed 232
Figure 5-73 Coating head configuration for EB coating (rollers W0 and W2 have a rubber EPDM cover) 235
Figure 5-74 Relation between footprint and negative gap in Bradford and correlation with Hannah equation [7] for both pilot line facility and Bradford case (error bar are error of measurement reading 0.1 for negative gap, 1mm in footprint) 237
Figure 5-75 Comparison between actual and predicted pilot line trial wet film thickness data 239
Figure 5-76 Picture of steel substrate with light in normal direction (left) and grazing light (right) 241
Figure 5-77 Picture of some white defect observed on coated samples 241
Figure A-1 Coating gap control with wedge adjustment system 266
Figure A-2 Coating roll drive with timing belt system 266
Figure A-3 Film thickness scrapper system (in contact with the roller) 271
Figure A-4 Roller speed calibration results 276
Figure A-5 Actual and set roller speeds in rig 278

Figure A-6 Heating and recirculation facility attached to the coating rig.....280
Figure A-7 Deformable roll coating with radiation curable coating in the lab 280
Figure 6-8 Fluid element with direction vectors.....284
Figure A-9 Piece of area in fluid 286
Figure A-10 Co-ordinate system for fluid system 287
Figure A-11 Normal stresses in fluid element.....287
Figure A-12 Effect of dilution on shear viscosity at 20°C.....288
Figure A-13 Flow curve for pre-treatment primer at 20°C [10% by wt dilution].....289
Figure A-14 Wet film thickness relation with roll speed.....291
Figure A-15 Wet film thickness relation with roll speed.....292
Figure A-16 Effect of speed ratio on applicator roll WFT at -0.2mm gap.....293
Figure A-17 Effect of speed ratio on applicator roll WFT at -0.4mm gap.....294
Figure A-18 Effect of speed ratio on applicator roll WFT at -0.6mm gap.....294
Figure A-19 Experimental set up for ribbing study [2].....295
Figure A-20 Rib wavelength against roll speed.....296
Figure A-21 Misting phenomena.....297
Figure A-22 Misting severity Vs process conditions 297
Figure A-23 Film thickness variation with speed at various viscosities and for gap - 0.5mm 298
Figure A-24 Film thickness variation with speed at various viscosities and for gap - 0.75mm 299
Figure A-25 Schematic diagram of various stages in the deformable roll coating of steel substrate.....303
Figure A-26 Linear flow rate criteria for various viscosity fluids 304
Figure A-27 Effect of negative gap on achieving target linear flow rate 306

LIST OF TABLES

Table 1-1 Wide range of coated products and applications [1] 3
Table 3-1 Static modulus measurement from coating rig 111
Table 3-2 Static modulus measurement from comparative studies [118,119] 112
Table 3-3 Strain of rubber cover at different gap distance 115
Table 3-4 Typical values of α, gap distance and strain rate 121
Table 5-1 CaBER results for EB coating 172
Table 5-2 Calculated Trouton results from CaBER 174
Table 5-3 Summary of rheological results of EB coating 177
Table 5-4 The PDMS model solutions 179
Table 5-5 Mixture details for PIB-Kerosene blends 181
Table 5-6 PIB-Kerosene blend details with viscosities 182
Table 5-7 Mixture details for PDMS and PIB-Kerosene blends (5 litres) 184
Table 5-8 Summary of exponents of the dimensionless groups from regression analysis 189
Table 5-9 Comparison of processing parameters with previous experimental studies 190
Table 5-10 Predicted film thickness values using Carvalho's equation (low speed)191
Table 5-11 Predicted film thickness values using Carvalho's equation (high speed) 193
Table 5-12 Model fluid relationship with viscosity of EB topcoat paint (Supplier A) 198
Table 5-13 Operating conditions for model fluid trials.....199
Table 5-14 Experimental film thickness (high speed) results for 45 Shore A 199
Table 5-15 Film thickness limits from high speed experimental studies.....200
Table 5-16 Operating conditions for O Cohu and A Magnin work [64] 203
Table 5-17 Summary of the experimental observations in case of Shore A 70,.....215
Table 5-18 Actual parameter and final wet film thickness on strip in pilot line trial 238
Table 5-19 Summary of the 3 roll deformable roll coating with nip feeding of an EB fluid (non pigmented) onto 0.1 mm gauge smooth CR steel substrate 242

KEYWORDS

Deformable Roll coating, Coil Coating, Rheology, High Speed, Film Thickness,

Ribbing, Misting

Nomenclature:

b (mm)	Rubber cover thickness
τ (Pa)	Shear stress
υ (s^{-1})	Shear rate
λ	Dimensionless flow rate
η_E (Pa)	Uniaxial extensional viscosity
Ca	Capillary number
DMA	Dynamic mechanical analysis
DFT (µm)	Dry Film Thickness
E (MPa)	Elastic modulus
E_{eff} *(MPa)*	Effective Elastic modulus
E' (MPa)	Storage modulus under bending mode
E'' (MPa)	Loss modulus under bending mode
EB	Electron Beam
FTIR	Fourier Transform Infrared Spectroscopy
G' (Pa)	Storage modulus under tensile mode
G'' (Pa)	Loss modulus under tensile mode
h (mm)	Gap between the rolls
L (mm)	Contact length
n	Power law index
N1	First normal stress
PTFE	Poly tetra fluoro ethylene
R (mm)	Radius of the roll
Re	Reynolds number
WFT (µm)	Wet Film Thickness
µ (Pa.s)	Viscosity
σ (N/m)	Surface tension
ρ (kg/m^3)	Density
Q (m^3/sec)	Volumetric flow rate
UV	Ultraviolet
W (N/m)	Applied load
We	Weissenberg number

Chapter 1 : INTRODUCTION

1.1 Introduction

This thesis examines the fluid mechanics of deformable roll coating at high speeds, up to 6 m/s, to produce thin films, 50 μm or less which are absolutely uniform for application in the continuous coating of steel. All published work on deformable roll coating prior to this study has been carried out at low speeds not exceeding 1-2 m/s and only with coating fluids that are rheologically simple, i.e. Newtonian. This research stems out from the need of the steel industry to coat steel coils fast and thin so that production costs are reduced. In these applications the coating fluids are "paints" that protect the steel from corrosion as well as giving aesthetic and other functionalities. These paints are naturally non-Newtonian and this affects the fluid mechanics of the operation. This study thus has a wider scope than previous work in that it considers the non-Newtonian flow features.

As deformable roll coating is a generic and fundamental coating flow, this introduction presents first generalities on the importance of coating and its application. A coating flow is then defined and its limitations described within the concept of a "coating window". As there is a variety of coating methods to produce a thin film onto a substrate, a classification of coating flows is presented. Coil coating is then identified within this classification and issues related to this operation are brought out in the content of this research. This leads to the final section of this introduction chapter which defines the aim and objectives of the research.

1.2 Coating and its application

Coating is the deposition of a film, originally as a liquid, onto a surface (substrate). The surface is usually a solid unless the coating is applied as a multilayer in which case the second and subsequent layers are coated onto a liquid. Once applied, the coating is then dried or cured to produce a solid layer. This definition applies to both stationary and moving substrates. In actual industrial operation, the substrate travels at speed as shown in *Figure 1-1*.

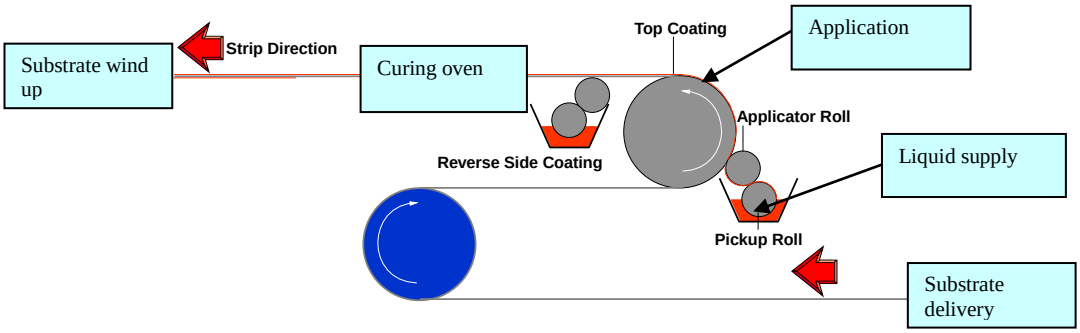

Figure 1-1 Simplified schematic diagram of industrial coating process

The function of the coated layer may be purely aesthetic but more generally it is functional hence the wide variety of coated products: audio and video films, printed paper and magazines, adhesive tapes, X-ray, solar cells, plastic electronics, medical drug release patches etc. The list is endless (see examples in *Table 1-1*) and demonstrates the huge economic importance of the coating industry.

Table 1-1 Wide range of coated products and applications [1]

Food packaging & food service
Flexible packaging
Interleaving sheets for separation
Heat seal films for pouch and food packaging
Barrier layer film to prevent moisture, vapour and oxygen transmission
Batteries
Battery separators
Rechargeable battery foils
Alternative energy
Photovoltaic cells
Solar films
Energy storage
Medical
Diagnostic strips for lab analysis
Electrodes for skin contact
Photographic films for medical, industrial, graphic arts and consumer use
Optical and magnetic media for audio and visual use data storage
Printing plates
Printed electronics
Multilayer ceramic capacitors
Liquid crystal display
OLED lighting
Smart labels
Logic circuits
RFID radio frequency identification devices
Graphics
Print adhesion layer for digital presses
OHP films
Various digital graphics display coatings
Protective coatings
Paints to protect the surfaces from corrosion and degradation
Packaging materials for electronic products
Metal coil coating
Industrial and automotive
Various adhesive layers for laminating
Chemically active thin surface layers
Dye surface coating
Flat belt coating
Conductive coating for self-heating film
Friction layers for high friction parts
Optical
Anti reflective coatings
Adhesive for optical laminations
Optical adhesive for clear labels
Tints for window film

Concurrent with the development of the vast range of products, there is also the development of the coating fluids, pastes and paints. These fluids by necessity contain the active solids (polymers, pigments and other particulates) and in turn can be complex (non-Newtonian) in their flow properties. As coating is the deposition of a film onto a surface, usually a solid, the characteristics of the substrate are also important. Surface properties such as roughness, porosity, surface energies all play a part not only in the deposition process but also with regard to adhesion and levelling of the film. Clearly coating as a technology and science is a complex interplay of fluid flow, rheology and interfacial effects. This is further complicated as there are many methods of applying a coating. A scientific framework becomes necessary first to define a coating flow and identify limitations of the flow and then classify all the coating methods available into simple categories all linked by common features. This is presented in the next section.

1.3 Coating flows: definition, limitations and classification

For most of the coating processes, the layers are in liquid form at the time of application. So it becomes imperative to have a fundamental understanding of the physical processes governing these fluid flows. A coating flow can be defined as a free surface flow with complex associated rheology, having static and dynamic wetting lines. These coating flows control the feasibility and operability of a specific coating process and subsequently the uniformity of the coated substrate surface.

Clearly the main objective when coating any substrate is to choose a right coating method and ensure that the operation produces the required film thickness and quality. Many different coating processes can be used to achieve the concerned

coating flow. Some of the common coating processes and their related flows in literature are schematically represented in *Figure 1-2*

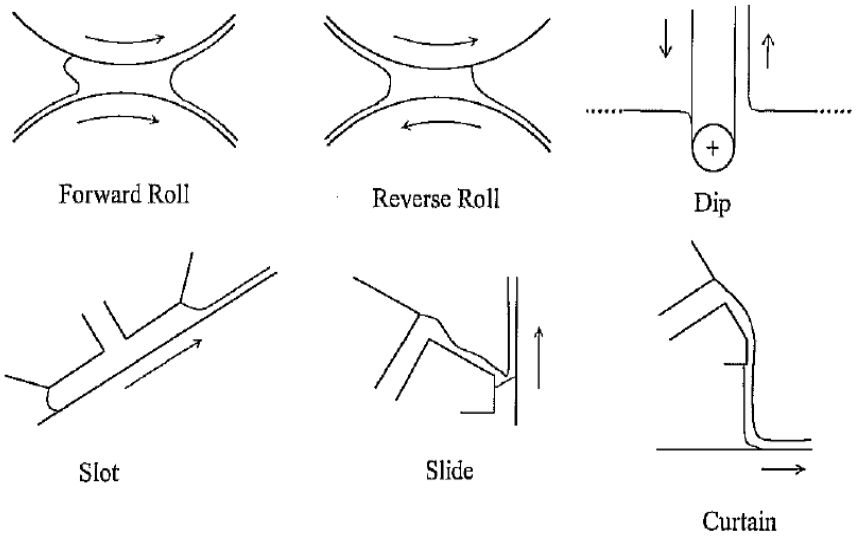

Figure 1-2 Various coating processes [2]

1.3.1 Classification of coating flows

Coating flows as explained above are many and varied, but can be organised according to their associated flow mechanism. As given below, Benkreira et.al [3] classified all known coating processes into four categories, progressing from basic coating flow with limited control to the one which gives higher control and accuracy.

(i) Free coating flow: A simple flow scheme in which a moving substrate or roll is withdrawing the liquid from a pool (as shown in *Figure 1-3*). Here the amount of fluid picked up, its stability and air entrainment depends on various process parameters like process speed, geometry, rheology of the liquid to be coated etc [4].

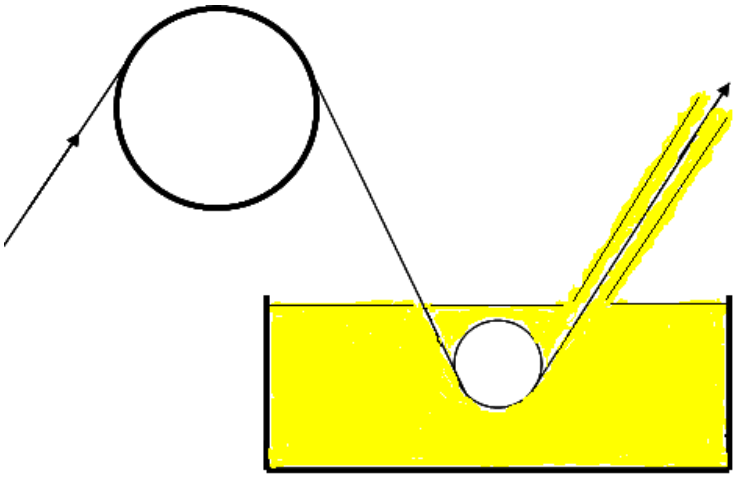

Figure 1-3 Dip coating process (a free coating flow)

These coating flows have been employed in various industrial applications such as the metallic coating of steel, application of polymeric material to conveyor belts, lubrication of moving machine parts, coating a photographic film etc.

(ii) Self metering flow: A flow in which excess amount of the liquid is delivered onto a given geometry and the required amount is metered (as shown in *Figure 1-4*). The extent of metered flow can be decreased through the application of an additional boundary such as jet of air flow, a rigid or flexible blade, rotating rolls or deformable rolls. Unlike free coating, self metering coating flows can deliver a range of film thicknesses using the control variables of roller speeds and gaps.

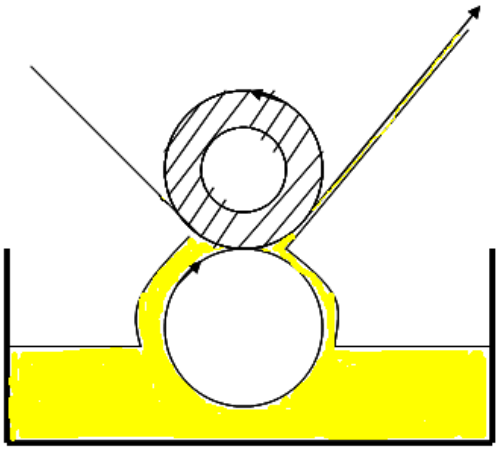

Figure 1-4 Roll coating process (a self metering flow)

(iii) Pre-metering flow: A flow in which an exact amount of liquid is delivered to the flow geometry and later on transferred onto a moving substrate (as shown in *Figure 1-5*). Curtain, slide and slot coaters are examples of exact coating mechanisms, where all the liquid fed into the coating head is transferred onto the substrate. Therefore, with pre-metering coating flow, for a given flow rate delivered by the coating head, the film thickness that forms on the substrate is controlled by the speed of substrate.

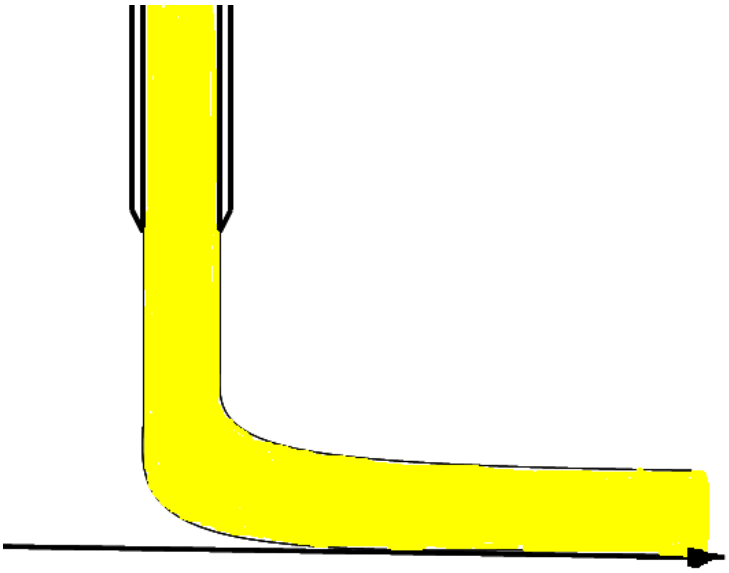

Figure 1-5 Curtain coating process (Pre-metering flow)

(iv)Gravure coating flow: A special case of flow in which a proportion of the liquid trapped inside the cells of a gravure roll is being wiped off by the moving substrate (shown in *Figure 1-6*). In gravure roll coating, in addition to roller speed, the cell volume controls the average coating thickness and it is the major determinant of the emptying behaviour. Clearly gravure coating can produce very thin films (1-5 μm) if the cell volume is very small.

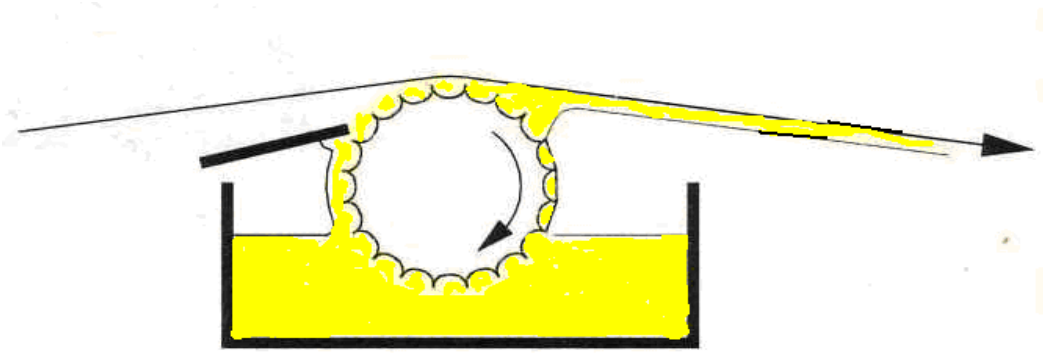

Figure 1-6 Gravure coating process

1.4 Background to the steel coil-coating industrial process

The steel coil coating industry dates back to the 1940's and compared to post-painting, coil coating offers a very cost effective, efficient and consistent route to manufacture a wide range of coated steel products [5]. Coated steel products have made great progress in terms of both production tonnage and technology in the last two decades [6]. The structure of pre-coated steel is usually composed of steel in the middle, on which initially a metallic coating is applied by hot dip coating process. Then different organic / inorganic coatings are applied on both sides, such as (i) a pre-treatment, mainly for the adhesion of the organic layer on metallic substrate, (ii) a primer used mainly for corrosion resistance and (iii) an organic topcoat used mainly for the aesthetic properties (see *Figure 1-7*). Depending on the requirements of the final product, there are different kinds of topcoat used, such as thermosetting solution coat, thermoplastic plastisol etc. These coatings will have different composition and flow properties along with a specific optimum applied wet film thickness.

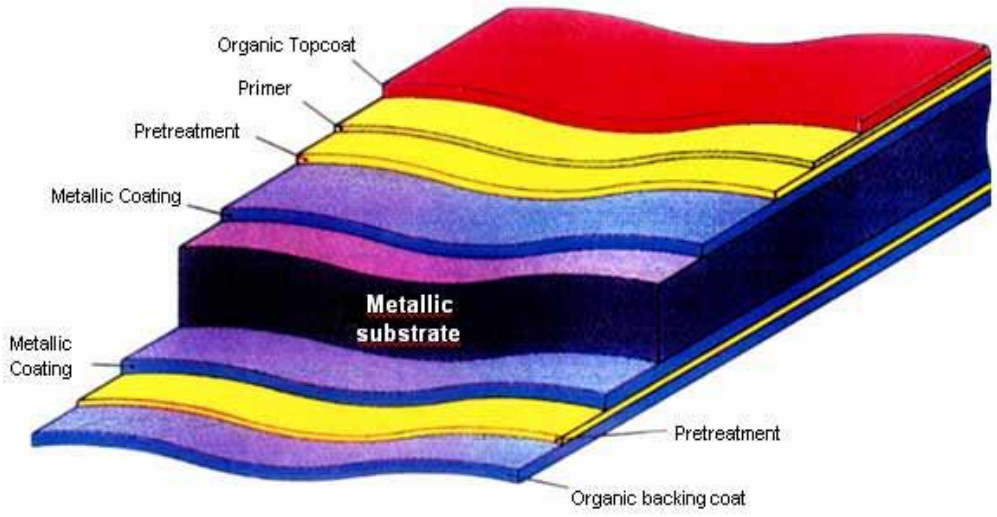

Figure 1-7 Cross section of precoated steel [7]

The organic coatings are applied continuously to coiled strips; which provides an efficient protective barrier for the underlying metallic coating together with an aesthetic appearance and other functionalities. The continuous application of organic coatings known as coil coating process is also used to produce pre-primed strip with only a primer coating. They are designed to receive a finish coating after downstream forming processes. Coil coating also produces ready-to-use pre-painted strips, with an additional aesthetic topcoat. Many coil coating lines (*Figure 1-8*), were built across the world to satisfy demand for pre-painted coil products with specific stringent requirements.

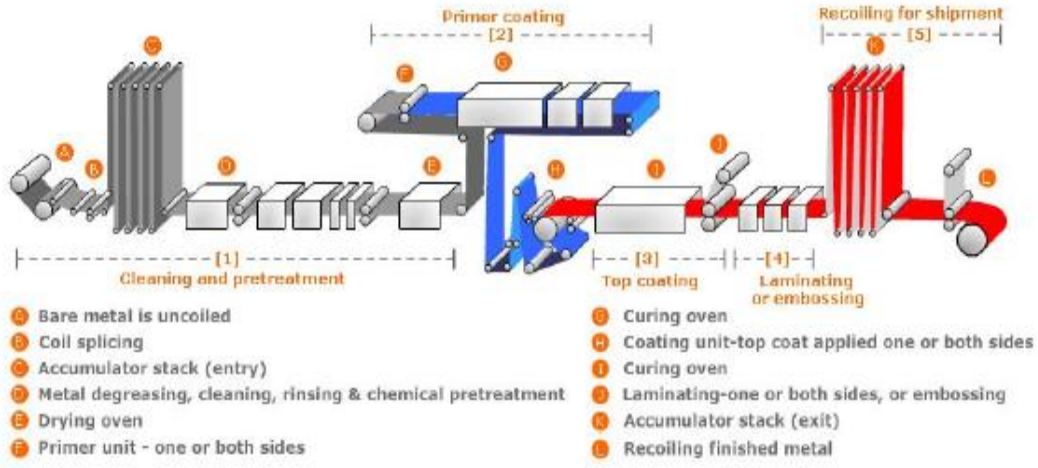

Figure 1-8 Typical coil coating line [7]

A schematic of a typical coil-coating line can be found in *Figure 1-8* and it operates at speeds of between 60-120 m/min. In this case, the web widths of up to 1850 mm and substrate thickness ranging from 0.3-2.0 mm are used. The majority of coating systems on steel consist of a pre-treatment layer (*section 1* in *Figure 1-8*) plus a primer (*section 2*) and a topcoat (*section 3*) layer. The layers are typically applied using a two or three roll deformable roller coating technique followed by heating to dry or cure each layer of coating individually (*section E, G, I* in *Figure 1-8*).

The use of continuous coil coating process has a number of technical and economical advantages:

- High productivity and yield, minimizing the cost of painting.
- The flexibility of coating processes, enabling to produce various types of coated products with colour and properties.
- High curing temperatures (220 to 250°C), allowing the use of a wide range of binders or polymers, with different film formation processes.
- The efficiency of waste treatment systems (e.g. incineration of solvent vapours), ensuring the environment protection.

1.5 Roller coating: product and process interaction

Since being introduced in the 1960's, Ultraviolet (UV) and electron beam (EB) curing of polymer coatings have been widely adopted in many industries such as automotive applications, telecommunications, electronics, adhesives, graphic arts, wood coatings, food packaging etc. In recent years, radiation curing applications have shown a steady growth of around 10% per annum and now constitute approximately 4% of the total industrial coatings market [7].

Given the advantages offered by radiation curing, it is not hard to see why the process is proving to be so popular. Radiation curing offers a number of perceived advantages over conventional thermal curing, including:

- Increased production speeds (due to near instant drying and little or no cooling of substrate required).

- In some cases, improved coating properties (e.g. better chemical and scratch resistance).
- Lower emissions of organic solvents, providing:
    - Lower handling costs
    - More environmentally friendly processes
    - More customer friendly

- Lower energy consumption (energy transferred mainly to coating, not to the substrate)

- Less waste; as 'flash off' can be re-cycled
- Less floor space required, as equipment is more compact

There are still, however a number of perceived disadvantages with radiation curing. These include:

- Difficulty in applying high viscosity radiation curable coating systems in uniform way with existing process methods

- Large initial capital costs (particularly for EB curing ovens)

- Difficulties associated with adhesion to certain substrates (such as steel)

- The raw materials can be more expensive, compared with conventionally cured materials

- There can be difficulties when using UV to cure pigmented and high build systems

However these barriers are gradually being reduced, opening up radiation curing to a host of new applications. In line with these fast drying or curing developments, the steel industry is now embarking on "speeding" up the coating operation from the low 1-2 m/s to very high 6 m/s. This is the topic of this research – to provide the intelligence for these key industrial developments.

In coil coating process, the coating formulation is usually applied with the forward or reverse roller coating method. The strip is moved over a rigid support roll and the coating is applied with an applicator roll made from a deformable elastomer material (*Figure 1-9*). Normally, a two or three roll configuration is chosen in order to meter the required thickness of the coating to be applied with specified accuracy.

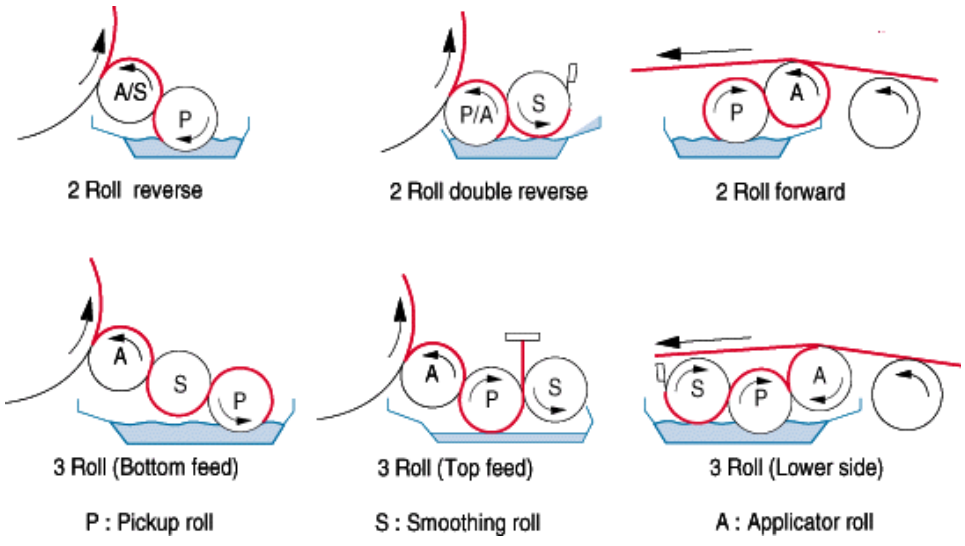

Figure 1-9 Some of the possible 2 and 3 roll configurations for coil coating [8]

The fluid behaviour in relation to the stress created by the coating process can be described by the fluid rheology. The rheological behaviour of fluids has been classified into various categories:

- Newtonian liquids: at a constant temperature, these liquids have a constant viscosity (η) regardless of the extent of the applied shear rate during the process (*Figure1-10(a)*).

- Non-Newtonian liquids: these liquids differ from Newtonian liquids in that their viscosity is sensitive to the applied shear rate. Some of them are shear thinning liquids meaning their viscosity is reduced as the applied shear rate increases (*Figure 1-10(a)*), which is common in many types of paints and coatings. Thixotropic liquids are another type of non-Newtonian liquids and these fluids can have a different viscosity at low shear rate (*Figure 1-10(b)*), that is their viscosity depends on both the applied shear rate and the shearing time.

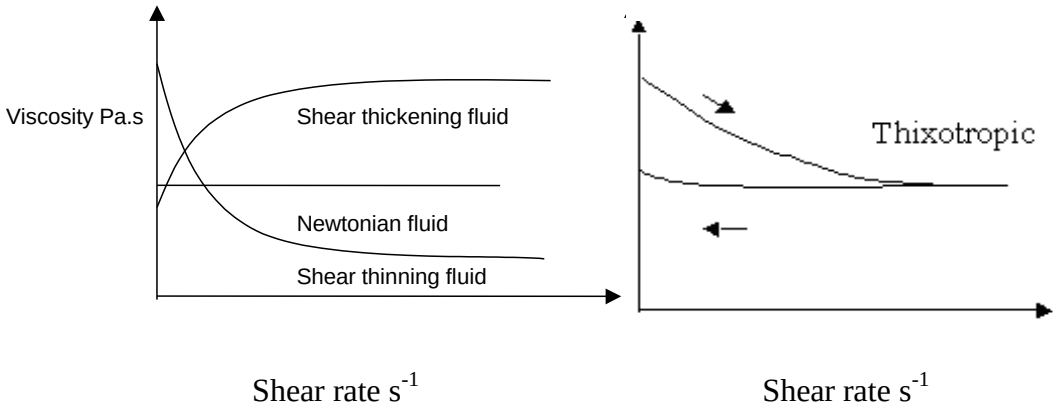

Figure 1-10 (a & b) Different rheological behaviour types

Another rheological parameter influencing the coating behaviour is the extensional viscosity (η_E) or the resistance to extensional rather than shearing flow. The ratio

between the shear viscosity (η) and the extensional viscosity (η_E) known as Trouton ratio. In the case of Newtonian fluids, Trouton ratio is a simple relationship with magnitude of 3. However, for polymeric non-Newtonian coatings this relation is not true anymore and the ratio of the viscosities can be as large as 10^4. Moreover with some coatings, at low stretch rate, η_E is constant but as the shear rate increases it initially increases then it decreases [8].

Coating viscoelasticity is the other main rheological feature. The description of shear viscosity and extensional viscosity highlighted above implies steady-state shearing. But the fluid behaviour during start up or under changing conditions in strain rates is described by a transient viscosity. This is due to the fact that non-Newtonian fluids are not only viscous but also show an elastic property.

The shear rates encountered in typical two or three roller systems instantaneously reduce the viscosity by several orders of magnitude for the majority of industrial coatings. This is because small coating gaps (less than 1 mm) and large roller speeds (larger than 1 m/s) result in very high shear rates (order larger than 10^6 s^{-1}). The viscosity values obtained in roller coating at these high shear rates are very difficult to measure with common commercial rheometers. Consequently, the low gradient viscosity measurement techniques used for quality assurance purposes bear no relation to the real viscosities encountered during the roll coating process. For a two roll configuration involving a contact between rigid roll and elastomer roll, the typical orders in magnitude of the process parameters are indicated in *Figure 1-11*.

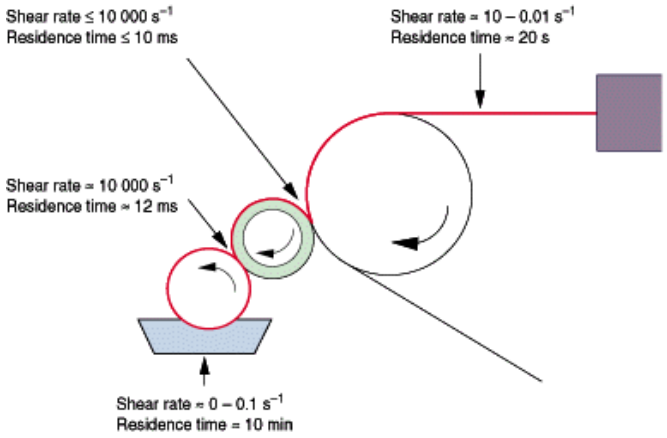

Figure 1-11 Time scale and typical values of process parameters in coil coating [9]

A particular feature of the forward roll coating mode is the appearance of a resonance or instability phenomenon, immediately after separation of the rolls and is called ribbing (*Figure 1-12*). It is identified as characteristic undulations in the wet film, with amplitude of several microns. Their appearance is related to the fluid properties, roll velocity, thinner coating and higher line speed. This effect is observed even in Newtonian fluids and has been extensively studied by Coyle et.al [10]. It is clearly an undesirable occurrence and understanding this phenomenon at high speed and with Newtonian as well as non-Newtonian fluids is an integral part of this research.

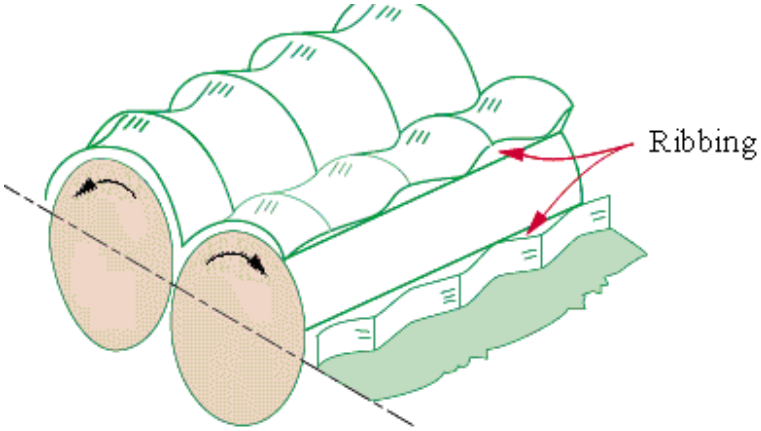

Figure 1-12 Ribbing phenomenon in forward mode [9]

1.6 Challenges in coating flows

Most of the coating processes have a narrow ‘stable operation window’ which will produce high quality products free from instabilities or defects. This operating window is difficult to predict due to dynamic wetting of fluids and free surface at the coating meniscus. When dynamic wetting fails, air is entrained at the dynamic wetting line where the solid substrate meets the fluid. Ribbing as described earlier is an instability on the top surface of the film caused by features in the actual flow. The coating window is thus delimited by two instabilities, air entrainment and ribbing. Their onset depends on many factors combined (roller speeds and gaps, fluid properties and substrate properties). As a result, industrial design and operation of coating processes become more of an art, relying on experience rather than fundamental knowledge.

Typically, a company has expertise in a few selected application techniques and new products are adapted using existing methods. Usually the cost and the time required to build a new facility is significantly higher than the cost to increase the speed of an existing line. Advanced knowledge of these existing and newer coating technologies are scattered throughout the literature in the form of scientific papers and patents.

The coating flows in general, meet different type and degree of challenges during the application, depending upon the type and roughness of the substrate to be coated, which may be another liquid or a solid substrate. The substrate may be permeable such as in paper coating or impermeable as seen in metal substrate coating. The coating solution may have different properties like paints, adhesives, inks, polymeric solutions etc, which behave differently during and after application. The coating

thickness requirement depends on the end use of the product, for example generally the coating layer thickness for an outdoor application coated steel sheet will be more compared to an indoor product. The required uniformity and integrity of the coated film again depends on the requirements of the specific industry.

The speed of the operation depends on the specific requirement of the industry and it can vary in a big margin. In an industrial context, coating speed can be an important determinant in the choice of coating processes. Some methods are inherently limited to certain speed ranges and in general, most of the methods can work in low speeds (exceptions: curtain coating and slide bead coating [11]) but all of them have an upper speed limit for a given coating thickness.

1.7 Aim and objectives of the research

The main aim of this research is to investigate the fluid mechanics of deformable roller coating process at speeds higher than normally operated and up to 360 m/min. The study will be largely experimental and will examine the film thickness and surface finish in relation to operating variables such as roller speeds, speed ratio, gap and load, as well as the coating solution properties (viscosity and surface tension). In respect of the fluid properties non- Newtonian characteristics, such as shear thinning will also be taken into consideration.

In order to achieve the above aim, the following objectives will be pursued:

- Develop a critical understanding of the fluid mechanics of coating flows in general, thorough a survey of available literature.

- Build on the above, and document in full details all previous work in relation to deformable roll coating.

- Identify from this literature, a rationale for how high speed coating can be accommodated. In other words, build a scientific steer to underpin the experimental work to be undertaken in this study.

- Rheological characterization of different commercial paint systems and based on the results to develop model fluids for coating experiments at higher speeds.

- Build or develop the experimental facilities necessary to undertake the research. The modifications would include high speed rig capabilities, measurement techniques, feeding zones, solvent handling etc.

- Develop the visualisation technique necessary to assess the surface finish and onset of ribbing and other instabilities of the film being formed at such high speeds.

- Carry out a systematic measurement of the variation of film thickness and film surface quality as a function of:

  - Roller speed
  - Roller speed ratio
  - Gap
  - Load
  - Viscosity

- Surface tension
- Non-Newtonian behaviour

- Underpin the observation made by simple fluid mechanic models of the flow.

- Conclude with Design-Operation parameters that can guide industrial operation at the required high speed.

Chapter 2 : LITERATURE REVIEW

2.1 Introduction

There are various types of coating flows and methods to produce films of different thickness in a range of speeds. It is important to review all of these coating flows and methods to get an understanding of the subject and identify areas of further research. This becomes a challenging task and will require reviewing almost everything written on the subject in the last hundred years. This is not at all intended here, but to focus on the production methods to produce very thin films of the order of 50 μm or less at speeds of above 100 m/min. Such application is of particular importance to the steel industry. In this chapter, various coating methods are reviewed briefly, especially from the point of view of producing thin and uniform films at higher speeds. In order to facilitate this process, in the first section the concept of a coating flow is introduced with its definition and associated features. Following this, a classification of all coating flows is presented giving advantages and limitations of the various methods. In the last section, the metered coating method of forward roll coating (both rigid and deformable) which is the subject of this research is reviewed in detail. This is done in terms of fluid mechanics aspects of film formation with thickness, surface flow instabilities (ribbing, cascade and others) and dynamic wetting failure (air entrainment). This review will present current knowledge as well as the research challenges that remain, and thus put in perspective the objectives set for this work and justification for this research.

2.2 Coating flows: definition & features

Thin film coating flows are viscous, free surface flows which form a film of liquid onto a solid substrate moving at speed. As coating is ultimately the deposition of solid onto another solid substrate after drying or curing, the coating formulation is typically a dispersion of fine particles or polymers into a solvent or water. These polymers or fine solid particles are well mixed with binders and other different additives, which after drying would form a continuous integral film adhering to the solid substrate. Because of their demanding final film requirements, clearly from their very nature, these coating fluids will be non-Newtonian in their flow characteristics. Adding to the non-Newtonian aspect, the presence of a three-phase or dynamic wetting line (as shown in *Figure 2-1*) and the surface tension effect on the free surface, makes the mathematical analysis of these coating flows very difficult.

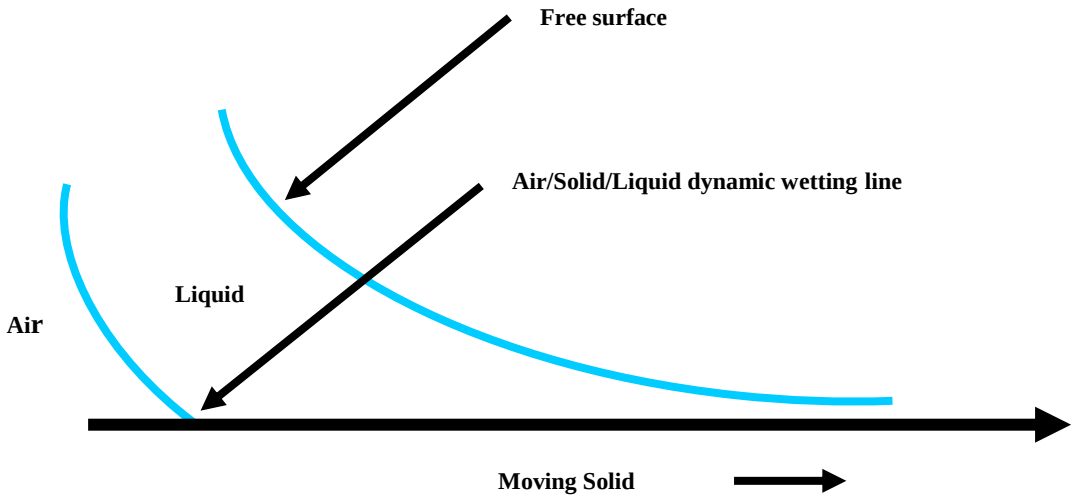

Figure 2-1 Coating flow with liquid sheet falling under gravity to coat a thin layer film

Like all other flows, coating flows are not always stable. Stable coated films are normally formed in a narrow window of operating speeds, gaps and physical properties, which is known as the "coating window". One of the main category of instabilities is free surface instabilities, which include ribbing (ribs on the film in the direction of flow), filamentation (ribs changing into filaments) when the coating fluid is viscoelastic and cascade (bars on the film in the transverse direction). Ribbing instability for example is controlled by viscosity and surface tension factors, for which the criterion of onset has been well studied in positive gap forward and reverse roll coating [12]. In negative gap (deformable) roll coating, the conditions for the onset of ribbing has however not been studied in length and this is an objective of this research. The other forms of instabilities are associated with air entrainment, resulting from wetting failure at the dynamic wetting line when the coating speed is increased beyond a threshold [13]. Whereas in principle ribbing instabilities analyses can be done mathematically by free surface perturbation analysis, dynamic wetting failure analysis are more difficult as we do not yet have unique conditions describing the dynamic wetting line in coating flows. This line is singular because on one hand it is "stationary" and on the other hand the whole surface is moving. Research in dynamic wetting failure is thus very challenging and one of the most exciting researches in coating flows [21].

There are many ways of achieving a coating flow, from the basic brushing (painting) action to the more complicated methods which involves specially designed dies, printed rollers, multiple rollers etc to deliver flow and film onto moving web. For convenience and better understanding, Benkreira et.al [3] classified and organised all these coating flows into four main categories. Any known coating method can be

included into these four broad fundamental categories. Hence, it becomes imperative to understand these basic coating flows and their fundamental differences in order to choose the right method for the right application. The aim of the next section is to briefly describe the fluid mechanics of these four classified categories of coating flows.

2.3 Classification of coating flows

Benkreira et.al [3] using the way in which the coating film is formed as a basis, suggested that thin film coating flows can be classified into the following four categories,

- Free coating flows
- Metered coating flows
- Transfer coating flows
- Gravure or Print coating flows

It is important to note that these are broad categories, which cover almost all coating processes in terms of the way in which the particular film is formed and later controlled. One interesting aspect of this classification is as you move from one category to the next; a reduction in film thickness is achieved towards very thin films at higher speed. In this aspect, the classification of Benkreira et al [3] is very helpful. Thus, moving from free coating flows up to gravure coating, lower thickness, better control and less dependency on process parameters are achieved.

2.3.1 Free coating flow

In free coating, a moving web or roller is allowed to enter a liquid pool, leaves with the same speed and it results in entraining a thin film as shown in *Figure 2-2a, b.*

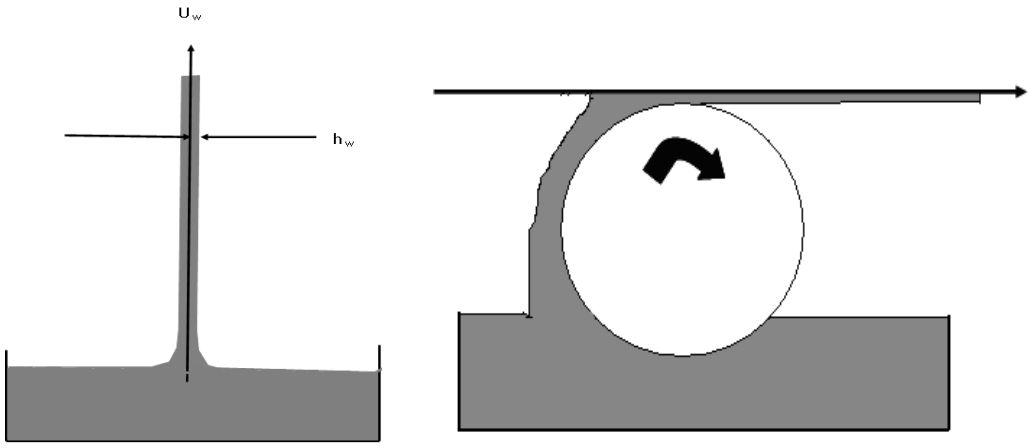

Figure 2-2 Dip coating a) with a flat substrate b) with a roller

Free coating flow, such as dip coating has been studied from very early times in coating processes, as it is the most basic way of forming a thin film. In free flow coating, the film thickness and associated instabilities depend on many factors, such as the speed of the substrate, fluid properties, surface properties of substrate etc. Here the main fluid properties include viscosity (μ), surface tension (σ) and density (ρ), while substrate surface properties include its roughness and wettability. The wettability of the substrate surface is expressed by the dynamic contact angle and it can be measured. In dip coating, the ratio of viscous force to surface tension force which is known as Capillary number ($Ca = \mu U_w / \sigma$) is found to be the controlling parameter. At high speeds, the ratio of inertial forces to viscous, known as the Reynolds number ($Re = \rho U_w h_w / \mu$) is also found playing a part. The non-dimensionless film thickness (H) will depend on the values of Capillary number (Ca) and Reynolds number (Re) and there are many experimental data available for a range encountered in practice. For example, Spiers et.al [14] (an early researcher at

Bradford University) solve the problem at low Ca values ignoring the inertia effect, and the solution found was:

$$H = 0.944Ca^{1/6}\left(\frac{\mu U}{\sigma g}\right)^{1/2} \qquad [2.1]$$

Looking at the above relationship, it is clear that in free flow coating the final coating thickness increases with increased viscosity and coating speed. This is not desirable as the high solid content coatings used in industry are inherently highly viscous and the coating speed demand is also higher. But the industrial expectation from these coating operations is to produce thinner coating films, and hence free coating flow related processes are limited in these applications.

Another interesting area of research in free coating flow is the effect of the angle of substrate withdrawal from the pool on coating thickness, because of its change in meniscus shape and gravitational effects [15]. Also because of the simplicity of the flow, this has been used extensively to understand the air entrainment phenomena.

These methods can generally coat on both sides of a flat substrate, as used in the case of dip coating for galvanised steel substrates. But with the use of a roller (as shown in *Figure 2-2b*), free coating flow can transfer the coating fluid from the pan to the web on one side as well. One of the key limitations of free coating flow is that, if one has to set the speed and the physical properties of the fluids, the film thickness cannot be controlled. In other words, there are no other variables that can be manipulated to reduce film thickness if so desired. This limitation leads naturally to

the search for other coating flows with more precision and control. The next category offers precisely this possibility.

2.3.2 Metered coating flow

In metered coating, a physical boundary, which could be stationary or moving, is added in the flow domain in order to reduce the extent of film formation. Metered coating flow is probably the most versatile coating flow category available, as it enables a wider range of parameters to be used to control the film thickness and stability of the concerned flow. With metered coating flow, the physical boundary produces a gap (h_0) to meter or reduce the film formed on the web. This boundary can be stationary as in the case of blade coating (*Figure 2-3*), or it could be moving as in the case of roll coating (shown in *Figure 2-4, 2-5, 2-6*). Hence in this category of coating flows, unlike the free coating flows described before, the flow is no longer free to establish itself. The hindrance introduced will restrict the flow in a way to limit flow rate as well as film thickness.

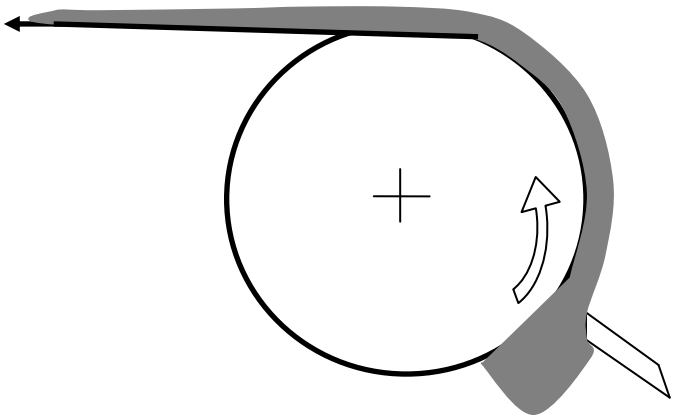

Figure 2-3 Metered coating flow- blade coating

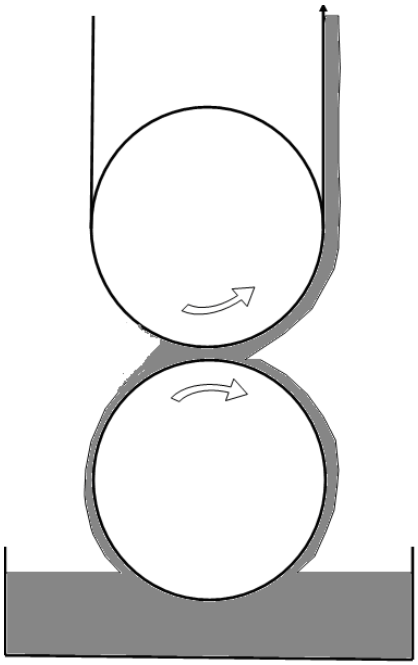

Figure 2-4 Metered coating flow- forward rigid roll coating

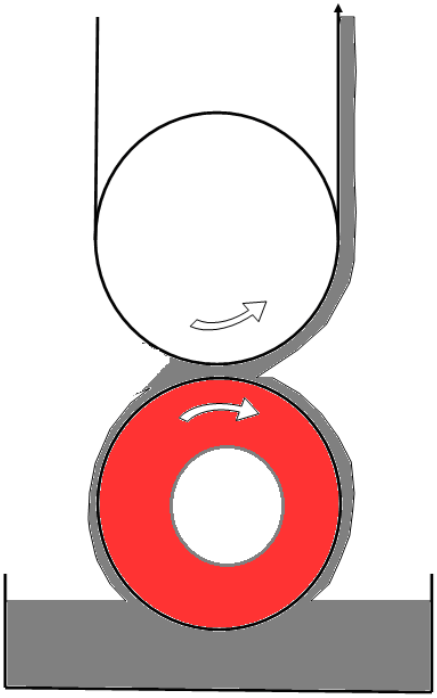

Figure 2-5 Metered coating flow- deformable forward roll coating

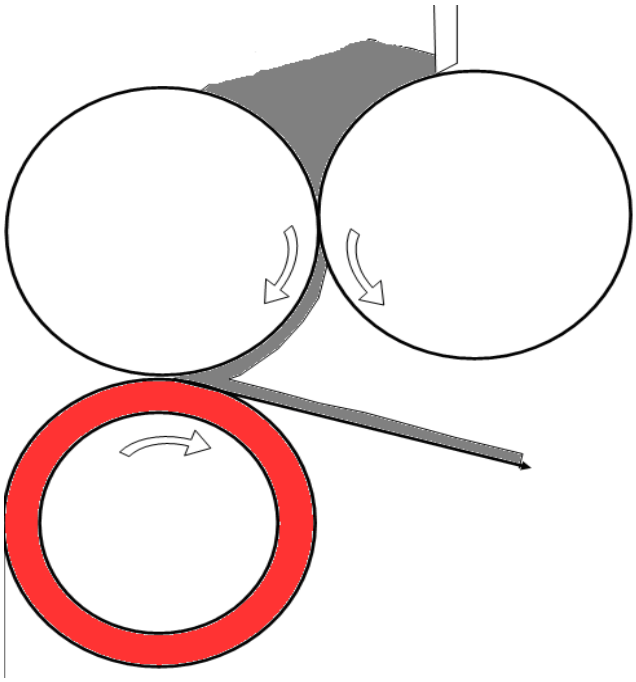

Figure 2-6 Metered coating flow- reverse roll coating

In forward rigid roll coating (see *Figure 2-4*), the film thickness on the moving web can be predicted analytically using the lubrication approximation [15]. The model is simply a balance of pressure (p) and viscous forces expressed by:

$$\frac{dp}{dx} = \frac{d\tau}{dy} \qquad [2.2]$$

The constitutive equation for Newtonian fluids can be used for stress τ ($\tau = \mu\, du/dy$) and the velocity profile in the gap can be obtained using the boundary conditions on the rotating rollers,

$$\frac{dp}{dx} = \mu\frac{d^2u}{dy^2} = \frac{12\mu}{h^2(x)\left[U - \frac{Q}{h(x)}\right]} \qquad [2.3]$$

U is the average speed of the rollers and h(x) the gap between them. To solve for flow rate (Q), approximate boundary conditions for pressure at the flow limits are needed. A typical solution presented by Benkreira et.al [16] gives Q as a simple fraction of the product of the gap and average speed or:

$$Q = \frac{4}{3h_0 U} \qquad [2.4]$$

Assuming that the rollers rotate at same speed, the film thickness on the web can be calculated as:

$$h_w = \frac{2}{3} h_0 \qquad [2.5]$$

Thus, this "extra" parameter (gap h_o) is the control parameter and a film thickness about 2/3 of the gap set is achieved independently of speed and physical properties of fluid, which is most interesting and desirable in practical applications.

The above prediction is however only approximate. Here the pressure boundary conditions are important in solving the problem and the exact position where flow separates is unknown. This stresses on the significance of having a proper model for film separation conditions in order to capture the full dependence of operating parameters which must include speed, physical properties as well as gap.

In deformable roll coating flow which is the focus of this research, at small gaps on wider rollers with viscous fluid, the pressure distributions will be so high that rollers will deform and the coating flow problem becomes coupled with a roller deformation problem [18], i.e. an elasto-hydrodynamic situation. When the roller speeds are unequal, Benkreira et.al [17] through a semi-empirical approach formulated the

condition that defines the distribution of the flow Q between two rollers. This is discussed in detail in later sections of this chapter.

In reverse roll coating, the metered coating flow (*Figure 2-6*) becomes more complex, (full 2D flow with recirculation) unlike when the two rollers are moving in the same direction at the nip (the forward case just described). The film of interest in reverse roll coating is the one that is formed by the leakage flux out of the nip. The transfer film can also be of interest. Here the nip does not need to operate at flooded condition at the inlet as in the case of forward, and the deformable nip with negative gap is also studied [19]. Even though progress has been made in understanding the metered flow, the position of dynamic wetting line or conditions for its failure (which results in air entrainment) is not fully understood. At the exit meniscus, the dynamic wetting line conditions would be helpful to predict other surface instabilities such as ribbing as well.

2.3.3 Exact or pre-metered coating flow

In exact coating flows (also known as transfer coating flow), the flow rate Q is set and it determines the coated thickness, independent of the liquid properties and substrate speed. Fixing the substrate speed, the required uniform coating thickness can be achieved by controlling the flow rate through a high precision liquid delivery system (such as those formed from accurately designed dies). The main types of exact coating flows are: (i) Slot coating (ii) Slide Coating and (iii) Curtain coating (shown in *Figure 2-7*)

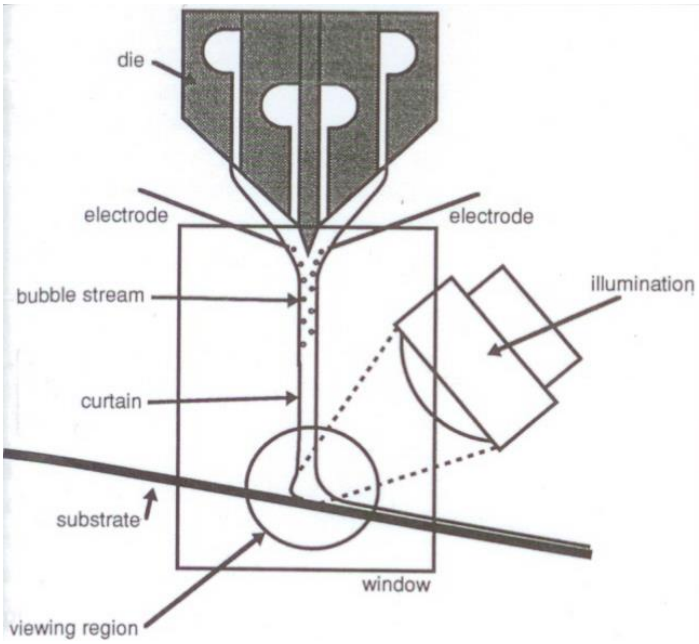

Figure 2-7 Curtain coating flow [20]

There are differences in the way these films are deposited: (i) in slot coating, the liquid is pumped through a die directly onto the substrate; (ii) in slide coating, the coating layers slide through a distance before being deposited, and (iii) in curtain coating, the die forms a curtain of fluid which impinges onto the moving substrate. In the curtain coating case, this impingement of liquid is good for delaying the air entrainment at higher web speeds. This feature is traditionally used by the photographic industry which requires multilayer (up to 12 layers simultaneously) curtain coating. Blake et.al [21] from Kodak explained that the impinging curtain "assists" dynamic wetting as a pressure is applied in the dynamic region by the curtain and this delays air entrainment to higher speeds thus enabling to reduce film thickness. This concept of dynamic wetting assist explains the reason why air is entrained at comparatively lower speeds in the case of other coating flows such as free coating and metered coating flows where the dynamic wetting region is not subjected to extra external pressure.

Lee et.al [22] studied experimentally slot die coating (experimental set up in *Figure 2-8*) and found that there is a critical capillary number (Ca) below which the minimum wet film thickness depend on coating speed and viscosity. This minimum dimensionless film thickness obtained in their study was around 0.6 to 0.7 for a gap of 0.2 to 1 mm.

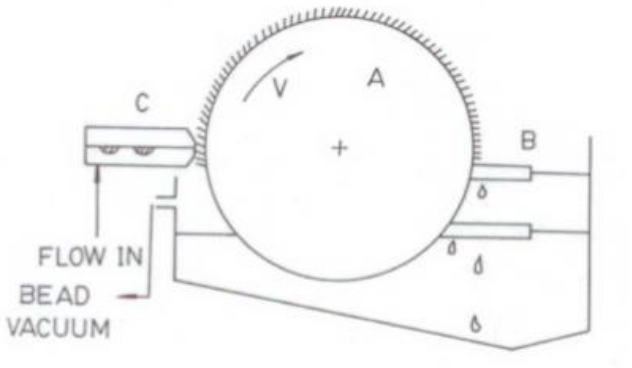

Figure 2-8 Slot die coating onto a roller [22]

Later Carvalho and Kheshgi [23] found a new region, different from Lee et.al [22] in which the minimum wet film thickness decreases as Capillary number (Ca) increases. Their results indicate that it is possible to get a 12.7 µm film using a 22 mPa.s liquid at the coating gap of 100 µm at 70 m/min. Chang et.al [24] studied low viscosity fluids and concluded that there are three regions where the stable minimum coated film can be achieved. Their study indicated towards different regions, one where Lee. et.al [22] work fits (minimum thickness independent of Ca) and one where Carvalho and Kheshgi [23] work fits (minimum thickness decreases as Ca increases). In their experiments, the minimum wet thickness is about 12 µm using a low viscosity fluid (1.2 mPa.s) with the coating gap of 200 µm at 72 m/min (*Re* =200). Meanwhile Romero and Carvalho [25] and Chin et.al [26] studied the importance of die lip geometry to minimise the wet film thickness and instabilities.

Although the minimum film thickness can be reduced by minimising the die gap, there is clear limitation to close this gap, because of possible clash of die with roll or substrate. As a solution to this problem, Lin et.al [27] studied experimentally the tensioned web slot die coating (*Figure 2-9*) and produced very thin films (0.5 to 1.5 µm), which was much thinner than conventional slot die coating.

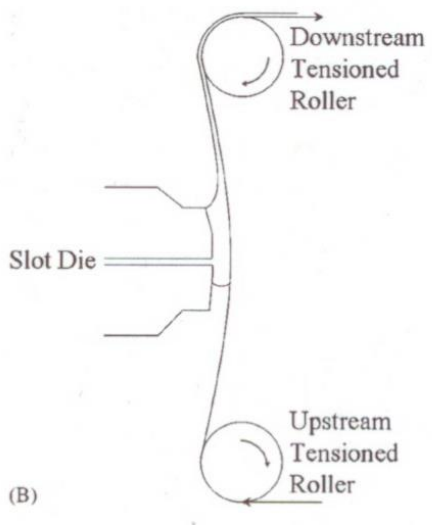

Figure 2-9 Tensioned web slot die coating (Lin et.al [27] arrangement)

Ning et al. [28] found that there is an optimum concentration of polymer additives in coating fluids at which a minimum thickness can be achieved. Romero et al. [29] studied the low flow limit in slot coating using low molecular weight polyethylene glycol and high molecular weight polyethylene oxide in water. From their experimental results, as extensional viscosity increased, the minimum wet thickness increased, i.e. there was no effect of adding high molecular polymer on reducing the minimum wet film thickness. However Romero et.al [30] studied theoretically and found that for low Weissenberg number (We = shear rate * relaxation time) and less flexible polymer molecules, the onset of the low flow limit occurs at lower flow rate

than the Newtonian liquids. They also concluded that above a critical Weissenberg value (We), the viscoelastic stresses destabilises the process. Chu et.al [31] found out that coating window is expanding with molecular weight, and after certain point, elasticity found to be significant. They also studied the effect of additives such as TiO_2 in the coating window, to conclude that higher interaction between particles and polymer solution increased the surface tension and in turn wider coating window.

Slide coating (as shown in *Figure 2-10*) is used in multilayer application, where many layers can be applied at one time. The low flow limit of coatability on slide coating was studied by Gutoff and Kendrick [32] and their data indicate that the maximum velocities with no bead vacuum are identical to that of dip coating. According to their data, the minimum wet film thickness was not less than 100 μm at a speed more than 60 m/min.

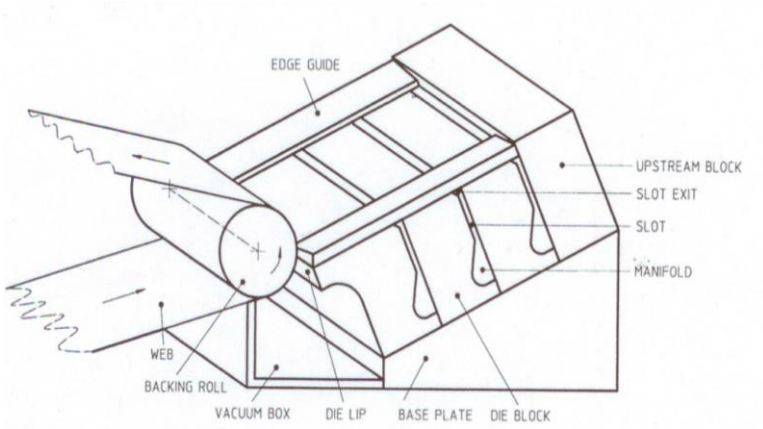

Figure 2-10 Slide coating system [33]

Benkreira and Cohu [15] found that having the dynamic wetting line not perpendicular to the substrate motion is an effective way to delay air entrainment in slide coating. Remember that the main challenges in slide coating are low wet film thickness (below 20 μm) thus increase in operation speed above the threshold of air entrainment is critical.

In the industrial context, curtain coating (*Figure 2-7*) is known for its high speed to deposit coating liquids onto substrates. Blake et.al [34] explained that in curtain coating, the liquid is delivered to the moving substrate as a freely falling liquid sheet; the onset of air entrainment can be postponed by increasing the height of curtain, adjusting the solution flow rate or angle of impingement etc. Here the minimum flow rate in curtain coating is typically about 1.0 cm^2s^{-1} and it would make it difficult to apply thin films (below 20 µm) at speeds above 100 m/min. Hence curtain coating does not seems to be the right application technique to make thin wet film lower than 20 µm at high speeds such as those required for the present research (up to 360 m/min).

In general, the challenge in pre-metered coating flows is the capability of the precise designed die to deliver a uniform coating layer thickness across the width of the substrate. In metered coating flows the gap set up between the substrate and the coating roll or blade delivers the thin films while in pre-metered flows the accurately designed die across the width of the substrate delivers the uniform thin coating layer. Hence here the die design for uniform deposition which is also free from associated instabilities such air entrainment or ribbing is one of the other issues.

2.3.4 Gravure or print coating flow

A simple practical model of gravure coating is the traditional brush which when used efficiently should only hold coating in between the hair of the brush [35]. Gravure coating flow (as shown in *Figure 2-11*) relies on an engraved roller which picks up the fluid from the pan, the fluid is lodged into the tiny cells, wiped clean so that only the cell volume contains the coating fluid and it is then transferred to the web to

produce a very thin film of order a few microns. Wiping can be achieved either by a doctor blade (direct gravure coating) or an impression deformable roller (indirect gravure coating). In direct gravure coating, the substrate can travel in the same direction as the roll direction or opposite to it resulting in forward direct gravure or reverse direct coating flows. Indirect gravure coating also can operate in forward or reverse mode using an intermediate deformable roll between the gravure roll and web.

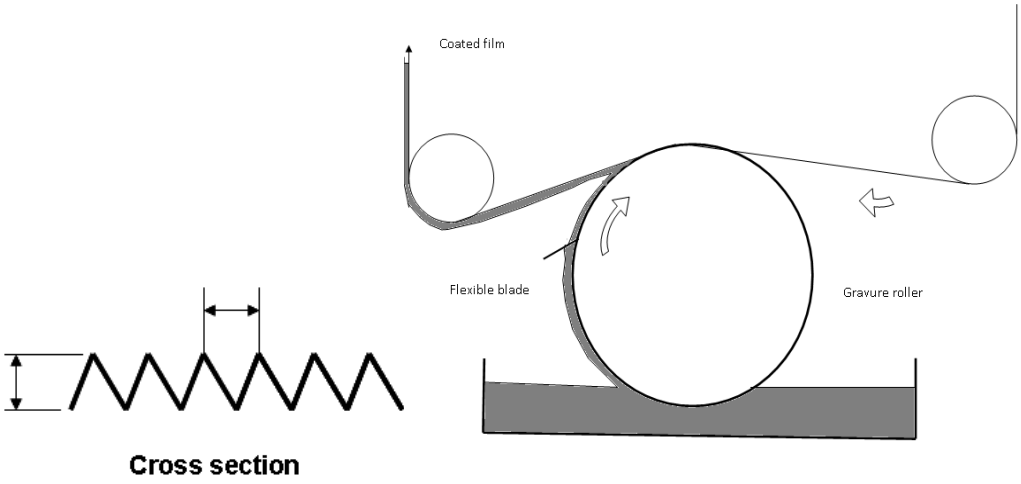

Figure 2-11 Direct gravure coating flow

Typical patterns in gravure coating are the quadrangular, trihelical and pyramidal geometries with cell volume per unit area of about 10 to 50 x10^{-6} m^3/m^2 as shown in *Figure 2-12a, b, c* respectively.

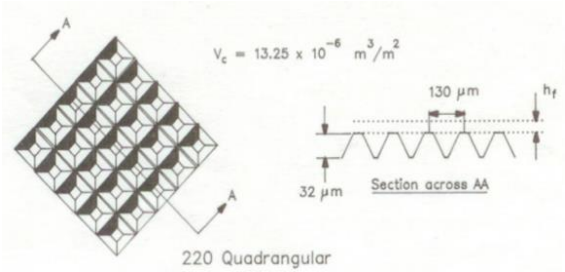

Figure 2-12a

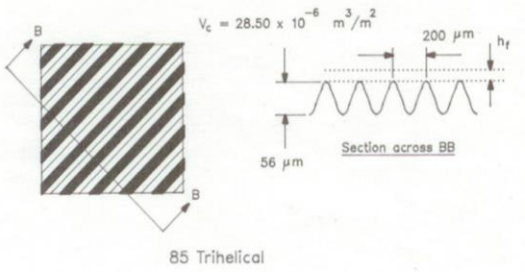

Figure 2-12b

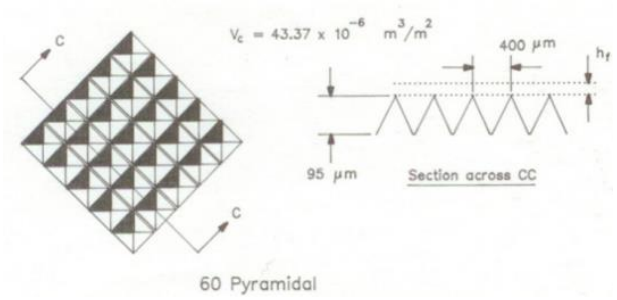

Figure 2-12c

Figure 2-12 a, b, & c, Common cell patterns used for gravure rolls [35]

2.4 Forward roll coating flows: film thickness

2.4.1 Introduction

In the previous sections, an overview of the literature on coating flow was given; explaining in particular the following important aspects:

1. The classification of coating flow, highlighting the importance of metering roll coating, forward roll coating in particular.
2. The limits of stable coating because of the inherent surface instabilities (ribbing, filamentation, cascade and others) and air entrainment.

In the following sections, more details of prior work on forward roll coating (rigid and deformable) is given and is presented along the line of film thickness, surface instabilities and air entrainment. Film thickness is chosen as a feature because of the interest in this coating research is in achieving very thin films.

Forward roll coating is an important industrial operation and modelling of this flow process has been extensively investigated [36]. This section is restricted to the examination of forward roll coating with the focus on film thickness related area.

This section is considered because of its direct relevance to the research study. The fundamental flow field is as shown in *Figure 2-13*

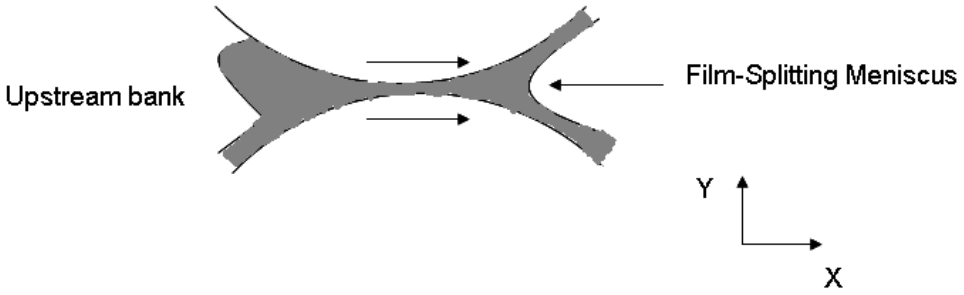

Figure 2-13 Forward roll coating film splitting flow

Usually an excess of coating fluid reaches the nip and this feed situation is known as a flooded nip as shown in *Figure 2-13*.Clearly the flooded nip case removes the dependence of the film thickness formed on the feed film. In cases where the feed film thickness is in the order of the size of the gap or less, the film thickness which forms will be highly dependent on the feed film thickness [37]. Coating flows are similar to lubrication flows [38], for example those in lubricated mechanical bearings. The common feature of lubrication flows is the fact that flow occurs in a very narrow but relatively long nip. In forward roll coating, fluid is dragged into the nip by the moving rollers through the action of coating fluid viscosity (μ) and roller speed (U). Here the geometry is converging and this result in a squeezing action that generates a high pressure on the inlet side of the nip. Conversely, the drag flow is diverging at the downstream side of the nip generating a comparatively lower pressure. This hydrodynamic pressure generation is governed by the geometric factor (h_0/R), which measures the slope between the roll surfaces. In the nip region, the flow is one dimensional because the cross-channel velocity can be considered as

negligible compared with down-channel velocity. But in the film-splitting region (meniscus), the flow is fully two dimensional and distinctly different than the lubrication flow in the nip. Here the flow is confined by a free surface which is controlled by the surface tension (σ) of the liquid. It gives rise to a dimensionless number known as Capillary number (Ca=μU/σ) which compares viscous effect forces with surface tension forces.

2.4.2 Rigid roll coating

There have been a number of fluid mechanics analyses of forward roll coating but the one by Coyle et. al [39] is the most complete as it considers the 2D aspects that are present in the separation zone (or film spilt meniscus as indicated in *Figure 2-14*) where the films form. It is this zone that presents a challenge as it is bounded by a free surface. Finding its shape as well as the size of the films formed is part of the solution challenge. Clearly such analysis will account for the effect of the capillary number Ca.

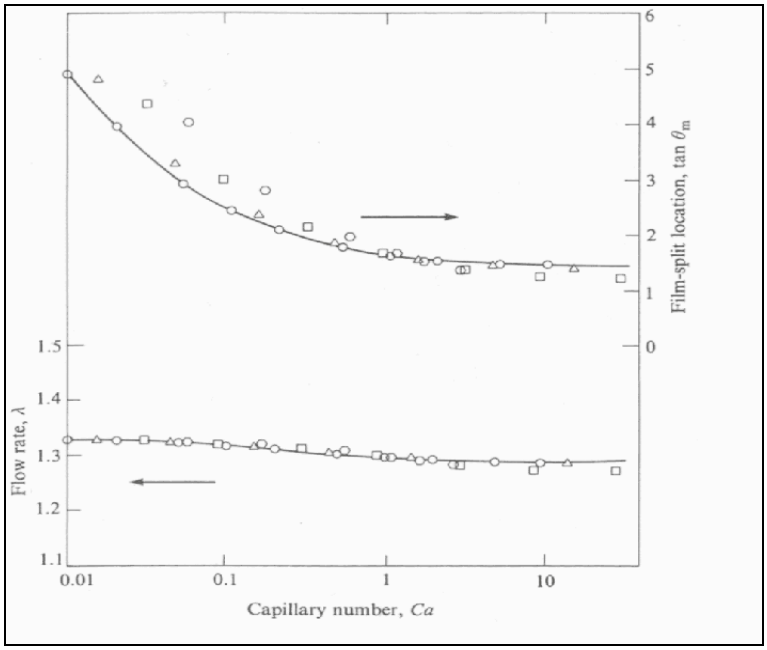

Figure 2-14 Flow rate and film split location predicted by Coyle et.al [39] ○, V=1; Δ, V=2; □, V=5; O, V=10

As shown in *Figure 2-14*, the results show that as capillary number is decreased the meniscus locates further away from the centre of nip and some recirculation starts to grow in size. Pitts and Greiller [40] also reported similar recirculation. At low capillary number, when roll speeds are unequal, the recirculation near the slow moving roll shrinks in size and detach from the meniscus. As for the size of the films formed, Coyle et.al [39] predicted for the symmetrical roll speed case where the two films formed are equal, a dimensionless flow rate λ ($=2UH/H_0$) of 1.301. Similar predictions of the film thickness can be obtained using simple lubrication analyses without the need of considering in detail the shape of the separation meniscus. As we shall demonstrate later, what is needed is the flow-pressure drop equation in the nip and appropriate pressure and/or velocity conditions at the flow exit. Pitts and Greiller [40], Greener and Middleman [41], Hintermaier and White [42], Sullivan and Middleman [43], Benkreira et.al [16] and several other researchers have all developed such simple lubrication models to predict λ values not far from those of Coyle et al full analysis, i.e λ~1.30.

When the rolls are running at unequal speeds, the analysis requires a model for how the flow split into the two films. Benkreira et.al [16] investigated this case, and measured the ratio of coating thickness on the rolls to be:

$$\frac{T_2}{T_1} = \left(\frac{U_2}{U_1}\right)^{0.65} \qquad [2.6]$$

Fortuitously, the same film split correlation can be found if one assumes the free coating prediction of Landau-Levich [4]:

$$H=1.34\ Ca^{2/3} \qquad [2.7]$$

Such correlation assumes that the flow in the nip has no bearing on how the film splits- the size of the film formed being the same as those dragged by two rollers from a bath of fluid. Using simple velocity conditions at the separation point (U (x_s) =dU/dy (x_s) =0), Coyle et.al [44] and Savage [45] predicted an exponent of 0.5 which clearly put in perspective the experimental correlation (equation [2.5]).

Dowson et.al [46] measured the pressure profile in the nip region between the rolls, which can be approximated as one dimensional in most of the region. As shown in *Figure 2-15*, it becomes two dimensional at the vicinity of the film-split meniscus, and found to be largely affected by the capillary number.

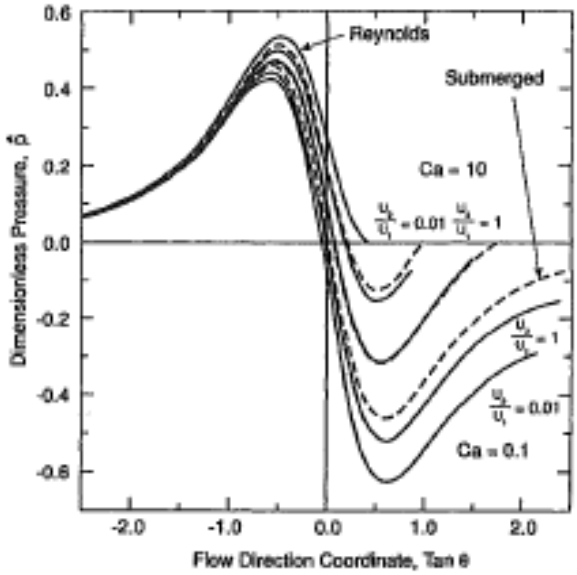

Figure 2-15 Measured pressures along the main flow direction in forward roll coating [46]

Coyle et.al [47] through their experiment proved that dimensionless flow rate (λ) should increase up to 1.4 as the power law index (n), which is a measure of the shear

thinning nature of non-Newtonian fluids decreases. Benkreira et.al [16] measured λ = 1.43 with carboxymethyl cellulose solution. The film split ratio for unequal speed was measured with varying power law index as shown in *Figure 2-16*.

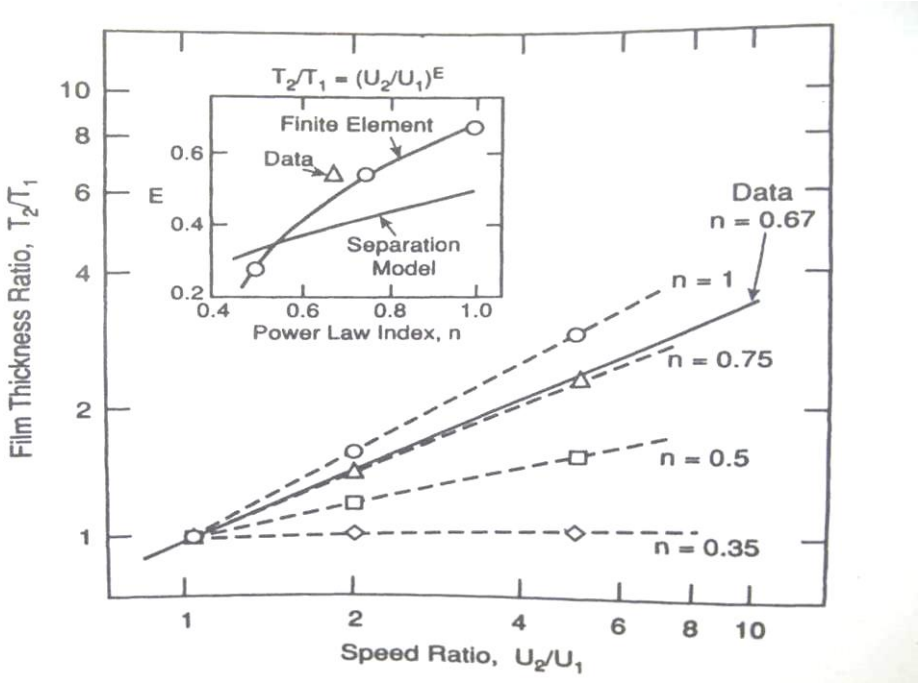

Figure 2-16 Effect of shear thinning on film thickness ratio [16]

As shown in *Figure 2-16,* for unequal speeds with non-Newtonian fluids, it can be concluded that as the power law index decreases (making the fluid more shear thinning) the film split becomes more symmetrical. Greener and Middleman [48] proposed a lubrication theory based model of forward roll coating with viscoelastic fluids. They concluded that the shear thinning effects tend to decrease the pressure generated in the nip far more than the viscoelastic effects.

As just described above, the fluid mechanics of rigid (positive gap) forward roll coating under the condition of a fully flooded nip are now well understood with both simple (lubrication) and involved (FE) models confirmed by experimental measurements. Savage and Gaskell [37] studied meniscus roll coating, where the

inlet film thickness is less than the set gap between the rolls and the resulting bead is maintained by solely surface tension effect. Preliminary results in this case show that, the fluid dynamics is quite different from the commonly used flooded configuration. Because the flows in these conditions are starved, the film thickness formed can be very small with surface tension having a critical effect. Such flows are inherently low speed phenomena and are not of interest to the present study.

Usually, the flow in a slowly varying channel can be analysed using the lubrication approximation with associated suitable pressure boundary conditions. When a film-forming meniscus is present, additional boundary condition (which is pressure gradient at the meniscus) are needed to determine its position. In small capillary number regime, Landau-Levich film forming equation [4] can be used and in this case, the surface tension force dominates the shape of the meniscus.

2.4.3 Deformable roll coating

The mechanism of flow in the deformable roll coating nip is similar to the elastohydrodynamic lubrication of bearings and gears [55]. Fluid is dragged into the nip by the moving roll surfaces through the action of viscosity. Since the geometry is converging, a squeezing action generates high pressures on the inlet side of the nip (as shown in *Figure 2-17*). This pressure can be high enough to cause elastic deformation of the rubber covered roll surface. This deformation changes the converging geometry and thus affects the hydrodynamic pressure.

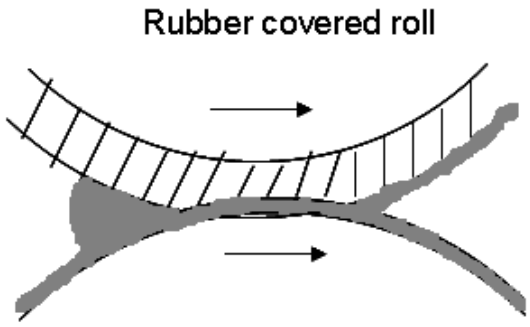

Figure 2-17 Deformable roll coating flow

The flow in the nip for deformable roll coating case is determined by the relative balance of viscous force, elastic force and externally applied force. In most of the cases, compared to the above forces the surface tension is insignificant and can be ignored. Deformable nip can be operated in constant gap or constant load configurations. In constant gap setting, the distance between the roll axes are fixed using mechanical stops and the load that tries to force the rolls apart is a function of the operating parameters. Normally, the gap setting would be a small negative number, meaning the rolls are pushed together such that they are deformed even at rest. In a second method, the movable roll is loaded either hydraulically or pneumatically up against the fixed roll. The gap between the rolls is now a function of operating parameters.

For constant load operation, if the viscous forces are small the load is supported by the elastic deformation of the roll surfaces and the situation is similar to the Hertzian contact between the cylinders. If the viscous forces are large the load is supported by the hydrodynamic pressure alone without much elastic deformation and the situation is basically the same as rigid rolls. The limiting cases for constant gap operation are

different and for positive gaps the rigid roll limit is reached at low viscous force, whereas higher viscous forces cause larger elastic deformations. For negative gaps there is no rigid roll limit.

The dependent variable of primary interest in a coating process is the coating thickness. For the symmetric roll speed case, the total coating thickness is equal to the local gap between deformed roll surfaces at the point of maximum pressure. The variables of interest are the pressure, gap profiles and the thickness of the deformable cover of the rolls. If the surface deformation is of the same order of magnitude as the cover thickness, the finite thickness becomes important. This relative importance of cover thickness can be evaluated by calculating the Hertizian dry contact half-width [56].

Dowson and Higginson [55] first published an accurate numerical solution of the coupled elastic and hydrodynamic problem. Many researchers (Dowson and Higginson [57], Archard et.al [58], Cheng [59]) followed previous work to come with a better iterative numerical solution or on the development of approximate analytic solution [60].

Herrebrugh [61] derived the first analytic results for a semi-infinite elastic medium with Newtonian fluids. This was followed by Hooke and O'Donoghue [62], who derived a large-deformation limiting solution for elastic solid layer of finite thickness.

They predicted that the minimum thickness in the gap, H_m for highly loaded systems with an incompressible elastomer layer is given by:

$$H_m = 3.12(\mu U_{avg})^{0.6} W^{-0.2} \left(\frac{4E}{3}\right)^{-0.4} R_{eff}^{\ 0.6} \qquad [2.8]$$

Here the maximum flux, Q_{total} passing through the nip can be approximated as,

$$Q_{total} = U_{ave} H_m \qquad \text{Giving:} \qquad [2.9]$$

$$Q_{total} = 3.12 \mu^{0.6} U_{avg}^{\ 1.6} R_{eff}^{\ 0.6} \left(\frac{4E}{3}\right)^{-0.4} W^{-0.2} \qquad [2.10]$$

Coyle [44] also analysed forward deformable roll coating using a simple 1D model for lightly and heavily loaded conditions. His prediction expressed in a form similar to in *equation [2.10]* gave:

$$Q_{total} = cons\tan t \times \mu^a \times U_{avg}^{\ b} \times R_{eff}^{\ c} \times E^d \times W^e \qquad [2.11]$$

The exponents in the above equation are:

a = 1.0, b = 2.0, c = 1.0, d = 0.0, e = -1.0 (Light loads)

a = 0.5, b = 1.5, c = 0.4, d = -0.33, e = -0.17 (Heavy loads)

It can be seen that in the case of heavy loads, *equation [2.10]* and *[2.11]* are similar.

Bapat and Batra [66] investigated the dry rolling contact of viscoelastic solid, while Coyle et. al [52] was the first to do corresponding analysis for the lubricated contact, although with limited range of material viscoelasic parameters. Later Coyle et. al [52] followed up with a study on nonlinear finite deformation of elastic solid layer and some preliminary results for viscoelastic solid layer. They computed pressure and gap profiles as function of load and speed parameters (as shown in *Figure 2-18*). As shown in figure, at high load there is an extended nearly parallel gap region over which the pressure profile is nearly Hertzian. At constant load, if the viscosity or speed is increased, the pressures in the inlet region increase and since the area under

each pressure curve is equal the pressure in the centre nip region falls. At the same time the rolls move apart and the inlet region takes on a less sharp gap profile.

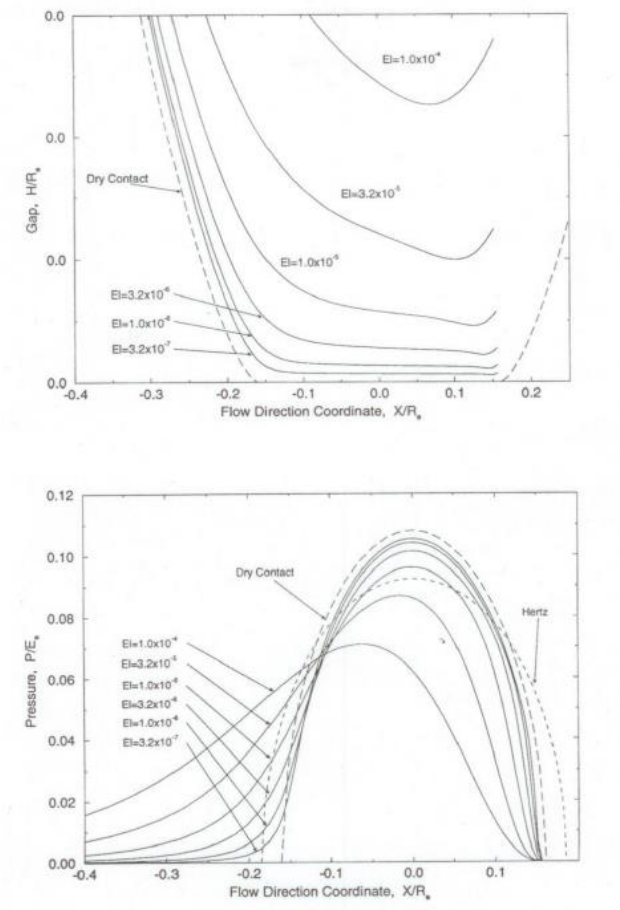

Figure 2-18 Computed pressure and gap profiles as a function of load and speed parameters [52]

Carvalho and Scriven [18, 67] confirmed the results by Coyle [65] with a one-dimensional model to describe the roll deformation. They also proposed a Hookean two-dimensional model for predicting the pressure distribution and roll profile in both positive and negative gap regime. In their model, applied load and hydrodynamic lubrication force are balanced mainly by the elastic deformation of the roll covers. At high loads (large solid deformation), an extended nearly parallel central nip region is formed where the pressure is nearly Hertzian. Here the thickness

of the cover becomes important, as thin covers can drastically reduce the coating thickness. Their expression predicts that H_{app} changes with the applied load W, but the system can operate with constant gap as well. In this case, Pranckh and Coyle [68] proposed a relationship between W (applied load) and H_o (gap between rolls), which leads to H_{app} as:

$$H_{app} \approx (\mu U_{avg})^{0.6} (-H_0)^{-0.2} E^{-0.6} R_{eff}{}^{0.2} \qquad [2.12]$$

Smith and Maloney [63] carried out one of the earliest comprehensive experimental investigation using some 700 data points measuring the dependence of the film thicknesses with viscosity, average roll speed, roll radius, elastic modulus and external applied load between rollers. They found:

$$h_m = 4.04 \times 10^4 \times \mu^{0.64} \times U^{0.58} w^{-0.34} E^{-0.35} R^{0.58} \qquad [2.13]$$

As shown in *Figure 2-19*, Coyle's predictions were confirmed by Cohu and Magnin [64] data, who also stressed that elastic modulus of rubber materials, may be time-dependent.

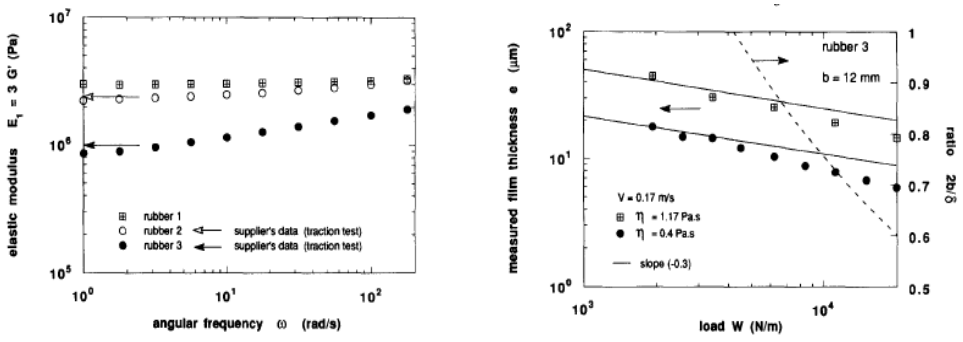

Figure 2-19 a) Elastic modulus as function of angular frequency b) Effect of thin cover on coating thickness [64]

Cohu and Magnin correlation is:

$$h_m \approx 0.4 \times R^{0.7} \times (\mu V)^{0.6} E^{-0.3} W^{-0.3} \qquad [2.14]$$

Later Coyle [65] presented results of an experimental study of the film thickness with around 200 data points fitting the following correlation:

$$h_m = 1.87 \times 10^4 \times (\mu U)^{0.49} w^{-0.43} E^{-0.41} R^{0.42} \qquad [2.15]$$

In an effort to relate operations in the constant load and constant gap modes, Young [69] analysis predicted that the relationship between W and H_o could be approximated by:

$$W = 1400 E R_{eff} \left[\frac{-H_0}{R_{eff}} \right]^{1.93} \qquad [2.16]$$

This leads to a maximum flux passing through the deformable nip as:

$$Q_{total} = 0.66 \times \mu^{0.6} \times U_{avg}{}^{1.6} \times R_{eff}{}^{0.786} \times E^{-0.6} \times (-H_0)^{-0.386} \qquad [2.17]$$

Kang et.al [70] is one of the few who carried out experiments at constant gap. Their correlation expressed as in equation [2.18] is however quite different:

$$Q_{total} = cst \times \mu^{0.5} \times U_{avg}{}^{1.5} \times R_{eff}{}^{0} \times E^{1.6} \times (-H_0)^{-0.47} \qquad [2.18]$$

Carvalho and Scriven [71] developed a two-dimensional model with a plane-strain, non-linear viscoelastic model of the elastomer which accounts for the roll cover

modulus and thickness for both pre-set load and pre-set gap. They derived the following correlations for thin and thick layers:

For thin layers ($L/R_{eff} < 0.1$)

$$Q_{total} = 1.34 \times \mu^{0.6} \times U_{avg}{}^{1.6} R_{eff}{}^{0.71} E^{-0.29} W^{-0.31} \left[\frac{L}{R_{eff}} \right]^{0.29} \quad [2.19]$$

For thick layers (L/Reff >= 0.1)

$$Q_{total} = 0.68 \times \mu^{0.6} \times U_{avg}{}^{1.6} \times R_{eff}{}^{0.71} E^{-0.29} W^{-0.31} \quad [2.20]$$

Adachi et.al [53] presented coating thickness data for a rubber-covered roll against a flat plate, operated at a constant gap condition. These results along with the theoretical predictions of Coyle et.al [52] are plotted in *Figure 2-20*.

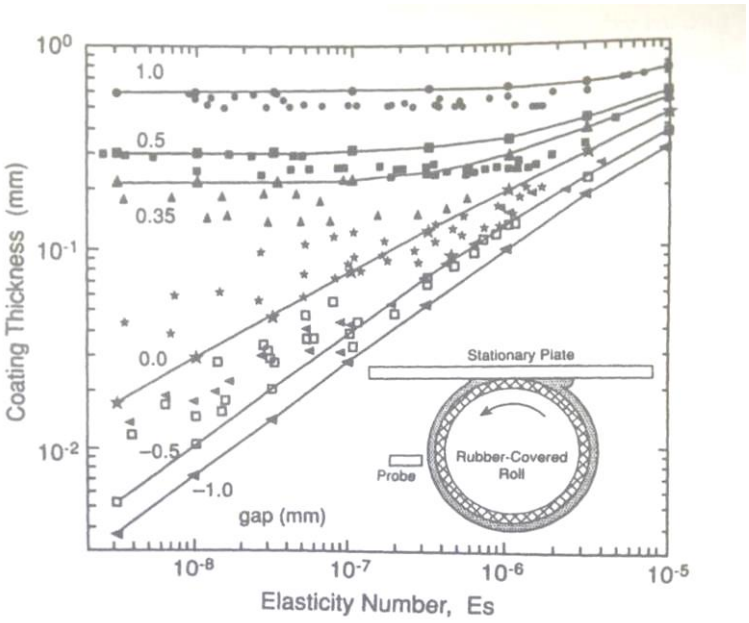

Figure 2-20 Comparison of theoretical predictions and experimental measurements [53]

For fixed positive gaps, the rigid roll limit is represented by the plateau of coating thickness at low elasticity number. At high elasticity number the coating thickness begins to increase as viscous forces overcome the resistance to elastic deformation. For negative gaps, there is no rigid roll limit and the coating thickness steadily increases with elasticity number and as the gap setting becomes more negative the corresponding reduction in coating thickness becomes less. The agreement of theory and experiment is good, except at large negative gaps and low elasticity number where the experimental film thickness is roughly a factor of two bigger than predicted. As the experimental film thickness in this cases where very low, the error in measurement could as become important.

Malvern [72] suggested that for a standard linear viscoelastic solid model there is a short-time elastic modulus and a characteristic relaxation time in addition to the long-time elastic modulus. Preliminary data on the roll covers indicate that short-time elastic modulus of about double the long-time ones, and the relaxation times varied from seconds to minutes (Coyle et.al [52]). Computations with this model showed the predicted coating thickness decreasing with increasing relaxation time (τ), but numerical scheme couldn't converge at high τ to confirm its role on the discrepancy. Such discrepancies could perhaps be expected in such experiments where the film thickness between the rolls is so small compared to the elastic deformations in the roll covers.

2.5 Forward roll coating flow: surface instabilities

2.5.1 Introduction

All coating processes are susceptible to flow instabilities or defects of one form or another. Often than not, attempts to apply continuous uniform viscous fluid layer onto solid substrate by various methods, produce uneven films. Commonly, the term 'instability' is associated with periodic variations in the film thickness in the web known as "Ribbing" (*Figure 2-21*). In forward roll coating, at low roll speeds the fluid flow is two dimensional and steady; as the roll speed is increased, the two dimensional flow becomes unstable and is replaced by a steady three-dimensional flow which results in regular stripes in machine direction. Ribbing is similar to the phenomenon in which a low viscous fluid displaces a high viscous one from a confined passageway, which Saffman and Taylor [73] mentioned as "viscous fingering". As it is flow instability associated with thin films, the ribbing phenomena can be observed in all coating processes including the common paint brushing, slot or knife coating [75], slide and curtain coating [76] etc.

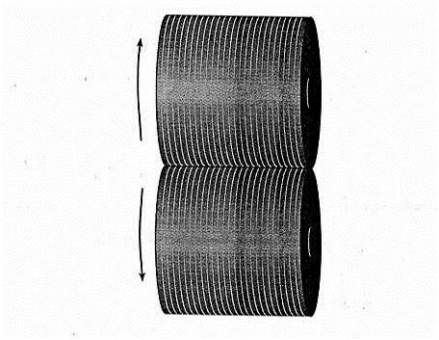

Figure 2-21 Ribbing instabilities in forward roll coating (74)

2.5.2 Rigid roll coating

In general the ribbing phenomenon being flow instability is avoided using low production speeds, low viscosity fluids and thicker films. These conditions are all

against the typical industrial requirements, expected to meet economic and ecological (less solvent) advantages through their processes. Furthermore, forward roll coating flows have a converging-diverging flow geometry leading to a film split separation region which creates a pronounced meniscus. Such a flow is easily destabilised because a positive gradient develops in the diverging section of the flow domain [51]. Films formed at sufficiently low capillary number are uniform because of the stabilizing effect from surface tension. The onset of ribbing can be predicted from standard linear stability analysis [52]. For Newtonian liquids, ribbing is related to a balance between the pressure (destabilising) at the meniscus and the surface tension divided by the local radius of curvature (stabilising). For a small disturbance of the layer thickness the pressure change at the surface should be smaller and then the change in force due to surface tension [77]:

$$\frac{d}{dx}\left(p+\frac{\sigma}{R}\right)<0 \qquad [2.21]$$

In which p denotes the pressure, σ the surface tension and R the radius of curvature at the centreline of the meniscus.

Pitts and Greiller [40] explained the mechanism of ribbing through a force balance as shown in *Figure 2-22*. The pressure under the rib (point 2) is different than the pressure in the unperturbed region (point 1), because there is a pressure gradient in the flow and also the radius of curvature of the meniscus has been changed. If the pressure under the perturbation is less than in the unperturbed location lateral flow would occur, resulting in a disturbance that grows into a "ribbing" pattern. In forward roll coating, the pressure gradient at the meniscus is always positive, and it always destabilises the flow making it prone to ribbing. Here the mechanism of

ribbing phenomenon can be understood as a competition between a pressure gradient that is destabilizing, and the stabilizing impact of surface tension force. This mechanism suggests that by manipulating the pressure gradient, the ribbing can be eliminated as in the case of reverse roll coating.

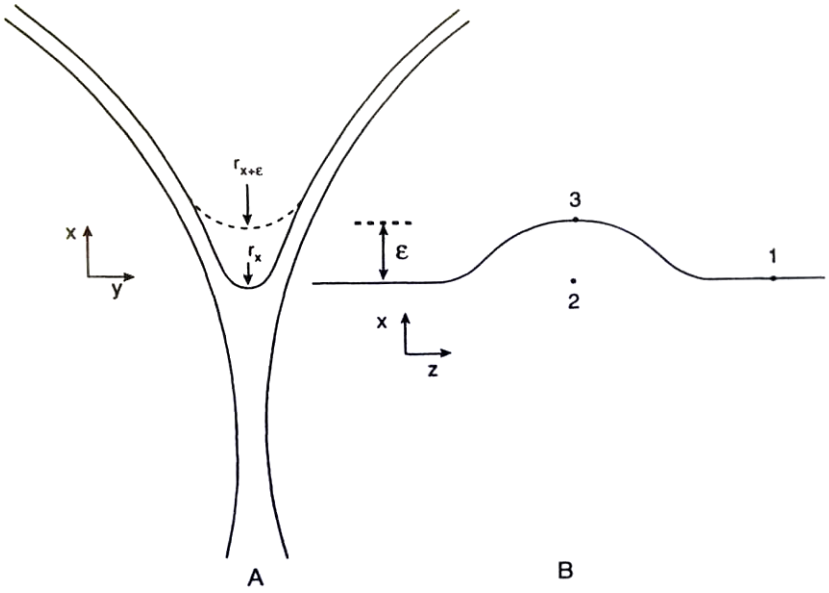

Figure 2-22 Film splitting meniscus and ribbing mechanism in forward roll coating [40]

Pitts and Grieller [40] and later Savage [78] confirmed the qualitative stability criteria for ribbing phenomena to occur at the film splitting meniscus,

$$\frac{dp}{dx} > \frac{1}{Ca}\left(\frac{1}{r^2}\frac{dr}{dx} + N^2\right) \qquad [2.22]$$

Where N is the wavenumber of the ribs (2π / wavelength) and r is the dimensionless radius of curvature of the meniscus. In forward roll coating, the pressure gradient at the meniscus is always positive, and the flow become stable only if the right hand side of the equation is greater than the pressure gradient value, which happens only in low capillary number regime.

Experimental measurements of the critical conditions for ribbing in roll coating have been performed by number of researchers (Pitts and Greiller [40], Mill and South [79], Greener et.al [80], Coyle et.al [52]). *Figure 2-23* compiles all available data for the onset of ribbing (expressed by a critical capillary number) in forward roll coating. A forward roll coating operation below this curve produces films with uniform thickness, and above this curve produces ribbed films. The speed ratio between the rolls has been found to have less effect on the critical capillary number. Rather, the average roll speed is found to be important (Benkreira et.al [17]). As the capillary number is increased further above the critical capillary number, the wavelength at first shrinks and then becomes constant. According to Pulkrabek and Munter [81] the wavelength of the ribs at high capillary number is proportional to the gap width.

In forward roll coating, non-Newtonian coatings show remarkable difference in ribbing behaviour with their Newtonian counter parts. This reinforces the critical role of viscous forces but also the importance of viscoelasticity. Theories are currently limited to shear-thinning viscous fluids [44]. Bauman et al [82] found that adding 10 ppm polyacrlamide reduced the critical capillary number by a factor of 2-5, even without any measurable difference in steady shear viscosity or normal stresses. They found that adding 100 ppm polyacrylamide; the critical capillary number is reduced by a factor of 10-30.

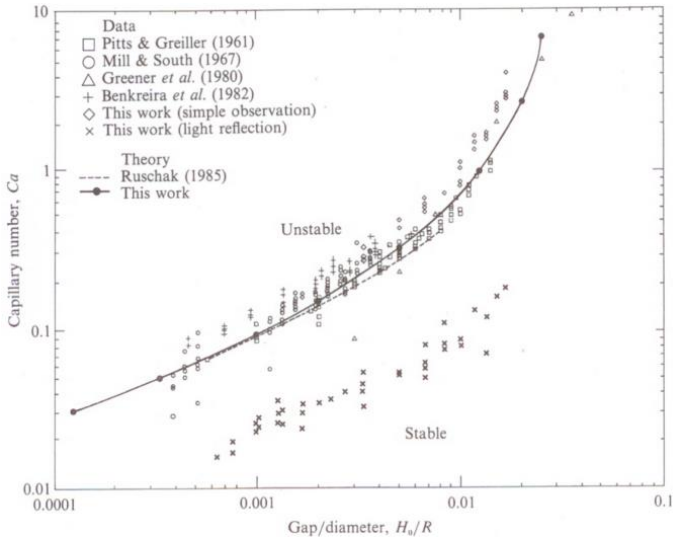

Figure 2-23 Experimental results of critical capillary number for two-roll coater and roll wall systems [81]

Extensive experimental studies of ribbing with non-Newtonian fluids were carried out by Glass et.al [83]. The flow field in film split meniscus region of forward roll coating is extensional in nature. They measured "dynamic uniaxial extensional viscosity", in order to correlate it with the ribbing behaviour of the non-Newtonian fluids.

G.A Zevallos et.al [54] analysed forward roll coating with viscoelastic fluids using Oldroyd-B and FENE-P models and the results indicate that the extensional flow downstream of the film splitting stagnation point leads to a high elastic stress at the free surface. They suggested that this high stress diminishes recirculation at the meniscus and the normal stress difference acting on the free surface grows with Weissenberg number. This increase in normal stress difference is suggested as the driving force of the ribbing instability. I.e. at any given capillary number, there is a critical Weissenberg number above which the flow becomes unstable.

J.H. Lee et.al [84] experimentally shown that, wet coating thickness decreases as coating gap or softness of the roll decreases and the viscoelasticity rises. They measured the viscoelasticity with rotational rheometry and CaBER technique and concluded that viscoelasticity aggravates the ribbing instability. T. Hasegawa et.al [85] studied the wavelength, depth of ribbing for rigid forward roll coating, and more importantly a method to eliminate ribbing. They used a string spanned near over the gap so as to touch the liquid in the gap in order to disturb the meniscus and thus eliminate the ribbing phenomenon (as shown in *Figure 2-24*)

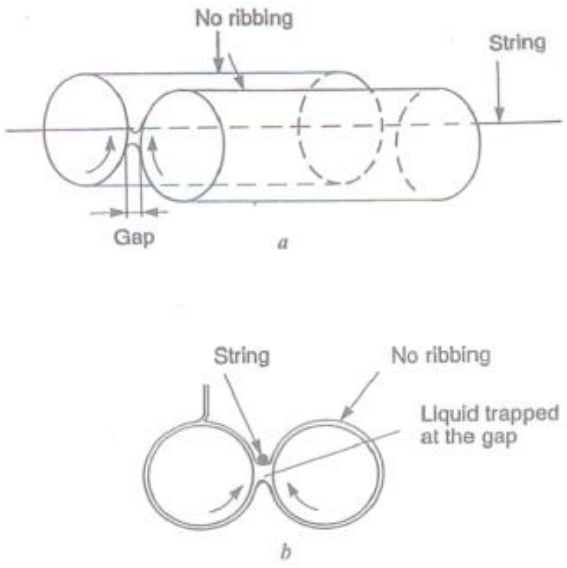

Figure 2-24 Side view of the experimental set up [85]

2.5.3 Deformable roll coating

Deformable roll coating is prone to ribbing defect such as rigid roll coating with a fixed gap condition. Pranckh and Coyle [68] suggest that ribbing is an unavoidable feature for deformable roll coating systems. Carvalho and Scriven [18, 86] considered the case with positive gap setting using linear stability analysis, and shown that the elastomeric cover has weakly stabilising effect on the onset of ribbing. Here the Navier-Stokes equations for fluid domain were coupled to a

constrained column model (CCM) for their analysis. With elastomeric cover in positive gap condition they were able to achieve 10% increase in roll speed compared to their rigid roll counterparts. This was later confirmed again by Chong [87] as shown in *Figure 2-25*

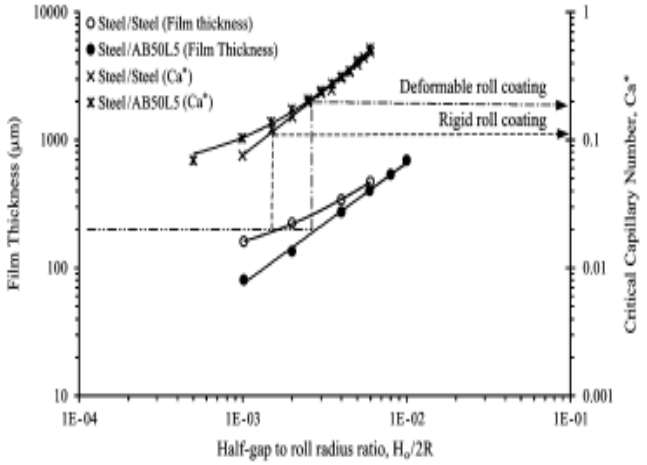

Figure 2-25 Effect of gap on film thickness and critical capillary number [87]

Chong et.al [87] also plotted critical capillary number as a function of the dimensionless positive gaps along with their data (present data in the *Figure 2-26*)

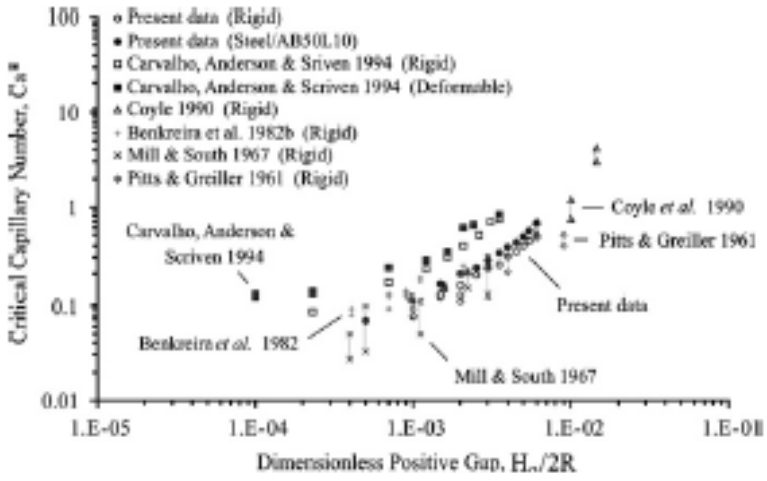

Figure 2-26 Critical capillary number as a function of the dimensionless positive gap (Chong et.al [87])

Gaskell et.al [49] performed a finite strip model (FSM) and predicted that softer thicker roll coverings enhance stability for small negative gaps but that thinner layers would be more stabilising under highly loaded conditions. Young [69] carried out a simple stability analysis for positive and negative gaps, and indicated that deformable layer had a stabilising effect in relation to the onset of ribbing for positive gaps and a possibility of film restabilisation in large negative gaps. Hence it would be interesting to study the effect of higher negative gap with higher speed of operation, and to analyse the effect of higher contact width on re-stabilizing this flow.

2.6 Forward roll coating flows: air entrainment & misting

2.6.1 Introduction

Air entrainment is a mode of coating failure in that the dynamic wetting line is susceptible to air entrainment at sufficient high coating speeds. Dynamic wetting line is an integral feature of all coating processes (curtain coating, roll coating etc.) and occurs at the line where a thin liquid film displaces air in contact with a moving dry solid substrate. These dynamic wetting lines are observed in the plunging area and a dynamic wetting failure results in air entrainment, which is a serious limitation to good and fast coating process. This entrained air into the fluid at the wetting line could cause a series of small air bubbles and craters on a coated film. Initially, Burley and Kennedy [89], Blake and Ruschak [90] and Burley and Jolly [91] investigated air entrainment with plunging dry tape into fluid bath. They showed that as contact angle approach 180° V-shaped cusps were formed on the interface between the fluid and tape.

2.6.2 Rigid roll coating

Coyle [88] suggest that rolling bank, which results from the excessive feeding of the inlet can cause runback effect which could contribute towards coating defects. The air entrainment could also be the result from the coating pan during the pick up of fluid, which results in a lower operating speed for a shallower immersion of the pick up roll.

Spiers et.al [92], Bolton and Middleman [93] studied air entrainment in a bath of fluid by partially submerged rotating roll (as shown in *Figure 2-27*). They observed the formation of a cusp on the surface linked to air entrainment and derived empirical correlations to relate the speed of the web and fluid properties to air entrainment. Bolton and Middleman [93] also indicated that in the case of viscoelastic polymer solutions, elasticity is a strong stabilizing factor. Spiers et.al [92] found that the critical speed decreased linearly with viscosity and increased linearly with surface tension. Innes [94] studied the source of air entrainment in roll coating with various feed mechanisms. Meanwhile, Bourgin and Tahiri [95] studied air entrainment in a curtain coating system at high speed. Adachi et.al [53] shown through experiments that as roll speed increases, the associated ribs become unsteady and ultimately spatter and spray occur.

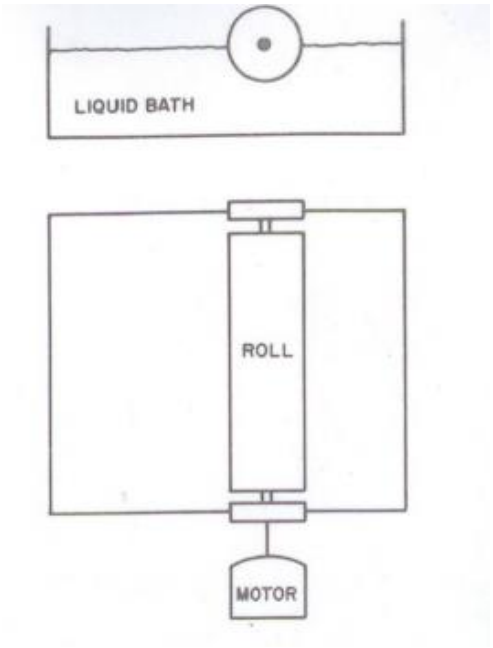

Figure 2-27 Experimental apparatus used for air entrainment studies [93]

Benkreira [96] studied experimentally the dynamic wetting in metering and pre-metered forward roll coating. He observed that dimensionless applicator flow rate (λ_A) is a key parameter in defining the dynamic failure occurring by air entrainment or cascade. This work also suggested that entrainment speeds for roll coating are similar to corresponding plunging tape flow case. It was also proven that cascade occurred in pre-metered regime because the dynamic wetting line moves near the minimum gap position as in the case of reverse roll coating. Carvalho et.al [18, 67] analysed the role of pressure on nip flow stability at low coating speed.

2.6.3 Deformable roll coating

Roper et.al [97] observed misting which accoding to them appears for speeds above 1000 m/min and defined as the ejection of fluid droplets during the film splitting at the exit of the transfer nip. They also revealed that as the solid content increased the severity of misting drastically reduced. Ascanio et.al [98] experimentally studied Newtonian fluids through the deformable nip at high speed (shown in *Figure 2-28*).

Experimental results indicate that both film splitting and air entrainment into the nip can be responsible for misting phenomena at low load, and at high load it could be reduced or even eliminated, which is something to investigate further.

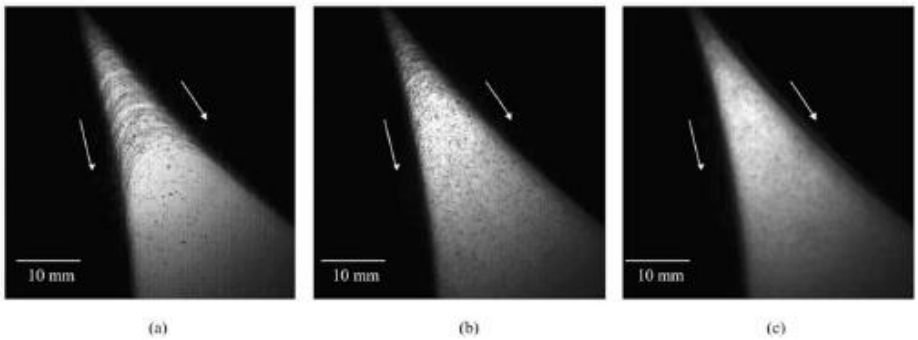

Figure 2-28 Images from the nip (μ = 0.63, W = 4 kNm^{-1}) a) 500m/min b) 800m/min c) 1100m/min [98]

They also concluded that the pressure drop in the gap was insufficient to cavitate the liquid. Gron et.al [99] suggested that under moderate application speeds, misting can be minimised by the selection of appropriate operating conditions. But as the need to operate at higher speeds grows, the option is limited and understanding of fluid parameters and their interaction with process parameters becomes critical.

Coyle et.al [39] has established the presence of a high fluid pressure region at the nip followed by a low pressure region at its exit. R.H Fernando et.al [100] suggested that the tensile stress developed at the nip-exit cause low pressure, which in certain cases drops below the vapour pressure of the coating liquid causing cavitation. This cavitation can lead to filament formation that breaks up to form mist droplets as shown in *Figure 2-29*

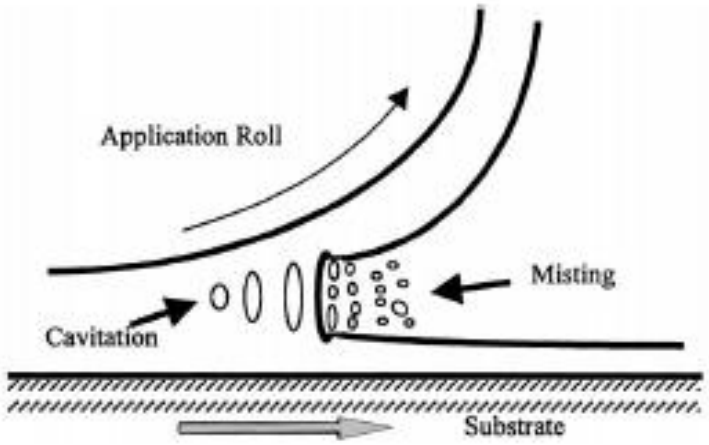

Figure 2-29 Cavitation and misting in roll coating [100]

MacPhee [101] suggested that at low speed the film splitting in counter rotating printing press rolls is smooth but as the roll speed increases the film splitting changes to ribbing, then to filamentation, cavitation and finally to misting at very high speeds. Cohu and Magnin [64] and Carvalho et.al [86] suggested that the film splitting depends not only on roll speed but also on the fluid properties, the rigidity of the surface rolls etc. Owens et.al [102] observed septa in forward roll coater, which they defined as the formation of curved thin sheets of liquid extending from the nip for both Newtonian and non-Newtonian fluids (*Figure 2-30*). They measured the droplet size, number of drops and mass concentration of mist to characterise misting.

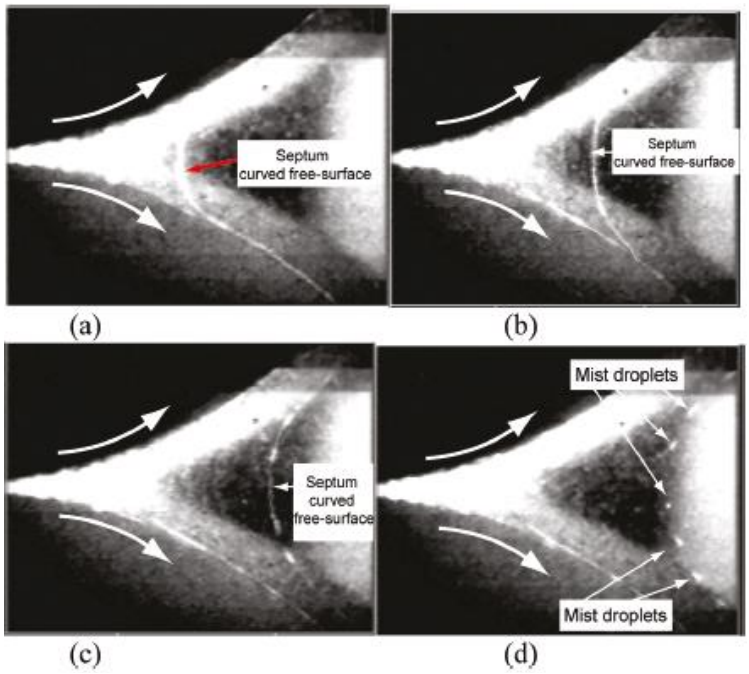

Figure 2-30 Sequence of side view images of a septum of deformable configuration [102]

Owens et.al [102], also shown that measured misting droplet count increases as (Viscosity)^3 as the roller speed increases (shown in *Figure 2-31*).

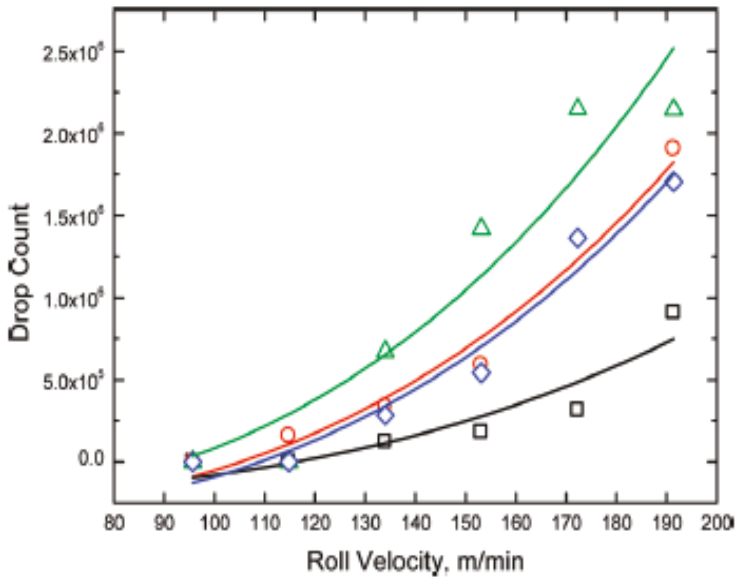

Figure 2-31 Drop count increase at 74 (□), 230 (◊), 282 (○) and 460 (Δ) mPa.s oils [102]

2.7 Research challenges in deformable roll coating

The comprehensive literature review presented above has enabled the identification of some key voids in knowledge and associated challenges to address in future studies of forward deformable roll coating:

- Although there have been many previous studies on deformable roll coating, the focus has not been on producing very thin stable films at high speeds. Most of the previous experimental work and simulations is related to film formation mechanism and associated instabilities below 100 m/min. In order to achieve thinner uniform films at higher speeds, the gaps used between the rolls should be lesser and fluid dynamics under such limiting conditions need to be understood.

- From the previous literature on deformable roll coating, it is clear that there are wide discrepancies among previous findings on symmetric and asymmetric film thickness values. It is also clear that there is no comprehensive experimental film thickness data or simulation results in the high speed regime going up to 360 m/min.

- New technological advances operate with a range of viscosities with Newtonian and non- Newtonian fluids, and the resultant metered film thickness or quality of thin films are not suitably correlated to process parameters in the case of forward deformable roll coating. This would evidently help to establish a "process window" for the given fluid and process conditions.

- In the case of characterisation of technologically relevant non-Newtonian fluids, there is no integrated approach, utilising a range of comparative rheometrical techniques, with a focus on measurement of: (i) high strain rate shear viscosity [η], (ii) high strain rate uniaxial extensional viscosity [η_E] (iii) high strain rate elasticity ($N1$). These rheological parameters are found to have some impact on the ”Process window”, but the effect is not well defined.

- At high roll speeds, ribbing and misting instabilities are interesting fluid mechanic phenomena and has been the subject of some studies, experimental and theoretical, over many years. Unlike ribbing, misting instabilities have received comparatively little attention. It becomes important to study them in detail, in order to develop operational strategies and coating formulations to avoid them in roll coating operation at the high speeds, which is required for high productivity.

2.8 Conclusions

In this chapter, a literature review on roll coating flows has been carried out to assess the important issues regarding how the film thicknesses and their stability depend on the design and operating conditions of the coater. It was found that forward rigid and deformable roll coating have been the subject of much research, both experimental and theoretical. Previous studies of this flow have however been limited to relatively large gaps (>100 μm), moderate to high viscosities (>100 mPa.s) moderate speeds (~1 m/s) and moderate rubber cover hardness (~ 50 Shore A). Clearly, research at gap approaching to higher negative gap with much higher speeds

and higher viscosities is required to meet the new technological demands of very thin films at high speeds. Forward roll coating is also known to be limited by instabilities at high roll speeds. One of these instabilities, ribbing has been well studied both theoretically and experimentally compared to the misting phenomena. Although film split in rigid forward roll coating is established in the literature, the same for deformable roll coating has not been studied in the high speed regime. The literature review also revealed that, although non-Newtonian fluids in deformable roll coating process have been studied before, there has been no integrated approach to combine studies with different rheometrical quantities to the concerned "process window". In conclusion, this literature survey has revealed that the aim and objectives set in the present research are novel and studying them either experimentally or theoretically will help to advance further our understanding of roll coating flows and thin film coating science and technology. In the final analysis, it is important to note that this work (high speed coating) is driven by economics but its study is of great academic importance (very fast coating flows).

Chapter 3 : EXPERIMENTAL METHOD & EQUIPMENT

3.1 Introduction

This chapter presents the experimental method and equipment used during this research. The aim of the experiments is to replicate a typical deformable roll coating operation producing stable films of thicknesses less than 50 μm at high speed up to 6 m/s. These are severe requirements for a laboratory rig and necessitated the provision of a well designed and instrumented rig. There is also the additional challenge of carrying out the experiments with model coating fluids that replicate the rheological and wetting behaviour of paints used in industry on steel coils as this is the industrial context of this research. A full rheological and wetting characterisation of typical industrial paints was thus an important part of the experimental work, in order to guide the development of model fluids. Another important consideration in the experimental programme is the physical and dynamic characterisation of the rubber sleeves used on the rollers. This is critical as a range of rubber hardness is used in practice and the rheological response of the rubbers used has to be established under the coating conditions not merely under static conditions.

3.2 Deformable roll coater rig design

In order to study the deformable roll coating process experimentally in a manner that leads to accurate and stable data at the high speeds sought (up to 6 m/s), it was necessary to design and construct a solid and well instrumented coating rig. For this purpose, the laboratory deformable roll coater rig in Bradford University was modified and adapted for high speed application. *Figure 3-1* shows the schematic diagram of the laboratory roll coater, which clearly replicates the essential features of the industrial operation. The rig can operate at either constant gap or constant load

over a wide range of conditions and is able to measure on-line the important operating parameters-roller speeds, roller gap (positive and negative) and the combined applied or hydrodynamic load. To meet these operational modes, the pick up roller (steel roller) bearing blocks are mounted in a fixed position, while the applicator roller (rubber covered roller) bearing blocks are mounted on linear slides, enabling the accurate adjustment of coating gap. The instrumentation required to achieve this important feature is shown schematically in *Figure 3-2*. In practice the coater was operated at constant gap whilst measuring both gap and load.

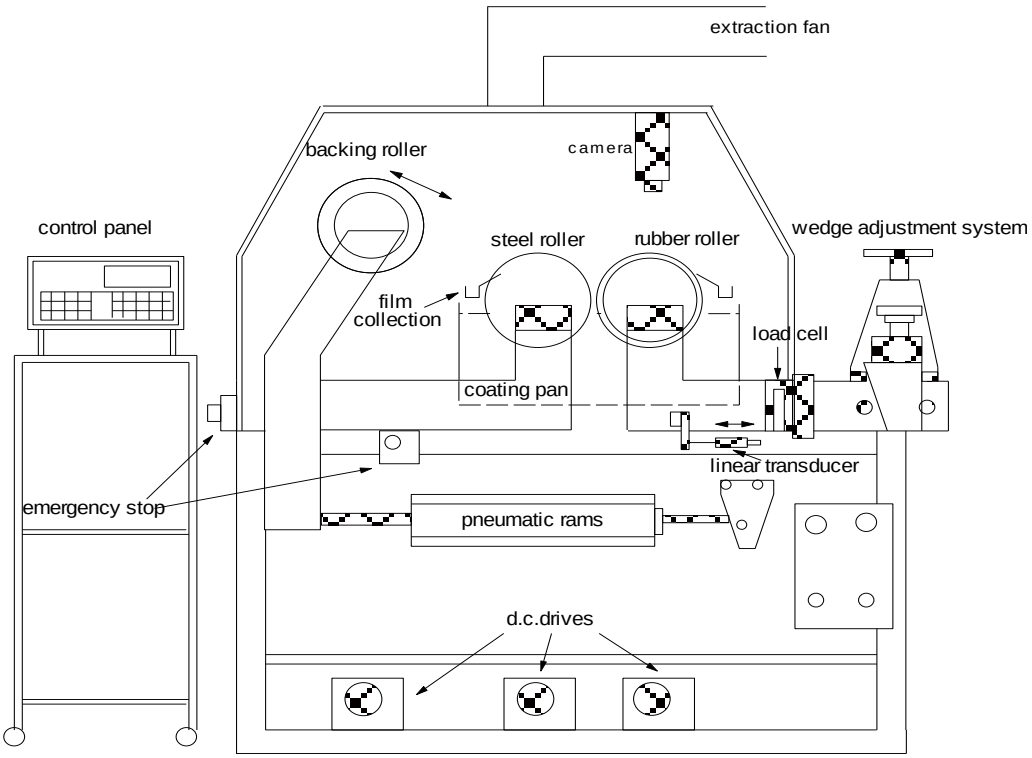

Figure 3-1 Schematic diagram [120] and photo (front view) of lab roller coater rig

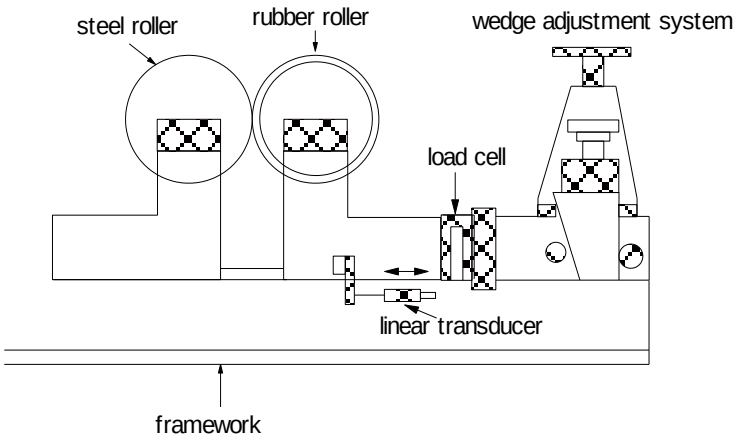

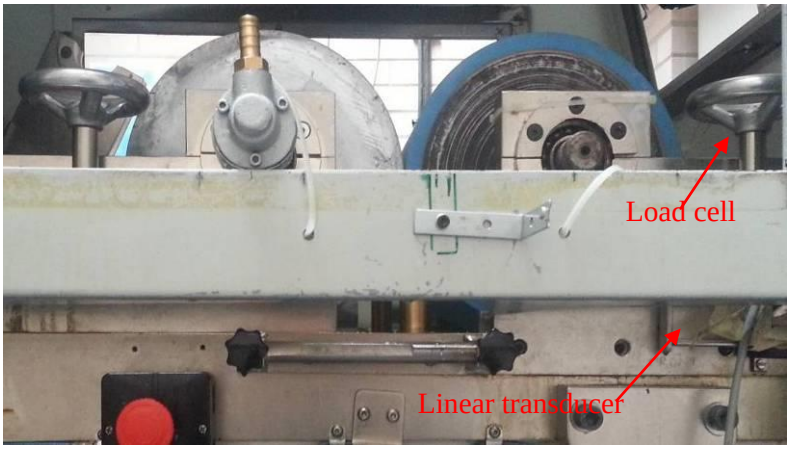

Figure 3-2 The experimental rig, feed & deformation control (gap & load) [120]

As shown in *Figure 3-1*, the coating gap between the pick up roller and applicator roller is controlled using a wedge adjustment system (*Figure 3-2*). The gap is monitored using the linear transducers mounted on linear slides in both sides of the rig. Load cells are fitted between the wedge adjustment system and applicator roller bearing blocks and these allow the measurement of applied and hydrodynamic loads.

Both rolls have an overall diameter of 250 mm. The steel roll was ground and chromed with an ultra-finished 100 μm chrome layer giving a maximum eccentricity of 5 μm. The applicator roll was made with a steel shell and a 15 mm thick rubber layer. The rubber cover thickness was kept constant throughout the experiments, and from previous literature it is found to have less effect on process output, unless it is very thin. Here we operate in the thick regime where effectively the entire deformable roller may be assumed to be made of rubber. Rubber covers, with different elastic properties and hardness were investigated during the experimental study.

As shown in *Figure 3-1*, the rig also provides a substrate handling facility, albeit limited. It uses a backing roller which can be manoeuvred pneumatically towards the pick up roller where contact can be made for a maximum duration of ¾ of a revolution. The backing roller is operated by a micro-switch linked to a timer that sends a signal to a solenoid valve controlling the movement of this third roller. The gap between the pick up roller and rubber covered backing roller is controlled using the mechanical stops. These arrangements allow a small length of substrate to be attached to the backing roller surface to produce a coated substrate sample for further examination.

All three rollers are driven by independent 1.5 kW DC drive geared motors with timing belts (*Figure 3-47* in *Appendix I*). As shown in *Figure 3-3*, in order to replicate the industrial process, the rollers were run in forward mode with different roll speeds at mostly negative gap configurations. In order to have an equal split of the flow at the nip region, both rolls need to run at the same speed (i.e. a speed ratio of 1). The splashing of fluid at higher speeds was controlled by fitting splash guards designed during the programme of work. The wet film thickness (WFT) of the fluid on the applicator roll was measured from the amount of fluid scraped across a specific width of the roll surface for finite time duration and later correlated with FTIR gauge readings. A detailed procedure including risk assessment for the operation of the deformable coating rig is given in *Appendix I.*

.

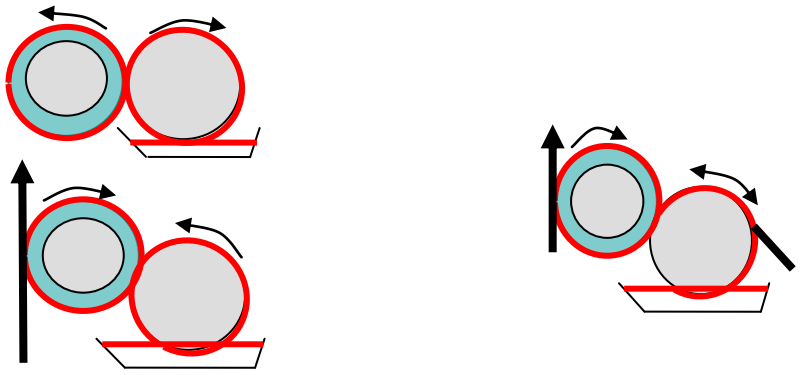

Figure 3-3 Schematic arrangement of different possible two roll deformable coater set up in coil coating line

The whole coating rig is housed in an enclosure constructed from steel and access doors made of perspex on all the four sides. The frame work made of steel is designed with the capability to withstand high loads, speeds and absorb vibrations. A flame proof light was placed inside the housing for visualisation purposes. For safety

reasons, an extraction fan was fitted at the top side of the housing to suck away any hazardous solvents or chemicals during the rig operation.

In addition to the above mentioned provisions of the experimental rig, the experimental programme at high speed faced many additional challenges. This includes the feeding related issues at high speed, wet film thickness measurement at high speed and visualisation of different instabilities at high speed. The following aspects of the laboratory deformable roll coating rig at Bradford University were modified in order to process different range of viscosity fluids at high speeds going up to 360 m/min.

3.3 Feeding and related problems

Feeding is an important consideration as the rollers rotate at high speed and a stable feed with no splash is required to be brought to the nip. In roll coating operations, it is desirable (see literature review) to operate with a flooded feed so that the feed itself does not control film thickness. The following feed systems were tried:

- Normal pan operation with the two rollers simply immersed in a trough containing the coating liquid. This required the control of splash
- Pressurised pan operation with the two rollers immersed partly so that only a thin layer of feed liquid is made available thus avoiding splash.
- Die feeding where a film of liquid is provided by a die onto the applicator roller. This method also avoids splash in principle.

Generally flooded condition is maintained throughout the experiments, although metered feeding was also tried without success (details in *section 3.3.1.1*). The pan feeding mechanism (both normal and pressurised) was employed in all trials and care was taken to maintain a constant level of fluid in the pan. Hence in the feeding aspect, the flooded condition in the nip area was ensured throughout the experiments.

Normally for feeding purposes with most of the coating fluids, going up to a maximum speed of 120 m/min roll speed, a normal open holding pan was used (*Figure 3-4*). In industrial coating process situation as well, this mode of simple open pan is used for feeding purposes. Using a normal holding tank, one of the major constraints in rigid or deformable roll coating at high speeds is the inevitable splashing phenomena from the edges of the rotating rolls. Properly designed splash guards (*Figure 3-5*) help to reduce the severity of the splashing, but still these guards tend to interfere with the experimental measurements at high speeds.

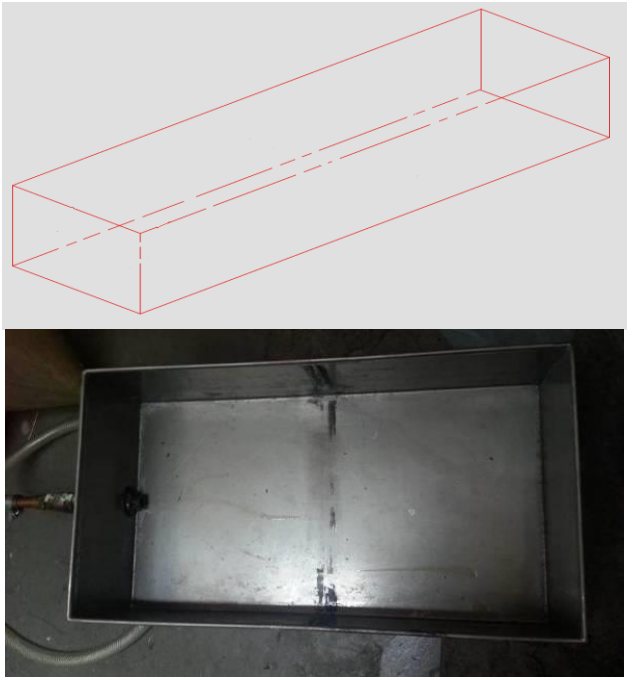

Figure 3-4 Open pan for feeding

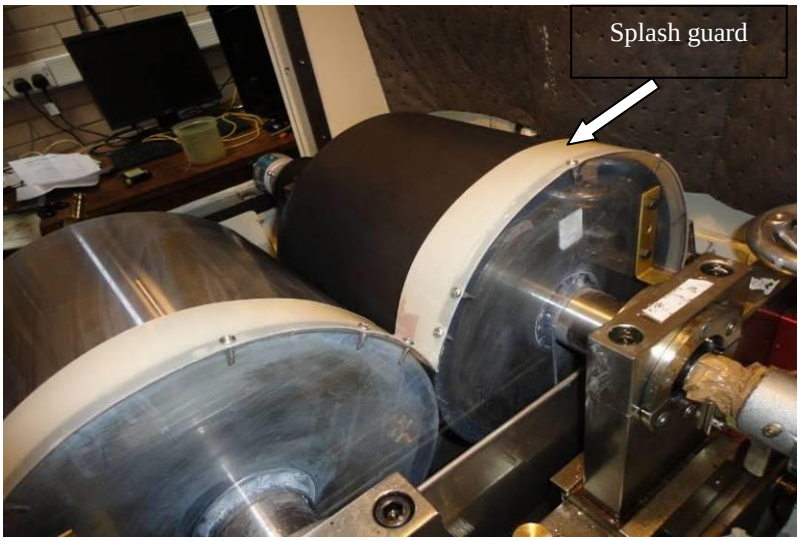

Figure 3-5 Splash guard fitted onto the roller coater rig

The open feed normal pan (*Figure 3-4*) could be used to get good control of coating thickness at lower speed however when this technique was tried in high speeds, it showed many disadvantages:

- The fluid may not be under pressure uniformly in all parts of the pan and could result in uneven coating thickness across the pick up roll.

- Air entrainment was observed at higher speeds in the open pan arrangement (as shown in *Figure 3-6*), and these could be detrimental for the film quality in long production runs.

- Exposed fluid could create differences in the viscosity due to solvent evaporation or temperature changes

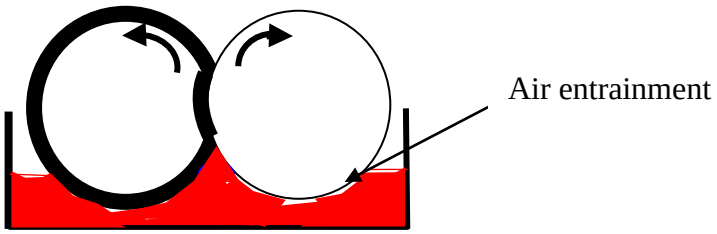

Figure 3-6 Air entrainment in open pan for feeding

- The amount of fluid picked up by the rolls depends largely on roll speed and it is very difficult to control the same. This increases the possibility of splashing of the excess fluid reaching the nip area.

3.3.1 Different feeding methods for high speed operation

The major disadvantages of using an open tray for feeding purpose is that it provides an uncontrolled amount of feed into the nip region between the rolls. This larger volume of fluid at nip area could contribute to the splashing phenomena; hence the controlled feeding of the fluid to the nip area of the rolls is critical for the high speed deformable roll coating process. In industrial scenario, a third roll would be used in the roll system configuration to control the amount of feed going into the nip region. But as this is not an option in current feasibility rig study, the following easier methods to control the feed have been explored:

3.3.1.1 Use of a properly designed feeding die

A die is directly delivering the premetered amount of fluid onto the pick up roller (as shown in *Figure 3-7b*). In this situation, the pick up roller is not dragging the fluid (the fluid is put onto it) and the propensity of air being entrained is reduced. Also, a

fresh, regulated amount is provided and this is beneficial for good quality operation. This also ensures a good fresh supply to the nip without too much excess.

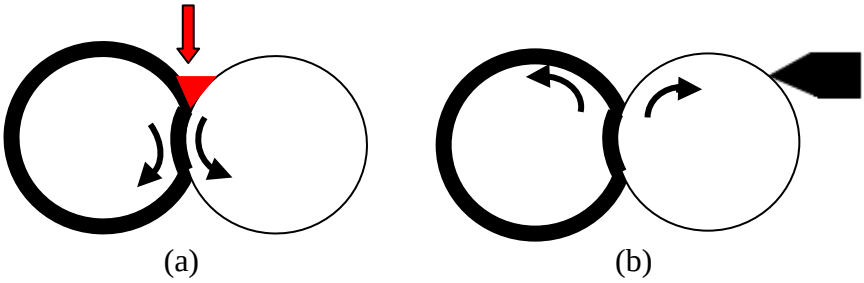

Figure 3-7 a) Feeding straight into nip b) Feeding from die onto roller

The whole idea of die feeding in the case of deformable roll coating for industrial purpose can be schematically represented in *Figure 3-8*

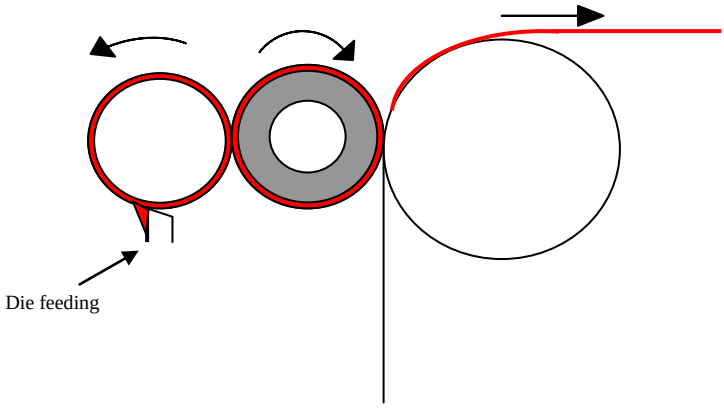

Figure 3-8 Example for industrial die feeding set up in roller coating

In order to replicate the industrial die feeding set up and to investigate the feasibility of die feeding onto the roller, following die feeding was arranged in lab. A feeding die is designed to be able to fit underneath the chromated pick up roll as shown in *Figure 3-9.*

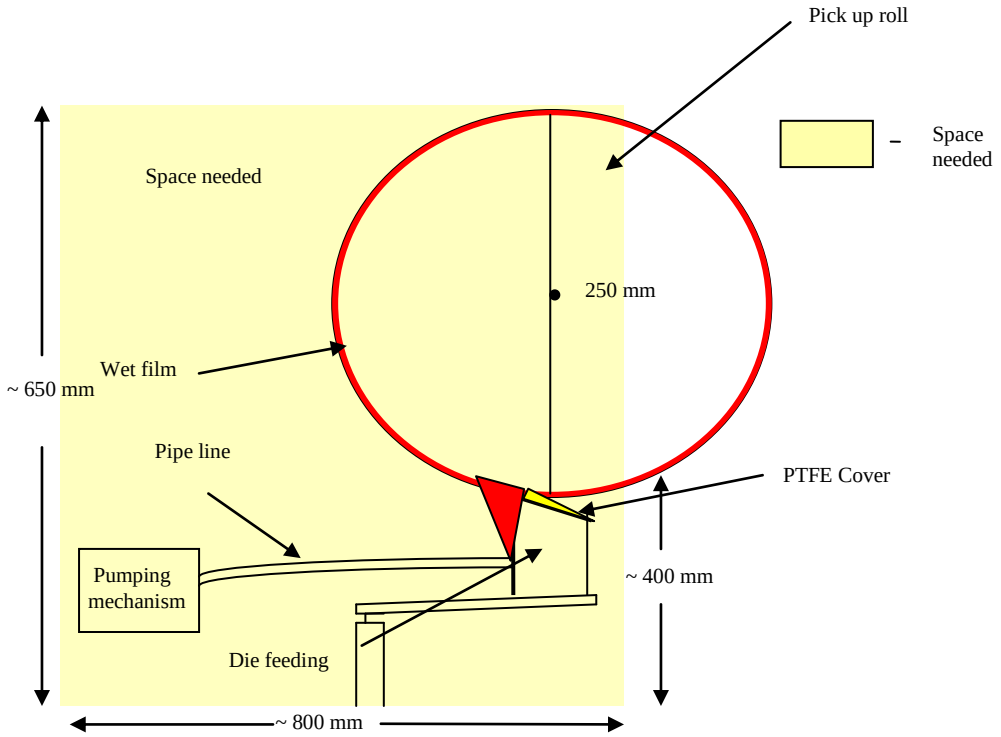

Figure 3-9 Die feeding set up for roller coater rig

Here the feeding die upper part that comes into contact with the steel roll is made of precisely machined PTFE to avoid the possibilities of scratches or other damages to the roll at high speeds. The die used in our experiments along with its dimensions are as shown in *Figure 3-10* (a & b).

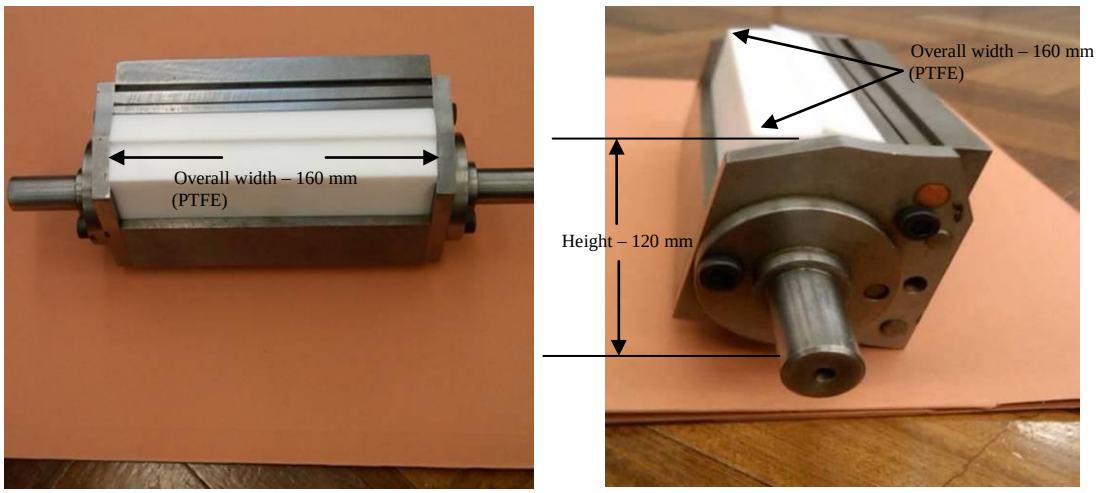

Figure 3-10 (a & b) Die design specifications

The properly designed die is fitted into the available space underneath the pick up roll (as shown in *Figure 3-11*). The feeding pipes connected to pressure vessel, which pump the fluid into the die and the fluid could be picked up by the pick up roll. The die was touching the pick up roll in all modes of operation.

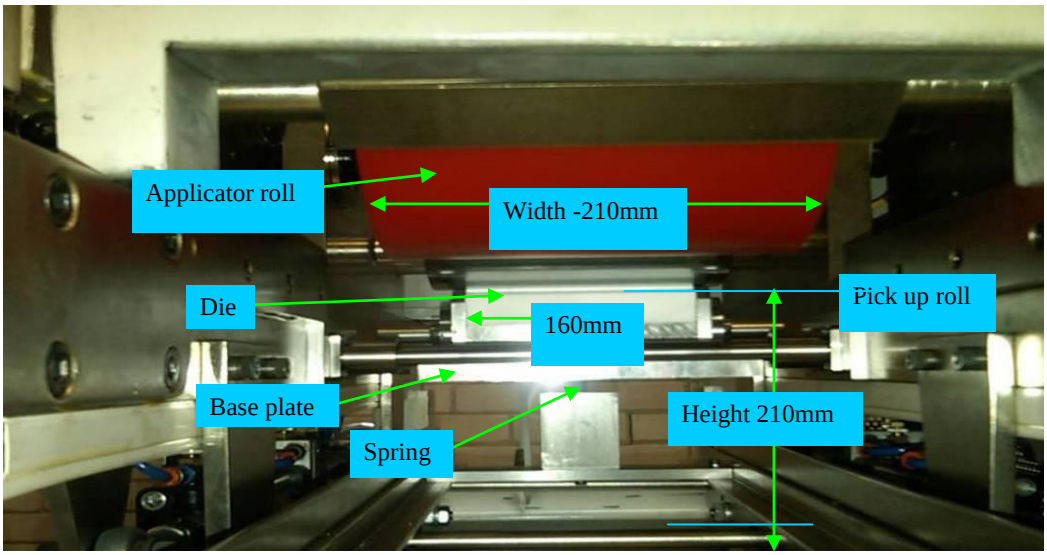

Figure 3-11 Die fitted onto the roll from a front view

The fluid for the experimental study is kept in a pressurised vessel (*Figure 3-12a*) and the pressure inside the container is controlled with an air pressure regulator. By regulating the air pressure into the pressure vessel, the flow rate of the fluid to the die exit could be controlled. The whole system is calibrated with the fluid, in order to get information of the flow rate against set pressure. The pressure vessel used for experiments with pipes is shown on *Figure 3-12a* and the two pressurised pipe inlets to the fitted die in *Figure 3-12b*.

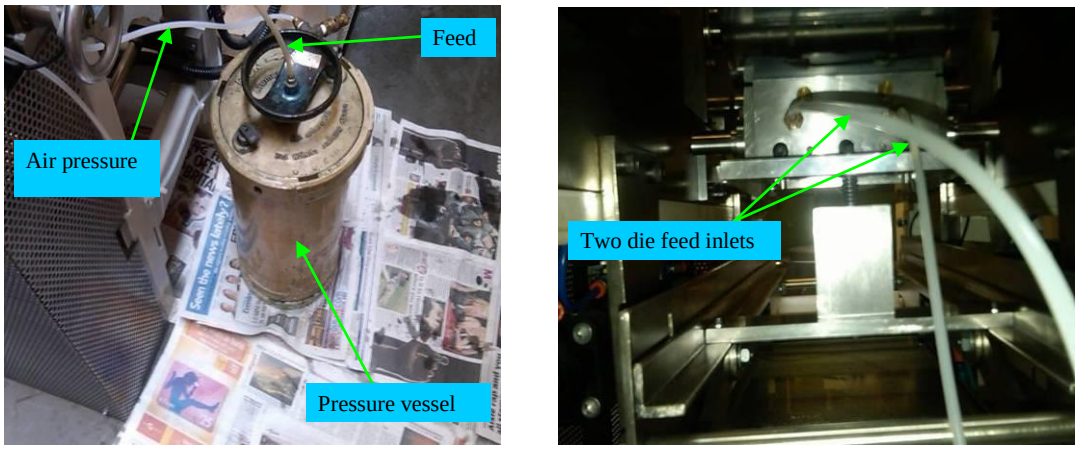

Figure 3-12 (a & b) Pressure vessel set up & die feeding inlet

Die feeding in theory should give more freedom to operate at higher speeds, as the wet film thickness onto the roll could be exactly controlled by the pressure of feeding fluid. This mode of feeding was found to give good results at lower roll speeds, but as the roll speeds increased the fluid find it hard to stick onto the rolls. The model fluid used in these trials was not able to wet the steel roll completely and fluid ended up gushing out from the die lip area. Also because of non-uniform pick up, the die feeding mode was not selected for the roller coater rig trials at high speeds.

3.3.1.2 Use of pressurised feeding pan

Because of all above listed reasons (*section 3.3*), the normal pan is changed with a pressurised pan in high speed mode of operation. The fluid flow mechanism is schematically given in *Figure 3-13*, and with this it is also possible to control the fluid level in the pan. From a holding tank in which one or both rollers are immersed, the fluid may or may not be under pressure depending on the intricacies of the pan design. Also the main aim here is to overcome air entrainment that occurs as the roller speed is increased. With a special design of the pan (*Figure 3-14*), the fluid pressure inside the pan is more uniform and the air entrainment possibilities are less.

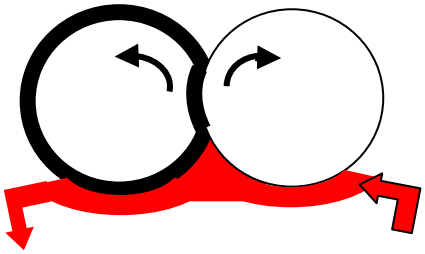

Figure 3-13 Mechanism of pressurised pan feeding

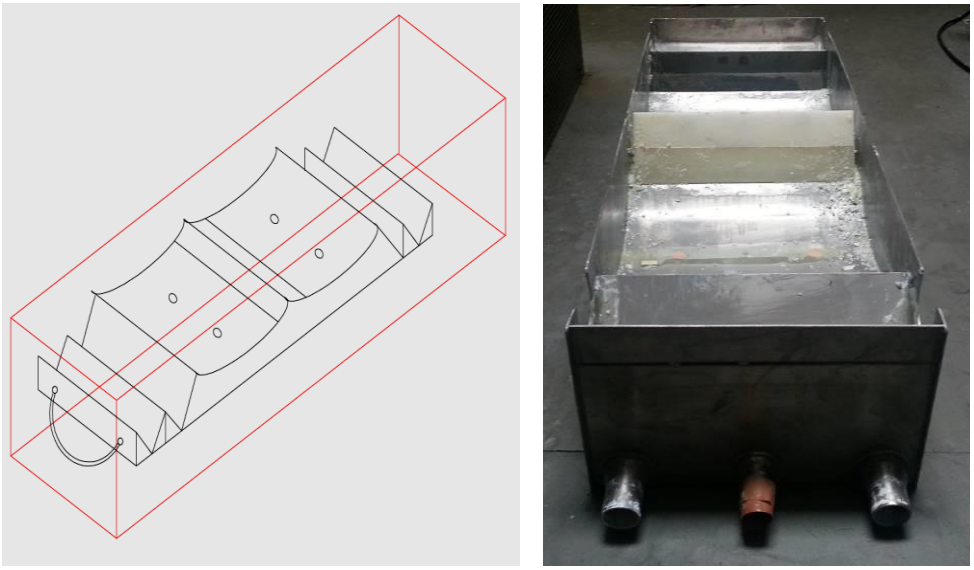

Figure 3-14 Schematic of pressurised pan feeding system

Because of continuous recirculation in pressurised feeding pan, it was possible to keep the fluid level constant throughout the trials. This fluid level was found to have a critical effect on the amount of fluid picked up by the rolls, uniformity of fluid picked up and air entrainment possibilities. The specific fluid level in the pan is measured as a height from the bottom surface (deepest point) of the pan in all the experiments. Throughout the experiments the nip area between the rolls was maintained in a flooded condition to avoid any possibilities of dry contact between the rollers. Higher speed operation trials with different model fluids and coatings are conducted using pressurised pan feeding system.

3.4 Wet film thickness measurement

The accurate measurement of the film thickness developed in the experiments is critical to the research programme. For this reason, two methods were used to allow good precision as the roller speed was increased:

- Scraping the film and weighing it (Contact method)
- Use of gauges (capacitance or infra-red) to measure film thickness (Non contact method)

3.4.1 Contact wet film thickness measurement

At lower roll speeds, the wet film thickness on the roll is measured with a contact technique, whereby a scrapping attachment in contact with the deformable roll collects the fluid for a specific time. With prior knowledge of the density of the fluid scrapped, the wet film thickness (WFT) of the fluid on the applicator roll was calculated from the amount of fluid scrapped across a specific width of the roll surface for a finite time duration (as shown in *Figure 3-15*). In this case, the average film thickness was calculated from the weight of the liquid scrapped and collected over the set time (10 to 300 seconds).

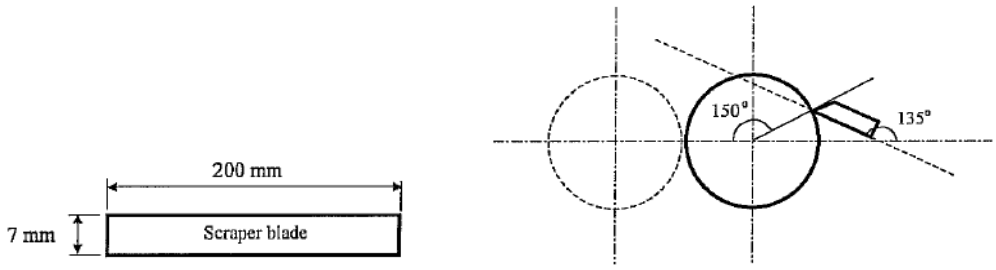

Figure 3-15 Scraper blade and holder dimensions and location in the rig [120]

The scrapping unit is usually made of aluminium which was used during the trial with hydrocarbon model fluids. But in the trials with polyester topcoat paint, it did not wet to the aluminium material surface properly (as shown in *Figure 3-16*)

Figure 3-16 Non uniform scrapping with aluminium scrapper

The wettability of different possible materials was tested using a pendent drop surface tension/contact angle measurement instrument. The contact angle results for the polyester topcoat on different materials are as follows,

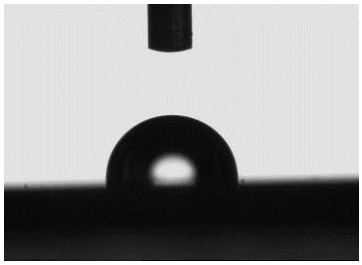

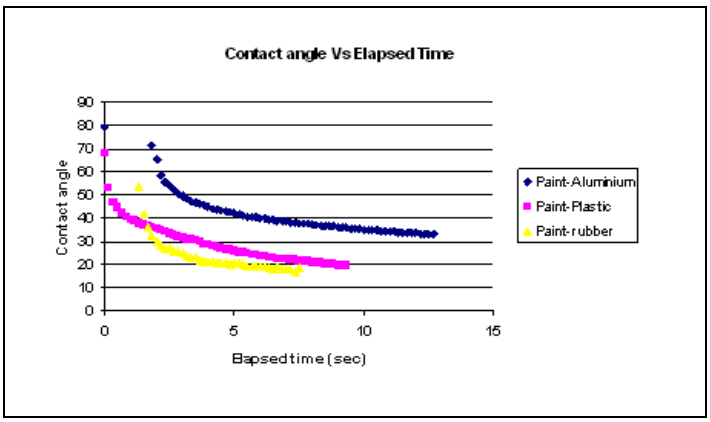

Figure 3-17 Contact angle of polyester topcoat drop with different scrapper substrates

From the wetting study, it became clear that contact angle for the aluminium material is higher than plastic material (Polyethylene) used under same conditions. Hence the material for the scrapper was changed to Polyethylene (and this design was used for future experiments).

3.4.2 Non contact wet film thickness measurement

At higher roll speeds, the scraping technique for wet film thickness measurement shows its limitations as:

1. It is very hard to collect the fluid at higher speeds without splashing

2. It is difficult for rolls to uniformly cover the scrapped area just immediately after scraping

3. For higher speeds, the volume of the scrapping container need to be large in order to collect the volume of fluid removed

4. Shorter time of scraping induces more measurement error.

Because of all the above reasons, a non-contact method of wet film thickness measurement for high speed operation is required. Of the techniques reviewed, the following were suitable for use on the roller coating rig:

1. Capacitor probe measurement

2. Infrared gauge measurement

3.4.2.1. Capacitor probe measurement

A capacitor probe (MB1, Wayne Kerr Co.Ltd), was assessed, but after the calibration stage it was decided not to use this technique, because of the requirement of close proximity of the capacitor probe head near to the rolls. For ±2 µm accuracy in wet film thickness measurement the specific capacitor probe head needs to be 5 mm close to the roll. This close fitting could be detrimental in high speed operation, and could damage the roll surface and probe head, if they come into contact during operation.

Principle of operation

The principle of this technique is to determine the dielectric constant of the fluid which is placed in an equivalent parallel plate capacitor. The experimental arrangement is as shown in *Figure 3-18*, such that the roller surface is being considered as one plate, and a capacitor probe surface as the other plate.

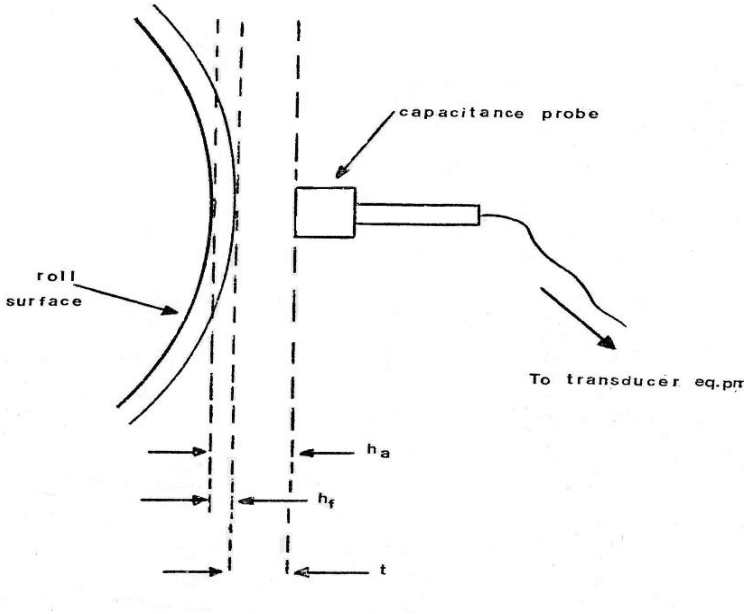

Figure 3-18 Capacitor probe arrangement

$$C_a = (E_0 E_a A) / (h_a - h_f) \qquad [3.1]$$

Where C_a is capacitance of free space measured, E_0 is the dielectric constant for the free space, E_a is the dielectric constant for air, A is the probe area, h_a is the air gap between the roll surface and probe. Similarly capacitance of fluid layer (C_f)

$$C_f = E_f E_0 A / h_f \qquad [3.2]$$

Depending on the type of fluid used, these capacitors could be in series or parallel and effective capacitance is measured. From the above relation the wet film thickness (h_f) could be calculated.

3.4.2.2 Infrared gauge measurement

The infraguage 710e (from NDC Infrared Engineering Ltd, UK) was used for non-contact measurement of WFT measurement. This infraguage is a 3 filter infrared absorption gauge and is used in other industries to analyse factors such as moisture, fat, protein measurement and the thickness of films.

Figure 3-19 Non contact wet film thickness (WFT) instrument in coating rig

Principle of operation

The new Infrared gauge was installed and commissioned on the Bradford University lab based roller coater rig for this part of the work (Installation details: *Appendix II*). The gauge works on the principle that different product constituents (such as OH or CH bonds) absorb Near Infra-red (NIR) radiation at specific wavelengths. The gauge emits NIR radiation at specific wavelengths and then accurately measures the amount of reflected radiation from the product. From this it can generate outputs that are directly proportional to the amount of each measured constituent in the product.

To start with, IR gauge needed to be separately calibrated for different model fluids and coatings (procedure described in *Appendix II*). Once the proper calibration of the particular fluid was done and the sensor head (as shown in *Figure 3-19*) location fixed over the top of the roll, it was cross checked with scrapping method at lower roll speeds.

Figure 3-20 Schematic IR gauge sensor head and mounting [121]

For this gauge, the spacing from the crown of the steel roller to the sensor window was 100 +/- 25mm (details in *Appendix II*). The sensor was mounted horizontally (as

shown in *Figure 3-19*). In addition there is a facility to be able to tilt the sensor at an angle relative to the horizontal (max 20°).

Method of operation

The gauge comprises of a sensor (sensing head), connected to an Electronic Control Unit (ECU) and it can be demounted as well. In the sensor, a quartz halogen lamp and three narrow-band filters are used to produce infrared light at carefully selected wavelengths.

Figure 3-21 Electronic control unit (ECU) for Infrared gauge

The proportion of light absorbed by the sample at each of these wavelengths is continuously measured and transmitted to the ECU. In the ECU, mathematical functions (Fourier transform related algorithms) convert this information into the thickness measurement of interest. The ECU has two channels, and with a sensor connected to each, its front panel LCD, provides three measurements, any of channels or differential measurement.

3.5 High speed visualisation of coating flow

As stated earlier in the aim and objective, the important consideration of the research was to assess the stability of the films formed as speed was increased. This

necessitated observation of the flow and films formed at the high speed. The camera used for visualisation of high speed roller coating experiment was a Vision Research Phantom 7.3 (*Figure 3-22*). The frame rate on the videos are varied from 7000/s to 30,000/s with the conditions of the experiment such as roll speed, roll gap etc. Along with the high speed camera, an infinity K2 microscope lens with a CF3 objective was used, which gives a field of view about 1.5 mm across, around 100 mm working distance. The camera sensor resolution is 800 x 600 pixels maximum, so ~2 µm/pixel. Microscope lenses usually have a very shallow depth of field, and to view the meniscus in the nip of the rollers, the lens needed to be at a shallow angle to the rollers. This setting allowed the meniscus to be in focus both in the nip and as it emerges from the nip (as shown in *Figure 3-23*). A very shallow angle can also be created by looking through from the ends of the rollers, but this did not work: the end meniscus on the rollers is larger than the others obscuring the view and covers the lens in coating.

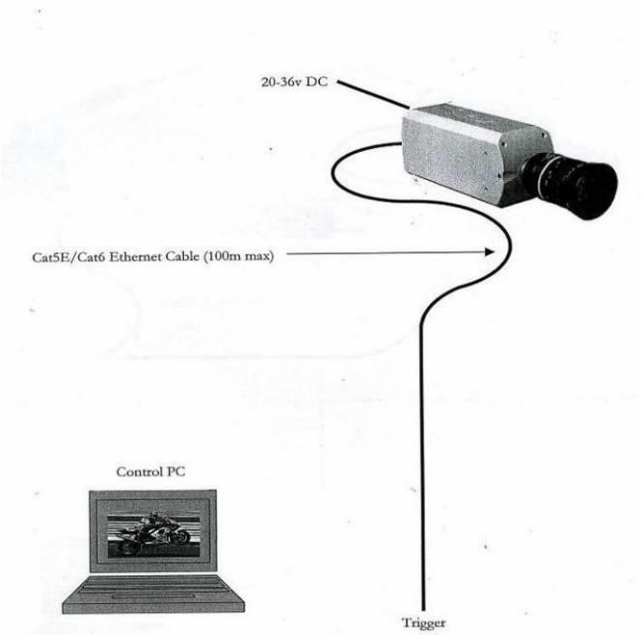

Figure 3-22 Single high speed camera set up

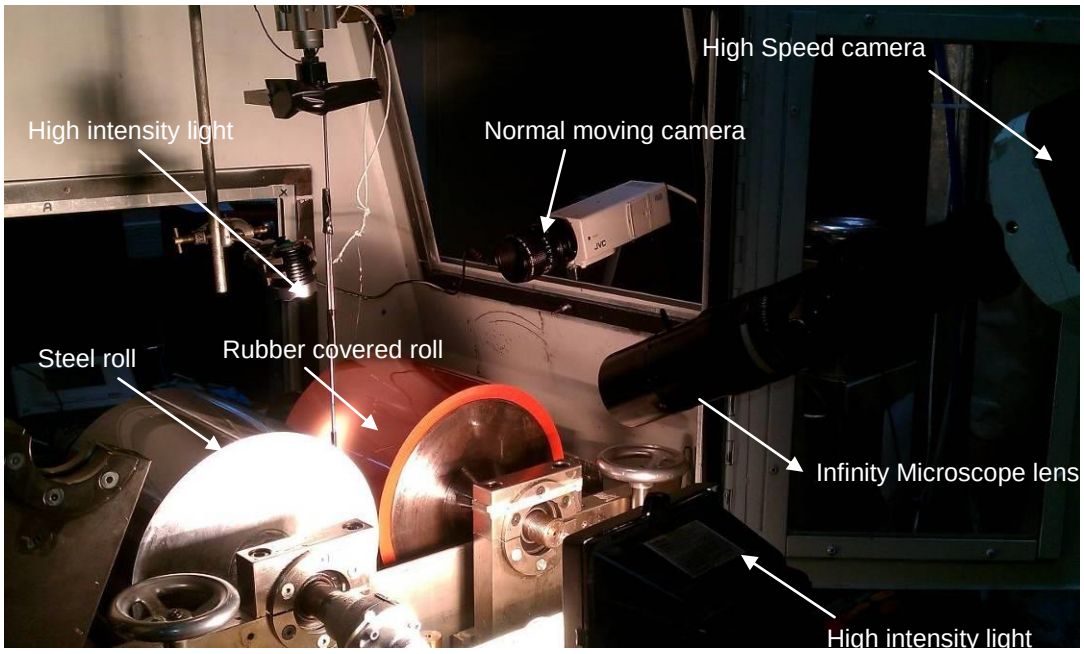

Figure 3-23 Experimental lab visualisation techniques

It was more successful getting the lens in line with the roller nip, at the shallowest angle possible, with the lens as close as possible to the top of rollers, as shown in *Figure 3-23*. This requires a lens with long working distance, and very precise positioning of the camera. In order to get these done, a tripod with a geared column was used to adjust the column in z direction, a geared tripod head to do the three axes of tilt, yaw and roll, and geared micro positioning plates to do x and y directions. The tripod fittings need to be strong as well as precise, the camera along with microscope lens is around 0.75 m long and weight of 7 kg. A high intensity machine-vision fibre light was used with precise positioning in line above the nip so that the light really was cast straight down into the nip.

Along with the high speed camera, a normal video camera was also used in experiments (JVC RRGB TK 1270 with 3.5X lens) positioned above the top of the deformable roll to capture pictures of the rib pattern formed under various process conditions. Ribs on the film were highlighted using a halogen light source, directed

onto its surface at an oblique angle. This cast the valleys of the ribs into shadow thereby allowing the average wavelength to be measured from the resulting image.

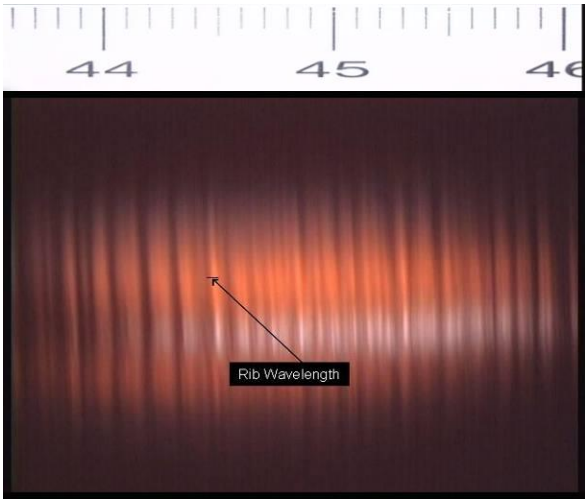

Figure 3-24 Photograph of the rib pattern from the model fluid rig trial (Conditions: -0.5mm gap/ 60 m/min roll speed)

These photographs were analysed through image analysis software (ImageJ) with use of a reference picture to calibrate the measurement (as shown in *Figure 3-24*). Setting up the gap, the roll speeds are changed and once the stable conditions are achieved two photographs under same experimental conditions are taken.

The visualisation technique was employed to study the misting phenomenon (ejection of droplets from coating nip) for both viscous model fluid and viscoelastic model fluids. In general, the observed misting phenomena can be defined by three different parameters that can be measured:

1. Misting height-h (mm)
2. Misting spread across the roll-w (mm)
3. Misting droplet size-d (mm)

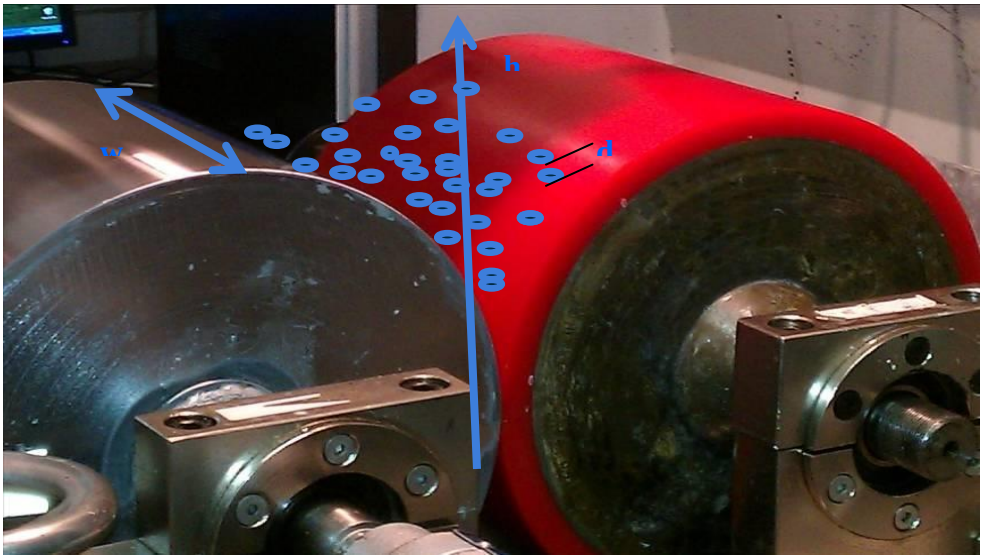

Figure 3-25 Schematic misting phenomena and measurement method

All three parameters are found to be significant in the context of misting analysis, and were therefore measured during the trials. The droplets were collected with a clear glass slide positioned at the top of the rolls. When removed the slide immediately checked under a microscope and the average droplet size is measured. The measurements made should be considered more as general indicators than absolute measurements.

As these three parameters found equally important at this initial stage of the study, a single term called “misting severity factor” is coined.

Misting severity factor = Misting height (mm) * Misting spread (mm) * Misting droplet size (mm).

3.6 Industrial coating full rheological characterisation

Introduction

As it may be expected, fluid rheology will strongly influence coating flow, hence the thickness and stability of the films formed. In industrial operations, this dependence may present problems as the thickness of films and stability are desired not to vary significantly with fluid formulation, hence the concept of operating within a 'rheological window' [104]. The purpose of this research is to assess how wide the variation of film thickness and stability with change in fluid rheology. Only by measuring this variation will we be able to develop this rheological window. Rheology of course must take into consideration, as the type of flows that occur during roll coating and these are not simple shear flows but also extensional flows. Most industrial coating laboratories are still reliant on shear rotational rheometry and do not assess extensional effects. Extensional rheological measurements present also many challenges such as experimental artefacts at high strain rates (fluid fracture, secondary flows and geometrical misalignment). Very few studies have focussed on high strain rate capillary techniques to characterise coating fluids. The work of Willenbacher et.al [104] is notable in highlighting wall slip and entrance pressure drop as predictors of blade coating performance. This was expanded upon by Dirking et al. [105], who used contraction flow and stagnation point techniques to relate extensional behaviour to atomisation / sprayability. In addition, the combined use of rotational and die swell experiments to determine normal stresses and its role on the onset of ribbing has been studied by Varela-Lopez et al. [106]. More recent work by Pipe et al [107] has highlighted the use of a micro fabricated slot die for high shear measurement of low viscosity complex fluids. This study has been

undertaken to characterise potentially high speed radiation curable paints (Ultra violet paint, Electron beam paint), solvent based topcoat, model fluids etc in order to correlate the rheological properties of the fluid system with concerned processing characteristics, giving better idea about their optimum processing range.

3.6.1 Significance of rheological measurements

In order to be applied successfully at high speed, coating formulations need to meet different demanding rheological properties. Very high shear rate measurements made in a capillary rheometer up to 10^6 s^{-1} range are able to simulate more realistically the conditions taking place in the coating head of a high speed coater. As shown in *Figure 3-26*, the ability of the rheometers to measure performance across a spectrum of shear rates that more closely mirror those observed through the whole coating process gives valuable information.

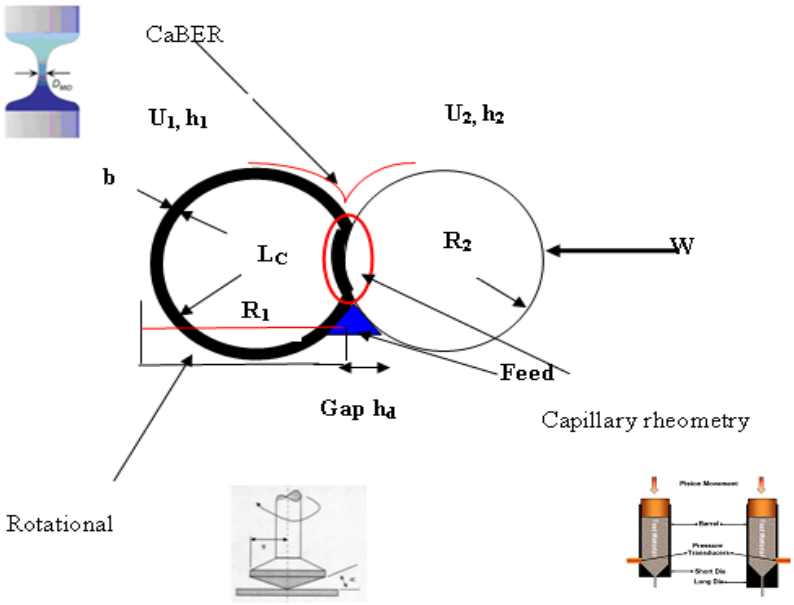

Figure 3-26 Integrated rheological measurement for roller coating

In addition to the above rheological studies, low shear viscosity will affect the storage, roller pick-up and levelling characteristics of the coating. A high low shear

viscosity will resist sedimentation but results in the pick-up of a heavier mass of the coating. It will also result in better levelling of the film (stability) [108]. The high shear rate viscosity provides information about the transfer properties of the coating and its mechanical stability. A low value of high shear viscosity will give better transfer properties between rollers and the substrate [108]. Viscosity-time characteristics will invariably determine the sample mechanical stability. The oscillatory tests, which give information about the structure of the system, could help in the comparison of similar shear viscosity coatings showing difference in processability and performance. Rheological experiments will inform the development of a range of tailored 'model' fluids, which will be tested in parallel with roller coating experiments. The rheometrical techniques to be employed in this research will include Capillary Rheometry [109]; Rotational rheometry [110] and Capillary Break-up Extensional Rheometry (CaBER) [111].

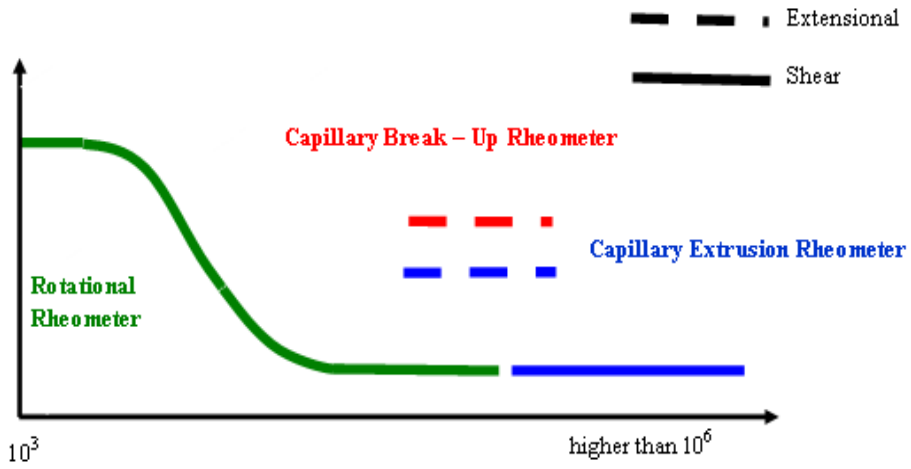

Figure 3-27 Paint map approach for an industrial coating feasibility with roller coater

The novelty of the research proposed lies in an integrated approach (as shown in *Figure 3-27*), utilising a range of comparative rheometrical techniques, with a focus

on measurement of: (i) high strain rate shear viscosity [η], (ii) high strain rate uniaxial extensional viscosity [η_E] (iii) high strain rate elasticity ($N1$).

3.7 Rheological techniques

3.7.1 Rotational rheometer

The rheometer used to carry out the experiments is the Anton Paar Physica MCR 301 (*Figure 3-28a*). This equipment can measure the rheology of the fluid in steady and dynamic modes with control of shear stress (CSS) and control the shear rate by a retrocalculation method. A cone and plate measuring device (*Figure 3-28b*) was used with the selection of suitable rotational test that gives the information on the rheology of the fluid up-to a medium range of viscosity.

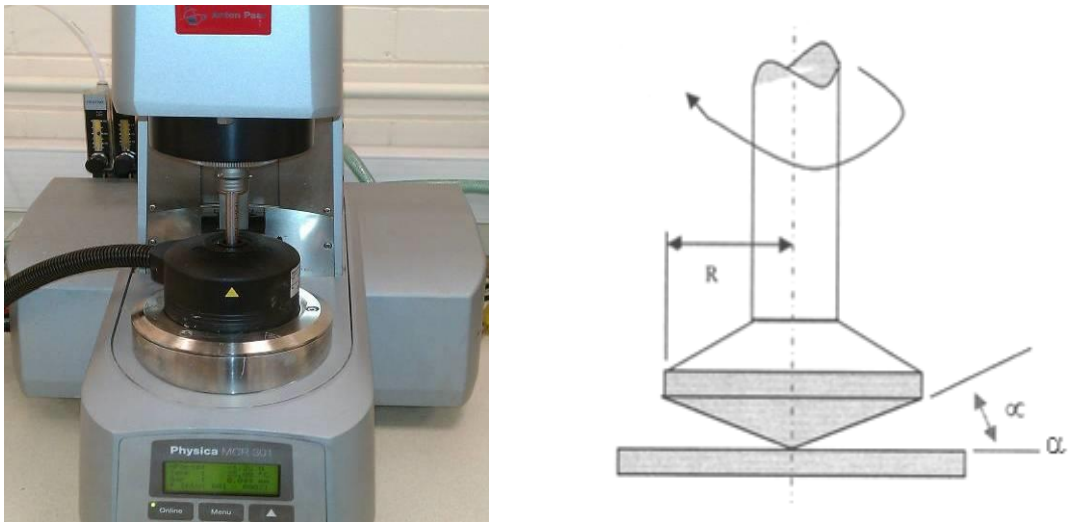

Figure 3-28 a) Rotational rheometer b) Cone and plate measuring system [113]

The geometrical dimensions of the cone are 25 mm cone radius (R) and 0.05 μrad cone angle (α) with a fixed plate having flat surface. During the rotational tests, 5 s^{-1} preshear followed by one minute rest was given before the testing to allow the

sample to reach equilibrium state, where the internal and external stress at the gap for the sample become ideally equal.

The rheometrical techniques to be employed will involve rotational rheometry as well as a number of techniques less commonly encountered in coating science and technology. As a common issue with high shear experiments, each of the techniques has an effective 'operability window', defined by the configuration of the measuring geometry and proposed fluid under test. Outside this window the contribution of errors increases and to counter these difficulties, overlap of data from complimentary techniques is sought to provide a higher level of confidence in results.

3.7.2 Capillary rheometry background

High speed roll coating generates very high shear in the narrow nip region between the rolls. The viscosity at these high shear rates becomes important, and only capillary rheometry is able to measure viscosities (both shear and extensional) at high shear rates (~ 10^6 s^{-1}). For better understanding of the high speed process and analysis of the instabilities associated with it, full characterisation of the concerned coating in shear and extensional modes is required. As the rotational rheometer available at Bradford University is limited to low and medium shear rates, different measurement method was chosen. This part of the work is done at Glyndwr University using sophisticated rheometry equipments like capillary rheometer, capillary Break-up Extensional rheometry (CaBER), other rotational rheometers etc. The full characterisation of coating itself was required for the following reasons:

- Generally the coatings have high loading of pigments and other components, which make it shear thinning and the extensional viscosity of this non-Newtonian

fluids become significant, especially at high extensional rates.

- Preliminary experiments using capillary rheometry [112] have demonstrated that high strain-rate uniaxial extensional viscosity is a much more effective predictor of the instabilities at high line speeds compared to the normal low-medium strain rate rotational measurements.

- Several academics [113, 114, 115] have indicated the importance of viscoelasticity in instabilities like ribbing and misting, which normally occur at high operation speeds.

Principle of operation

Capillary rheometry is a technique whereby a set volumetric flow rate of sample is extruded through a die of defined dimensions and the shear pressure drop across the die is recorded (*Figure 3-29*).

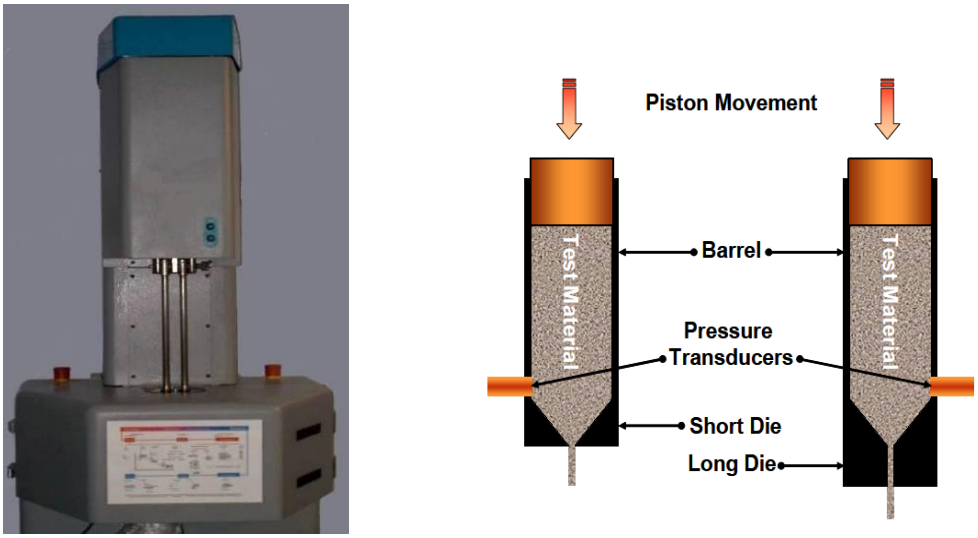

Figure 3-29 Mechanism of capillary rheometer

Capillary rheometers are comprised of temperature controlled barrel incorporating one or more precision bores fitted with capillary die at the exit. The pressure transducers are mounted immediately after the dies to record the pressure drop as the coating being tested undergoes extrusion through the dies.

Method of operation

In an extensional viscosity measurement test, the coating sample is pushed by a piston (driven at a defined speed) through a capillary die and the pressure is monitored above the die. The pressure builds up until an equilibrium condition is reached, at which point the pressure is recorded and the speed is changed to the subsequent measurement point. This process is repeated over a number of speeds (6 different speeds in this study). The range of speeds selected, correspond to the shear rate range of interest and it ranges from 0.5 mm/min to 250 mm/min in these trials. The fundamental rheological measurements at each speed are volume flow rate (defined by piston speed and piston diameter) and pressure drop.

$$\text{Shear stress } (\zeta) = \Delta P r / 2L \qquad [3.3]$$

$$\text{Shear rate } (\surd) = 4.Q / \pi.r^3 \qquad [3.4]$$

Where ΔP is the measured pressure drop, r is radius of die, L is the length of die and Q is the volumetric flow rates associated. From these measurements, viscosity (Y-axis) can be plotted against corresponding shear rate (X-axis). When experiments are performed on the twin-bore capillary rheometer systems, extensional viscosity can be simultaneously measured with shear viscosity. Capillary die diameters of 0.5 mm are used in all experiments with short and long die lengths (5.8 mm and 51 mm

respectively). Cogswell's equations, given below is used to calculate extensional viscosity along with the shear viscosity calculation,

$$\mu = 9/32 * (n+1)^2 / \eta * (P_0 / \sqrt{})^2 \quad [3.5]$$

Where power law index (n), shear viscosity (η) could be obtained from shear viscosity experiments. While entry pressure (P_0), in the extensional flow case to be obtained additional and it help to calculate the extensional viscosity.

3.7.3 CaBER test background

The Capillary Break up Extensional Rheometer (CaBER) is another extensional viscosity measurement technique (shown in *Figure 3-30*), which measures the extensional value at much lower shear rate values (~500 s^{-1}) compared to capillary rheometers (~6000 s^{-1}).

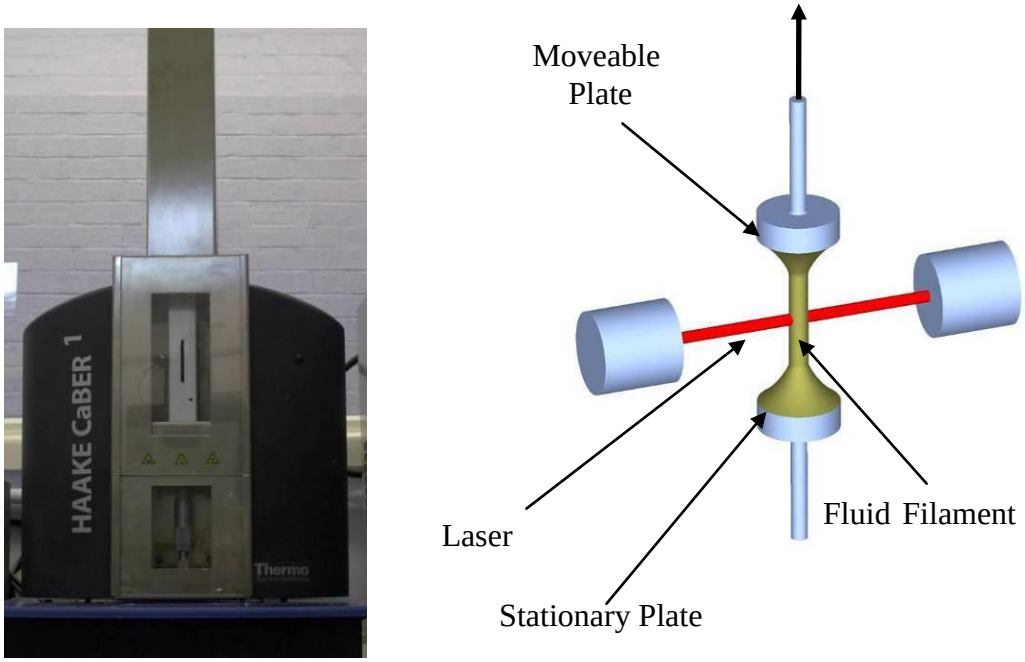

Figure 3-30 Mechanism of capillary break up rheometer [112]

This method gives different extensional viscosity information compared to capillary test, but was used to compare and reconfirm the trend under different testing conditions. Also in the case of misting, the fluid undergoing break-up is non-Newtonian, and therefore the transient extensional viscosity of the fluid plays an important role in controlling the dynamics and eventual means of break-up. This dynamical process can be extremely rapid at high speeds and depending on the composition of the fluid; the viscous, elastic and inertial forces will resist the capillary forces to form droplets. So it is expected that the CaBER plots of different formulations can provide a better rheological understanding of the misting phenomena in the high speed process.

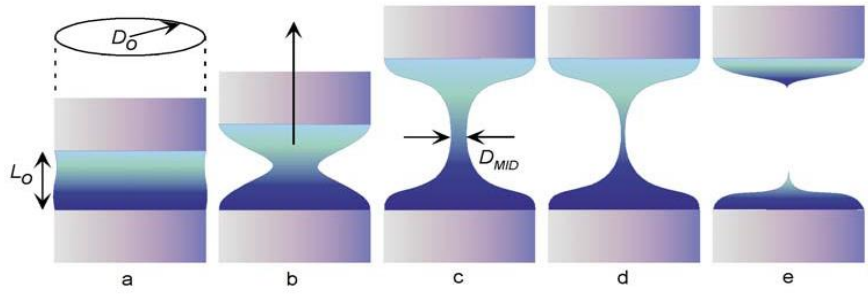

Figure 3-31 Flow mechanism during CaBER test [116]

CaBER is based on the formation of an unstable fluid filament caused by imposing a rapid axial step-strain of a prescribed magnitude (*Figure 3-31*). The filament is then allowed to relax till break-up under the action of its own dynamics. The relaxation and decay of the necked sample is governed by the viscous, elastic, gravitational and capillary forces [117] and the evolution of the filament diameter can be monitored.

3.8 Measurement of wetting property

Surface tension is the tangential force that keeps a fluid together at the air/fluid interface and is considered as an important aspect in the wetting property (as shown

in *Figure 3-32*). This property has an important role on the formation of surface instabilities, such as ribbing and other defects that may occur during coating. Surface tension together with surface energy of the coated substrate determines the extent of wetting. In order to coat the sample properly, the dynamic surface tension of the coating solution should be lower than the surface energy of the substrate

The contact angle was measured using the pendent drop measurement technique, as shown in *Figure 3-33*,

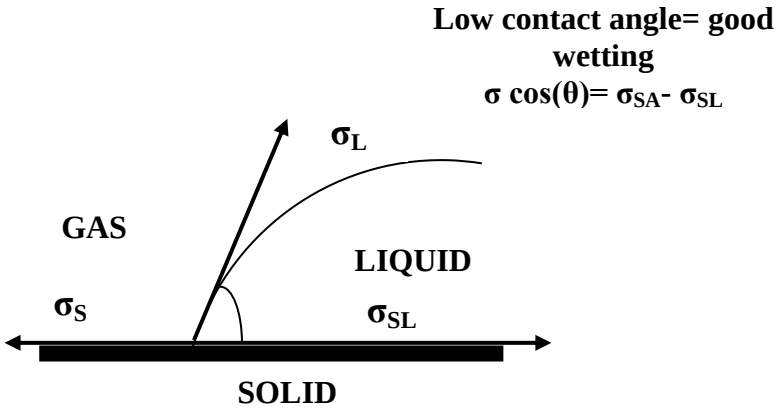

Figure 3-32 Principle of contact angle measurement

Figure 3-33 Pendent drop contact angle measurement technique

3.9 Generation of model fluids

After the thorough rheological characterisation of different industrial coatings, a suitable model fluid, designed to mimic the coating. The more advanced viscoelastic model fluids were required because:

- Earlier model fluids (lubricating oils) used for initial feasibility study matched the coating in shear viscosity only. The effect of extensional viscosity, which has major role in the quality of the thin film formed, was very different.

- Longer exposure to some of the industrial coatings is not preferred because of health and safety concerns. For example, Electron beam paint (Confidential supplier) needed to be heated to 55°C and as it is based on acrylate monomers, had different health hazards involved. Longer experiments using these materials were not ideal in lab conditions; hence an alternative safer fluid was used which closely matched the paint in rheological terms (but did not require heating).

- It is easier to modify the rheology of the model fluids than of a radiation curable coating, therefore model fluids could give better fundamental understanding of the effect of elasticity in the formulation to the instabilities (such as misting) observed in high speed process.

3.10 Rubber cover physical and mechanical characterisation

Establishing the deformation properties of rubber sleeve during coating (dynamic situation) is a difficult problem and itself an interesting area of research. The scope here is not to cover the intricacies of this problem but rather to arrive at some

property (elastic modulus) that can be used to correlate the measurement. The critical aspect is to use properties in a consistent manner.

3.10.1 Dynamic mechanical analysis (DMA) experiments

DMA setup

Dynamic mechanical measurements of rubber samples were carried out by TA Instrument model Q800 DMA (shown in *Figure 3-34*) on prismatic specimens deformed in a dual-cantilever clamping mode, with a span length between the clamps 17.5 mm.

Figure 3-34 Q800 Dynamic mechanical analysis instrument

The Q800 DMA is operated by applying force and measuring strain by displacement sensors. The schematic diagram of the dual cantilever clamping system is shown in *Figure 3-35*. The force and amplitude data are the raw signals recorded by the machine. Stiffness of the sample is then calculated from force and amplitude and modulus is calculated from the stiffness times the geometry factor, which is related to the geometry of the sample and the type of clamps. The geometry factor for dual cantilever clamp in the experiment is calculated by:

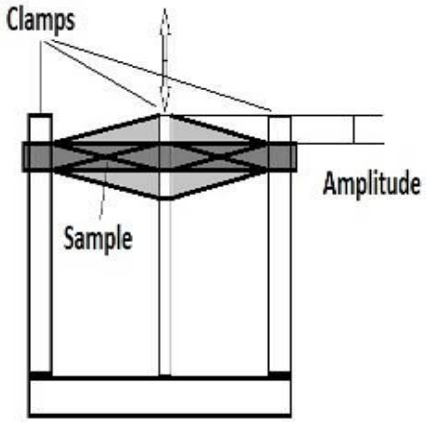

Figure 3-35 Dual cantilever clamps in DMA test machine

$$\text{Geometry Factor} = \frac{1}{F}\left[\frac{L^3}{192I} + \frac{S(1+\nu)L}{2A}\right] \qquad [3.6]$$

Where:

A = Cross section area of the sample (mm^2)

L = length of the specimen (distance between clamps) (m)

I = Geometric moment (mm^4)

For rectangular samples I = $\frac{1}{12}T^3W$ $\frac{1}{12}T^3W$

T = thickness of the sample

W = width of the sample

ν = Poisson's Ratio (normally 0.44)

F = Clamping Factor (normally 0.9)

S = Shearing Factor (normally 1.5)

As the test results of DMA are related to the geometry and dimensions of the test samples, it is important that due care is taken in measurement of the sample dimensions. A digital calliper was used in these tests and the average of length,

width and thickness at 3 different locations was recorded. The test method used in this DMA test was isothermal linear frequency sweep from 0.01 Hz to 20 Hz with 15 data points. The amplitude used in these tests was an optimised 2 mm, after trying different amplitudes such as 1 mm, 2 mm and 3 mm.

Sample preparation for the DMA test

Due to the softness of rubber, there was a conflict between the clamping of the rubber samples in the DMA test machine and the possible damage of the samples during the test as well as the inaccurate measurement of the mechanical properties. In order to overcome these problems, rubber was adhered to aluminium tags by superglue to provide tight clamping of the tags by the DMA machine and hence avoid either potential damage to the rubber samples, or slippage during the test. The glue was enough to fill the gap between the rubber and the aluminium tags thoroughly. The schematic diagram of the combination of the rubber and the aluminium tag as well as the dimension of the aluminium tag is displayed in *Figure 3-36*.

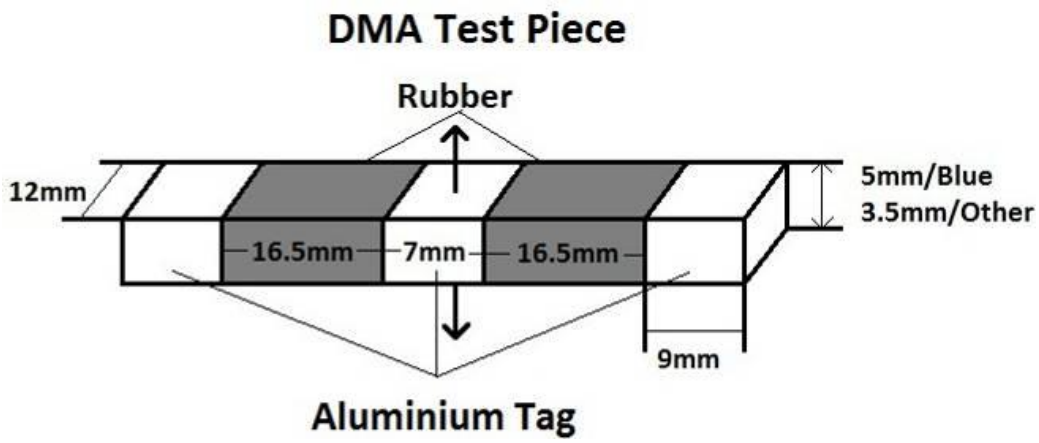

Figure 3-36 Schematic diagram of DMA test piece

According to the sample specification of DMA machine, the distance between the clamps is 35 mm. But the total actual length rubber part between the aluminium tags is 33 mm in order that the clamping of the sample is on the aluminium tag. The aluminium tags are 12 mm long. Two different aluminium tags with 7 mm and 9 mm in width were adhered in the middle and at the two ends of the sample. The rubber part was cut to a rectangular shape with 16.5 mm in length and 12 mm in width by a razor blade mounted in a vertical cutter to give a square and smooth cut.

The thickness of the aluminium tags depends on the thickness of the rubber. The blue rubber has the largest thickness, around 4.5 mm. Therefore, the thickness of the aluminium tag was prepared at 5 mm. The thickness of the aluminium tags was larger than the thickness of rubber but no larger than twice of the thickness of rubber, otherwise the relative position between the rubber and the aluminium tags would not be parallel and affect the final results of dynamic properties. Examples of the prepared DMA test pieces are shown in *Figure 3-37*.

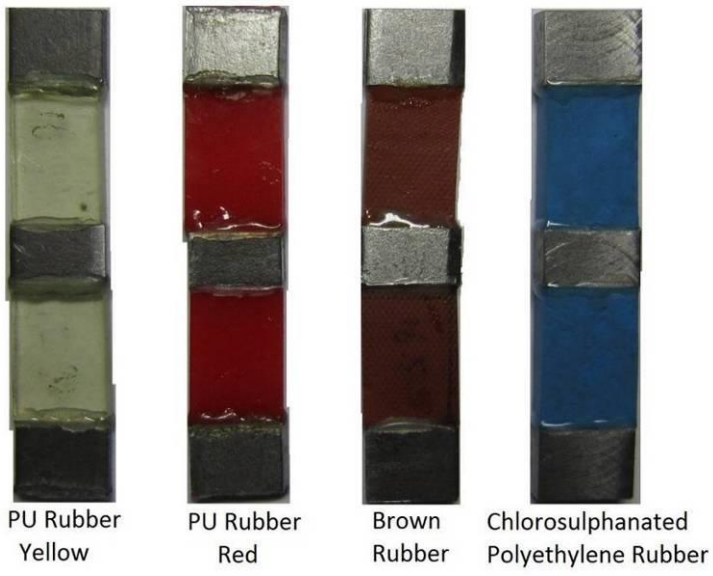

Figure 3-37 DMA test pieces of the rubbers

3.10.2 Measurement of elastic modulus by coating rig

The coating rig was used to measure the elastic modulus. The deformable roller was pressed against the rigid roller to the set negative gap and the corresponding Load (W) was measured using the load cell (as shown in *Figure 3-38*). The value of the elastic modulus (E) is obtained by evaluating the contact length (L_c) in conjunction with the measurement of W and the negative gap:

$$L_c = \sqrt{\frac{4WR}{\pi E}} \qquad \text{with} \qquad \frac{1}{R} = \frac{1}{2}\left(\frac{1}{R_1} + \frac{1}{R_2}\right) \qquad [3.7]$$

In the above equation, W is the applied load per unit width roller, E is the Young's modulus of the elastic roller (the entire roller is assumed rubber made), L_c is the contact length between the two rollers and R their equivalent radius. Now the contact length L_c is also related to geometry (equivalent radius R and negative gap h_d) as:

$$L_c = 2\sqrt{R^2 - \left(R - (h_d / 2)\right)^2} \qquad [3.8]$$

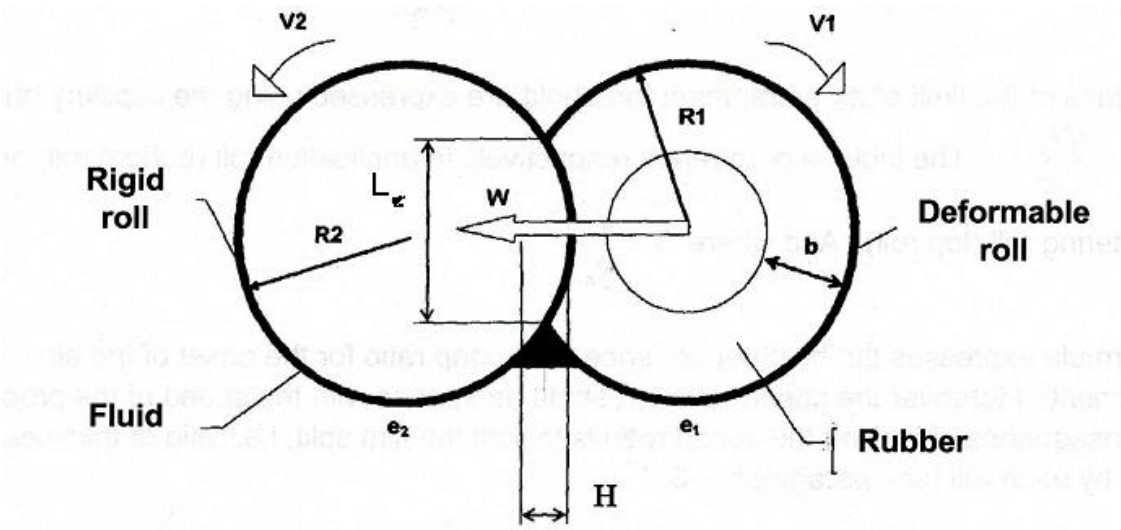

Figure 3-38 Roller coater arrangement for measuring elastic modulus [64]

In the rotating conditions, the duration of stress is simply the contact length divided by speed or:

$$t = L_c / U \qquad [3.9]$$

This corresponds to an angular frequency:

$$\varpi = 2\pi / t = 2\pi U / L_c = \pi U / \sqrt{R^2 - \left(R - (h_d / 2)\right)^2} \qquad [3.10]$$

Therefore E can be measured both statically (rollers stationary) leading to E_{Static} or dynamically (rollers moving at equal speed U) leading to $E_{Dynamic}$. Note that the Poisson's ratio for rubber is assumed to be 0.5 (incompressible with no volume change).

The three rubber covers used in trials had hardness values 45, 55 and 70 Shore A. These three rolls had the same rubber cover thickness of 15 mm with a 250 mm overall roll diameter. *Figure 3-39* shows the static load against the negative gap

measured in the case of 55 Shore A PU rubber cover, while *Table 3-1* gives its detailed data.

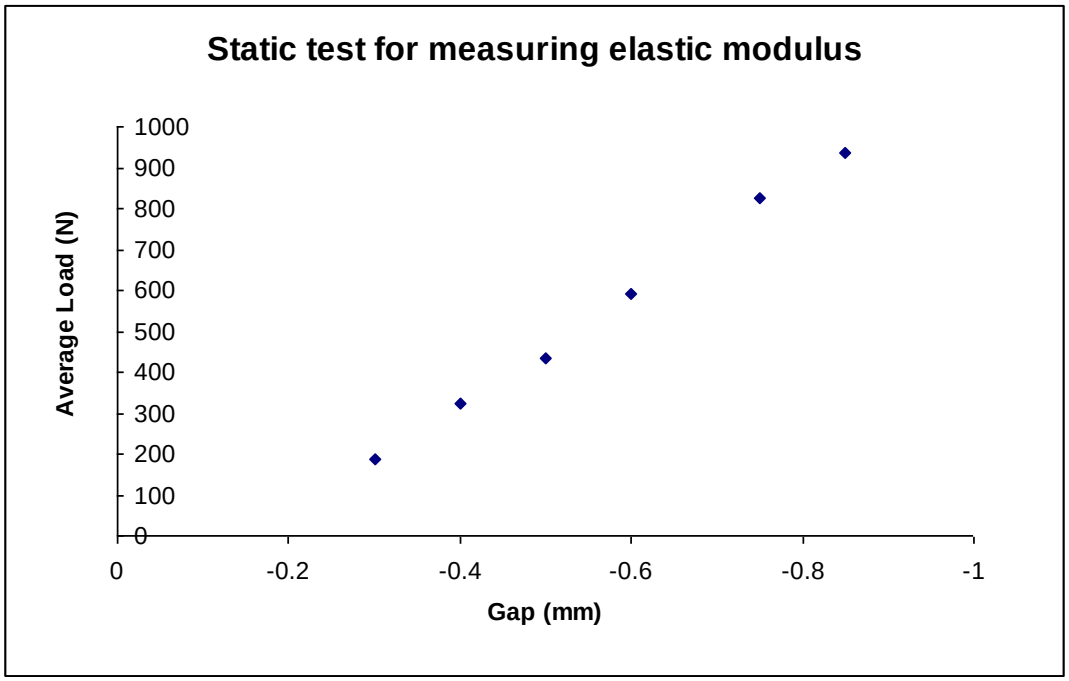

Figure 3-39 Static load variation with gap

Table 3-1 Static modulus measurement from coating rig

Static modulus measurement	**Static tests: R=0.125m, b=15mm, PU Rubber Shore hardness 55**						
Negative	Contact		Load	Load	Load	Mean Load	Elastic
Gap	Length	Delta	Front	Back	Mean	per m roll	Modulus
(mm)	mm	(m)	(N)	(N)	(N)	(N/m)	(MPa)
-0.3	12.3	0.01224	196	186	191	940.9	2
-0.4	14.16	0.01414	309	325	317	1561.6	2.49
-0.5	15.8	0.0158	407	434	421	2071.4	2.64
-0.6	17.31	0.01731	544	590	567	2793.1	2.97
-0.75	19.32	0.01935	744	826	785	3867	3.29
-0.85	20.61	0.0206	903	935	919	4527.1	3.4

From Hannah's theory [118] static and dynamic moduli for three rubber covers is calculated as follows,

Table 3-2 Static modulus measurement from comparative studies [118,119]

Shore A	**Estimated elastic modulus (MPa)** [118]	**Calculated static modulus*(MPa)** [119]
45	2.04	1.3-1.9
55	2.98	2-3.4.0
70	5.54	7.1-9.0

3.11 Deformation of rubber roll cover during roll coating process

During the actual roll coating process, the rubber roll cover experiences a complex deformation including compression, extension and shear, as rubber is bonded to the metal roll. Since rubber is normally considered as an incompressible material, the thickness of the rubber cover decreases when passing through the gap between the rolls and the volume change is balanced by the increase in thickness at the free boundary. Therefore, simple models are proposed initially in the following section considering the range of strain and strain rates that the rubber could encounter during the roll coating process. Suitable conditions for the DMA test can therefore be determined accordingly.

3.11.1 Maximum strain

The maximum strain the rubber cover experience is along the outer surface of the roll cover, when the rubber passes through the gap. In order to simplify and visualize the calculation, a typical example is taken when the diameter of the metal roll is 250

mm and the thickness of the roll cover is 30 mm (thick rubber cover regime). *Figure 3-40* shows the deformation of the rubber at the gap between the rolls.

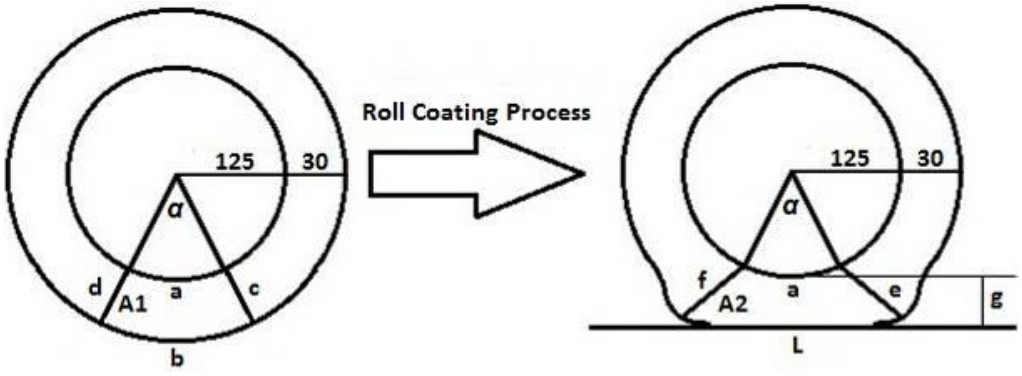

Figure 3-40 Deformation of rubber during roll coating process

It is assumed that the rubber is incompressible and so the cross section area of rubber cover remains the same before and as it passes through the gap. Therefore, the area A1 and A2 in *Figure 3-40* are the same. When the gap distance between the rolls is set at '*g*' mm, the corresponding angle of the compressed area of rubber cover is defined as '*α*' and the relative length of rubber cover along the inner roll, '*a*' is a part of the circumference of the circle of the inner roll. The length of the outer surface of the corresponding roll cover segment is defined as '*b*'.

Where:

$$a = \frac{\alpha}{360}\pi \times 250 \text{ mm}$$

$$b = \frac{\alpha}{360}\pi \times (250 + 2 \times 30)\text{mm} = \frac{\alpha}{360}\pi \times 310 \text{ mm}$$

During the roll coating process, the inner surface of the cover is bonded to the metal roll and the deformation is restricted. The outer surface of the roll cover is free to deform and there is normally no slippage between the rubber cover and the other

metal roll. The rubber is squeezed in the direction radial to the rolls and stretched in the circumferential direction to bulge out at the free boundary on either side of the gap (as shown in *Figure 3-40*). The maximum strain is then obtained when the initial length of the roll cover '*b*' is extended to '*L*'. The strain is a combination of shear, compression and tensile. Rubber is suffering from compression and strain at the middle of the gap while the roll is rotating. The rubber is stretched and elongated along the contact plane of the rubber cover and metal roll. In this model it is assumed that the amount of elongation is uniform along the whole length of contact, 'L'. The initial boundary of the rubber cover to pass through the gap '*c*' and '*d*' is deformed and approximated to straight lines '*e*' and '*f*'. For easier calculation, the cross section area of deformed roll cover after passing through the gap '*A1*' is approximated to be a Trapezoidal and the length of upper base is approximated to '*a*'.

Therefore, the strain can be obtained when '*A1*' equals '*A2*':

$$\mathbf{A1} = \frac{\alpha}{360}(\pi \cdot 155^2 - \pi \cdot 125^2) = \frac{70}{3}\pi\alpha$$

$$\mathbf{A2} = \frac{1}{2}(a + L) \times g = \frac{25}{72}\pi\alpha g + \frac{1}{2}Lg$$

$$\mathbf{A1} = \mathbf{A2}$$

$$\frac{70}{3}\pi\alpha = \frac{25}{72}\pi\alpha g + \frac{1}{2}Lg$$

$$L = \frac{140}{3}\frac{\pi\alpha}{g} - \frac{25}{36}\pi\alpha$$

The strain is $\frac{L-b}{b}$ $\frac{L-b}{b}$

$$b = \frac{\alpha}{360}\pi \times 310 \text{ mm}$$

$$\text{Strain} = \frac{L-b}{b} \times 100\% = \frac{\frac{140}{3}\frac{\pi\alpha}{g} - \frac{25}{36}\pi\alpha - \frac{31}{36}\pi\alpha}{\frac{31}{36}\pi\alpha} \times 100\%$$

$$= \left(\frac{1680}{31g} - \frac{56}{31}\right) \times 100\% = \frac{56}{31}\left(\frac{30}{g} - 1\right) \times 100\% = \frac{5600}{31}\left(\frac{30}{g} - 1\right)\%$$

According to the equation, the strain of the roll cover is independent of the angle 'α' but only depend on the gap distance between the rolls. The equation is reasonable as the strain increases with decreasing gap between the rolls. The plot of strain against gap distance is illustrated in *Figure 3-41*. Some typical values of strain at different gap distance are tabulated in *Table 3-3*. The strain gets infinite when the gap distance between the rolls decreases to zero and the strain is zero when the gap distance is 30 mm, i.e., no stress is applied on the roll cover. The strain increases quickly when the gap distance decreases, the strain gets to 100% when the gap distance reduces to 19.33 mm.

Table 3-3 Strain of rubber cover at different gap distance

Gap distance (mm)	29.5	28	26	24.5	22.5	20
Strain (%)	3.06	12.90	27.79	40.55	60.22	90.23

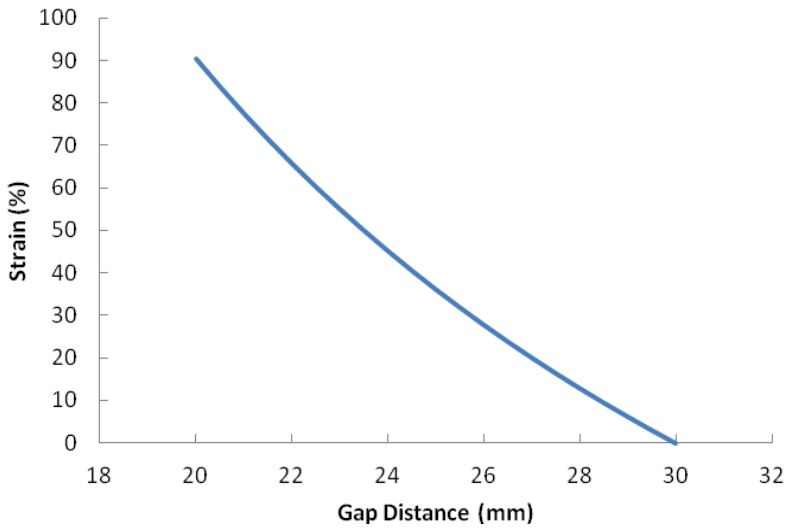

Figure 3-41 Strain versus gap distance

3.11.2 Frequency and strain rate

In the roll coating process, the speed is determined by the line speed. So the frequency of the operation is obtained by the line speed divided by the circumference of the roll (covered by rubber). If the coating process typically operates at a line speed of 2 m/s, the frequency at this speed can be calculated by:

$$\text{Frequency} = \frac{2 \times 1000}{\pi \cdot (250 + 60)} = 2.05\text{Hz}$$

From the research point of view, the target frequency is up to 7 Hz, which gives an even higher strain rate of rubber. The rubber around the circumference of the roll cover is not stressed for the complete cycle. Rather, as each individual point around the rubber cover passes through the gap between the rolls, it experiences one strain action. It is then relaxed during the rest of the cycle, until it approaches the gap again. *Figure 3-42* illustrates the strain of the roll cover against operating time.

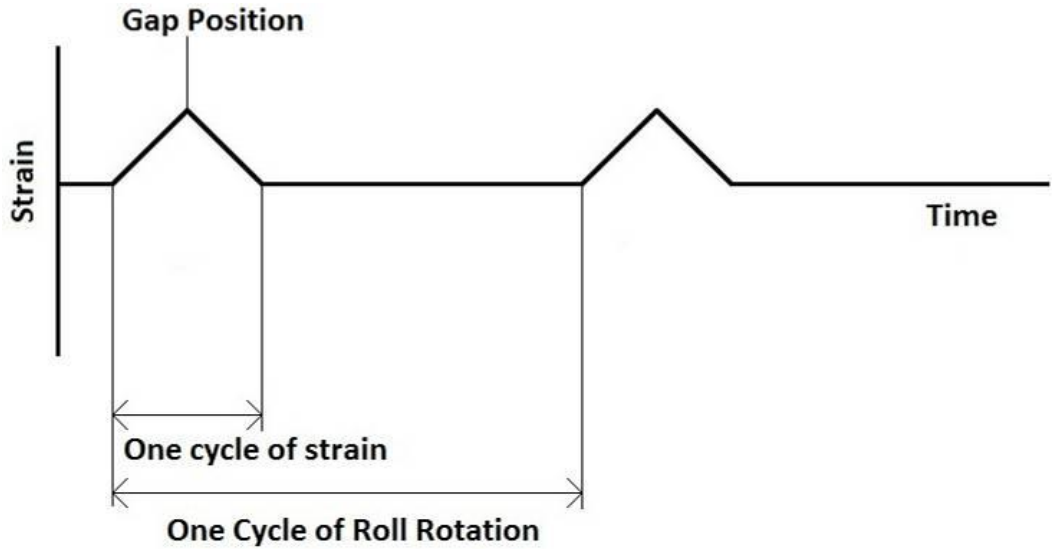

Figure 3-42 Strain of roll cover versus operating time

The strain rate depends on the time the roll cover is stressed during each roll rotation. Therefore, the strain rate is related to both the angle 'α' and the gap distance 'g'. It is obvious that α increase with decreasing gap value as α is zero when the gap distance is larger than 30 mm. The value of α is hard to decide as the boundary condition is difficult to determine without Finite Element Analysis. But if not considering the deformation of the rubber at the free boundary, the estimated α value can then be obtained through Pythagoras' Theorem and trigonometric functions from the isosceles triangle of the intersections between the rolls along the rubber cover and the centre of the rubber cover roll. The schematic of the triangle is demonstrated in *Figure 3-43*.

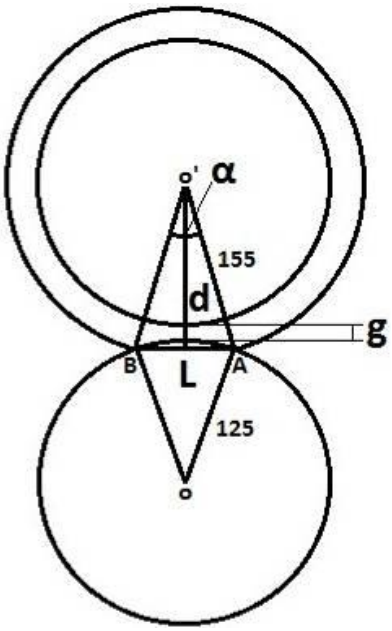

Figure 3-43 Triangle of gap condition of rolls

The length of sides is the radius of the rubber covered roll, i.e., 155 mm. The relationship between α and the gap distance 'g' can be calculated through the following equations:

The length of the base side of the triangle, 'L':

$$\mathbf{L = 2\sin\frac{\alpha}{2} \times 155 = 310\sin\frac{\alpha}{2} mm}$$

The height of the isosceles triangle O'AB is'd' and it can be obtained from the length between the two centre of the rolls minus the height of Δ OAB:

$$\mathbf{Height\ of\ \Delta OAB = \sqrt{125^2 - \left(\frac{L}{2}\right)^2} = \sqrt{125^2 - 155^2\sin^2\frac{\alpha}{2}}}$$

$$\mathbf{d = 125 + 125 + g - Height\ of\ \Delta OAB}$$

$$= 250 + \mathbf{g} - \sqrt{\mathbf{125^2 - 155^2\sin^2\frac{\alpha}{2}}}$$

'*d*' is also obtainable in the isosceles triangle O'AB by trigonometric functions:

$$\mathbf{d} = \cos\frac{\boldsymbol{\alpha}}{\mathbf{2}} \times \mathbf{155mm}$$

Therefore, the relationship between α and gap is:

$$250 + \mathbf{g} - \sqrt{\mathbf{125^2} - \mathbf{155^2}\sin^2\frac{\boldsymbol{\alpha}}{\mathbf{2}}} = \cos\frac{\boldsymbol{\alpha}}{\mathbf{2}} \times \mathbf{155}$$

$$\mathbf{g} = \mathbf{155}\cos\frac{\boldsymbol{\alpha}}{\mathbf{2}} + \sqrt{\mathbf{125^2} - \mathbf{155^2}\sin^2\frac{\boldsymbol{\alpha}}{\mathbf{2}}} - \mathbf{250}$$

Figure 3-44 displays the relationship between α and gap showing α to increase with decreasing gap.

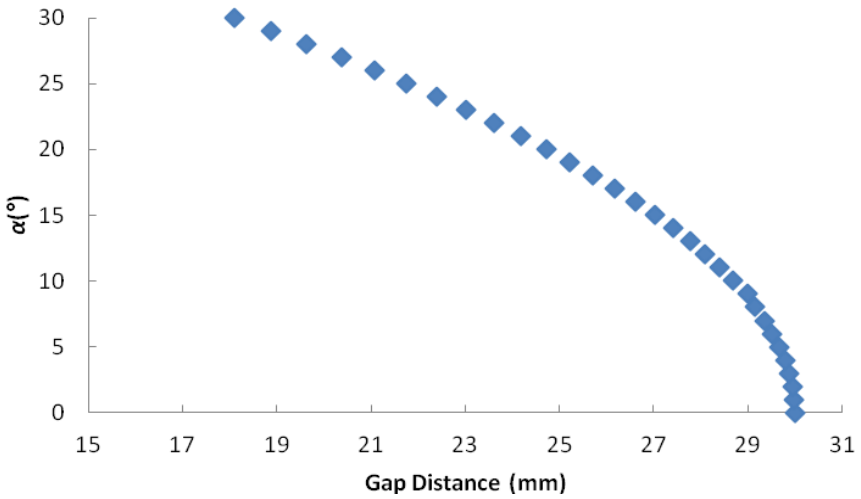

Figure 3-44 Relationship between gap distance and 'α'

Therefore, the frequency of the rubber cover during the strain action in the roll coating process can be calculated by the incorporation of α and gap. When the roll coating process operates at speed of 2 m/s, the time period for the rubber cover to

experience one strain action is the length of compressed circumference divided by the linear speed at 2 m/s:

$$\text{Time} = \frac{\frac{\alpha}{360} * \pi * 0.31\text{m}}{\frac{2\text{m}}{\text{s}}} = 0.\frac{4869}{360}\alpha\text{s}$$

The frequency is then the inverse of the time:

$$\text{Frequency} = \frac{1}{0.\frac{4869\alpha}{360}} = 739.\frac{4}{\alpha}\text{Hz}$$

Thus, the frequency of the roll cover can be plotted against the gap distance, as shown in *Figure 3-45*. The frequency at large gap distance is very high as the time for the strained rubber to pass through the gap is very small. When the gap distance increases, the angle α increases, more rubber is strained and takes more time to pass through the nip between the two rolls. Typical values of the angle, gap distance and the frequency are tabulated in *Table 3-4*. Although the frequency at large gap distance, i.e., small α angle, is very large, the strain, according to *section 3.11.1*, is rather small.

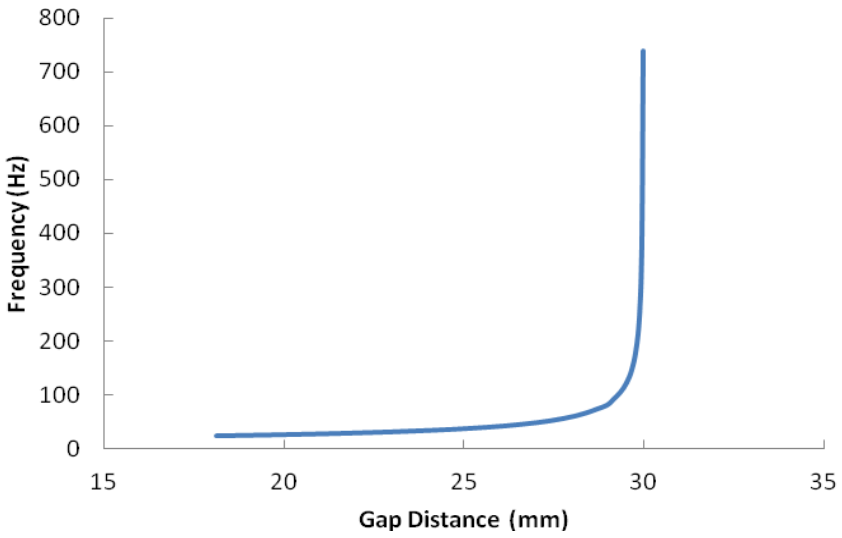

Figure 3-45 Strain rate versus gap distance

Table 3-4 Typical values of α, gap distance and strain rate

α (°)	1	8	12	15	17	20	23	27
Gap distance (mm)	29.99	29.15	28.10	27.03	26.18	24.71	23.01	20.37
Frequency (Hz)	739.4	92.43	61.62	49.29	43.49	36.97	32.15	27.39
Strain (%)	0.078	5.24	12.24	19.88	26.36	43.56	54.90	85.45

It is reasonable for the rubber cover to experience a high frequency during the roll coating process, but due to the restrictions of the machine limitations and the bonding between the metal and the rubber, it was not possible to measure the DMA at both high frequency and high strain. Therefore, the appropriate test conditions for DMA test was determined to have a highest frequency of 20 Hz. Nevertheless, the storage modulus of the DMA test plateaus out with increasing frequency at a certain amplitude. Thus, it is acceptable to test the dynamic properties of the rubber at the frequency of 20 Hz.

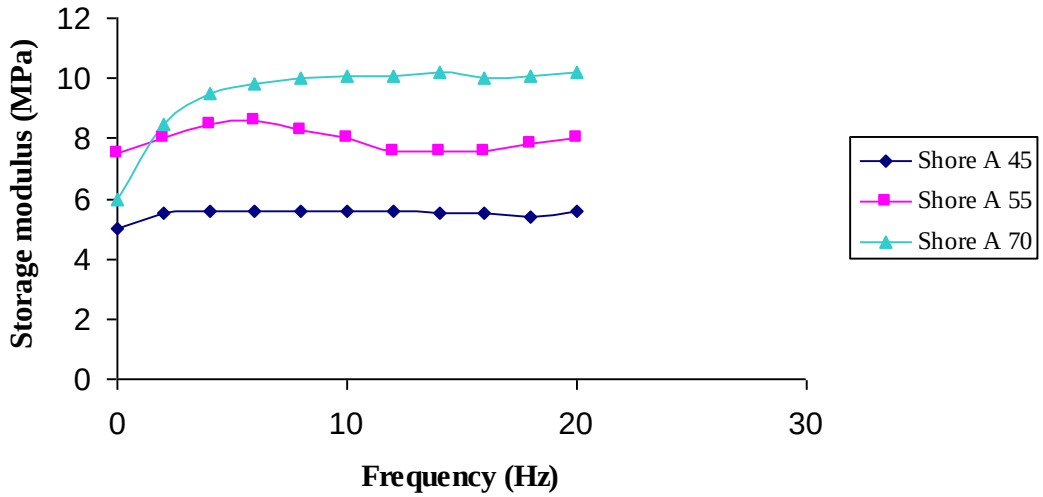

Figure 3-46 Storage modulus measured with DMA at 2 mm amplitude

The DMA results for different rubbers up to 20 Hz frequency is given in *Figure 3-46*.

3.12 Conclusions

The detailed theoretical and experimental study of deformable roller coating process resulted in the design and construction of state of the art coating rig at Bradford University. This coating rig was later modified to accommodate the high speed operation and measurement of the most important fluid parameters. This included the full rheological characterisation of complex Newtonian and non-Newtonian fluids and their wetting properties. At higher speeds, several feeding options were investigated and an optimum method was chosen to control the instabilities. Wet film thickness was measured with both scraping and a non contact gauge method, particularly suited for high speed operation. Flow and flow instabilities were observed using a high speed visualisation technique. Dynamic properties of the rubber cover used were studied in order to understand and evaluate the elastic parameters relevant to high speed roll coating rather than relying on a static elasticity

value. These various techniques and associated processes were developed to collect the important data to enable a good understanding of high speed deformable roll coating.

Chapter 4 : THEORETICAL STUDIES

4.1 Introduction

The goal of theoretical analyses is to gain a fundamental understanding of a physical phenomenon using the laws of physics, in this case the laws of fluid dynamics, without any recourse to experimental data (*details in Appendix IV*). Clearly the more rigorous and comprehensive the analytical treatment, the more accurate the predictions will be. Often however, a rigorous treatment is not feasible as the solution of the mathematical equations describing the theoretical model become very difficult to achieve. Deformable roll coating is a case that presents such difficulties as it is a coupled flow and rubber deformation problem with the flow bound by a free surface and a dynamic wetting line and the rubber deformation being dynamic and a-priori viscoelastic. This coupled problem is further complicated as the coating fluids are normally non- Newtonian. Here we develop models of this problem using first a Newtonian one dimensional analysis of rigid roll coating (no rubber and hence no deformation), then a Newtonian lubrication model of the coupled flow-deformation case and finally a numerical more comprehensive simulation using a software package OpenFoam. The main aim of these analyses is to predict flow rate (coating thickness), interface locations, velocities, pressures, forces, deflections, flow recirculation and instabilities and to compare these predictions with the measured data.

4.2 Rigid roll coating of Newtonian fluids

The approach here is to use the lubrication approximation [38] to describe the flow of a thin film of liquid between two rollers rotating in the same direction at the nip.

As the flow gap is long and thin, one dimensional flow can be assumed. However, the flow is not pure drag as the gap whilst being long and thin; it also converges and diverges to produce at the outlet two separate films as shown in *Figure 4-2*. We observe immediately that whilst we may assume the inlet pressure to be atmospheric, the outlet pressure may not be. Also whilst we may assume a known position of the inlet, the outlet position (where the two films form) is not known. The solution to the problem clearly hinges on the choice of pressure and separation flow boundary conditions at the outlet.

The fundamental flow of fluid between parallel plates is given in *Figure 4-1*

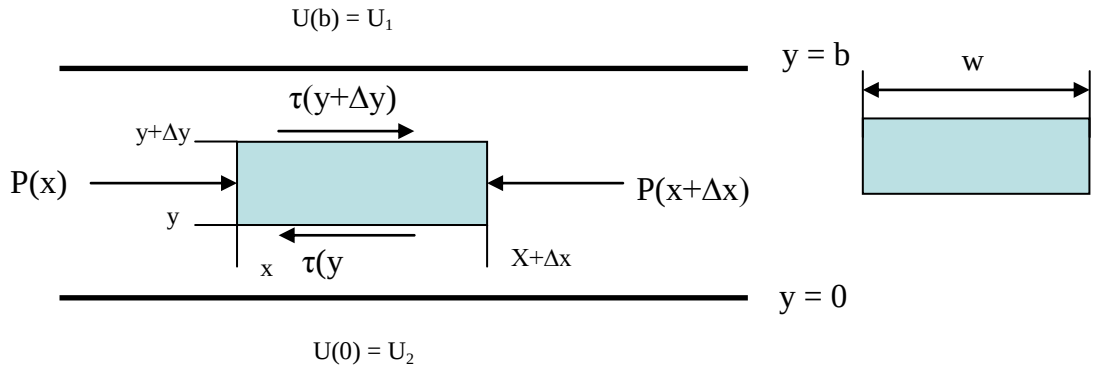

Figure 4-1 Fluid element between parallel plates

For steady state, applying the second law of motion to the differential volume element gives:

$$\sum Fx = M_{y+\Delta y} - M_y = 0$$

$$P(x)A(x) - P(x+\Delta x)A(x+\Delta x) - \tau(y)A(y) + \tau(y+\Delta y)A(y+\Delta y) = 0 \text{ --------- [4.1]}$$

Where

$$P(x) = P$$

$$P(x+\Delta x) = P + \frac{dp}{dx}\Delta x$$

$$\tau(y) = \tau$$

$$\tau(y + \Delta y) = \tau + \frac{d\tau}{dy}\Delta y$$

$$A(x) = A(x + \Delta x) = w\Delta y$$

$$A(y) = A(y + \Delta y) = w\Delta x$$

Now putting the above values into *equation [4.1]* gives:

$$\frac{dP}{dx} = \frac{d\tau}{dy}$$ ---------- [4.2]

Equation [4.2] is the principal model equation relating shear stress to pressure. Integration of this equation gives:

$$\tau(y) = \left(\frac{dP}{dx}\right)y + c_1$$ ---------- [4.3]

We now require a rheological constitutive equation to describe the shear flow and bring in the simple Newtonian model:

$$\therefore \tau = \mu\frac{du}{dy}$$

$$= \frac{1}{\mu}\left(\frac{dP}{dx}\right)y + \frac{c_1}{\mu}$$ ---------- [4.4]

Integration of the above equation gives:

$$u = \frac{y^2}{2\mu}\left(\frac{dP}{dx}\right) + c_1 y + c_2$$ ---------- [4.5]

Velocity boundary conditions are now required to solve the above equation and these are given using no slip velocity boundary conditions at the plates: $u = u_2$ for $y = 0$

$u = u_1$ for $y = b$ .This gives the velocity distribution in the nip as:

I.e. $u = \frac{-1}{2\mu}\left(\frac{dP}{dx}\right)\left(by - y^2\right) + \frac{y}{b}(u_1 - u_2) + u_2$ ---------- [4.6]

We may now integrate the velocity distribution across the nip width to obtain the flow rate per unit width as:

$$q = \int_0^b u(y)dy$$

$$= \int_0^b \left[-\frac{1}{2\mu}\frac{dP}{dx}(by - y^2) + \frac{y}{b}(u_1 - u_2) + u_2 \right] dy$$

$$= \left[\frac{-b^3}{12\mu}\frac{dP}{dx} + \frac{b}{2}(u_1 + u_2) \right]$$

i.e $q = \left[U_m b - \frac{b^3}{12\mu}\frac{dP}{dx} \right]$ where $U_m = ½ (u_1+u_2)$----------[4.7]

The analysis just described was presented for the flow between two parallel plates, in general. It can now be applied to the roll coating geometry shown below:

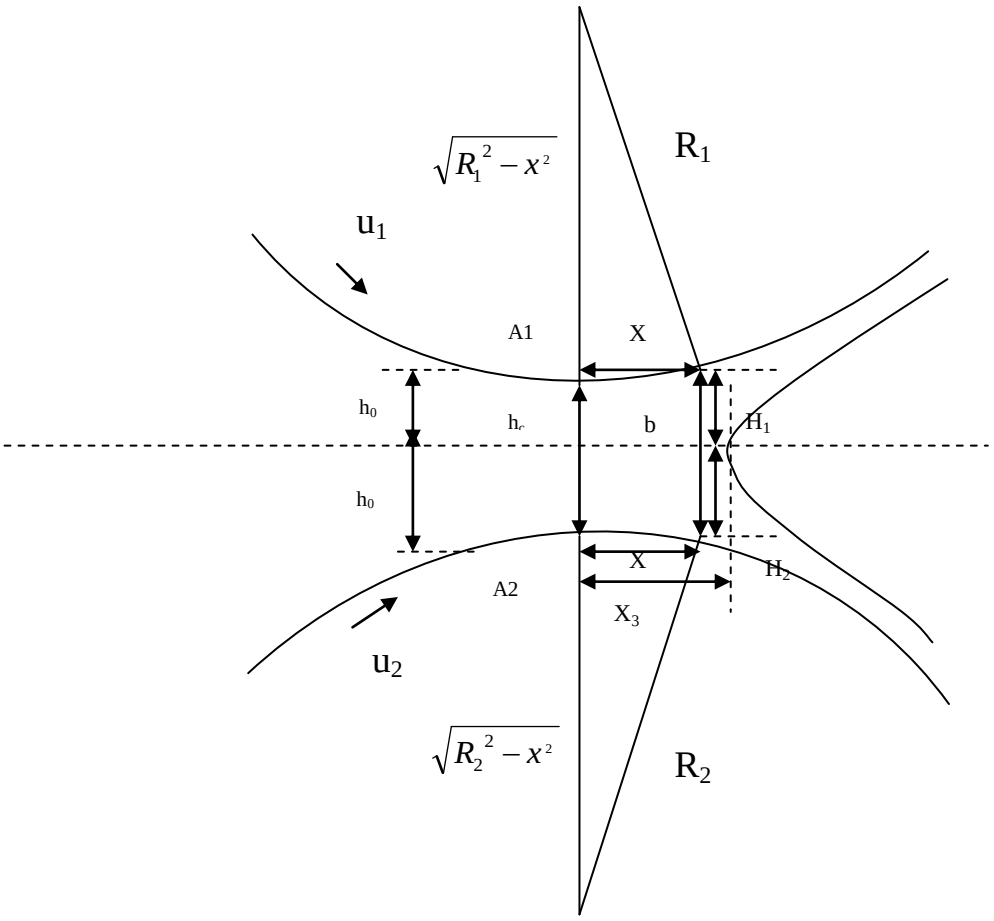

Figure 4-2 Roll coating flow geometry

The position of the top and bottom rollers is now related to minimum gap, roller radius and x direction by:

$$H_1 = h_0 + R_1 - \sqrt{R_1^2 - x^2}$$

$$H_2 = h_0 + R_2 - \sqrt{R_2^2 - x^2}$$

Expansion of the square roots using the binomial theorem gives:

$$H_1 = h_0 + R_1 - R_1(1 - \frac{x^2}{2R_1^2} + ...)$$

$$H_2 = h_0 + R_2 - R_2(1 - \frac{x^2}{2R_2^2} + ...)$$

Thus to a first order approximation, the gap **b** becomes:

$$b = H_1 + H_2 = 2h_0 + \frac{x^2}{2}(\frac{1}{R_1} + \frac{1}{R_2})$$

$$= h_c + \frac{x^2}{2}(\frac{1}{R_1} + \frac{1}{R_2}) \text{ ---------- [4.8]}$$

Having established the model equation linking pressure with flow rate, we can now solve it with appropriate boundary conditions. We require boundary conditions upstream and downstream and these are given as follows:

Upstream boundary conditions

Considering the fact that the flow channel is long and thin and flooded at the inlet, we see that the inlet is positioned relatively very far upstream thus:

$x_{in} \rightarrow -\infty$ and $p_{in} \sim p_{atm} = 0$

Downstream boundary conditions

The downstream conditions are less easily resolved as the position of the separation point (xs, ys) is not known and a separation meniscus forms. Strictly the pressure on the separation meniscus will not be zero as the convex meniscus will have negative pressure balanced by surface tension. However it may be approximated to be zero as a first approximation. As for finding the position (xs, ys) where the flow terminates at exit, we will adopt the Prandtl-Hopkins conditions which state that both the velocity and velocity gradient are zero. Thus the boundary conditions at exit are:

P=-σ/rc or 0; u (xs, ys)=du/dy (xs,ys)=0

With $\Delta u = u_1 - u_2$, *equation [4.6]* can be written as,

$$u = u_2 + \frac{\Delta u}{b} y - \frac{1}{2\mu} \frac{dP}{dx}(by - y^2) \text{ ---------- [4.9]}$$

Where the film splits, $x=x_s$, it is assumed that at some value of y the velocity is zero. At that location $\frac{du}{dy}$ is also zero. Computing $\frac{du}{dy}$ from *equation [4.9]* and setting the result to zero, we get:

$$\frac{du}{dy} = \frac{\Delta u}{b} - \frac{1}{2\mu}\frac{dP}{dx}(b - 2y_s) = 0$$

$$\therefore \frac{\Delta u}{b} - \frac{1}{2\mu}\frac{dP}{dx} + \frac{y_s}{\mu}\frac{dP}{dx} = 0$$

From which the separation point is found to be:

$$y_s = \mu(\frac{dP}{dx})^{-1}\left[\frac{b}{2\mu}\frac{dP}{dx} - \frac{\Delta u}{b}\right]$$

$$y_s = \frac{b}{2} - \mu\frac{\Delta u}{b}(\frac{dP}{dx})^{-1} \text{ ---------- [4.10]}$$

Now, since u=0 at $y=y_s$, Putting *[4.10]* into *[4.9]* and setting the result to zero gives:

$$u = u_2 + \frac{\Delta u}{b}\left[\frac{b}{2} - \mu\Delta u(b\frac{dP}{dx})^{-1}\right] - \frac{1}{2\mu}\frac{dP}{dx}\left[\frac{b}{2} - \mu\Delta u(b\frac{dP}{dx})^{-1}\right]\left[\frac{b}{2} - \mu\Delta u(b\frac{dP}{dx})^{-1}\right] = 0 \text{ --- [4.11]}$$

Or $u_2 - \frac{1}{2\mu}\frac{dP}{dx}\left[\frac{b}{2} - \mu\Delta u(b\frac{dP}{dx})^{-1}\right]^2 = 0$ ---------- [4.12]

Let $\frac{1}{2\mu}\frac{dP}{dx} = A$ i.e. $\frac{1}{\frac{dP}{dx}} = \frac{1}{2A\mu}$

Rearranging *[4.12]* gives:

$$u_2 - A\left[\frac{b}{2} - \frac{\mu\Delta u}{2Ab\mu}\right]^2 = 0$$

$$u_2 - A\left[\frac{b}{2} - \frac{\Delta u}{2Ab}\right]^2 = 0$$

$$u_2 - A\left[\frac{b^2}{4} + \frac{\Delta u^2}{4A^2b^2} - \frac{\Delta u}{2A}\right] = 0$$

$$u_2 - \frac{Ab^2}{4} - \frac{\Delta u^2 A}{4A^2b^2} + \frac{\Delta uA}{2A} = 0$$

$$u_2 + \frac{\Delta u}{2} - \frac{Ab^2}{4} - (\frac{\Delta u}{b})^2 \frac{1}{4A} = 0$$

$$u_m - \frac{Ab^2}{4} - \left(\frac{\Delta u}{b}\right)^2 \frac{1}{4A} = 0$$

Where $U_m = U_2 + (\Delta u / 2)$

Multiplying throughout by 4A gives:

$$4AU_m - A^2b^2 - (\frac{\Delta u}{b})^2 = 0$$

I.e. $b^2A^2 - 4AU_m + (\Delta u / b)^2 = 0$ ---------- [4.13]

Roots of above equation are:

$$\frac{1}{2\mu}(\frac{dP}{dx}) = A$$

$$\therefore \frac{\mu}{(\frac{dP}{dx})} = \frac{1}{2A}$$

$$A = \frac{1}{2\mu}\frac{dP}{dx} = \frac{4U_m \pm \sqrt{16Um^2 - 4b(\Delta u / b)^2}}{2b^2}$$

$$= \frac{4U_m \pm \sqrt{4(4U_m{}^2 - (\Delta u)^2}}{2b^2}$$

$$A = \frac{4U_m \pm 2\sqrt{4Um^2 - (\Delta u)^2}}{2b^2}$$

$$= \frac{2U_m \pm \sqrt{4Um^2 - (\Delta u)^2}}{b^2}$$

The negative sign should be discarded, because the corresponding y_s obtained from equation is:

$$y_s = \frac{b}{2} - \frac{\Delta u}{2Ab}$$

$$= \frac{b}{2} - \frac{\Delta u}{2} \frac{b}{2U_m - \sqrt{4Um^2 - (\Delta u)^2}}$$

I.e. $y_s = \frac{b}{2}\left[1 - \frac{\Delta u}{2U_m - \sqrt{4Um^2 - (\Delta u)^2}}\right]$ ---------- [4.14]

$2Um > \Delta u,$

Since $\frac{\Delta u}{2U_m - \sqrt{4Um^2 - (\Delta u)^2}} = \frac{1}{\Delta u}(2U_m + \sqrt{4U_m 2 - (\Delta u)^2} > 1$

Hence the y_s given in *equation [4.14]* are negative. Since only positive y_s is admissible,

$$\frac{1}{2\mu}\frac{dP}{dx} = \frac{2U_m + \sqrt{4U_m{}^2 - (\Delta u)^2}}{b^2}$$ ---------- [4.15]

With this root,

$$y_s = \frac{b}{2}\left[1 - \frac{\Delta u}{2U_m + \sqrt{4U_m{}^2 - (\Delta u)^2}}\right]$$

$$y_s = \frac{b}{2}\left[1 - \frac{1}{\Delta u}\left(2U_m - \sqrt{4U_m{}^2 - (\Delta u)^2}\right)\right]$$ ---------- [4.16]

Re-arranging *equation [4.16]*

$$b^2 = \frac{(2U_m + \sqrt{4U_m{}^2 - (\Delta u)^2}\, 2\mu}{(\frac{dP}{dx})}$$ ---------- [4.17]

From equation [4.7], $\frac{dP}{dx} = \left(\frac{U_m b - q}{b^3}\right)12\mu$

Substituting for (dP/dx) in *[4.17]* gives:

$$12\mu b^2\left(\frac{U_m b - q}{b^3}\right) = \left(2U_m + \sqrt{4Um^2 - (\Delta u)^2}\right)2\mu$$

I.e. $(U_m b - q)\frac{6}{b} = 2U_m + \sqrt{4U_m{}^2 - (\Delta u)^2}$

$$\therefore \frac{6q}{b} = 4U_m - \sqrt{4U_m{}^2 - (\Delta u)^2}$$

$$\therefore b = \frac{6q}{4U_m - \sqrt{4U_m{}^2 - (\Delta u)^2}} \text{ ---------- [4.18]}$$

$$c = \frac{\Delta u}{2u} = \frac{u_1 - u_2}{u_1 + u_2} = \frac{r_s - 1}{r_s + 1}$$

$$\Delta u = u_1 - u_2$$

Where $u = \frac{u_1 + u_2}{2}$

$$rs = \frac{u_1}{u_2}$$

$$c^2 = \left(\frac{r_s - 1}{r_s + 1}\right)^2 = \frac{r_s{}^2 - 2r_s + 1}{r_s{}^2 + 2r_s + 1}$$

$$(1 - c^2) = 1 - \frac{r_s{}^2 - 2r_s + 1}{r_s{}^2 + 2r_s + 1} = \frac{r_s{}^2 + 2r_s + 1 - r_s{}^2 + 2r_s - 1}{r_s{}^2 + 2r_s + 1} = \frac{4r_s}{(r_s + 1)^2}$$

$$(1 - c^2)^{1/2} = \frac{2r_s{}^{1/2}}{(r_s + 1)}$$

$$1 + (1 - c^2)^{1/2} = \frac{r_s + 1 + 2r_s{}^{1/2}}{r_s + 1} = \frac{(1 + r_s{}^{1/2})^2}{1 + r_s}$$

$$\frac{c}{1 + (1 - c^2)^{1/2}} = \left(\frac{r_s - 1}{r_s + 1}\right)\left(\frac{1 + r_s}{(1 + r_s{}^{1/2})^2}\right) = \frac{r_s - 1}{(1 + r_s{}^{1/2})^2}$$

$$1 - \frac{c}{1 + (1 - c^2)^{1/2}} = \frac{(1 + r_s{}^{1/2})^2 - r_s + 1}{(1 + r_s{}^{1/2})^2} = \frac{1 + 2r_s{}^{1/2} + r_s - r_s + 1}{(1 + r_s{}^{1/2})^2}$$

$$= \frac{2(1+r_s^{1/2})}{(1+r_s^{1/2})^2} = \frac{2}{(1+r_s^{1/2})}$$

Equation [4.15]

$$\frac{1}{2\mu}\frac{dP}{dx} = \frac{2U_m + (4U_m{}^2 - (\Delta u)^2)^{1/2}}{b^2} = \frac{2u}{b^2}\left(1+(1-c^2)^{1/2})\right)$$

$$= \frac{2u}{b^2} + \frac{2u}{b^2}(1-(\frac{\Delta u}{2u})^2)^{1/2}$$

$$= \frac{2u}{b^2} + \frac{2u}{b^2}(1-(\frac{\Delta u^2}{4u^2})^{1/2}$$

$$= \frac{2u}{b^2} + \frac{2u}{b^2}\left(\frac{4u^2-\Delta u^2}{4u^2}\right)^{1/2}$$

$$= \frac{2u}{b^2} + \frac{2u}{b^2.2u}\left(4u^2-\Delta u^2)\right)$$

$$= \frac{2u+(4u^2-\Delta u^2)}{b^2}$$

From *Equation [4.16]*

$$ys = \frac{b}{2}\left[1-\frac{\Delta u}{2U_m + (4U_m{}^2 - \Delta u^2)^{1/2}}\right] = \frac{b}{2}\left[1-\frac{c}{1+(1-c^2)^{1/2}}\right]$$

$$= \frac{b}{2}\left[1-\frac{\frac{\Delta u}{2u}}{1+(1-(\frac{\Delta u}{2u})^2)^{1/2}}\right]$$

$$= \frac{b}{2}\left[1-\frac{\frac{\Delta u}{2u}}{1+(1-\frac{\Delta u^2}{4u^2})^{1/2}}\right]$$

$$= \frac{b}{2}\left[1 - \frac{\frac{\Delta u}{2u}}{1+\left(\frac{4u^2 - \Delta u^2}{4u^2}\right)^{1/2}}\right]$$

$$= \frac{b}{2}\left[1 - \frac{\frac{\Delta u}{2u}}{1+\frac{1}{2u}\left(4u^2 - \Delta u^2\right)^{1/2}}\right]$$

$$= \frac{b}{2}\left[1 - \frac{\Delta u}{2u + (4u^2 - \Delta u^2)^{1/2}}\right]$$

$$y_s = \frac{b}{2}\left[1 - \frac{c}{1+(1-c^2)^{1/2}}\right]$$

$$y_s = \frac{b}{2}\left[\frac{2}{1+r_s^{1/2}}\right]$$

$$ys = \frac{b}{1+rs^{1/2}}$$

$$\therefore y_s^{\,2} = \frac{b^2}{(1+r_s^{1/2})^2}$$

And $y_s^{\,3} = \frac{b^3}{(1+r_s^{1/2})^3}$

Derivation for flow rate q

$$\frac{1}{2\mu}\left(\frac{dP}{dx}\right) = \frac{2u}{b^2}\left(1+(1-c^2)^{1/2}\right)$$ ---------- [4.19]

$$q = ub - \frac{b^3}{12\mu}\left(\frac{dP}{dx}\right)$$ ---------- [4.20]

$$\left(\frac{dP}{dx}\right) = \frac{4\mu u}{b^2}\left(1+(1-c^2)^{1/2}\right)$$ ---------- [4.21]

Now: $c = \frac{\Delta u}{2u} = \frac{u_1 - u_2}{u_1 + u_2} = \frac{(\frac{u_1}{u_2}) - 1}{(\frac{u_1}{u_2}) + 1} = \left(\frac{r_s - 1}{r_s + 1}\right)$ ---------- [4.22]

$$\therefore c^2 = \left(\frac{r_s - 1}{r_s + 1}\right)^2 = \frac{r_s{}^2 - 2r_s + 1}{r_s{}^2 + 2r_s + 1}$$

Substituting *[4.22]* into *[4.21]* gives:

$$\left(\frac{dP}{dx}\right) = \frac{4\mu u}{b^2}\left[1 + \left(1 - \frac{r_s{}^2 - 2r_s + 1}{r_s{}^2 + 2r_s + 1}\right)\right]^{1/2}$$

$$\left(\frac{dP}{dx}\right) = \frac{4\mu u}{b^2}\left[1 + (\frac{r_s{}^2 + 2r_s + 1 - r_s{}^2 + 2r_s - 1}{r_s{}^2 + 2r_s + 1}\right]^{1/2}$$

$$\left(\frac{dP}{dx}\right) = \frac{4\mu u}{b^2}\left[1 + (\frac{4r_s}{(r_s + 1)^2})\right]^{1/2}$$

$$\therefore \left(\frac{dP}{dx}\right) = \frac{4\mu u}{b^2}\left[1 + \frac{2r_s{}^{1/2}}{r_s + 1}\right] = \frac{4\mu u}{b^2}\left[\frac{r_s + 1 + 2r_s{}^{1/2}}{r_s + 1}\right]$$ ---------- [4.23]

Substituting *[4.23]* into *[4.20]* gives:

$$q = ub - \frac{b^3}{12\mu}\frac{4\mu u}{b^2}\left[\frac{r_s + 1 + 2r_s{}^{1/2}}{r_s + 1}\right]$$

$$q = ub - \frac{ub}{3}\left[\frac{r_s + 1 + 2r_s{}^{1/2}}{r_s + 1}\right]$$

$$= ub - \frac{ub}{3}\left[1 + (\frac{2r_s{}^{1/2}}{r_s + 1})\right]$$

$$= ub - \frac{ub}{3} - \frac{ub}{3}\left(\frac{2r_s{}^{1/2}}{r_s + 1}\right)$$

$$= \frac{2}{3}ub - \frac{2}{3}ub\left(\frac{r_s^{1/2}}{r_s+1}\right)$$

$$q = \frac{2}{3}ub\left[1 - \frac{r_s^{1/2}}{r_s+1}\right]$$

$$q = \frac{2}{3}ub\left[\frac{r_s+1-r_s^{1/2}}{r_s+1}\right]$$

$$\therefore q_1 = q - q_2$$

$$q = \int_{ys}^{b} udy = q - q_2$$

$$= \frac{2}{3}ub\left(\frac{r_s+1-r_s^{1/2}}{r_s+1}\right) - \frac{2}{3}ub\left(\frac{1}{r_s+1}\right)\left(\frac{1}{1+r_s^{1/2}}\right)$$

$$= \frac{2}{3}ub\left[\frac{r_s+1-r_s^{1/2}}{r_s+1}\right] - \left(\frac{1}{r_s+1}\right)\left(\frac{1}{1+r_s^{1/2}}\right)$$

$$= \frac{2}{3}ub\left(\frac{1}{r_s+1}\right)\left[r_s+1-r_s^{1/2} - \frac{1}{(1+r_s^{1/2})}\right]$$

$$= \frac{2}{3}ub\left(\frac{1}{r_s+1}\right)\left[\frac{r_s+r_s^{1/2}+1+r_s^{1/2}-r_s^{1/2}-r_s-1}{1+r_s^{1/2}}\right]$$

$$= \frac{2}{3}ub\left(\frac{1}{r_s+1}\right)\left[\frac{r_s^{1/2}}{1+r_s^{1/2}}\right]$$

$$\therefore q_1 = \frac{2}{3}ub\left(\frac{r_s}{r_s+1}\right)\left(\frac{r_s^{1/2}}{1+r_s^{1/2}}\right)$$

$$q_2 = \int_{0}^{ys} udy \qquad \text{---------- [4.24]}$$

$$= u_2 y_s + \frac{\Delta u}{2b} y_s^{\,2} - \frac{1}{2\mu}\frac{dP}{dx}\left(\frac{by_s^{\,2}}{2} - \frac{y_s^{\,3}}{3}\right)$$

Now: $u_2 y_s = \dfrac{bu_2}{1+r_s^{1/2}}$

$$\frac{\Delta u}{b}\frac{y_s^{\,2}}{2} = \frac{\Delta u}{2b}\frac{b^2}{(1+r_s^{1/2})^2} = \left(\frac{u_1-u_2}{2}\right)\frac{b}{(1+r_s^{1/2})^2} = \frac{r_s-1}{2}\frac{u_2 b}{(1+r_s^{1/2})^2}$$

$$= \frac{u_2 b}{2} \frac{r_s - 1}{(1 + r_s^{1/2})^2}$$

$$\frac{b y_s^{\,2}}{2} = \frac{b^3}{2(1 + r_s^{1/2})^2}$$

$$\frac{y_s^{\,3}}{3} = \frac{b^3}{3(1 + r_s^{1/2})^3}$$

$$\frac{b y_s^{\,2}}{2} - \frac{y_s^{\,3}}{3} = \frac{b^3}{2(1 + r_s^{1/2})^2} - \frac{b^3}{3(1 + r_s^{1/2})^3} = \frac{b3}{(1 + r_s^{1/2})^2} \left[\frac{1}{2} - \frac{1}{3(1 + r_s^{1/2})} \right]$$

$$\therefore \frac{1}{2\mu} \frac{dP}{dx} = \frac{2u}{b^2} \left[1 + (1 - c^2)^{1/2} \right] = \frac{2u}{b^2} \left[\frac{(1 + r_s^{1/2})^2}{(1 + r_s)} \right]$$

$$\frac{1}{2\mu}\frac{dP}{dx}\left(\frac{by_s{}^2}{2}-\frac{y_s{}^3}{3}\right)=\frac{2u}{b^2}\left[\frac{(1+r_s{}^{1/2})^2}{(1+r_s)}\right]\frac{b^3}{(1+r_s{}^{1/2})^2}\left[\frac{1}{2}-\frac{1}{3(1+r_s{}^{1/2})}\right]$$

$$=\frac{2ub}{(1+r_s)}\left(\frac{1}{2}-\frac{1}{3(1+r_s{}^{1/2})}\right)$$

$$=\frac{ub}{1+r_s}-\left(\frac{2}{3}ub(\frac{1}{1+r_s})(\frac{1}{1+r_s{}^{1/2}})\right)$$

$$\therefore q_2=\frac{u_2b}{(1+r_s{}^{1/2})}+\frac{u_2b}{2}\left(\frac{r_s-1}{(1+r_s{}^{1/2})^2}\right)-\frac{ub}{(1+r_s)}+\frac{2}{3}ub\left(\frac{1}{(1+r_s)}\right)\left(\frac{1}{(1+r_s{}^{1/2})}\right)$$

$$q_2=\frac{u2b}{(1+rs1/2)}+\frac{u2b}{2}\left(\frac{rs-1}{(1+rs1/2)2}\right)-\frac{(rs+1)}{2}u2\frac{b}{(1+rs)}+\frac{2}{3}ub\left(\frac{1}{1+rs}\right)\left(\frac{1}{1+rs^{1/2}}\right)$$

$$q_2=\frac{u_2b}{(1+r_s1/2)}+\frac{u_2b}{2}\left(\frac{r_s-1}{(1+r_s{}^{1/2})^2}\right)-\frac{u_1b}{2}+\frac{2}{3}ub\left(\frac{1}{1+r_s}\right)\left(\frac{1}{1+r_s{}^{1/2}}\right)$$

$$=u_2b\left[\frac{1}{(1+r_s{}^{1/2})}+\frac{1}{2}\left[\frac{(r_s-1)}{(1+r_s{}^{1/2})^2}-\frac{1}{2}\right]\right]+\frac{2}{3}ub\left(\frac{1}{1+r_s}\right)\left(\frac{1}{1+r_s{}^{1/2}}\right)$$

$$=u_2b\left[\frac{(1+r_s{}^{1/2})+\frac{1}{2}(r_s-1)-\frac{1}{2}(1+r_s{}^{1/2})^2)}{(1+r_s{}^{1/2})^2}\right]+\frac{2}{3}ub\left(\frac{1}{1+r_s}\right)\left(\frac{1}{1+r_s{}^{1/2}}\right)$$

$$=u_2b\left[\frac{(1+r_s{}^{1/2})+\frac{1}{2}\left(r_s-\frac{1}{2}\right)-\frac{1}{2}(1+2r_s{}^{1/2}+r_s)\ )}{(1+r_s{}^{1/2})^2}\right]+\frac{2}{3}ub\left(\frac{1}{1+r_s}\right)\left(\frac{1}{1+r_s{}^{1/2}}\right)$$

$$=u_2b\left[\frac{1+r_s{}^{1/2}+\frac{1}{2}r_s-\frac{1}{2}-\frac{1}{2}-r_s{}^{1/2}-\frac{1}{2}r_s}{(1+r_s{}^{1/2})^2}\right]+\frac{2}{3}ub\left(\frac{1}{1+r_s}\right)\left(\frac{1}{1+r_s{}^{1/2}}\right)$$

$$=ub\left[\frac{1+r_s{}^{1/2}+\frac{1}{2}r_s-\frac{1}{2}-\frac{1}{2}-r_s{}^{1/2}-\frac{1}{2}r_s}{(1+r_s{}^{1/2})^2}\right]+\frac{2}{3}ub\left(\frac{1}{1+r_s}\right)\left(\frac{1}{1+r_s{}^{1/2}}\right)$$

$$q_2=\frac{2}{3}ub\left(\frac{1}{(1+r_s)}\right)\left(\frac{1}{1+r_s{}^{1/2}}\right)$$

$$\frac{q1}{q2} = \frac{\frac{2}{3}ub\left(\frac{r_s}{r_s+1}\right)\left(\frac{r_s^{1/2}}{1+rs^{1/2}}\right)}{\frac{2}{3}ub\left(\frac{1}{r_s+1}\right)\left(\frac{1}{1+r_s^{1/2}}\right)}$$

$$= \left(\frac{r_s}{r_s+1}\right)\left(\frac{r_s^{1/2}}{1+r_s^{1/2}}\right)\left(\frac{r_s+1}{1}\right)\left(\frac{1+r_s^{1/2}}{1}\right)$$

$$\therefore \frac{q_1}{q_2} = r_s^{3/2} = \left(\frac{u_1}{u_2}\right)^{1.5} \text{ ---------- [4.25]}$$

As shown in *equation [4.25]*, the flux ratio in rigid roll coating has been calculated from lubrication analysis and the power factor is 1.5.

4.3 Lubrication modelling of deformable roll coating flow

Coating with deformable rollers is a complex mathematical problem and no complete solution is available for several reasons:

- The coupled flow and deformation problem can be non-linear when the rubber layer is small and viscoelastic properties of the rubber are required in this case, and it complicates the solution.
- Similar to any other coating flow analysis, the boundary conditions are unknown in terms of the position of flow geometry and associated pressures.
- At differential roll speeds, the criterion for the film split at exit of the nip is unknown as well.

The mathematical model follows from Reynolds lubrication analysis. In the lubricated contact between the two rollers, a convergent wedge of lubricant is formed and it is the convergence, coupled with the viscosity of the lubricant and the

speed of the moving roller surfaces that generates a pressure profile within the fluid. In the analysis reference is made to the co-ordinates in *Figure 4-3*.

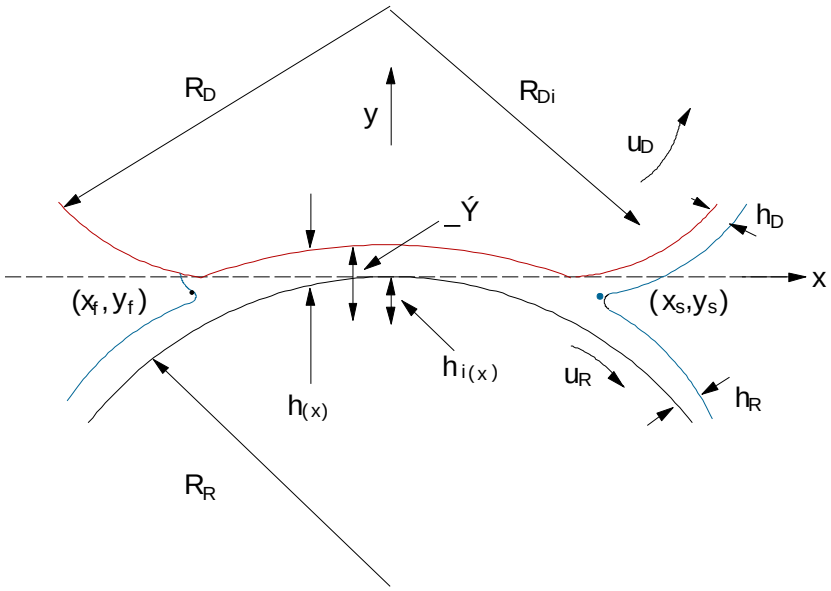

Figure 4-3 Flow field and co-ordinates system

It can be seen that the properties of deformable roll coating are precisely those encountered in lubrication flows, namely flow is largely one dimensional across a minimum length of contact. In the regions approaching the inlet and outlet of the flow situation the lubrication approximation breaks down, however in the region where the lubrication approximation holds and considering Newtonian fluids and constant viscosity, the Navier-Stokes equations (*equation [4.26]*) can be reduced to a balance between pressure and viscous forces as shown below.

Navier-Stokes equation:

$$\rho(\frac{du}{dt} + u.\nabla u) = -\nabla P + \mu\nabla^2 u + \rho g \text{ ---------- [4.26]}$$

As the flow is considered only in the direction "x",

$$\rho(\frac{du}{dt} + u\frac{du}{dx} + v\frac{du}{dy} + w\frac{du}{dz}) = -\frac{dP}{dx} + \mu(\frac{d^2u}{dx^2} + \frac{d^2u}{dy^2} + \frac{d^2u}{dz^2}) + \rho g_x$$

Now mass continuity equation is given as,

$$\frac{d\rho}{dt} + \nabla.(\rho u) = 0$$

When the density is constant (incompressible assumption), the mass continuity equation simplifies to a volume continuity equation:

$$\nabla.u = 0$$

If the flow is one dimensional (x direction),

"u" is constant in X direction, therefore

$$\frac{du}{dt} = 0 \quad \frac{du}{dx} = 0$$

$$\frac{d^2u}{dx^2} = 0$$

v = w = 0

If only x-y dimension is considered and no z-direction and gravity effect,

$$\frac{du}{dz} = 0, \ \frac{d^2u}{dz^2} = 0, \ g_x = 0$$

In case of one dimensional Newtonian liquid flow, the complex Navier-Stokes equation can be simplified as,

$$\frac{dp}{dx} = \mu \frac{d^2u}{dy^2}$$ ---------- [4.27]

This equation is the starting point for the model. The unknowns in *equation [4.27]* are *p*, the hydrodynamic pressure and *u*, the x-component of the velocity vector. Since pressure is strictly a function of position within the gap, (i.e. *x*), *equation [4.27]* is solved by integrating twice subject to the following velocity boundary conditions

$$\frac{1}{\mu}\frac{dp}{dx} = \frac{d^2u}{dy^2}$$ ---------- [4.28]

This equation can be integrated twice with respect to y:

$$u = \frac{1}{\mu}\frac{dp}{dx}\frac{y^2}{2} + c_1 y + c_2 \text{ ---------- [4.29]}$$

Here c_1 and c_2 are constants of integration.

Velocity boundary conditions are,

$$u = u_r \text{ at } y = y_r$$
$$u = u_d \text{ at } y = y_d$$

Using the velocity boundary conditions the following two equations can be derived.

At y = y_r $$u_r = \frac{1}{\mu}\frac{dp}{dx}\frac{y_r^{\,2}}{2} + c_1 y_r + c_2 \text{ ----------[4.30]}$$

At y = y_d $$u_d = \frac{1}{\mu}\frac{dp}{dx}\frac{y_d^{\,2}}{2} + c_1 y_d + c_2 \text{ ----------[4.31]}$$

Subtracting *[4.30]* from *[4.31]* gives:

$$u_r - u_d = \frac{1}{\mu}\frac{dp}{dx}\left(\frac{y_r^{\,2}}{2} - \frac{y_d^{\,2}}{2}\right) + c_1(y_r - y_d) \text{ ---------- [4.32]}$$

$$c_1 = \frac{u_r - u_d}{y_r - y_d} - \frac{1}{2\mu}\frac{dp}{dx}(y_r + y_d) \text{ ---------- [4.33]}$$

Substituting *[4.33]* in *[4.31]*

$$c_2 = u_d - \frac{1}{\mu}\frac{dp}{dx}\frac{y_d^{\,2}}{2} - \frac{u_r - u_d}{y_r - y_d}y_d + \frac{1}{2\mu}y_d\frac{dp}{dx}(y_r + y_d) \text{ ---------- [4.34]}$$

Substituting *[4.33]* and *[4.34]* into *[4.29]*

$$u = \frac{1}{\mu}\frac{dp}{dx}\frac{y^2}{2} + \left[\frac{y(u_r - u_d)}{(y_r - y_d)}\right] - \frac{1}{2\mu}\frac{dp}{dx}(y_r + y_d)y + u_d - \frac{1}{\mu}\frac{dp}{dx}\frac{y_d^{\,2}}{2} - \frac{u_r - u_d}{y_r - y_d}y_d + \frac{1}{2\mu}y_d\frac{dp}{dx}(y_r + y_d$$

[4.35]

$$h = y_r - y_d \qquad r_s = \frac{u_r}{u_d}$$

$$u = \frac{1}{2\mu}\frac{dp}{dx}(y^2 - (y_r + y_d)y + y_r y_d) - \frac{1-r_s}{h}(y - y_d)u_d + u_d$$ ---------- [4.36]

[4.36] divided by u_d gives:

$$U = \frac{1}{2\mu u_d}\frac{dp}{dx}(y^2 - (y_r + y_d)y + y_r y_d) - \frac{1-r_s}{h}(y - y_d) + 1$$ ---------- [4.37]

It is convenient to introduce dimensionless variables:

$$X = \frac{x}{\sqrt{Rh_0}} \qquad Y = \frac{y}{h_0} \qquad H_{(X)} = \frac{h_{(X)}}{h_{i(0)}}$$

$$\frac{1}{R} = \frac{1}{2}\left(\frac{1}{R_R} + \frac{1}{R_{Di}}\right) \qquad \overline{U} = \frac{U_R + U_D}{2} \qquad U = \frac{\overline{U}}{U_R}$$

$$\lambda_T = \frac{q_T}{\overline{U}h_{i(0)}} \qquad r_S = \frac{U_R}{U_D} \qquad r_R = \frac{R_R}{R_D}$$

$$P = \frac{h_{i(0)}^2 p}{6\mu(U_D + U_R)\sqrt{Rh_{i(0)}}} \qquad \mathrm{K} = \frac{k\,6\mu(U_D + U_R)\sqrt{Rh_{i(0)}}}{h_{i(0)}^2}$$

Referring to the dimensionless variables, the equation for the dimensionless velocity distribution is given as

$$U = \frac{1}{2}\frac{dP}{dX}\left(Y^2 - \left(Y_D + Y_R\right)Y + Y_D Y_R\right) - \left(\frac{1-r_S}{H}\right)\left(Y - Y_R\right) + 1$$ ---------- [4.38]

Here approximations are used for Y_D and Y_R

$$Y_D = \frac{y_D}{h_0} = \frac{1}{2}\left(1 + \frac{2X^2}{1+r_r}\right)$$

$$Y_R = \frac{y_R}{h_0} = -\frac{1}{2}\left(1 + \frac{2r_r X^2}{1+r_r}\right)$$ ---------- [4.39]

Leading to

$$H = Y_D - Y_R = 1 + X^2 \quad \text{---------- [4.40]}$$

If we integrate the velocity distribution across the width of contact, the flow rate per unit length through the nip can be determined from

$$q = \int_{y_R}^{y_D} u \, dy \quad \text{---------- [4.41]}$$

This equation gives a direct relationship between the flow rate, q, through the nip, the pressure gradient, $\frac{dp}{dx}$ within the nip and the gap, $h_{(x, y)}$.

$$q = w \int_0^{h(x)} u(y) dy$$

$$= w \int_0^{h(x)} \left[-\frac{1}{2\mu} \frac{dP}{dx} (h_{(x)} y - y^2) + \frac{y}{b} (u_d - u_r) + u_r \right] dy$$

$$= w \left[\frac{-1}{2\mu} \frac{dP}{dx} \left(\frac{h_{(x)} y2}{2} - \frac{y3}{3} \right) + \frac{y2}{2h_{(x)}} (u_d - u_r) + u_r y \right]^0 h_{(x)}$$

$$= w \left[\frac{-1}{2\mu} \frac{dP}{dx} \left(\frac{{h_{(x)}}^3}{2} - \frac{{h_{(x)}}^3}{3} \right) + \frac{{h_{(x)}}^2}{2h_{(x)}} (u_d - u_r) + u_r h_{(x)} \right]$$

$$= w \left[\frac{-1}{2\mu} \frac{dP}{dx} \frac{{h_{(x)}}^3}{6} + \frac{h_{(x)}}{2} (u_d - u_r) + u_r h_{(x)} \right]$$

$$= w \left[\frac{-{h_{(x)}}^3}{12\mu} \frac{dP}{dx} + \frac{h_{(x)}}{2} (u_d - u_r + 2u_r) \right]$$

$$= w \left[\frac{-{h_{(x)}}^3}{12\mu} \frac{dP}{dx} + \frac{h_{(x)}}{2} (u_d + u_r) \right]$$

i.e $q = w\left[U_m h_{(x)} - \frac{h_{(x)}^{\ 3}}{12\mu}\frac{dP}{dx}\right]$ where $U_m = ½ (u_d+u_r)$

I.e. Discharge per unit width is

$$q = U_m h_{(x)} - \frac{h_{(x)}^{\ 3}}{12\mu}\frac{dP}{dx}$$

$$q = \frac{u_d + u_r}{2} h_{(x)} - \frac{h_{(x)}^{\ 3}}{12\mu}\frac{dP}{dx} \text{ ---------- [4.42]}$$

After integration and rearranging of *[4.42]* as shown above, we obtain

$$\frac{dp}{dx} = \frac{12\mu}{h_{(x)}^2}\left[\frac{u_d + u_r}{2} - \frac{q}{h_{(x)}}\right] \text{ ---------- [4.43]}$$

In deformable roll coating, it is assumed that deformation ***δ (x)*** of the rubber sleeve varies linearly with pressure ***p(x)*** regardless of the thickness of the sleeve ***b***, we can write:

$$\delta(x) = \frac{b}{E} p(x) = k \cdot p(x) \text{ ---------- [4.44]}$$

E is the static Young modulus of the rubber material.

Now the flow gap h(x) can be expressed as the difference between the gap deformation and the initial gap set or:

$$h_{(x)} = \delta - h_{i(x)} \text{ ---------- [4.45]}$$

From geometry of the system we have:

$$h_{i(x)} = h_{i0} - \left[\left(R_{Di} - \sqrt{R_{Di}^2 - x^2}\right) + \left(R_R - \sqrt{R_R^2 - x^2}\right)\right] \text{ ---------- [4.46]}$$

Therefore

$$h_{(x)} = \delta_{(x)} - h_{i(x)} =$$

$$\delta_{(x)} - \left(h_{i(0)} - \left[\left(R_{Di} - \sqrt{R_{Di}^2 - x^2} \right) + \left(R_R - \sqrt{R_R^2 - x^2} \right) \right] \right) \text{---------- [4.47]}$$

If we substitute *equation [4.45]* into *equation [4.43]* then we obtain equation describing elastohydrodynamic lubrication, thus

$$\frac{dp}{dx} = 12\mu \left[\frac{u_d + u_r}{2\left(\delta_{(x)} - h_{i(x)}\right)^2} - \frac{q}{\left(\delta_{(x)} - h_{i(x)}\right)^3} \right] \text{---------- [4.48]}$$

If we substitute *equation [4.44]* into *equation [4.48]*, we obtain

$$\frac{dp}{dx} = 12\mu \left[\frac{u_d + u_r}{2\left(kp - h_{i(x)}\right)^2} - \frac{q}{\left(kp - h_{i(x)}\right)^3} \right] \text{---------- [4.49]}$$

In terms of dimensionless variables *equation [4.49]* becomes

$$\frac{dP}{dX} = \frac{1}{\left[\mathrm{KP} - 1 + X^2\right]^2} - \frac{\lambda_T}{\left[\mathrm{KP} - 1 + X^2\right]^3} \text{---------- [4.50]}$$

This is the final equation (*equation [4.50]*) we need to solve to calculate λ_T (the flux metered and which ends up as a film on the rollers, equal split if the two rollers are going at the same speed) by integrating P subject to knowing pressure boundary conditions at inlet and outlet.

4.4 Simulation on forward roll coating with a positive gap

4.4.1 Introduction

Forward roll coating is used in many of the processes to apply coatings. The current trend is to increase the application speed. Errors like ribbing occur more frequently with higher application speeds. A model could help to predict errors up front. Current models found in literature are based on finite elements. Yet these models

cannot predict a splashing of the fluid, and require an initial prediction of the meniscus. These problems could be solved by using a finite volume model. This study describes the first setup of a finite volume model to predict errors that can occur in forward roll coating. This is only an initial investigation and the study describes a 2-D model of a forward roll coating process with rigid rolls and a positive gap. The model was developed in OpenFoam, an open source computation fluid dynamics package. At the very beginning of the activity, some simulations were performed in CFX, yet these did not give a reliable result.

4.4.2 Setup of the simulation

The numerical grid of the gap section between the rolls was created in Gmesh, an open-source mesh-generator. The gap direction was assumed to be vertically positioned, with the bottom half of the roll submerged in the liquid (*Figure 4-4*).

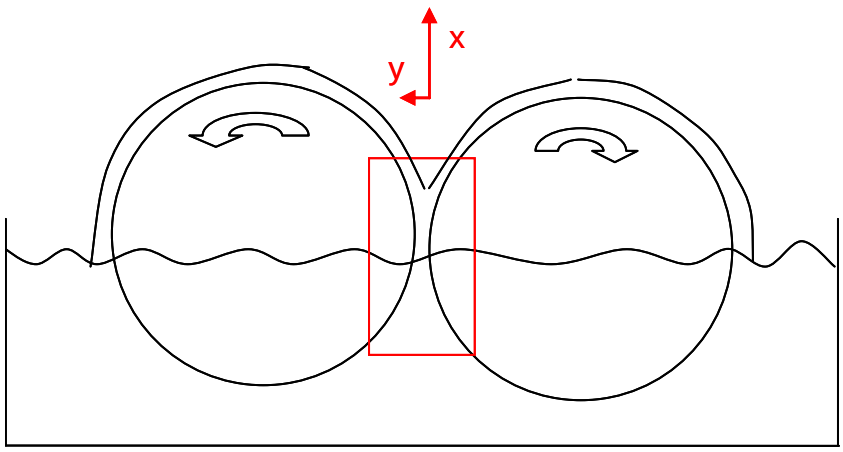

Figure 4-4 Overall view of the rigid roll coating process

An overview of the boundary conditions on the simulations can be seen in *Figure 4-5*.

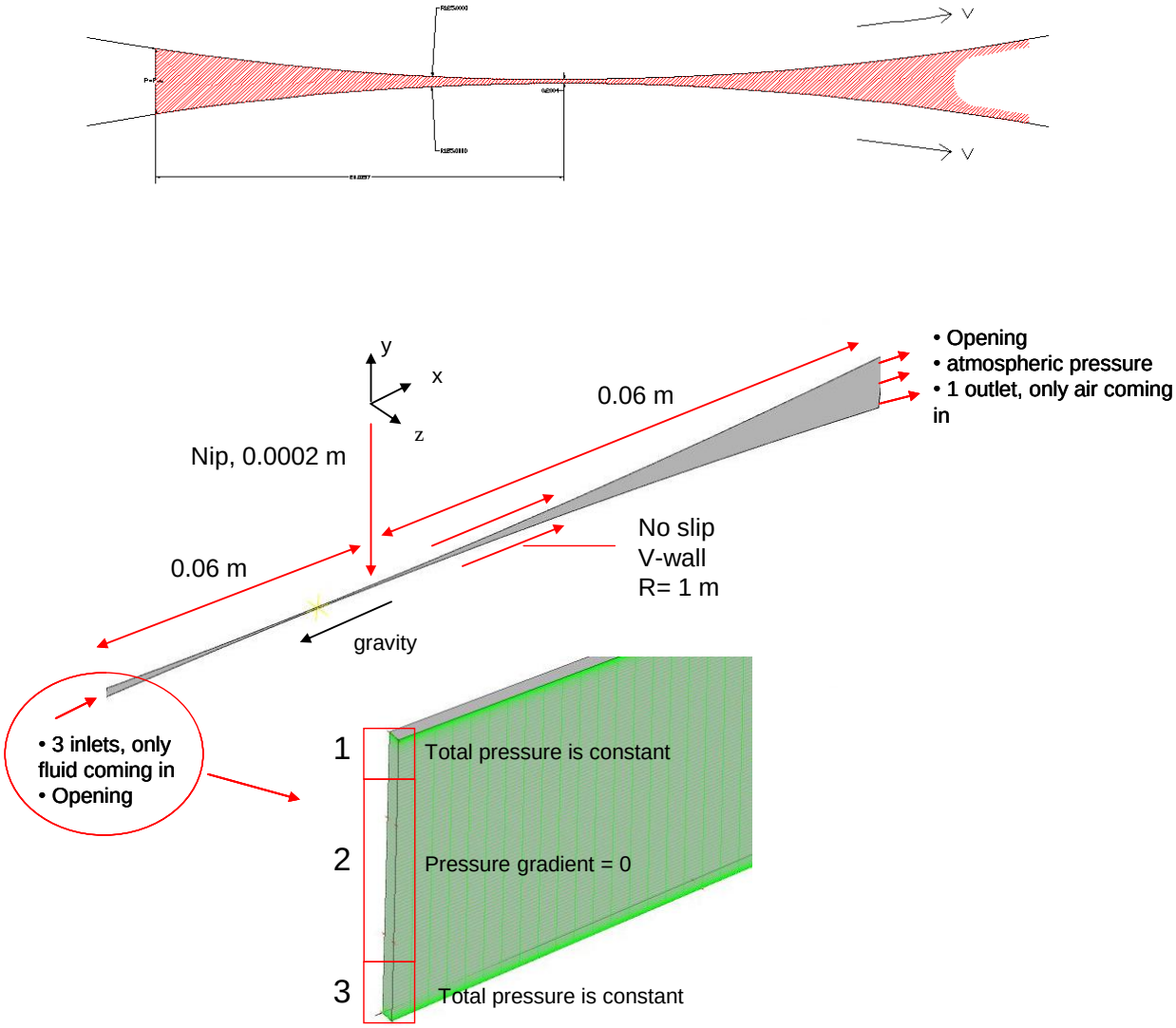

Figure 4-5 Overview of the boundary conditions

At the top outlet of the rolls an opening boundary condition is assumed where an atmospheric pressure of P_0 is imposed and both fluids (liquid and gas) can freely move in and out of the domain. If the fluid moves into the domain (in case of recirculation), the liquid fraction is set to zero, which implies that at the top outlet only air can flow back in between the rolls. The inlet of the model at the bottom of the rolls also is an opening boundary, however, now the inward moving fluid is

assumed to be only liquid. Imposing a total pressure over the whole inlet would cause an over-determined system, because the pressure at the inlet should follow from flow distribution caused by the flow pattern at the inlet. For this reason, a total pressure equal to the hydrostatic pressure was set only over two slides near the rolls (referred to as section 1 and 3 in *Figure 4-5*). Over the mid section 2, a zero pressure gradient was imposed. In this way, a naturally inflow of fluid was established in which liquid is allowed to move in and out of the system depending on the local flow conditions. It was assumed that the flow in between the rolls was laminar because the Reynolds number, based on the gap width and the fluid velocities relatively to the rolls, is smaller than 1.

Since the position of the meniscus was unknown, the distance before and after the gap were varied. For the same reason, the element size was varied across the height and across the length. In the end, the mesh size was about 300,000 hex elements. Since the element size is small, the courant number easily becomes larger than 1, which would give instability problems with the solver. To prevent this, the time step must be kept small, 1E-5 s. This results into long calculation times (on 4 CPU around 5-7 days).

Currently a Newtonian fluid was used with a fixed viscosity. The surface tension was set to 30 mN/m and the contact angle was set to (first guess) 45°. Two series of simulations were run to test the model on the position of the meniscus. First, the viscosity of the liquid was varied from 50-200 mPa.s. After this, a second series (viscosity= 150 mPa.s) was run with different capillary numbers from 1-10 (varying the roll speed 2-20 rpm).

4.4.3 Results: variation of viscosity

In the first series the viscosity was varied from 50-200 mPa.s. A simulation was found to have converged when the average of the liquid fraction across the domain was constant. A global flow field can be seen in *Figure 4-6*.

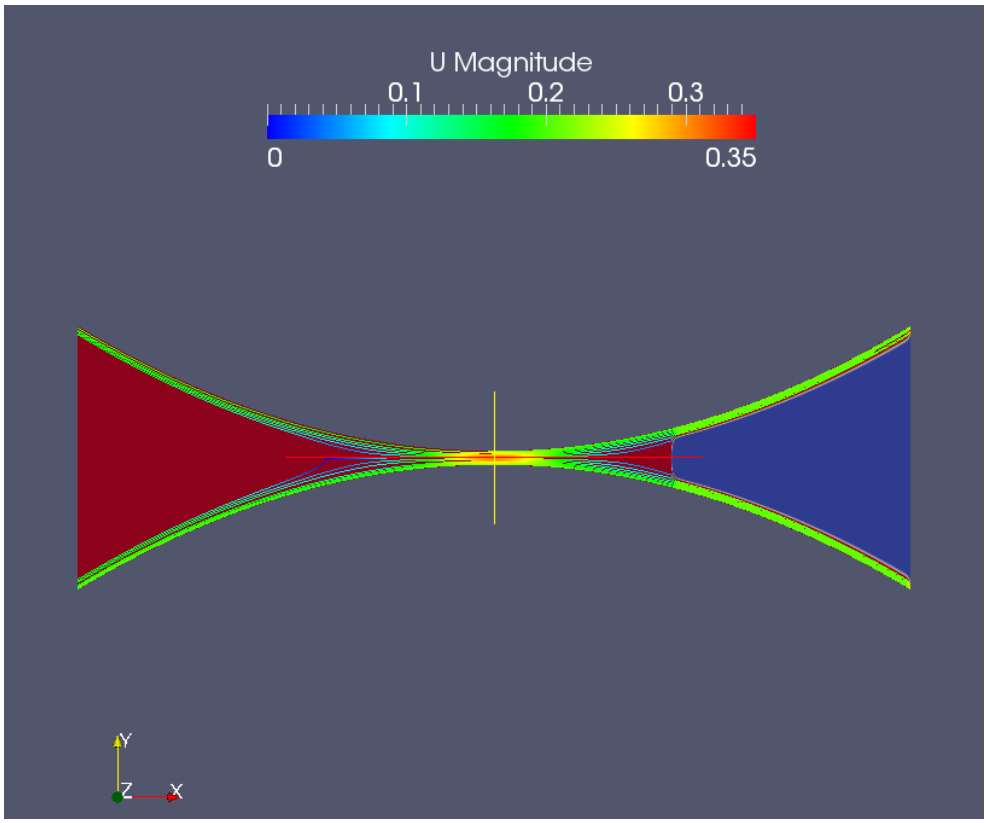

Figure 4-6 Global overview of a flow field (150 mPa.s, 2rpm)

The position of the meniscus is shown in *Figure 4-7*. The figure shows the volume fraction across the centre line of the model (y coordinate =0 m).

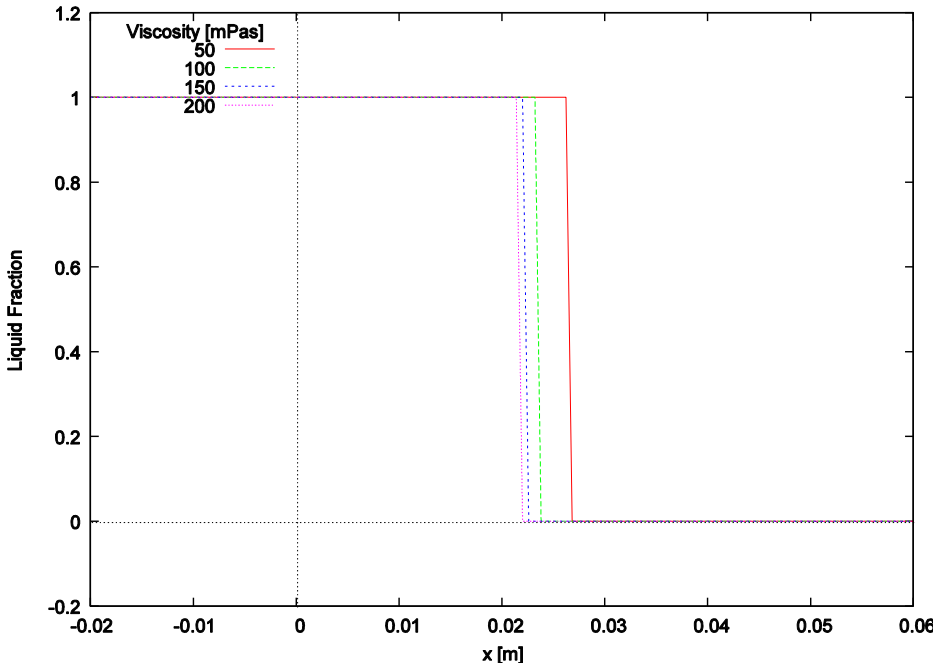

Figure 4-7 Position of the meniscus with increasing viscosity

Figure 4-7 shows that the meniscus moves towards the gap as the viscosity is increased. The reason for this can be found when the situation just before the meniscus is inspected. *Figure 4-8* shows a recirculation that is formed when the viscosity drops below the 50 mPa.s, which coincides with a capillary number of about 0.35.

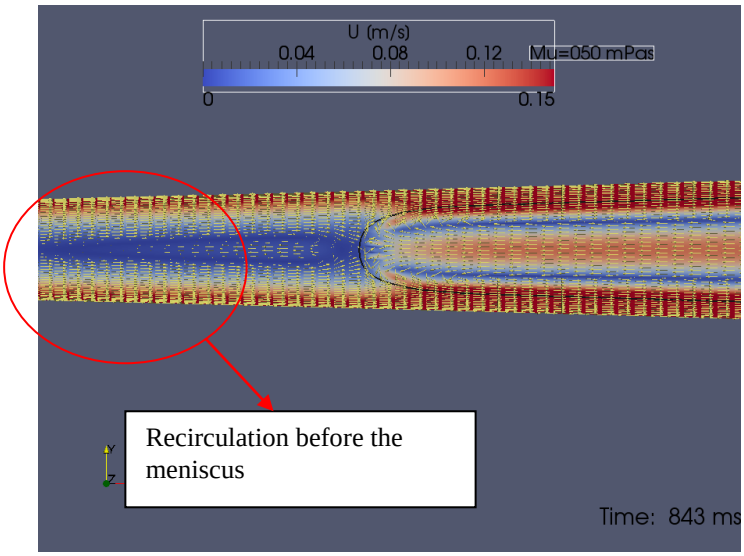

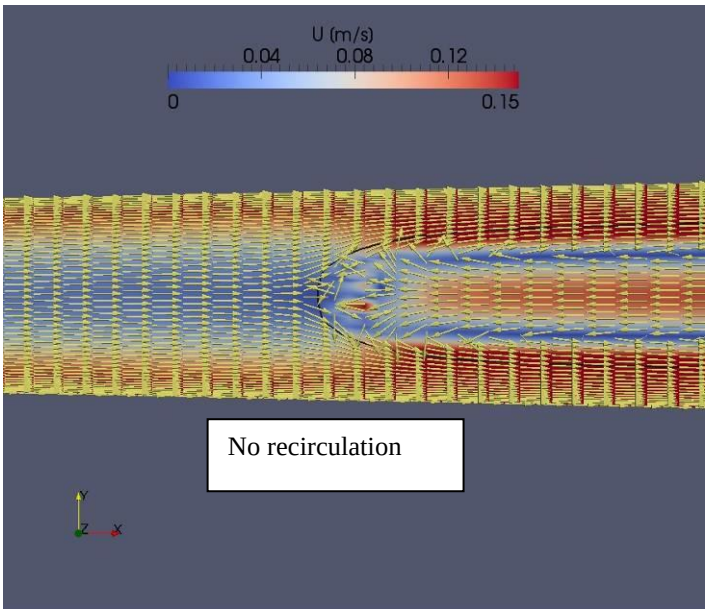

Figure 4-8 Comparison of the situation just before the meniscus. Top: viscosity=50 mPa.s bottom: viscosity =200 mPa.s

Due to the recirculation, the meniscus is pushed further away from the gap. This is supported by findings in literature [39]. *Figure 4-9* show in more detail, how the velocity profiles look at fixed positions before and after the gap.

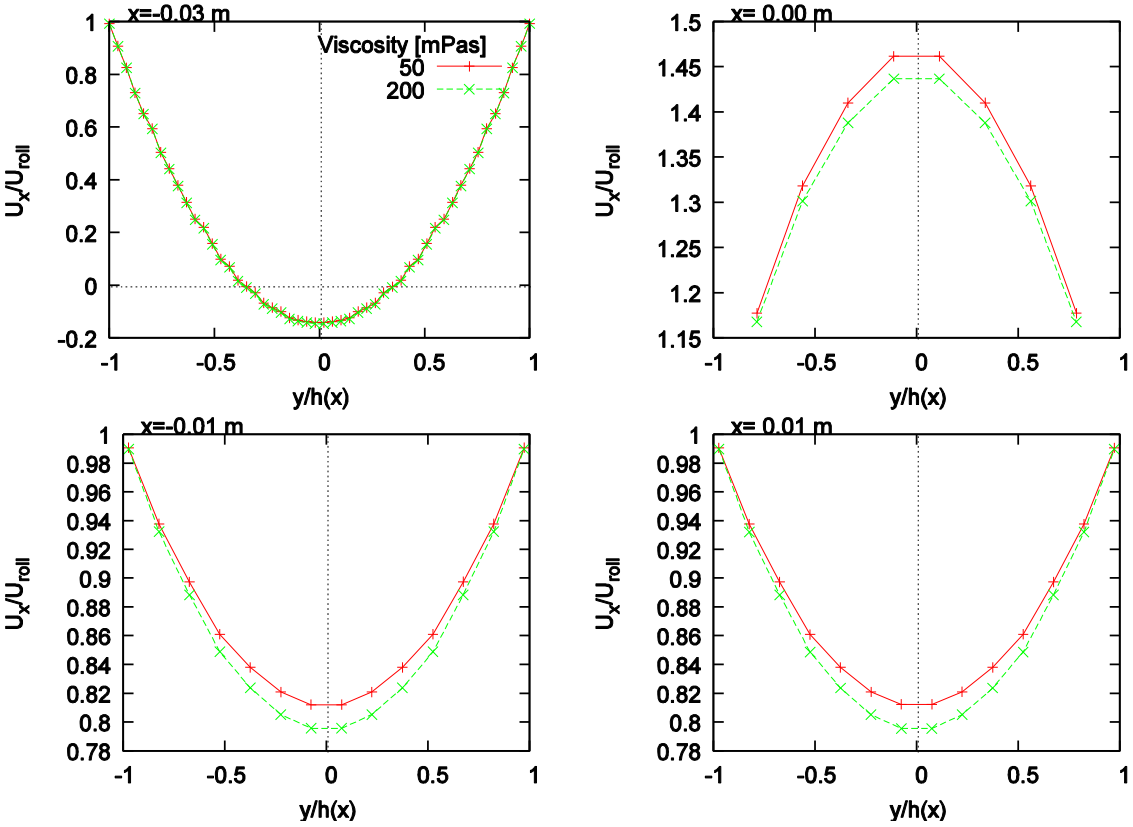

Figure 4-9 Velocity profiles just before and after the gap

It can be seen that the fluid is first dragged in by the rolls (higher velocity at the wall as in the middle) and then pushed through the nip. These distributions are linked to the pressure distribution across the x-axis (*Figure 4-10*).

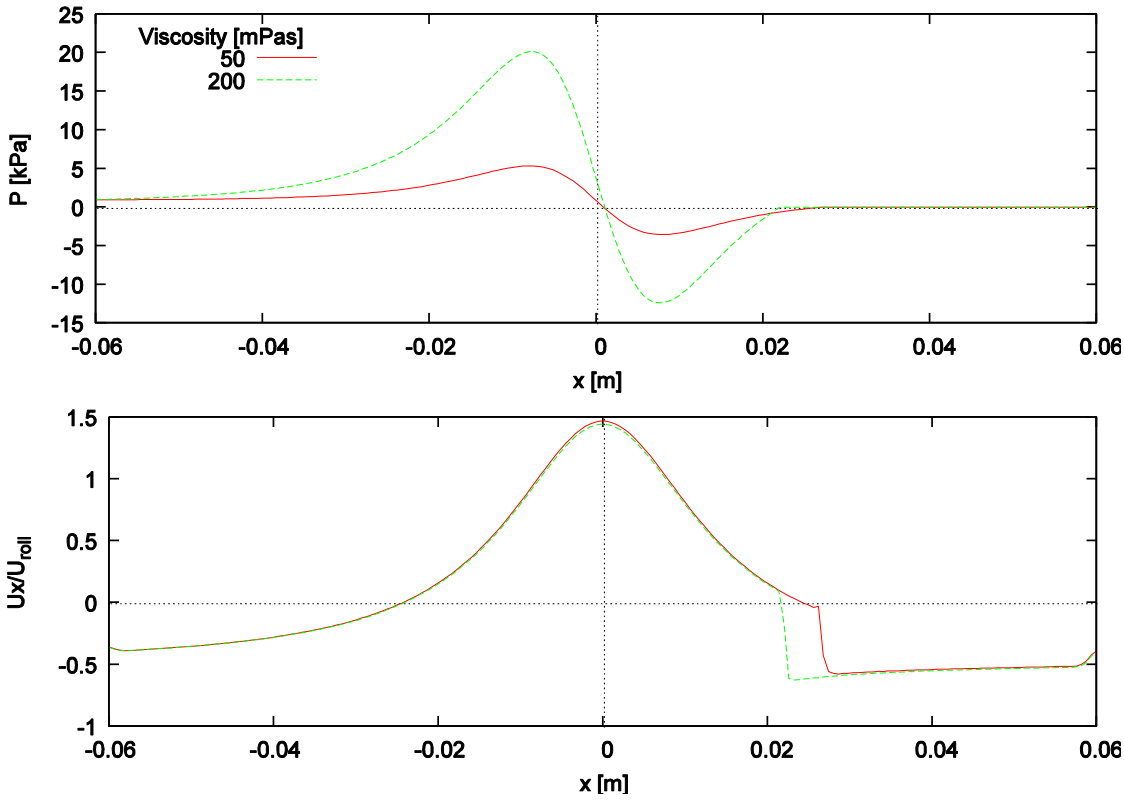

Figure 4-10 Pressure distribution and velocity across the x-axis (y=0m)

Figure 4-10 shows that a lower pressure creates a possibility for recirculation, driving the meniscus further away from the gap. Next, the film thickness on the top roll is evaluated. In order to determine the thickness of the film, the volume fraction across a line (from the centre of the top roll to a position well behind the meniscus) is plotted. The results can be found in *Figure 4-11*.

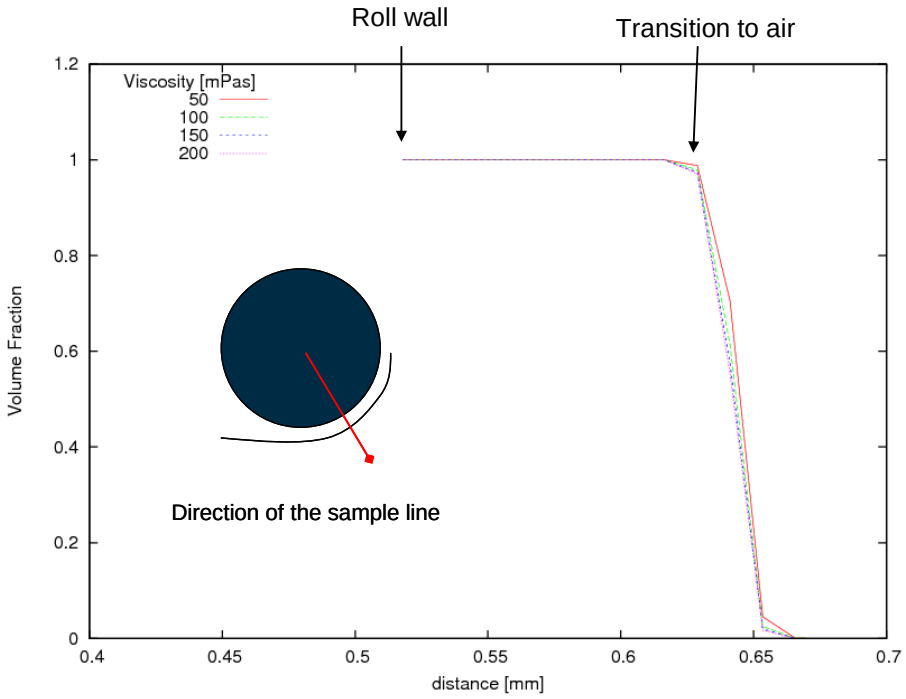

Figure 4-11 Determination of the film thickness

Figure 4-11 shows that the thickness of the film does not depend on the viscosity. This is confirmed by literature. Closer examination of the data shows a film thickness of about 0.086 mm.

4.4.4 Results: variation of roll speed

In a second series of simulations, the roll speed of both rolls was increased from 2 to 20 rpm. This leads to a variation in capillary number from 1 to 10. The viscosity was 150 mPa.s. *Figure 4-12* shows the position of the meniscus. The volume fraction is set out across the x-axis (y-coordinate=0 m).

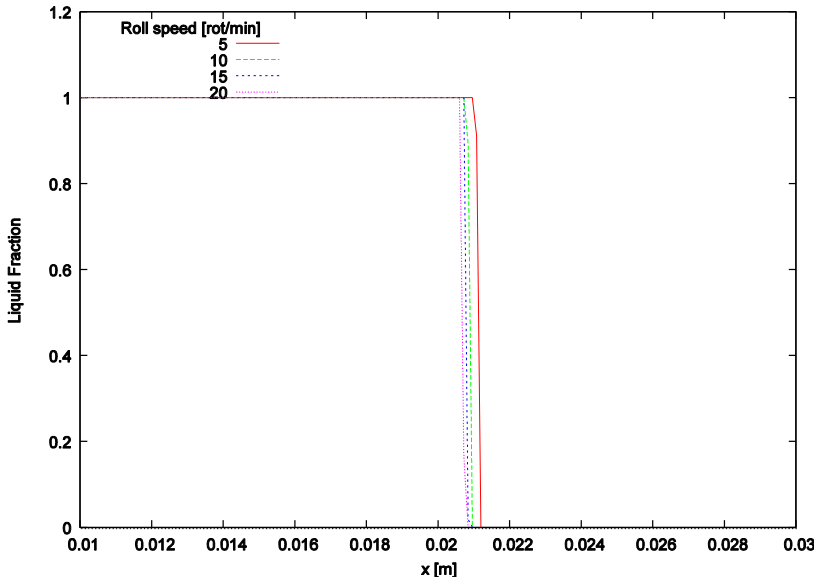

Figure 4-12 Position of the meniscus

Figure 4-12 shows that although the differences are not so explicit, an increase in roll speed leads to a reduced position of the meniscus. The velocity field just before the meniscus can be seen in *Figure 4-13*.

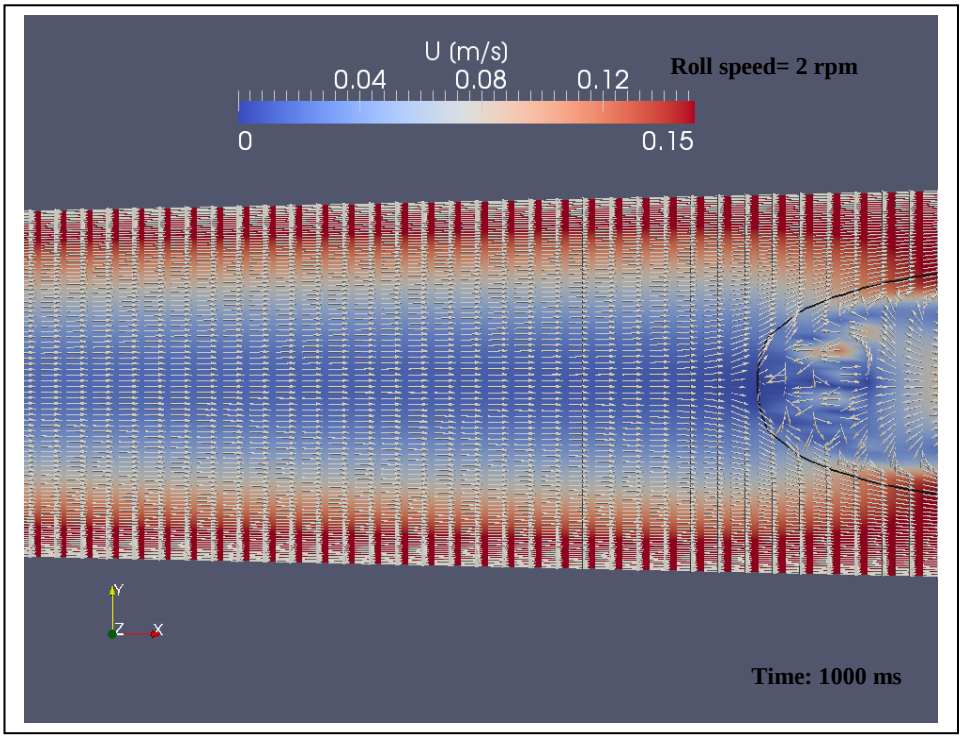

A large area with lower velocities, start of a recirculation zone. This picture is slightly moved to the right, to see the meniscus.

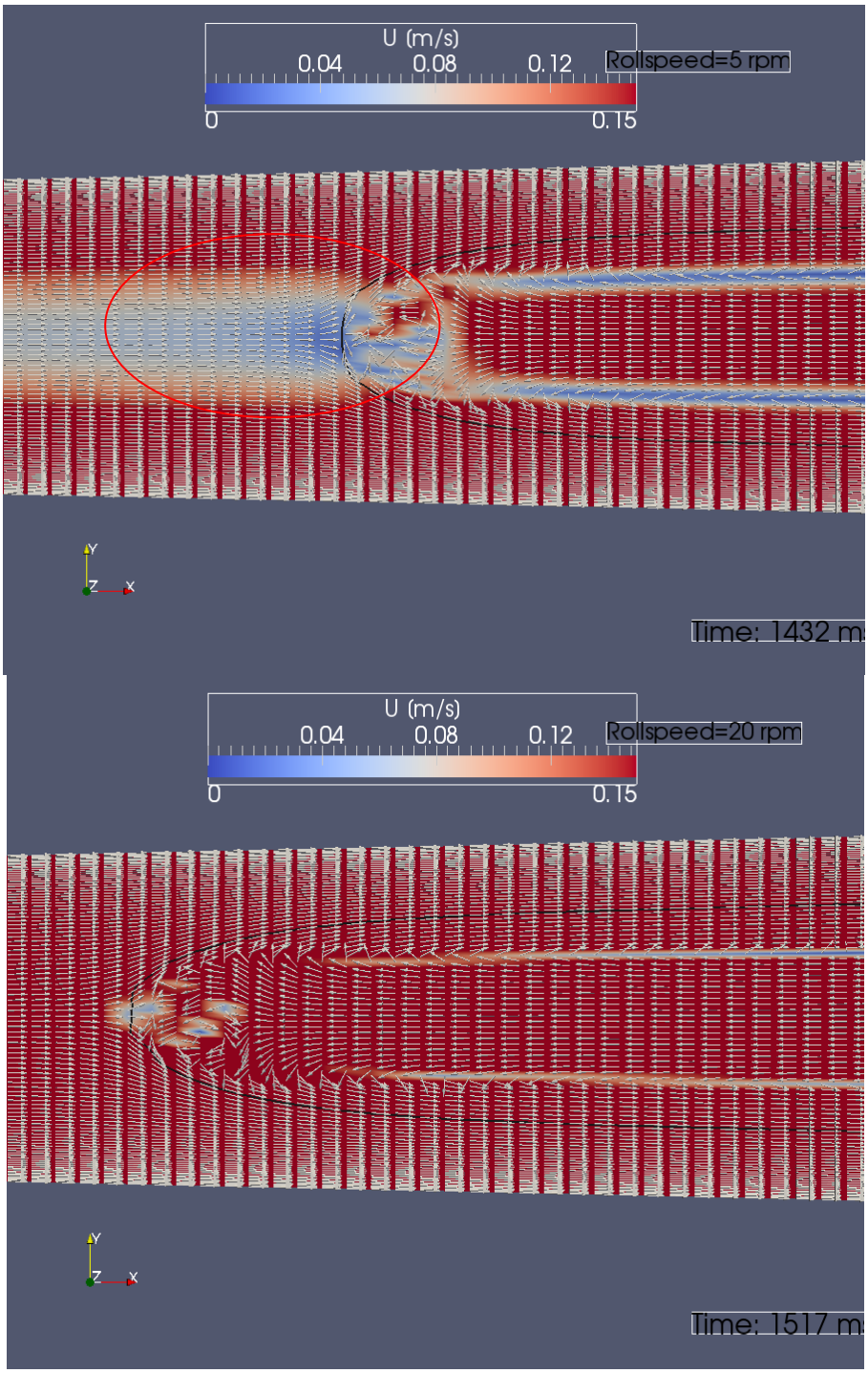

Lower velocities, start of a recirculation area.

Figure 4-13 Velocity field just before the meniscus, 2 rpm top, 5 rpm middle, 20 rpm bottom

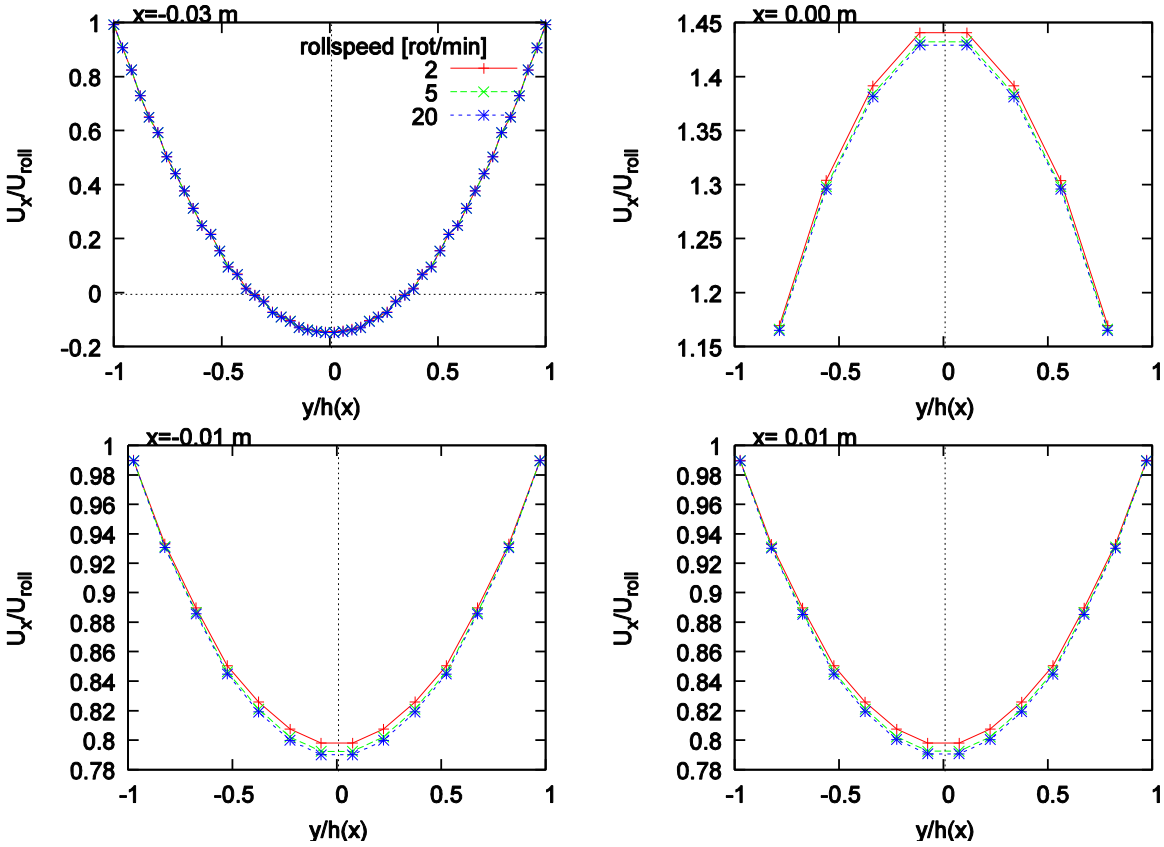

Figure 4-14 Velocity profiles just before and after the gap

This is caused by the same reason as mentioned before, a lower pressure drives the meniscus further backwards towards the outlet, in case of lower roll speeds. The same image is seen when the pressure distribution is studied (*Figure 4-15*).

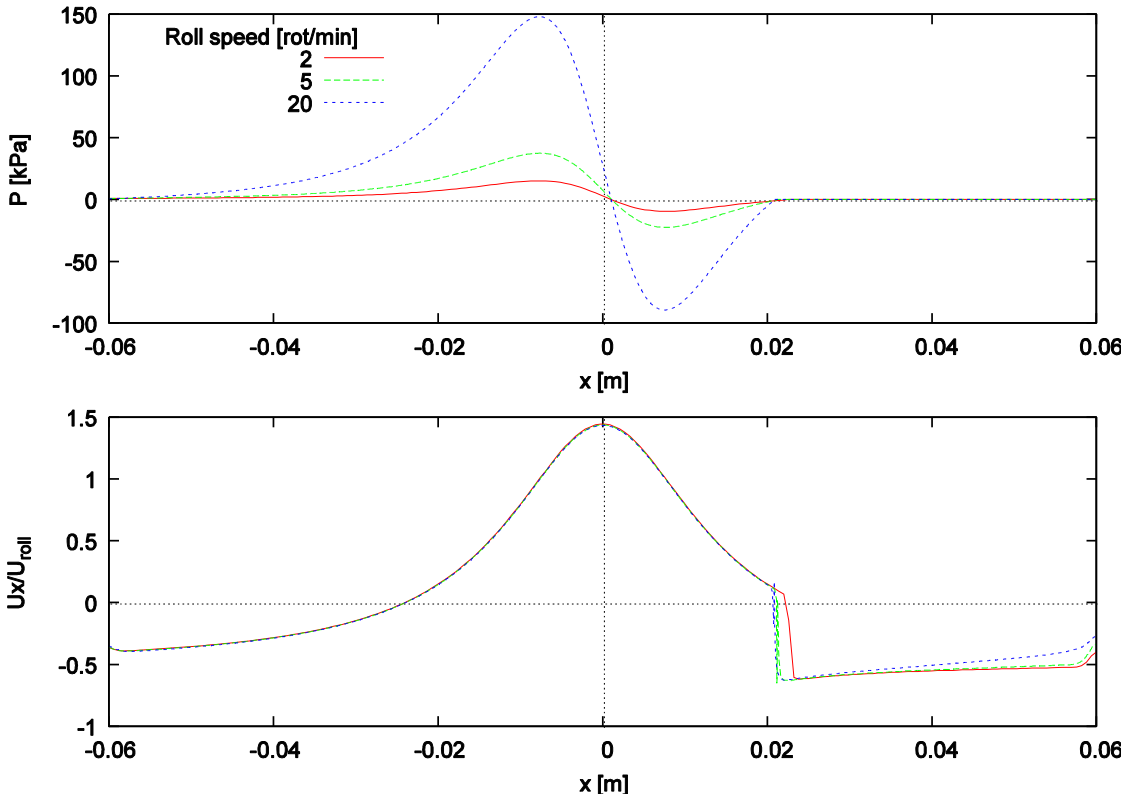

Figure 4-15 Pressure distribution and velocity across the x-axis (y=0m)

Figure 4-15 shows that a bigger difference is seen in the position of the meniscus when the velocity is increased from 2 to 5 rpm then from 5 -20 rpm. This is again the result of a lower capillary number, the appearance of recirculation areas. This was also confirmed by literature, see *Figure 4-17*.

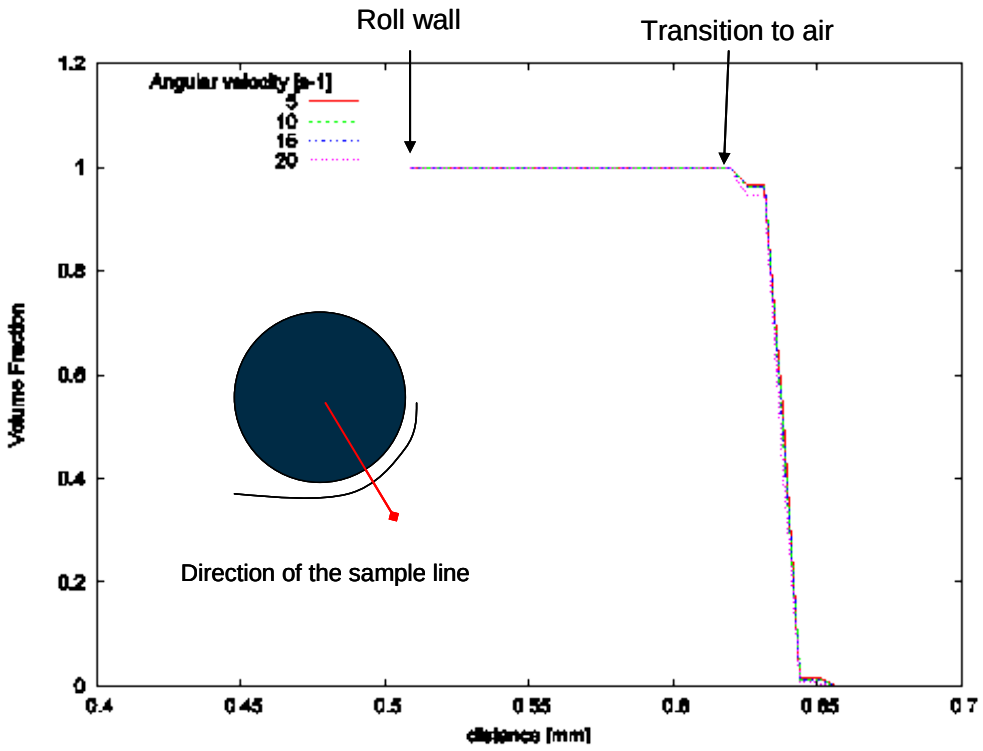

Figure 4-16 Thickness of the film on the top roll

Figure 4-16 shows that, when the velocity of both rolls is increased there is no influence on the thickness of the film after the gap.

4.4 Comparison with literature

Next, the results of these eight simulations are compared with data found in literature [39]. The results are compared on the position of the meniscus (split position), and on the flow rate through the gap (*Figure 4-17* and *Figure 4-18*). Relations used to create these figures:

- Capillary number=Ca= $\frac{\mu * \overline{V}}{\sigma} = \frac{\mu * (\frac{1}{2} * (V_{top} + V_{bottom})}{0.03E-3}$ ---------- [4.49]

- roll velocity= $V_{top} = 2 * \pi * R_{top} * n_{top}$, with n in rotations per sec second---- [4.50]

- $\tan(\theta) = \frac{X}{\sqrt{RH_0} * \sqrt{2}}$ ---------- [4.51]

Where X is the split position (m) and H0 is half of the gap (m).

- Flow rate = $\lambda = \frac{\frac{1}{2} * \int_{H1}^{H2} U dy}{\overline{V} * H_0}$ ----------[4.52]

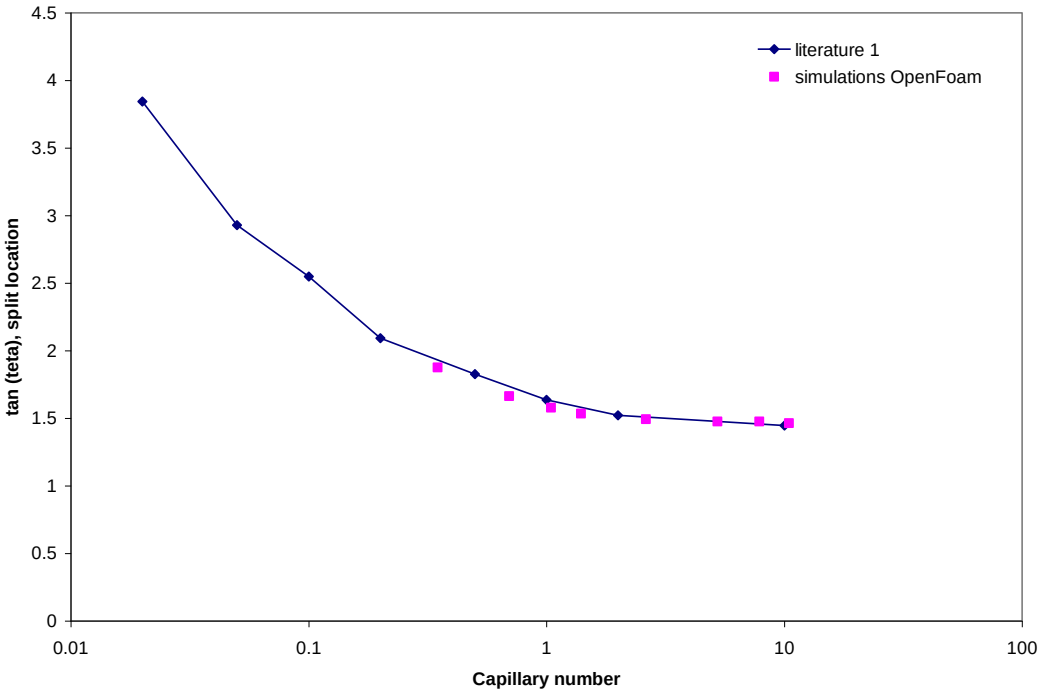

Figure 4-17 Position of the meniscus in relation to the capillary number

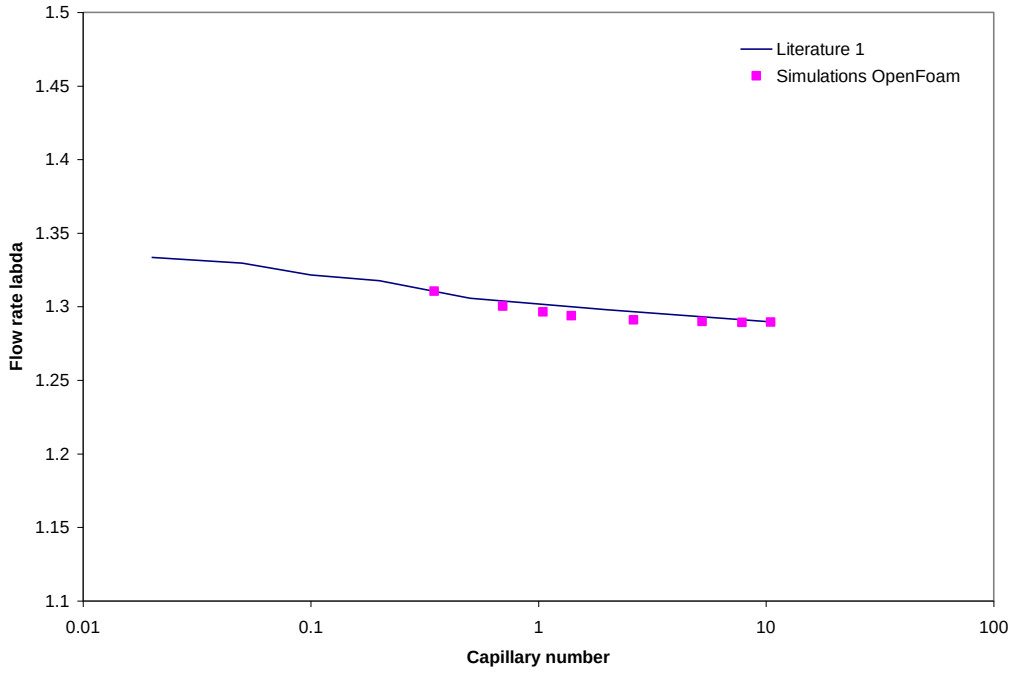

Figure 4-18 Normalised flow rate in relation to the capillary number

Both the figures show a good agreement between the data from the literature and the simulations that were performed with OpenFoam. The data that was used for the graph is the data that is valid for asymptotic results. This means that the value $(H0/R)^{1/2} \to 0$. In our case this is nearly correct: 1E-7. The raw data for the graphs can be found in appendix 1.

4.5 Conclusions and recommendations

A reliable model was created in OpenFoam 2.0.1. Results were:

- When the viscosity is increased, the position of the meniscus moves towards the gap.

- When the velocity is increased, the position of the meniscus moves towards the gap.

- Both viscosity and roll velocity seem to have no effect on the film thickness, taking into account that both rolls have the same velocity.

Chapter 5 : EXPERIMENTAL RESULTS AND DISCUSSION

5.1 Introduction

This chapter presents the results of the experimental programme carried out in this study. The approach was not only to develop a fundamental understanding of flow and stability in deformable roll coating for low to very high speeds but also to put it in the context of the coating of steel coils. To that effect, an integral part of the study was to characterise the industrial paints used in steel coil coating in order to inform the choice of the model fluids to be used in the experimental rig. Also, in order to test the validity of the finding in the experimental rig, industrial trials were carried out in a pilot plant. This was to inform the application of the data collected on the rig to actual industrial practice.

In the experimental programme, Newtonian and non-Newtonian fluids were used as the coating fluids, while film thickness and stability measurements were taken over a wide range of operating conditions. These measurements were performed on a roll coater specially designed for this study. As discussed in chapter 3, the coater did not have a good substrate handling capability. Thus the film thickness measured were those formed on the rotating rollers and stability was assessed by observing the flow and films formed. The data were processed using dimensionless analysis into correlations for the total flux and flux ratios which were then compared with theoretical predictions and experimental correlations from previous studies.

In the pilot plant trials, the measurements were taken on the steel substrates rather than on the rollers. In particular, instability was judged on the basis of visual

observation of samples of the coated steel coils. This is indeed the real test in actual practice.

5.2 Coatings used & their characterisation

Coating formulations are usually a complex mix of solvents or water, the particulates or macromolecules that are to be coated, additives and the binder that will hold the particulate together into the final dry or cured film. These formulations are thus non-Newtonian and their rheological behaviour must be established under conditions that occur during roll coating, where rapid high shear and elongation rates develop. The rheological characterisation should thus include the determination of high strain rate viscosity, elasticity and tensile behaviour. All these were measured during this programme.

In order to make the study relevant to academic aspects as well as the coating of steel, two representative industrial coating formulations were used. The first step was to characterise these formulations rheologically then develop model fluids which are equivalent to these formulations and also consider variations from these behaviours.
The two industrial coating formulations chosen are:

- Water based pre-treatment primer- Newtonian fluid (WBPP)
- Electron Beam Radiation curable topcoat - non-Newtonian fluid (EBR)

5.2.1 Industrial coatings

Water based pre-treatment primer (WBPP)

The rheology was measured with an Anton Paar rotational rheometer (MCR501 SN80061700) in a range of shear and temperatures with the coating stirred before measurement to prevent sedimentation of pigments. The solid content by weight for

the pre-treatment primer (WBPP) was measured to be 56±1%. *Figure 5-1* displays the viscosity flow curve measured at ambient temperature (20°C) indicating a strong shear thinning behaviour reaching a lower viscosity plateau of 0.035 Pa.s at about 500 s^{-1} shear rate. This suggests that during the coating operation (a high shear rate flow), the WBPP behaves essentially as a Newtonian fluid with a viscosity of 0.035 Pa.s. This makes finding a model fluid for WBPP a straight forward task.

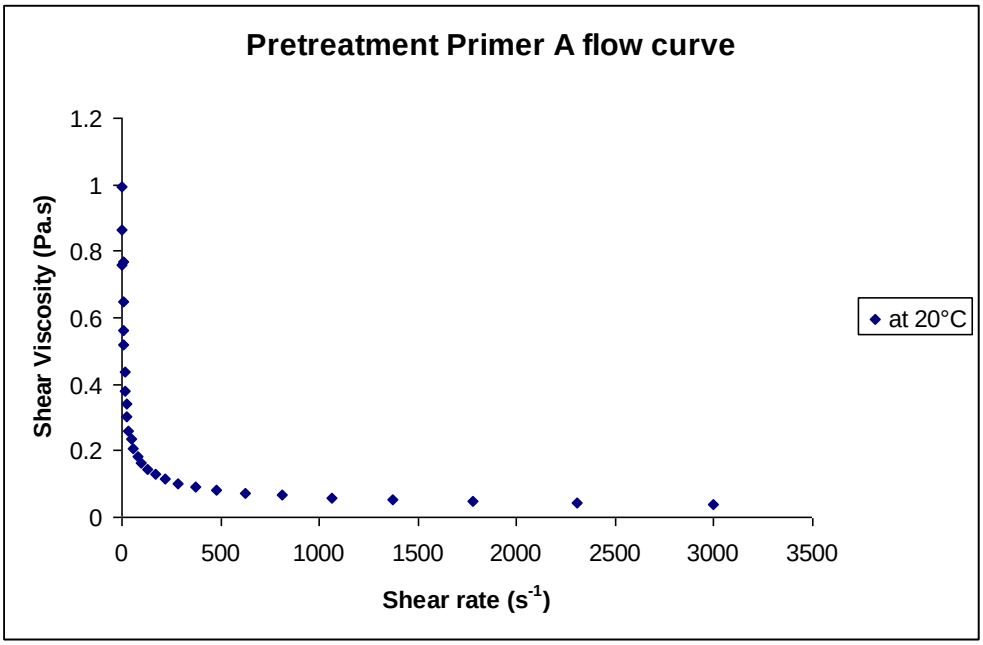

Figure 5-1 Flow curve for pre-treatment primer (WBPP) at 20°C

Electron beam radiation curable (EBR) topcoat

Different radiation curable coatings (representative industrial formulations) were rheologically characterised in the earlier stage of the study. An electron beam (EB) coating was chosen from this screening as the preferred option because it meets the industrial criteria for high speed coating, in particular a fast curing capability [7]. The challenges with this type of coating are high viscosity and elasticity, therefore the possibility of restriction in getting a very thin uniform layer at high speeds and the need to carry out both shear and elongational rheological characterisation.

Shear rheometry results

The results of the measurements, carried out in an Anton Paar rotational rheometer (MCR501 SN80061700) with cone and plate geometry (as shown in Fig 3.28), are presented in *Figure 5-2*. They too show a strong shear thinning behaviour to begin, which levels off to a low viscosity plateau of 0.350 Pa.s after a shear rate of about 500 s^{-1}. The electron beam (EB) coating is thus more viscous than the pre-treatment primer coating (WBPP) and will be difficult to roll coat to achieve a thin uniform film of 10-20 µm at high speeds. As indicated in the literature survey, viscous fluids are known to display ribbing instabilities in roll coating at high speeds. There will be a need during industrial applications to reduce this viscosity, by heating. *Figure 5-3* which gives shear viscometry results carried at various temperatures shows how the appropriate temperature may be chosen. This data, carried out at constant shear rate of 50 s^{-1} will need to be supplemented in actual practice with the data at higher shear rates (typically 1000 s^{-1} and higher).

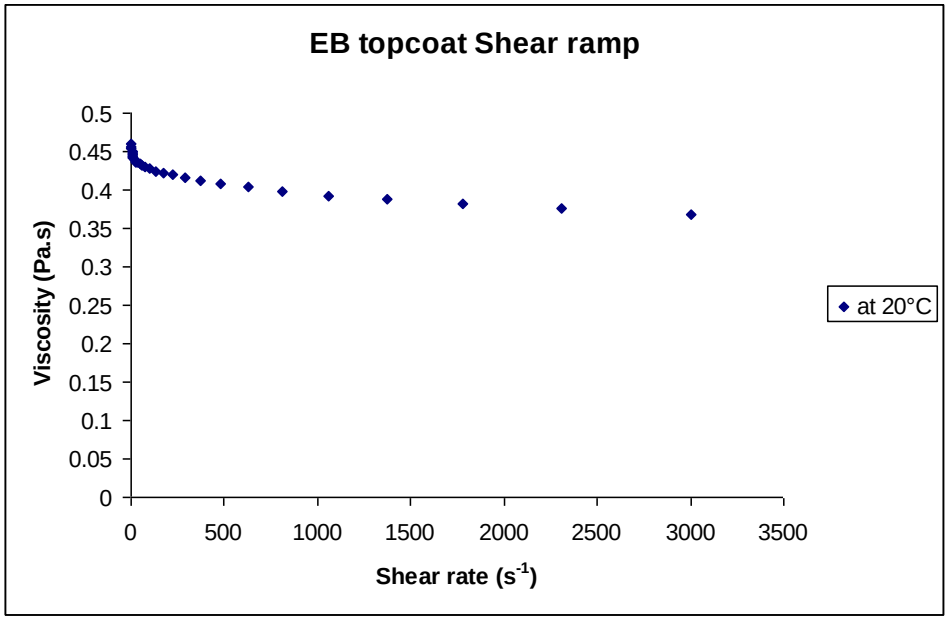

Figure 5-2 Flow curve for EB topcoat coating

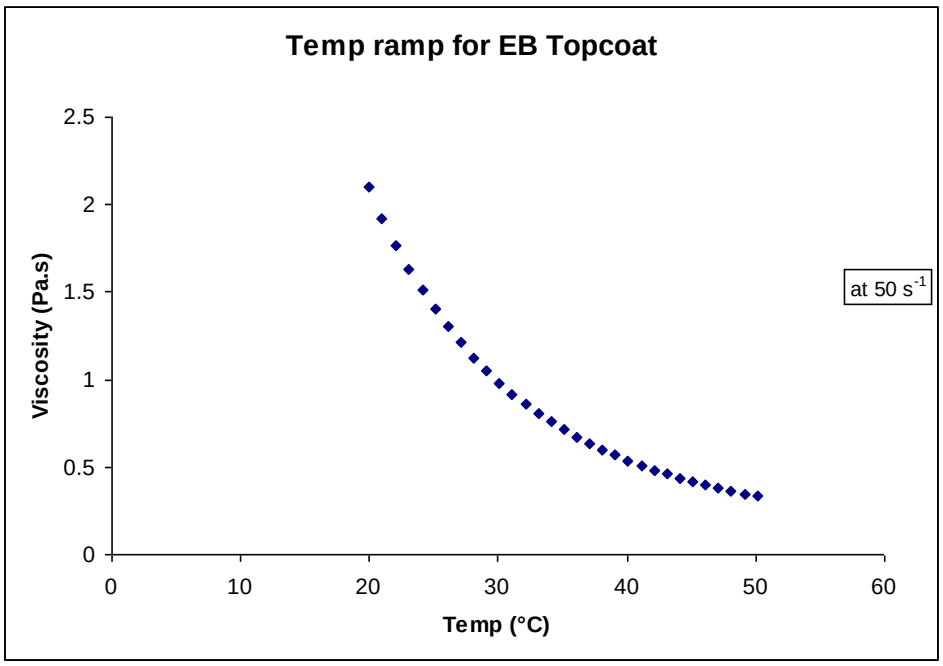

Figure 5-3 Temp ramp for EB topcoat

Although the EBR coating displays a constant viscosity at high shear rate, its behaviour under extension needs to be evaluated as it is manifestly elastic to start with. This is explained in following sections.

Capillary breakup extensional (CaBER) results

As explained previously (*section 3.7.3*), CaBER rheometry is based on the formation of an unstable fluid filament (see *Figure 5-4*) by imposing a rapid axial step-strain of prescribed magnitude and mode (linear or exponential as shown in *Figure 5-5*)

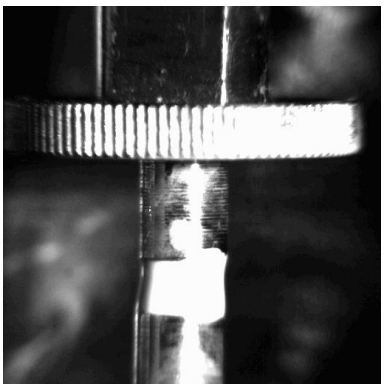

Figure 5-4 Image of CaBER experiment with EB coating

Figure 5-5 Stretch profiles used in CaBER experiments

The following relationships describe the linear and exponential stretch profiles:

$$h(t) = h_0 + (h_f - h_0)\frac{t}{t_s}$$

$$h(t) = h_0 + \frac{(h_f - h_0)\ e^{(t\,R)-1}}{e^{(t_s\,R)-1}}$$

h_0 = initial height in mm, h_f = final height in mm t = actual time in ms,

t_s = strike time in ms, R = Fundamental rate in 1/s

In the experiments, 4 mm diameter plate geometry was used with a 1.99 mm initial sample height at 20°C temperature. The final sample height was measured at 8.91 mm, with a maximum of 80 ms linear strike time and a Hencky strain of 1.50. *Figure 5-6* shows the temporal evolution of the mid-filament diameter of the EB coating, which is decreasing with time. The solid lines are Papageorgiou's fits [122] used in the calculation of the transient viscosity. This data enable the computation of

extensional viscosity parameters (*see equations in Chapter 3*) which are displayed in *Figure 5-7* and *Table 5-1*.

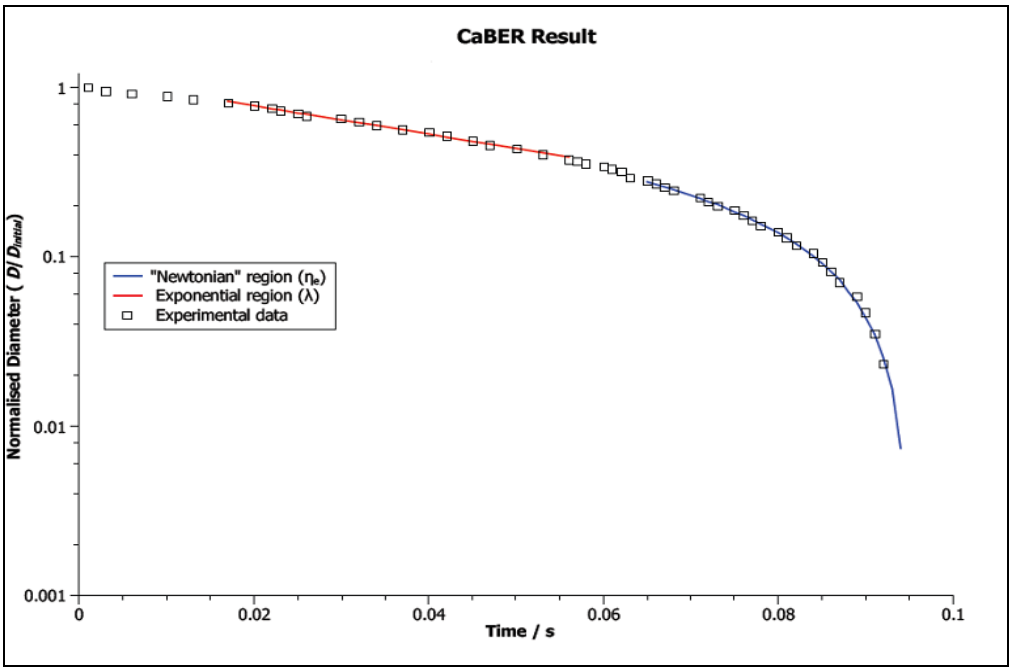

Figure 5-6 Mid-filament diameter for EB coating (from CaBER results)

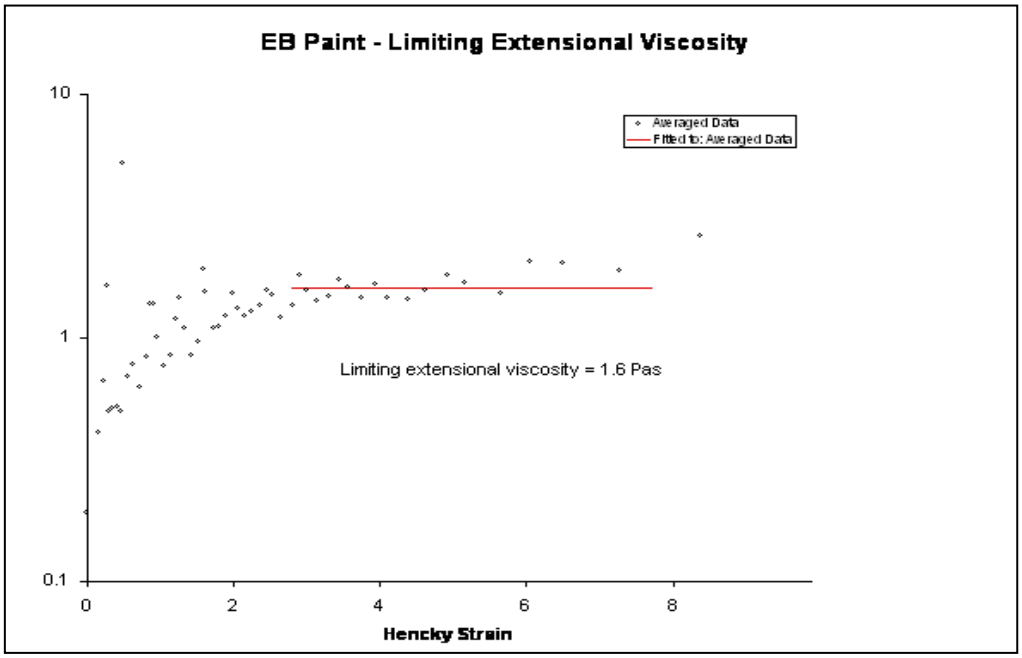

Figure 5-7 Limiting extensional viscosity for EB paint

Table 5-1 CaBER results for EB coating

	λ(relaxation time) /ms	η_E (extensional viscosity) /Pa.s
Mean	17.33	1.601
σ (standard deviation)	2.07	0.068
max	20.5	1.857
min	14.6	1.671

Figures 5-8 and 5-9 give data showing how the extensional viscosity and the relaxation time decrease (exponentially) with increasing temperature. This change is not permanent and found to be reversible when the temperature was ramped back.

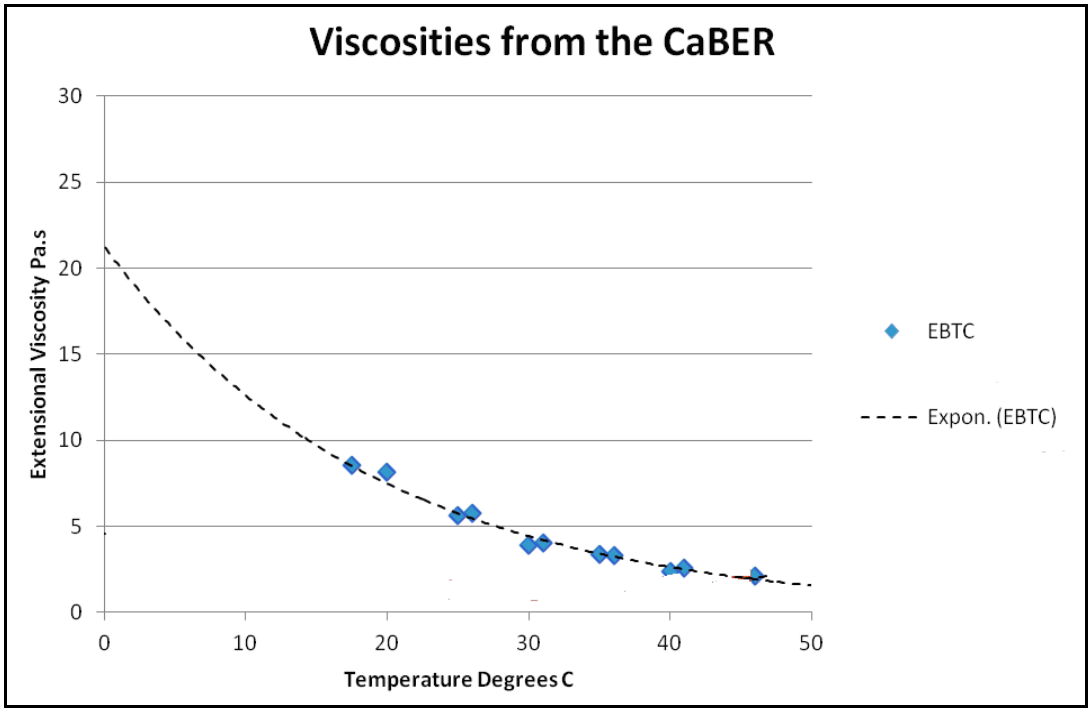

Figure 5-8 EBR coating temperature ramp results from CaBER

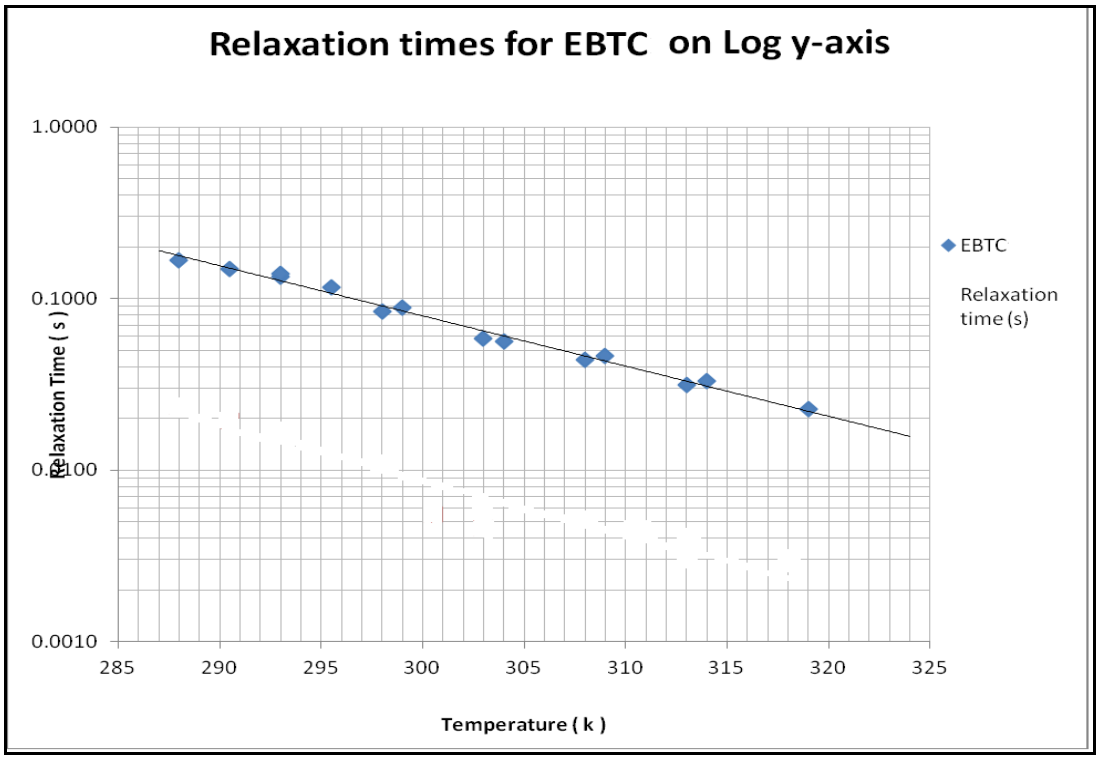

Figure 5-9 Relaxation time from CaBER experiments

Having carried out viscosity measurements in both shear and elongation mode, we can now combine the data as in *Figure 5-10* and *Table 5-2* to give the Trouton ratio in the temperature range measured. Values larger than 3 (Trouton ratio for a Newtonian fluid) and in the range up to 5 were found, indicative of elastic behaviour.

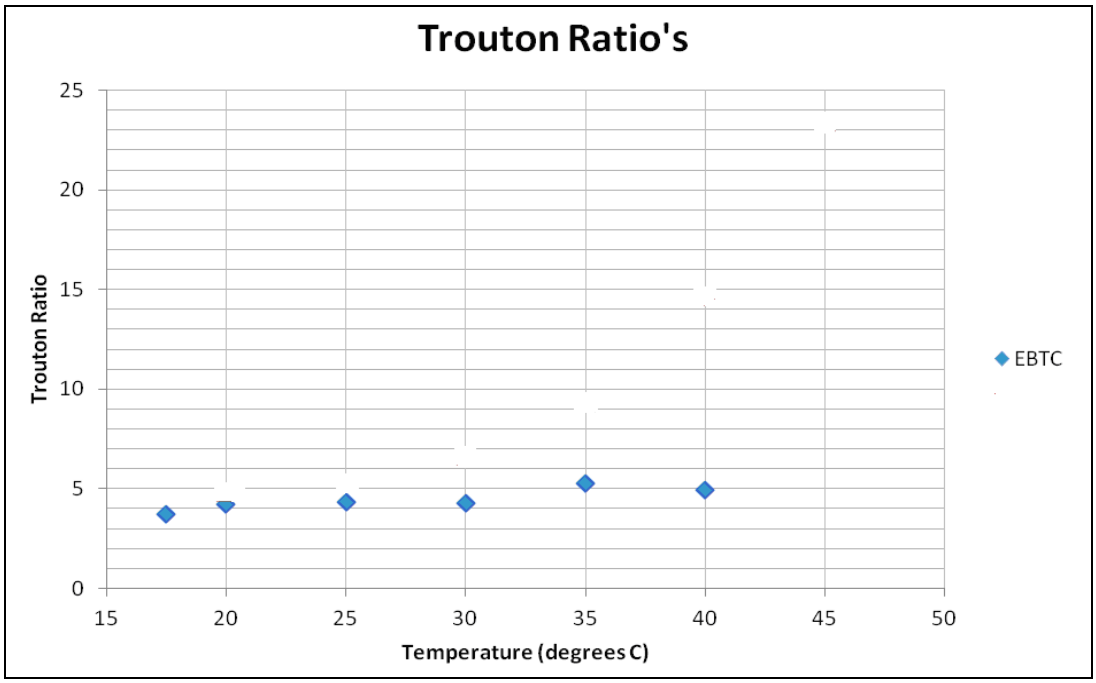

Figure 5-10 Trouton Ratio's of EB paint

Table 5-2 Calculated Trouton results from CaBER

Temperature (°C)	EB Paint Trouton ratio
20	4.2
25	4.4
30	4.3
35	5.3
40	4.9

Capillary extrusion rheometry results

The data obtained at high strain with capillary extrusion (*see Chapter 3 for method and relevant relationships*) are presented. *Figure 5-11* gives the raw data of recorded die pressure against ramming piston speed. The pressure builds up until an equilibrium condition is reached, at which point the pressure is recorded and the speed is changed to the subsequent measurement point. In the experiments, repeated several times (6) and a range of speeds (0.5-250 mm/min) were selected to correspond to the shear rate range of interest.

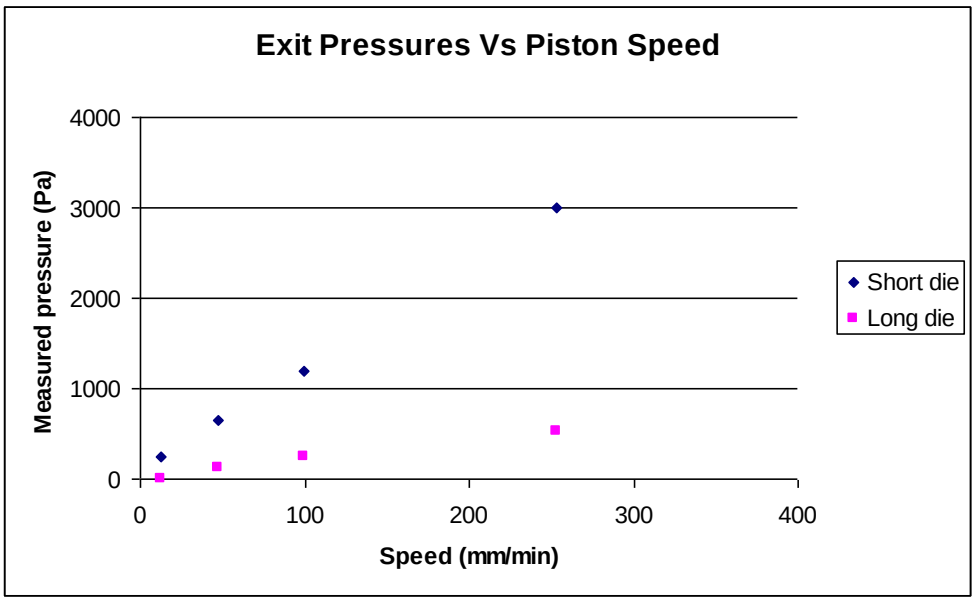

Figure 5-11 Capillary rheometer measurement for EBR coating

From these measurements, as shown in *Figure 5-12*, a graph of shear viscosity against shear rate is produced.

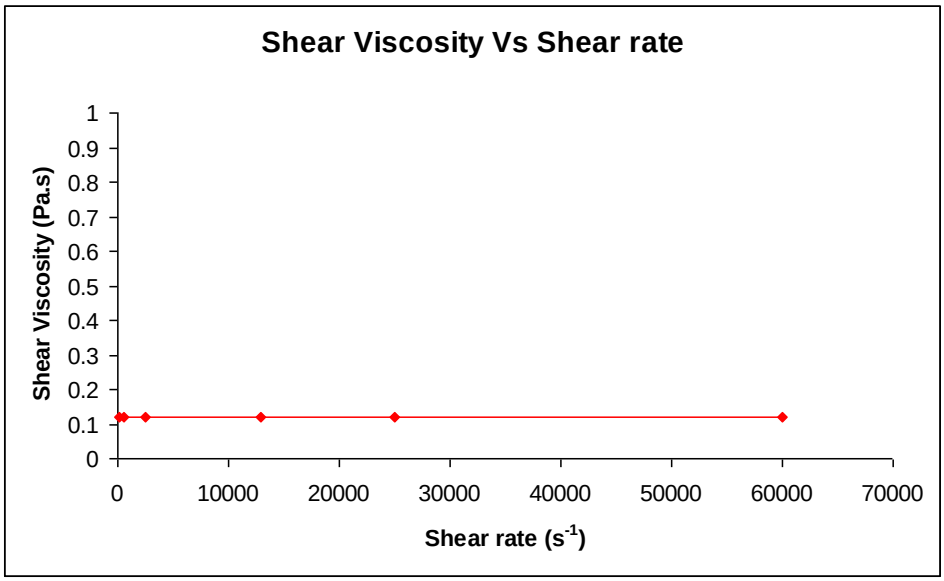

Figure 5-12 Flow curve for capillary rheometry

As these experiments were performed in a twin-bore capillary rheometer system, extensional viscosity could be simultaneously measured with shear viscosity. Capillary die diameters of 0.5 mm were used in all the experiments with short and

long die lengths (5.8 mm and 51 mm respectively). The extensional viscosity calculated for EB coating is given in *Figure 5-13* and it was found to be around 3.9 Pa.s at higher extensional rates compared to the 1.6 Pa.s limiting value found in the CaBER experiments. This difference is mainly to do with the strain rates and flow mechanisms involved in these two different methods of measurement.

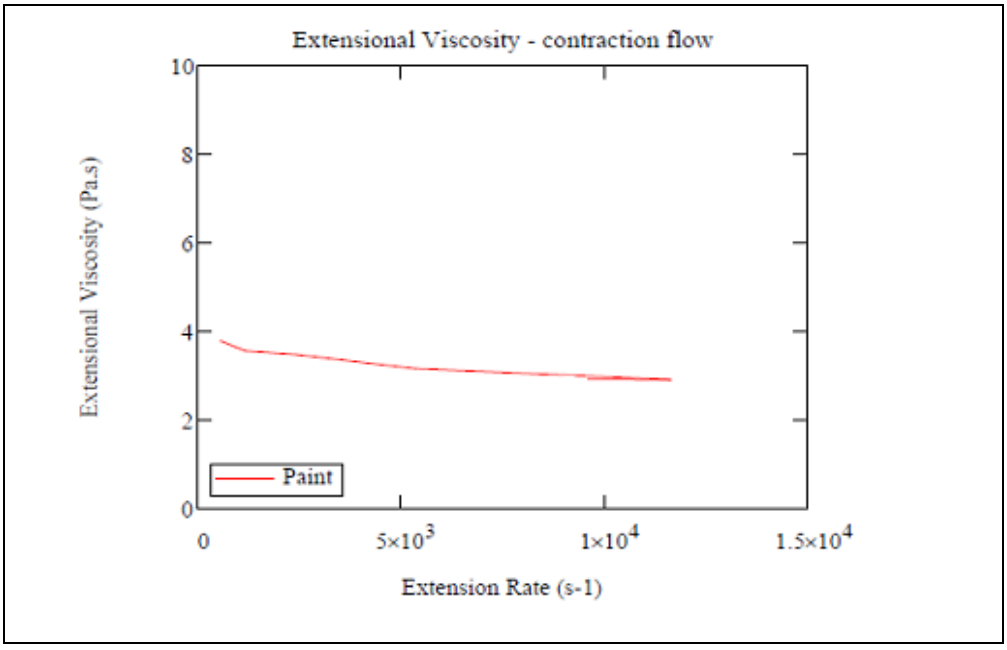

Figure 5-13 Extensional viscosity for EB coating

Concept of coating map

As explained earlier (*section 3.6.1*), the novelty of the research proposed lies in an integrated approach, utilising a range of comparative rheometrical techniques, with a focus on measurement of: (i) high strain rate shear viscosity (η) (ii) high strain rate uniaxial extensional viscosity (η_E) (iii) high strain rate elasticity (N1). The major rheological results for the EB coating formulation using each of the different techniques are summarised in *Table 5-3*.

Table 5-3 Summary of rheological results of EB coating

Category	Shear viscosity (Pa.s)		Extensional viscosity (Pa.s)	
Technique	**Capillary**	**Rotational**	**Capillary**	**CaBER**
Shear/extensional range	~ 60,000 s^{-1}	~ 1000 s^{-1}	~ 6000 s^{-1}	~ 500 s^{-1}
Result	0.118	0.103	3.9	1.6

The coating map for the EB paint, including all the relevant rheometrical results is shown in *Figure 5-14*.

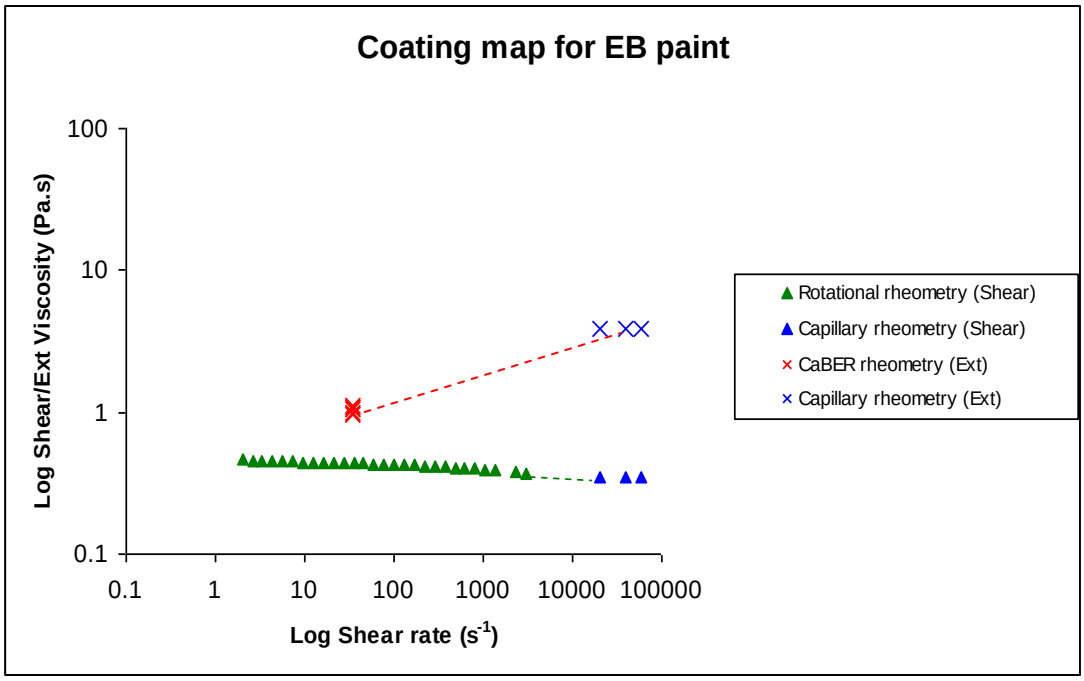

Figure 5-14 Coating map for EB coating

5.2.2 Model fluid generation

In comparison with the pre-treatment primer (WBPP) whose model fluid is any Newtonian fluid of viscosity 0.035 Pa.s with a surface tension value of 0.072 N/m (i.e. a water based solution), a model fluid for the radiation curing paint is more problematic as it has to combine the values of shear and elongational viscosities as

described above. The generation of such model fluids was in itself a separate larger project in collaboration with Glyndwr University. The level of details obtained from different type of model fluids is explained in *Figure 5-15*.

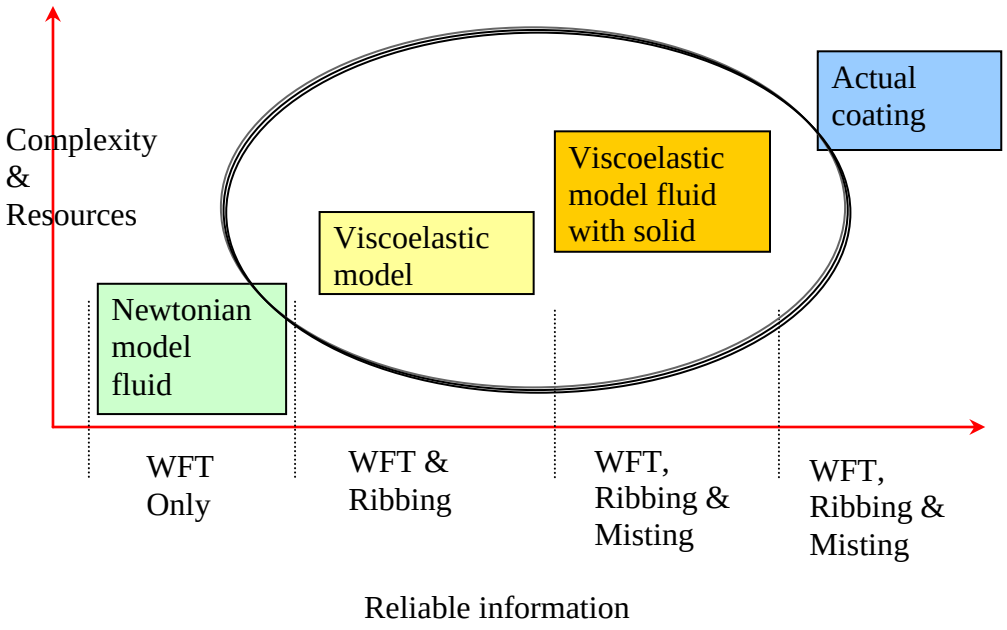

Figure 5-15 Coating fluids against available process information

Two set of non-Newtonian model fluids were considered:

- Poly dimethyl siloxane (PDMS) blend
- Poyisobutene (PIB) and Kerosene mix

PDMS fluids of polydispersities in the range 2.1-3.8 and viscosities 50 mPa.s, 1000 mPa.s, 600000 mPa.s and 1000000 mPa.s were obtained from Fluorochem, Glossop, UK. Various solutions were prepared (see *Table 5-4*) by mixing the high molar mass PDMS additives at concentration up to 50% by weight with the base PDMS fluid (50 mPa.s). Whereas the lower viscosity solutions could be prepared fairly quickly (2 hours of mixing), the more viscous solutions took as long as 2-3 days to be deemed fully mixed.

The rheology of these solutions was then evaluated in both shear and extension using the rheometers described earlier. The measured data on shear and extensional viscosities are shown in *Figure 5-16* to *5-18*; (See full data set in *Appendix III*). These data enabled the choice of the appropriate concentrations of high molecular weight PDMS into the base PDMS to obtain particular values of shear and extensional viscosities.

Table 5-4 The PDMS model solutions

Required mPa.s	50 mPa.s + 1,000 mPa.s (%)	50 mPa.s + 30,000 mPa.s (%)	50 mPa.s + 100,000 mPa.s (%)	50 mPa.s + 600,000 mPa.s (%)	50 mPa.s + 1,000,000 mPa.s (%)
100	82 / 18	96 / 4	95 / 5	96.74 / 3.26	97.23 / 2.77
200	62.5 / 37.5	88 / 12	90.5 / 9.5	93.69 / 6.31	94.88 / 5.12
300	47.5 / 52.5	82 / 18	87 / 13	91.95 / 8.05	93.37 / 6.63
400	37 / 63	80.5 / 19.5	85 / 15	90.42 / 9.58	92.21 / 7.79
500	27.5 / 72.5	78 / 22	83 / 17	89.13 / 10.87	91.24 / 8.76

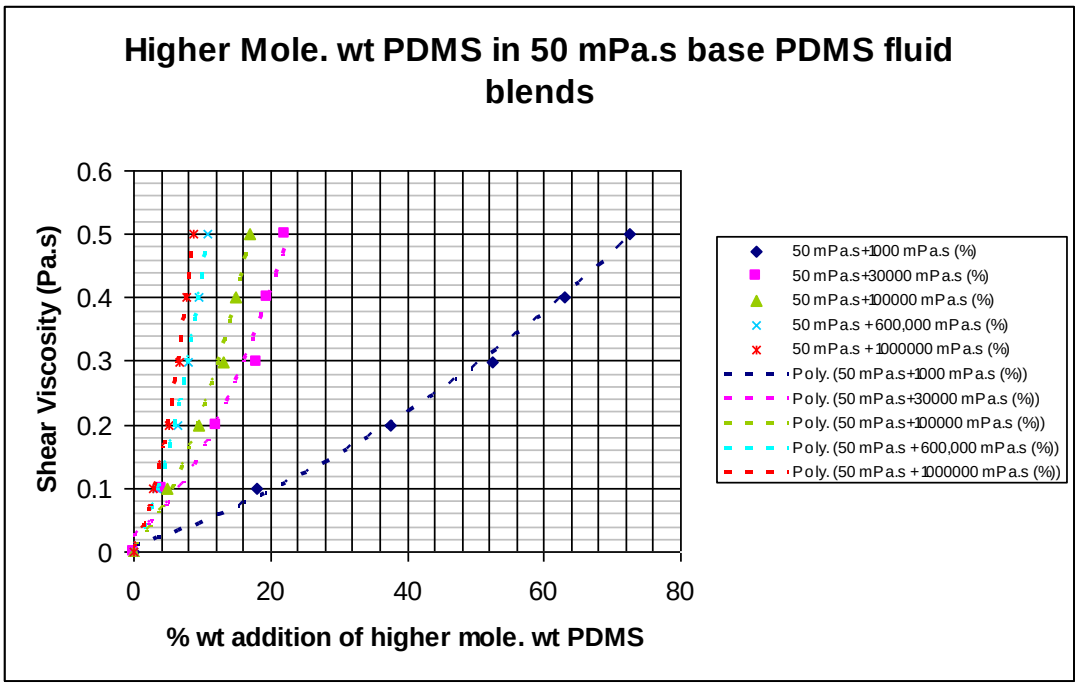

Figure 5-16 Trend lines for shear viscosity for 50 mPa.s base with corresponding higher molecular weight addition blends

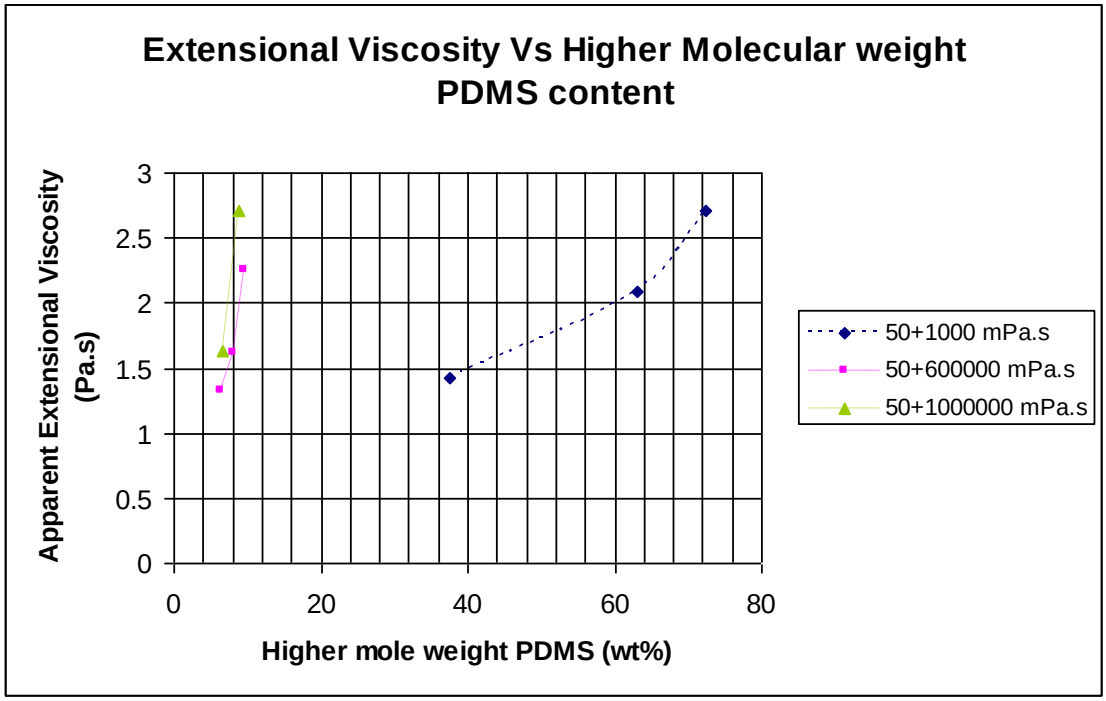

Figure 5-17 Measured apparent extensional viscosity (CaBER) against higher mole. wt PDMS addition (wt% in 50 mPa.s base solution)

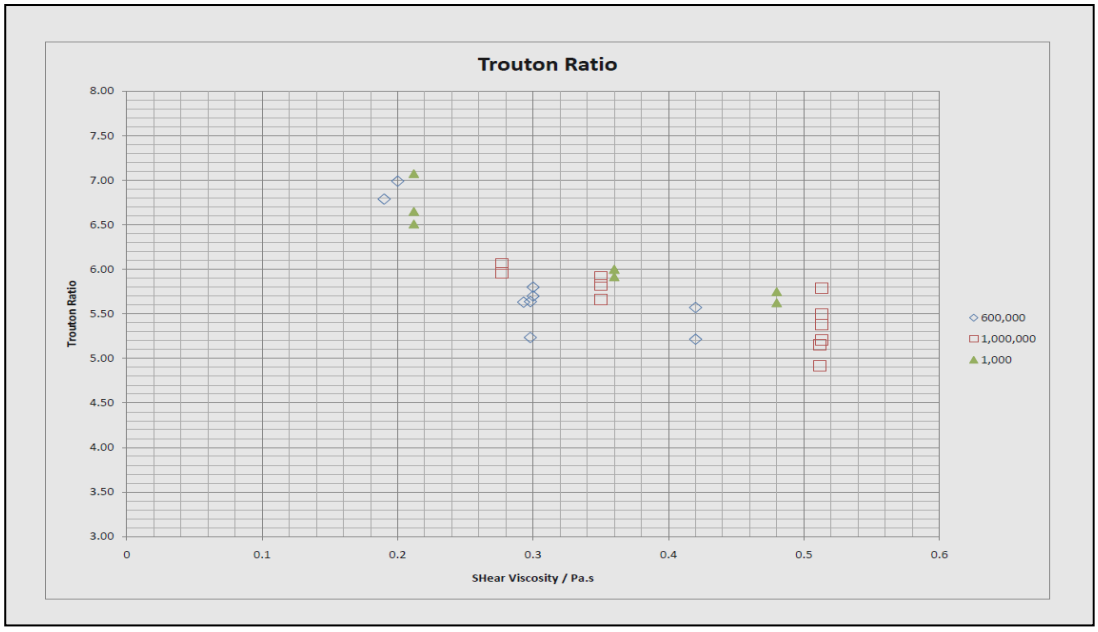

Figure 5-18 Measured Trouton ratio against shear viscosity for different PDMS blends

The same approach was used when preparing the PIB-Kerosene solutions (see *Table 5-5* and *5-6*) which are known to exhibit high normal stresses compared with the PDMS solutions (shown in *Figure 5-21*). The shear and extensional data for these

solutions are shown in *Figure 5-19* to *5-21* and a comparison of the extensional data with the PDMS solutions is given in *Figure 5-22*. Having measured the rheology over a range of concentration, it was then possible to establish the model solutions with the required shear and extensional viscosities. This is shown in *Table 5-5*.

Table 5-5 Mixture details for PIB-Kerosene blends

Required Pa.s	% Poly_025 in Kerosene	% Poly_30 in Kerosene
0.1	72	53
0.2	78	58
0.3	81.5	61
0.4	84	63
0.5	86	65

N.B. Poly_025 Molecular weight = 640 +/- 30

Poly_30 Molecular weight = 1300 +/- 100

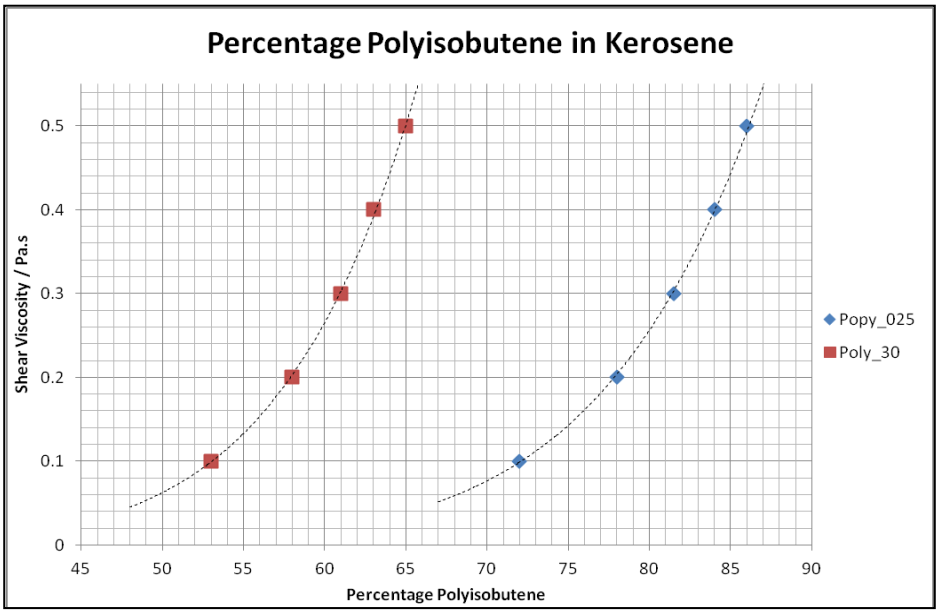

Figure 5-19 PIB-Kerosene blending to achieve specific high shear viscosity

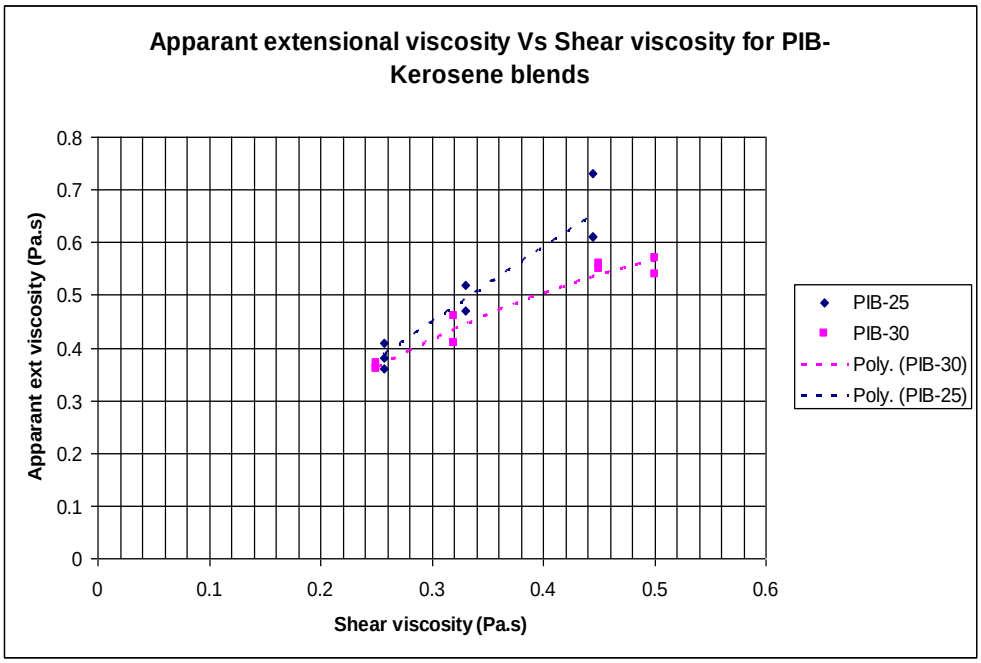

Figure 5-20 Apparent extensional against shear viscosity for PIB-Kerosene blends

Table 5-6 PIB-Kerosene blend details with viscosities

Name	PIB wt (%)	Kerosene wt (%)	Shear Viscosity (Pa.s)	Ext Viscosity (Pa.s)	Trouton ratio
Poly-25	85	15	0.45	0.65	1.46
Poly-25	80	20	0.26	0.38	1.48
Poly-25	82.5	17.5	0.33	0.5	1.52
Poly-30	60	40	0.25	0.36	1.44
Poly-30	62	38	0.32	0.43	1.34
Poly-30	65	35	0.50	0.56	1.12
Poly-30	64	36	0.45	0.56	1.24
Poly-heavy	89.7	10.3	0.23	0.56	2.48
Poly-heavy	87.6	12.4	0.44	0.6	1.38

Table 5-6 describes the rheological results for various PIB-Kerosene blends.

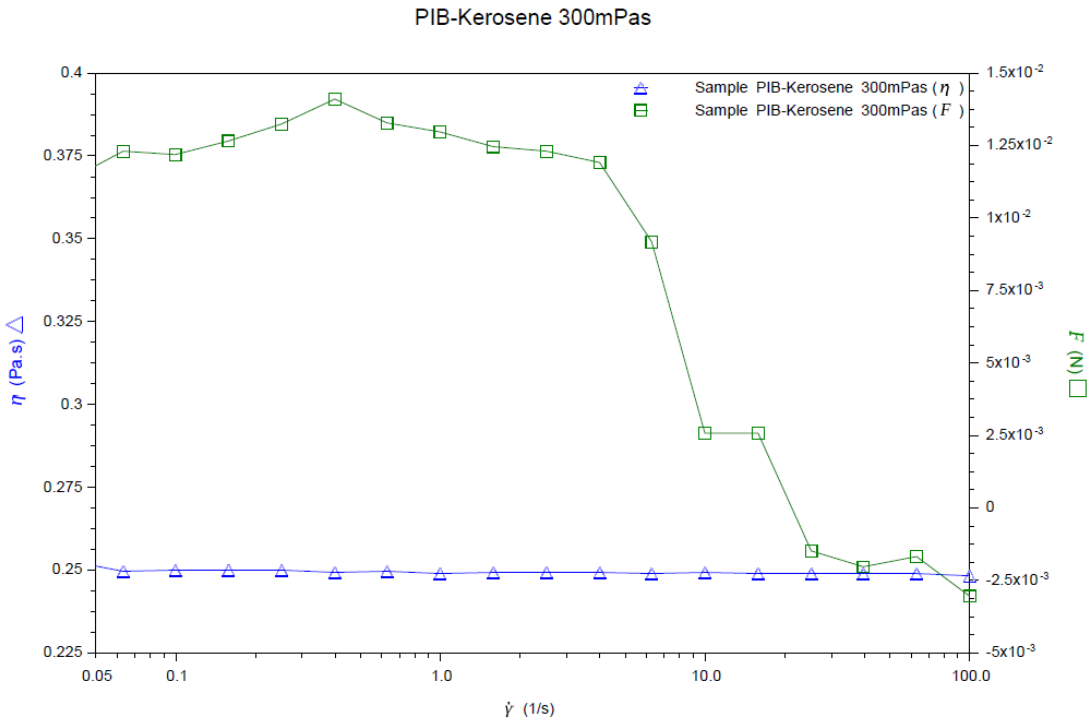

Figure 5-21 Normal axial force (N1) measured against increasing shear rate

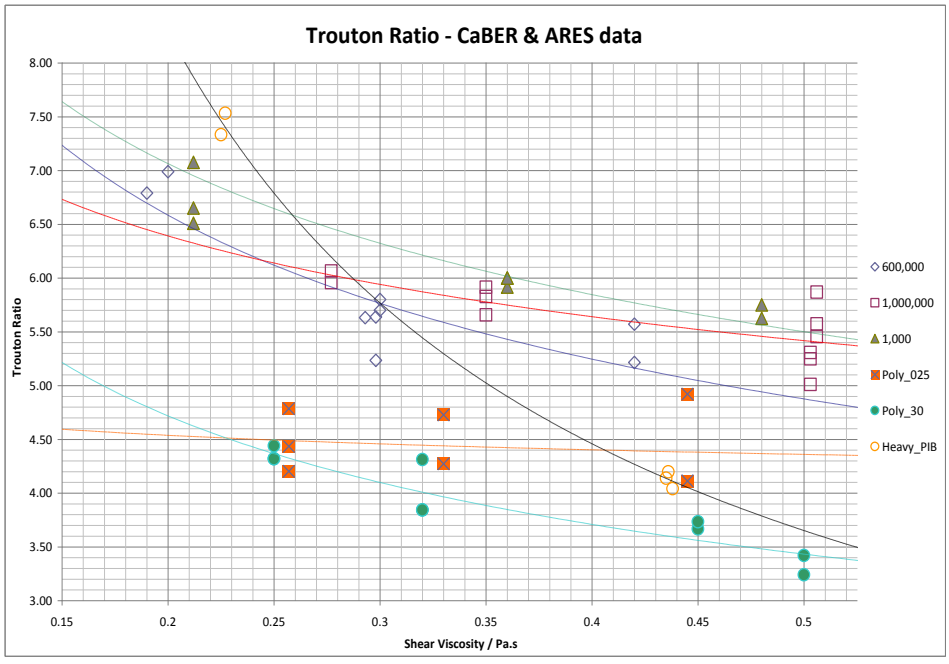

Figure 5-22 Rheologies of different non-Newtonian model fluids

Table 5-7 Mixture details for PDMS and PIB-Kerosene blends (5 litres)

Blend (A) + (B)	**Amount of (A)**	**Amount of (B)**	**Blend time / Total**
50cS + 1,000cS PDMS	2375ml	2625ml	2 days / 5000ml
50cS + 600,000cS PDMS	4584ml	401g	3 days / 5000ml
50cS + 1,000,000cS PDMS	4655ml	330.5g	4 days / 5000ml
Poly_025 + Kerosene	4075ml *[3749g]*	925ml	3 days / 5000ml
Poly_30 + Kerosene	3050ml *[2806g]*	1950ml	4 days / 5000ml
B 30 SF + Kerosene	504g *459.7g*	3996g *3645.3g*	5 days / 5481ml *5days / 5000ml*

N.B. Working off the principle of 1ml = 0.965g for PDMS.

5.3 Coatings used & their film thicknesses

Here, the film thicknesses measured with the model fluid solutions at the pick up and metering stages are presented. Also results from pilot line trials on steel substrate are discussed at the end, to give an insight on the validity of the data obtained in the laboratory on the roll coater without substrate.

5.3.1 Pick up roller feed film

First, the film thickness on the pick-up roll was measured in order to establish the required feeding condition to the deformable roll coating flow in the nip. The data, presented in *Figure 5-23* for a range of immersion angle (depth), show the effect of immersion angle is negligible at angle higher than about 30°. In all cases the film picked up was thick enough (5-7 mm) so that the nip would always be flooded. This consideration is important as it makes the film produced independent of the feed

conditions. This served to base the subsequent experiments at angles above 30°. The dependence of film thickness with roller speed and shear viscosity was also measured and the data are presented in *Figure 5-24*. Again the film thickness produced were always larger (order of mm) than the coating gap which is in the order of microns. Instabilities were observed at the higher speed but these will not be transmitted through the metering deformable gap.

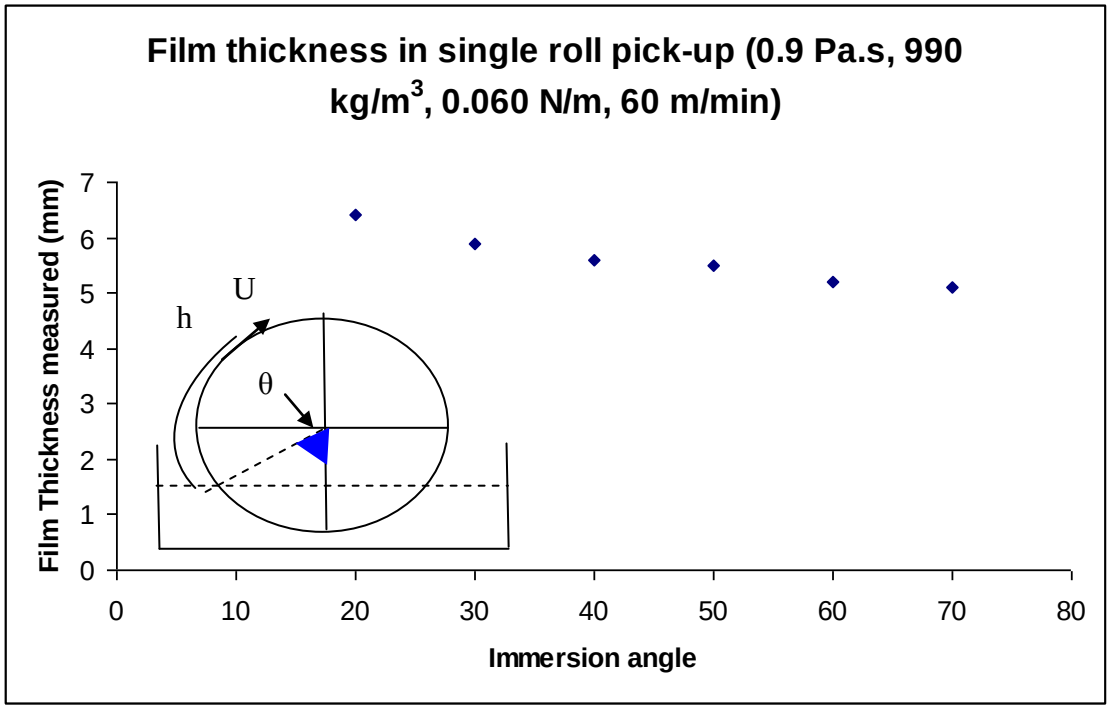

Figure 5-23 Single roll pick up film thickness at different immersion depths

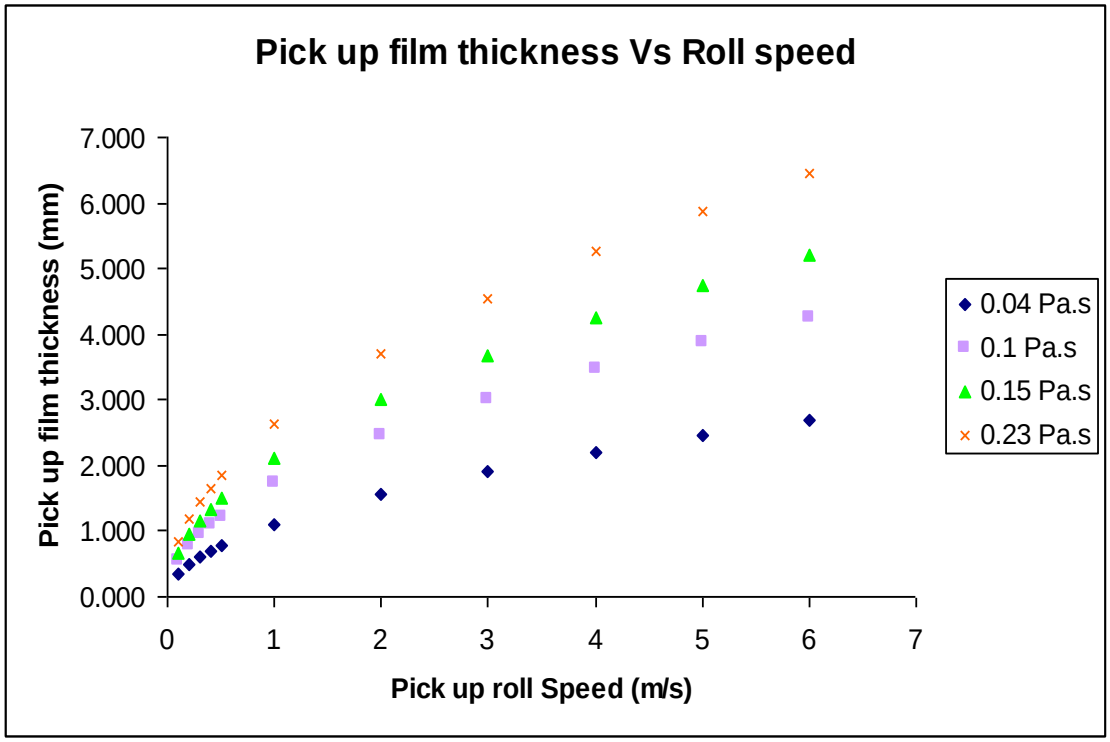

Figure 5-24 Film thickness with increase in pick up roll speed

5.3.2 Film thickness at equal roll speeds

Deformable roll coating is a complex multi-variables problem (as shown in *Figure 5-25*) with many design and operation variables such as roll speed, gap, rubber hardness and fluid properties. We can express the flow rate through the nip (total flow rate) Q_T and the flow rates on each of the two rollers (deformable and rigid) Q_D and Q_R and their ratio Q_D/Q_R as:

$$Q_T, Q_D, Q_R, Q_D / Q_R = f\left(R_d, R_r, b, U_d, U_r, E_d, E_r, h_d \text{ or } W, \rho, \mu, \sigma\right)$$

The dependency can be reduced if we combine the radii and elastic moduli of the rollers into an equivalent radius R of elastic modulus E.

$1/R=1/2\ (R_d + R_r)$ and $E = \frac{E_1}{(1-\nu_1^{\ 2})} + \frac{E_2}{(1-\nu_2^{\ 2})}$

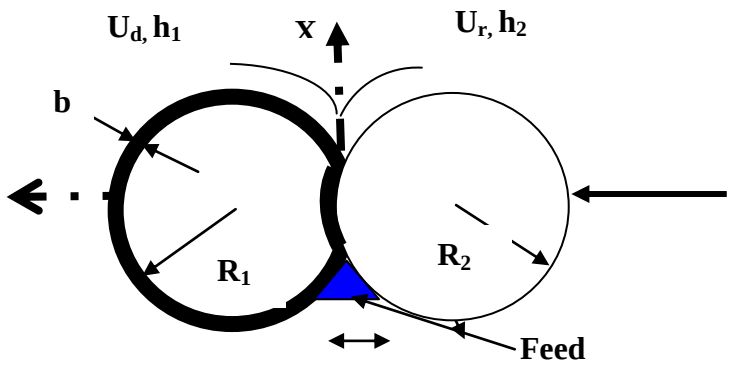

Figure 5-25 Deformable roll coating: Operating variables

We thus obtain:

$$Q_T, Q_D, Q_R, Q_D / Q_R = f\left(R, b, U_d, U_r, E, h_d \text{ or } W, \rho, \mu, \sigma\right)$$

We can apply dimensional analysis to the situation of constant gap or constant load.

Constant Gap Operation

$$\frac{Q_T}{\bar{U}R,}\frac{Q_D}{UR,}\frac{Q_R}{UR,}\frac{Q_D}{Q_R} = f\left(\frac{h_d}{R}, \frac{U_d}{U_r}, \frac{\mu\bar{U}}{ER}, \frac{b}{R}, \frac{\rho h_{io} U}{\mu}\right) = \left[\frac{h_d}{R}\right]^{e1}\left[\frac{U_d}{U_r}\right]^{e2}\left[\frac{\mu\bar{U}}{ER}\right]^{e3}\left[\frac{b}{R}\right]^{e4}\left[\frac{\rho h_{io} U}{\mu}\right]^{e5}$$

Constant Load Operation

$$\frac{Q_T}{\bar{U}R,}\frac{Q_D}{\bar{U}R,}\frac{Q_R}{\bar{U}R,}\frac{Q_D}{Q_R} = f\left(\frac{W}{ER}, \frac{U_d}{U_r}, \frac{\mu\bar{U}}{ER}, \frac{b}{R}, \frac{\rho h_{io} U}{\mu}\right) = \left[\frac{W}{ER}\right]^{e1}\left[\frac{U_d}{U_r}\right]^{e2}\left[\frac{\mu\bar{U}}{ER}\right]^{e3}\left[\frac{b}{R}\right]^{e4}\left[\frac{\rho h_{io} U}{\mu}\right]^{e5}$$

The groups specific to deformable roll coating are the load number (*W/ER*), which expresses the magnitude of load applied relative to the elastic forces developed and the elasticity number ($\mu U/ER$), which describes the magnitude of the viscous forces relative to the elastic forces developed. In deformable roll coating the compliant surface can deform linearly or not, depending on the rubber cover thickness ***b***, and its viscoelasticity. Therefore both the theoretical treatment and the data should be separated according to "thin" or "thick" sleeve, using ***b/R>0.1 or b/R<0.1*** respectively as the criterion. Also importantly, the value of E is critical and strictly should be measured under rolling not static conditions (*section 3.10)*.

In the case of equal roll speeds, the total flow rate Q_T through the nip splits equally into Q_D and Q_R so only one correlation is needed (Q_T) and checking that it is the case will give a test on the accuracy of data. So we also present for the equal speed data, the flow distribution Q_D/Q_R. An empirical fit of all the Newtonian fluid data from roller coating study (above 1400 data points) was obtained using Microsoft Excel® regression analysis option with Linest function. For ease of comparison with previous work which was carried out at low speeds and with Newtonian fluids only, this large data set was split into low speed (up to 50 m/min average speed- Reynolds number below 4100) and high speed (up to 160 m/min average speed- Reynolds number above 4100). The actual set of data used for regression analysis is given in *Appendix IV*. The results are as follows:

Total flux low speed regime:

$$\lambda_T = \frac{Q_T}{UR} = \left(\frac{\mu u}{ER}\right)^{0.68}\left(\frac{u_1}{u_2}\right)^{-0.001}\left(\frac{h_d}{R}\right)^{-1.36}\left(\frac{\mu u}{\sigma}\right)^{-0.07}\left(\frac{\rho h_d u}{\mu}\right)^{-0.01}$$

Total flux high speed regime

$$\lambda_T = \frac{Q_T}{UR} = \left(\frac{\mu u}{ER}\right)^{0.67}\left(\frac{u_1}{u_2}\right)^{-0.001}\left(\frac{h_d}{R}\right)^{-1.36}\left(\frac{\mu u}{\sigma}\right)^{-0.08}\left(\frac{\rho h_d u}{\mu}\right)^{-0.01}$$

Flux ratio low speed regime

$$\left(\frac{q_1}{q_2}\right)_{h_d} = \left(\frac{\mu u}{ER}\right)^{-0.0003}\left(\frac{u_1}{u_2}\right)^{1.53}\left(\frac{h_d}{R}\right)^{0.001}\left(\frac{\mu u}{\sigma}\right)^{-0.0007}\left(\frac{\rho h_d u}{\mu}\right)^{-0.0002}$$

Flux ratio high speed regime

$$\left(\frac{q_1}{q_2}\right)_{h_d} = \left(\frac{\mu u}{ER}\right)^{-0.005}\left(\frac{u_1}{u_2}\right)^{1.55}\left(\frac{h_d}{R}\right)^{0.016}\left(\frac{\mu u}{\sigma}\right)^{0.008}\left(\frac{\rho h_d u}{\mu}\right)^{-0.002}$$

These correlations are summarised in *Table 5-8* giving the exponents of the dimensionless groups of the measured functions, Q_T/UR, Q_D/Q_R.

Table 5-8 Summary of exponents of the dimensionless groups from regression analysis

Low speed regime	**Elasticity number (Es)**	**Speed ratio (S)**	**Gap Number (GN)**	**Capillary number (Ca)**	**Reynolds number (Re)**
Q_T / UR	0.68	-0.001	-1.36	-0.07	-0.01
q_1/q_2	-0.0003	1.53	0.001	-0.0007	-0.0002
High speed regime	**Elasticity number (Es)**	**Speed ratio (S)**	**Gap Number (GN)**	**Capillary number (Ca)**	**Reynolds number (Re)**
Q_T / UR	0.67	-0.001	-1.36	-0.08	-0.01
q_1/q_2	-0.005	1.55	0.016	0.008	-0.002

We observe from the regression analysis of the whole data set:

- The flux distribution data at speed ratio=1 shows the flow to split equally between the rollers giving confidence in the accuracy of our film thickness measurements.
- The flux distribution correlation at speed ratio≠1 shows that it depends only on the speed ratio, the exponents of the other groups being essentially zero.
- The total flux depends essentially only on the elasticity number (Es), the load or gap numbers (GN) and the rubber thickness number (not varied in this study) and not on capillary number and Reynolds number, their exponents being found to be essentially 0. This is expected as this flow is elastohydrodynamic with inertia and surface tension effects being secondary.
- There is little or no difference in the data correlation at low (Re < 4100) and high speed (Re > 4100) as the concerned factors are all similar in their values.
- In case of flux distribution, speed ratio between the rolls is the only concerned factor and it is shown by value of power to be around 1.53-1.55.

5.3.2.1 Operating parameters for experimental studies

The operating parameters chosen in this study cover a wider range compared to previous studies and this enables the assessment of stretching the process window for deformable roll coating process, as compared in *Table 5-9*. It is necessary to note that the important consideration of the data presented in this thesis is (i) the nature of the fluids used (Newtonian and viscoelastic non-Newtonian) which were designed to replicate industrial coating application and (ii) the range of speed pertinent to high speed coating whereas previous data were limited to Newtonian fluids coated at low speeds.

Table 5-9 Comparison of processing parameters with previous experimental studies

	Unit	**Kang**	**Cohu**	**Jones**	**This work**
Fluid Shear Viscosity	Pa.s	0.01-1	0.08-1.2	0.014-0.235	0.014-**0.235**
Fluid extensional viscosity (CaBER)	Pa.s	–	–	–	1.3-**2.7**
Roll Speed	m/s	0.014-1.5	0.17-1.67	0.16 - 0.83	0.13 – **6.4**
Negative gap	mm	0.05-0.2	–	0.2 - 1.0	0.25 - **0.75**
Load	N/m	–	1932 - 19,963	580 - 14,250	500 - **17,200**
Elastic modulus of the rubbers	MPa	5,6,16.2	0.9,3,15	0.74 - 4.65	1.8 – **7.6**

5.3.2.2 Application of previous theoretical solutions to current conditions

Under symmetric roll speed condition the roll speeds are same and the corresponding film thickness on each roll (pick up and applicator) will be the same. In this case, a theoretical solution using FE analysis was proposed by Carvalho [19]:

$$\frac{Q}{2VR} = 0.34\left(\frac{\mu\bar{U}}{ER}\right)^{0.6}\left(\frac{W}{ER}\right)^{-0.31}$$

Here the rubber cover thickness condition is *b/R >0.1* and *Table 5-10* predicts the wet film thickness following above relationship. Although during coating process, load (W) is expected to differ from our measured load under dry contact, the loads

do not vary significantly with speed. *Figure 3-39* show that the load varies linearly with gap only and not with roller speeds. In this situation, measured dry loads (W) are used in the film thickness predictions (Using above theoretical equation) which is presented in *Table 5-10*,

Table 5-10 Predicted film thickness values using Carvalho's equation (low speed)

Hardness of rubber cover : 55 Shore A- Low speed: 20, 30, 40 m/min						
Viscosity (mPa.s)	14	40	60	100	190	235
Gap (mm)						
-0.25	4.86 6.24 7.37	9.13 11.71 13.83	11.64 14.94 17.64	15.82 20.29 23.97	23.25 29.83 35.23	26.41 33.88 40.03
-0.5	3.25 4.17 4.93	6.1 7.83 9.25	7.78 9.98 11.79	10.57 13.57 16.02	15.54 19.94 23.55	17.65 22.65 26.76
-0.75	2.55 3.27 3.87	4.79 6.15 7.26	6.11 7.84 9.26	8.3 10.65 12.58	12.2 15.65 18.49	13.86 17.84 21.00

Inspection of the predicted results of *Table 5-10* suggests that Carvalho's equation provides a good estimation and it can be used as the theoretical guideline to assess trend and variations of the film thickness with the individual parameters. In order to assess these results more easily, such trends are presented in graphical form below (see *Figures 5-26-5-27*).

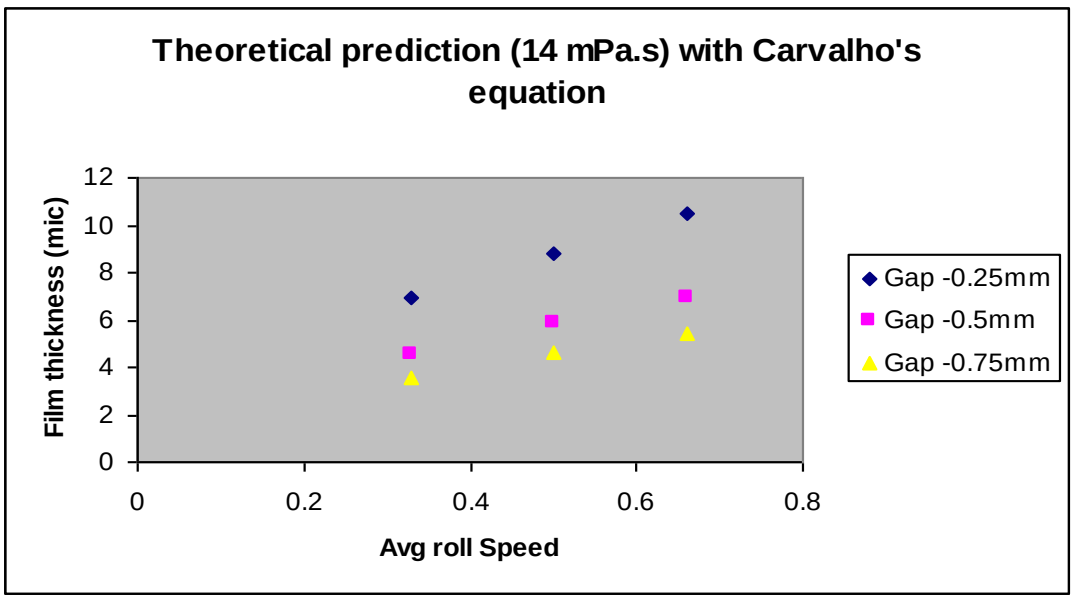

Figure 5-26 Film Thickness variation (Carvalho equation) with speed at various gaps and for viscosity 14 mPa.s

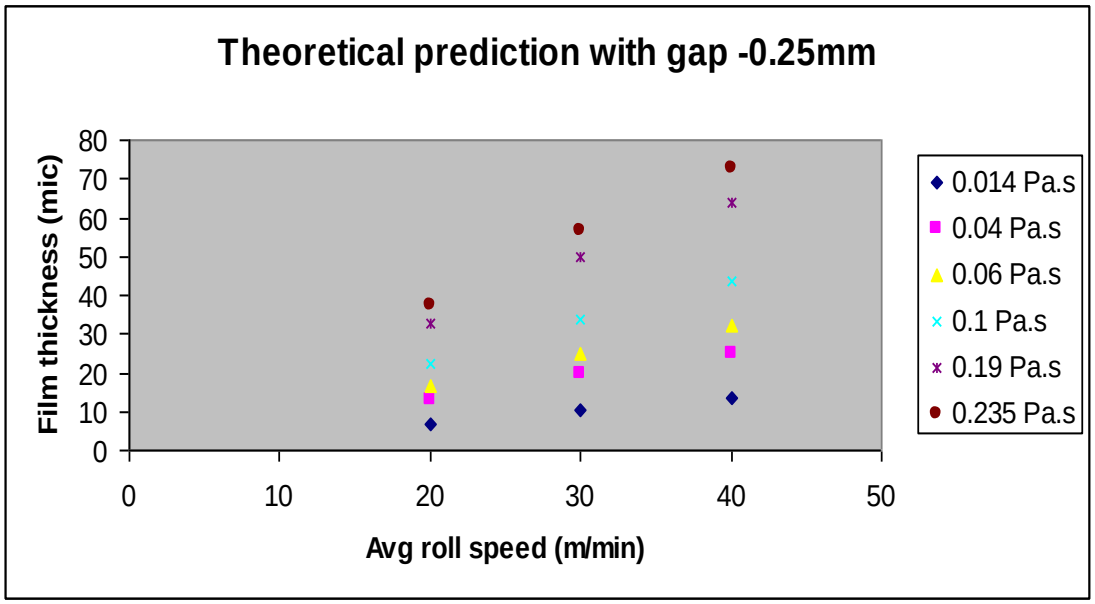

Figure 5-27 Film thickness variation with speed at various viscosities and for gap -0.25 mm

From the above graphs, it is clear that the predicted film thicknesses depend on viscosity and roll speed. Although the above relationship is plotted for low speed (upto 40 m/min), the same can be extrapolated to high speed regime (up to average roll speed of 240 m/min) as shown in *Figure 5-28*.

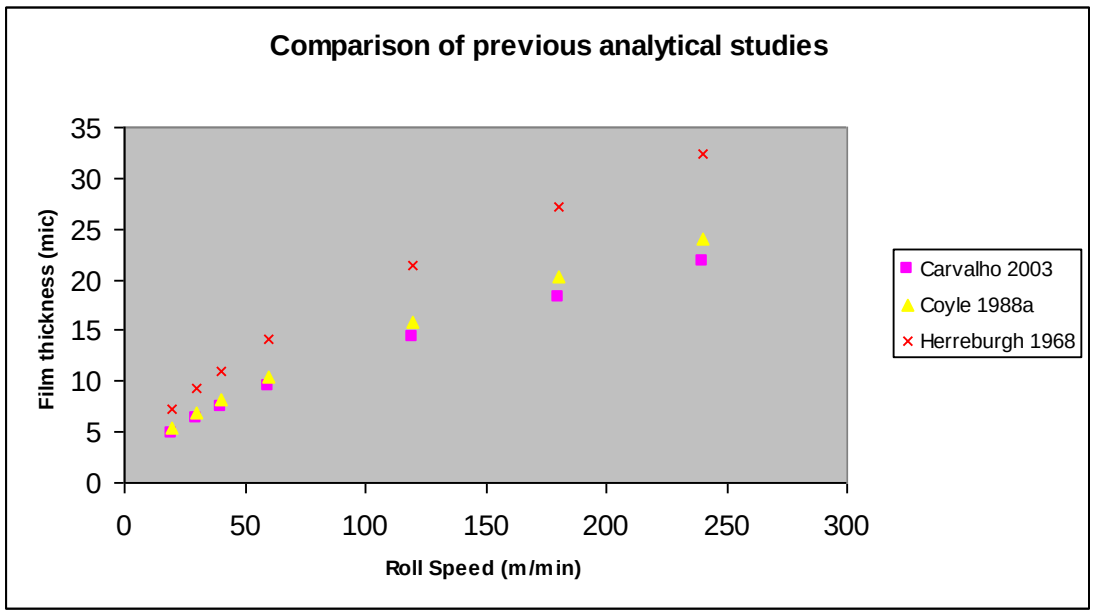

Figure 5-28 Predicted Film thickness variation with speed in previous analytical studies (0.014 Pa.s, 55 Shore A, -0.25mm gap)

Table 5-11 below presents the predicted film thickness results using Carvaho's equation at higher speeds.

Table 5-11 Predicted film thickness values using Carvalho's equation (high speed)

Hardness of rubber cover : 45 Shore A- High speed: 60, 120, 180, 240 m/min						
Viscosity (mPa.s)	14	40	60	100	190	235
Gap (mm)						
-0.25	13.4 20.32 25.91 30.8	25.17 38.14 48.65 57.82	32.1 48.65 62.05 73.74	43.61 66.10 84.30 100.19	64.1 97.15 123.91 147.25	72.81 110.37 140.76 167.28
-0.5	8.86 13.43 17.13 20.36	16.64 25.22 32.16 38.22	21.22 32.16 41.02 48.75	28.83 43.70 55.73 66.23	42.37 64.23 81.92 97.35	48.14 72.96 93.06 110.59
-0.75	6.96 10.54 13.45 15.98	13.06 19.79 25.24 30	16.56 25.24 32.20 38.26	22.63 34.3 43.75 51.99	33.26 50.41 64.3 76.41	37.78 57.27 73.04 86.8

Looking at the above prediction, negative gap in the range -0.75 mm can produce wet film thickness in the range 10-15 µm at 240 m/min for 0.014 Pa.s. The thickness obtained will be 15.98, 20.36 and 30.8 µm for negative gaps -0.75, -0.5 and -0.25 mm respectively. Thus the minimum thickness that is obtained at 240 m/min will be 15.98 µm and will require a negative gap of -0.75 mm. If a thinner film is required a larger negative gap or a harder roller will be necessary but this would require very large applied loads. Carvalho's equation shows keeping all other conditions the same, the film thickness varies with elastic modulus and load as follows:

$$\bar{h} \propto E^{-0.29} W^{-0.31}$$

Now for fixed rubber cover thickness (b), roll radius (R) and negative gap (h_d), operation at constant gap h_d will lead to a constant contact length L_C from which the static elastic modulus can be calculated as:

$$E = \frac{8WR}{\pi (L_c)^2} \quad \text{or}$$

$$E \propto W \text{ or } \frac{E_1}{E_2} = \frac{W_1}{W_2} \text{ or}$$

$$\frac{\bar{h}_1}{\bar{h}_2} = \left(\frac{E_1}{E_2}\right)^{-0.60}$$

Therefore to achieve a reduction from 15.98 µm (this is the value predicted with the

present rubber at -0.75 mm gap) to 5 µm, keeping the gap at -0.75 mm the elastic modulus will have to vary from the current 1.8 MPa to:

$$\frac{15.98}{5} = \left(\frac{1.8}{E_2}\right)^{-0.60} \text{ or}$$

E_2= 12.5 MPa

Alternatively we can use a thinner roll cover (*b).* Using above equation keeping all operating variables constant (speed 240 m/min, viscosity 14 mPa.s, same rollers and same rubber), we observe that to achieve a reduction from 15.98 µm down to 5 µm, require a layer thickness of

$$\frac{\bar{h}_1}{\bar{h}_2} = \left(\frac{b_1}{b_2}\right)^{0.29} \text{or}$$

$$\frac{15.98}{5} = \left(\frac{17}{b_2}\right)^{0.29} \text{ or}$$

b_2= 0.3 mm

Clearly a 0.3 mm layer is not practical, so a combination of a harder roller (Shore A Hardness 70) and a cover thickness of 17 mm is used which should reduce the film thickness. Alternatively operation at speed ratio less than 1 (i.e.) will also reduce the film thickness, which will be investigated in later section.

5.3.2.3 Low speed coating of model fluids to reflect WBPP

Figure 5-29 presents a comparison between our data at low speed and data from previous studies suggesting the closest fit to be with the data of Jones [120] and the largest discrepancy with the data of Smith and Maloney [63] which also deviate from all other data.

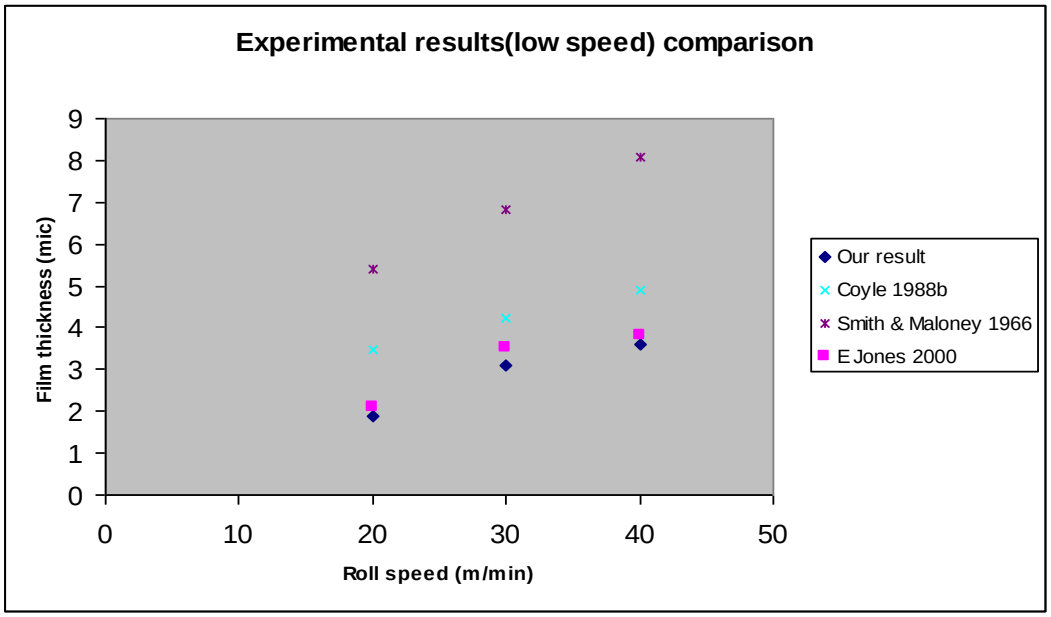

Figure 5-29 Comparison with previous experimental (low speed) roller coating studies

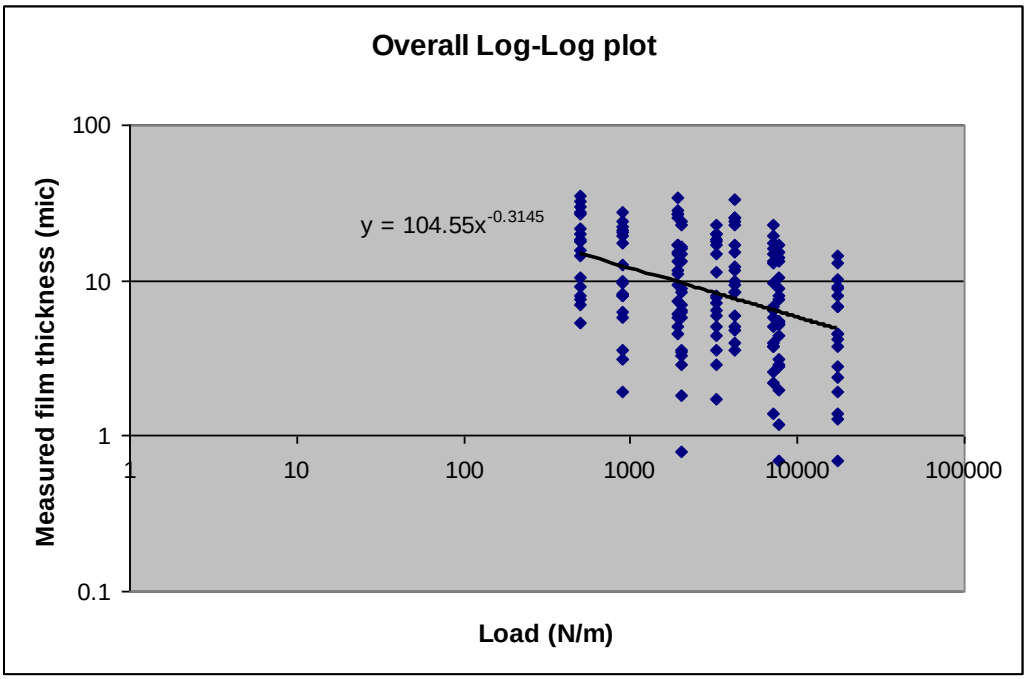

Figure 5-30 Influence of the external load on the coating thickness (thick rubber cover regime)

In *Figure 5-30* the change in film thickness as a function of the applied load is plotted. A large scatter in the data is observed and this is due to the very small film thicknesses measured which is in the range less than 2 µm size. A best fit to the data

shows an exponent of -0.3 for variation with load which is similar to the prediction of Coyle [44] and the data of Cohu et.al [64].

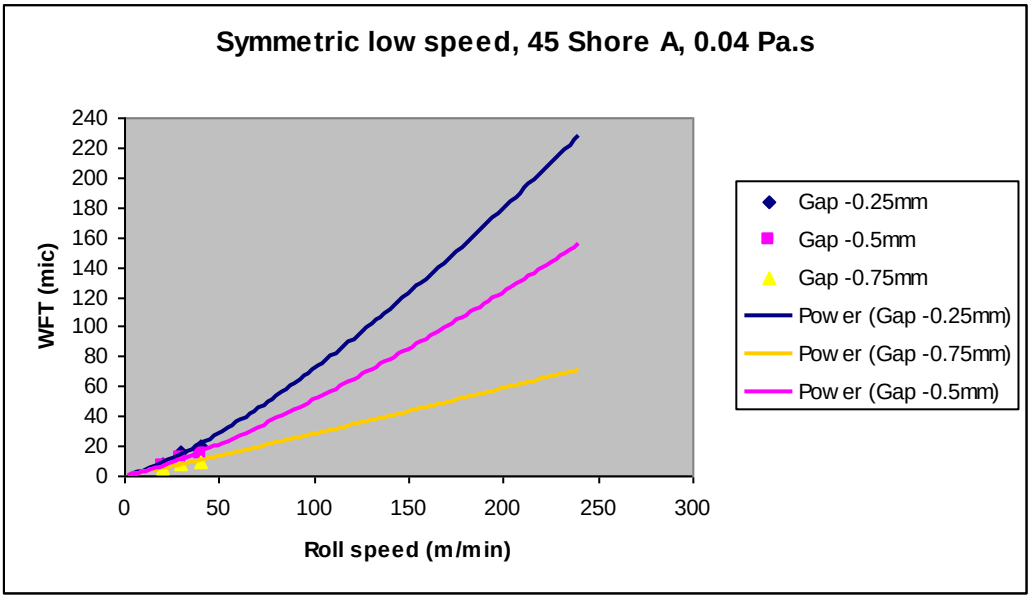

Figure 5-31 Film thickness measured at lower speed and extrapolation to higher speed

Figure 5-31 shows data at low speeds of the Newtonian model fluid (Millmax 10) extrapolated to high speeds for different gaps. This is done to understand the effect of extrapolating lower speed thickness results to higher roll speeds.

5.3.2.4 High speed coating of model fluids to reflect WBPP

Figure 5-32 shows typical data obtained for the model fluid with viscosity of 40 mPa.s at 3 negative gaps indicating that a linear extrapolation with speed is not appropriate (as shown in *Figure 5-31*). For example, extrapolation results give around 150 µm for -0.5 mm gap at 240 m/min. In real measurement at high speed, this thickness was found to be as low as 40 µm. The full results for all six Newtonian model fluids are presented in *Appendix III* and indicate the same observation.

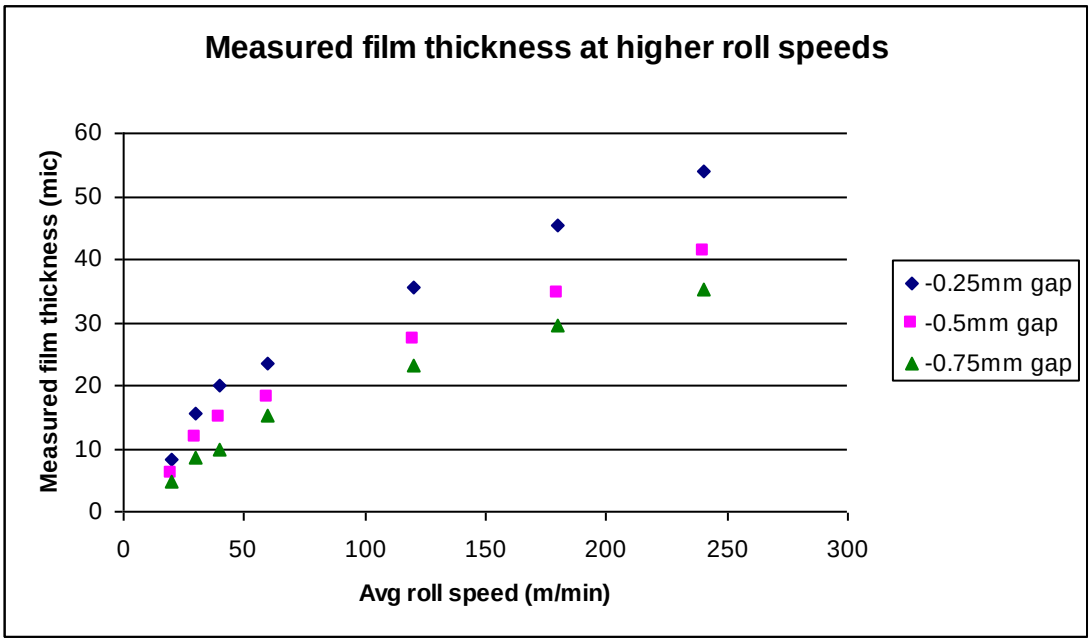

Figure 5-32 Measured film thickness data with model fluid (0.04 Pa.s, 45 Shore A)

5.3.2.5 High speed coating of model fluids to reflect EBR

The Electron Beam Radiation (EBR) curable coating system (Supplier- Confidential) for the study was characterised in rheological terms and these results show that at ambient temperatures the coating is moderately viscous, up to 600 mPa.s at higher shear rates.

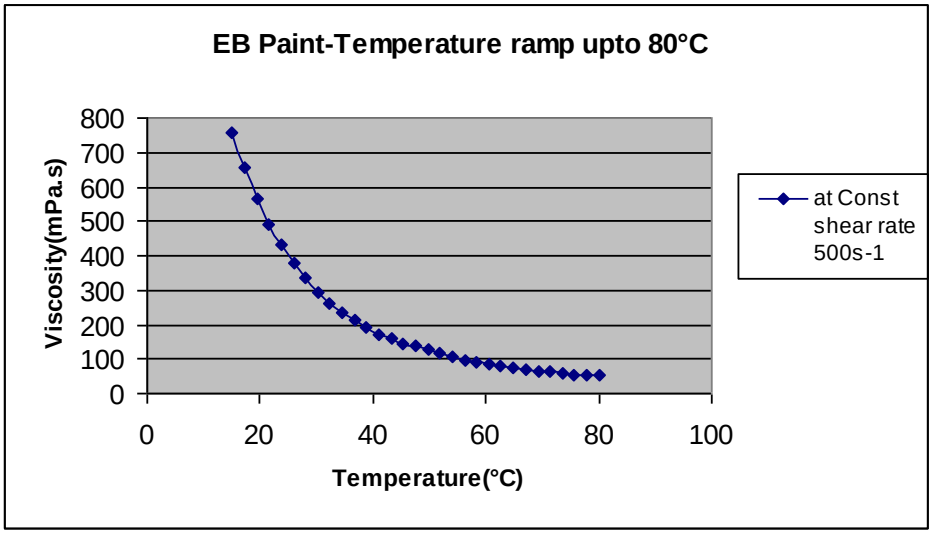

Figure 5-33 Shear viscosity Vs Temperature for EB topcoat paint at constant shear rate (500 s^{-1})

The temperature ramp (using Anton Paar MCR 301 rheometer) on the coating fluid (*Figure 5-33*) shows that the viscosity of the coating system is dependent on the temperature. The temperature upper limit of 80°C was chosen because the flash point for the coating was 120°C. According to these results, six different Newtonian model fluids (lubricating oil) were chosen for study with different relevant shear viscosities, as listed in *Table 5-12*.

Table 5-12 Model fluid relationship with viscosity of EB topcoat paint (Supplier A)

Model fluid	**Shear viscosity at 20°C (mPa.s)**	**Temperature for EB paint to achieve the viscosity (°C) [Ref. Fig. 5.33)]**
Millmax 10	14	90
Millmax 15	40	80
Millmax 32	60	70
Millmax 37	100	55
Millmax 68	190	40
Millmax 100	235	35

The studies with model fluids tried to mimic the shear viscosity of the heated EB paint system at different temperatures. The lubricating oil was chosen as model fluid, because its surface tension properties found to be closer to that of real paint. Initially the coater was operated at low speed (up to 40 m/min) in order to compare with previous experimental studies and validate the results (*Figure 5-29, 30*).

The above analysis was important in as much as it can guide the assessment of the experimental data. One important observation is however no previous theory or experiment have been carried out for speed in excess of 1 m/s and this was precisely the objective of the present work which was also to achieve target thickness (5-15 μm) up to speeds of 5-6 m/s. Here we present the data at these very high speeds with the model fluids and to assess them in relation to previous work (theoretical and practical). The operating conditions used in high speed roller coating trials are given in *Table 5-13*.

Table 5-13 Operating conditions for model fluid trials

Fluid viscosity (Pa.s)	0.014 - 0.235
Average Roll Speed (m/s)	0.33 - 4
Applied load between rolls (N/m)	500 - 17200
Negative Gap between rolls (mm)	0.25 - 0.75
Hardness of the applicator roll cover (Shore A)	45 - 70
Roll radius (mm)	125
Rubber cover thickness (mm)	15
Fluid level in pressurised pan from bottom surface (mm)	20 - 30

Table 5-14 Experimental film thickness (high speed) results for 45 Shore A

Hardness of rubber cover : 45 Shore A- High speed: 60, 120, 180, 240 m/min						
Viscosity (mPa.s)	14	40	60	100	190	235
Gap (mm)						
-0.25	11.12 16.84 21.48 25.52	23.4 35.55 45.36 53.91	24.94 37.80 48.19 57.30	31.61 47.92 61.11 72.63	59.76 90.54 115.52 137.25	60.32 91.44 116.64 138.6
-0.5	8.48 12.88 16.44 19.52	17.95 27.22 34.69 41.26	19.09 28.91 36.9 43.84	31.1 47.16 60.12 71.46	45.72 69.3 88.38 105.03	46.16 70 89.24 106.08
-0.75	7.28 11 14.04 16.68	15.34 23.26 29.65 35.28	16.31 24.71 31.54 37.50	26.6 40.32 51.44 61.11	39.11, 59.27, 75.6, 89.82	39.48 59.84 76.32 90.72

The experimental data for high speed roller coating is reinforcing the strong effect of viscosity, where thin films (below 10 μm) at high roll speeds (240 m/min) is formed only with low viscosity fluids. The limits of film thickness formed at high speed with current roller coating conditions are given in *Table 5-15*.

Table 5-15 Film thickness limits from high speed experimental studies

Viscosity (Pa.s)	Hardness (Shore A)	Gap (mm)	Roll Speed (m/min)	Film thickness (μm)
0.014	70	-0.75	240	7.16
0.04	70	-0.75	240	7.6
0.06	70	-0.75	240	15.02
0.1	70	-0.75	240	20.4
0.19	70	-0.75	240	38.6
0.235	70	-0.75	240	38.92

5.3.2.6 Comparison with theory and data

In *section 5.3.2.2*, Carvalho's theoretical relationship for roller coating thickness was examined but this is only valid at low speeds. In our experiments, we have accumulated bank of data at low speed (below 40 m/min) and large rubber cover thickness (b) and they correlate to similar form as:

$$\frac{\bar{h}}{R} = 0.17\left(\frac{\mu\bar{u}}{E\ R}\right)^{0.71}\left(\frac{W}{ER}\right)^{-0.23}$$

In *Figure 5-34*, measured film thickness at higher roll speeds is compared with extrapolated lower speed film thickness.

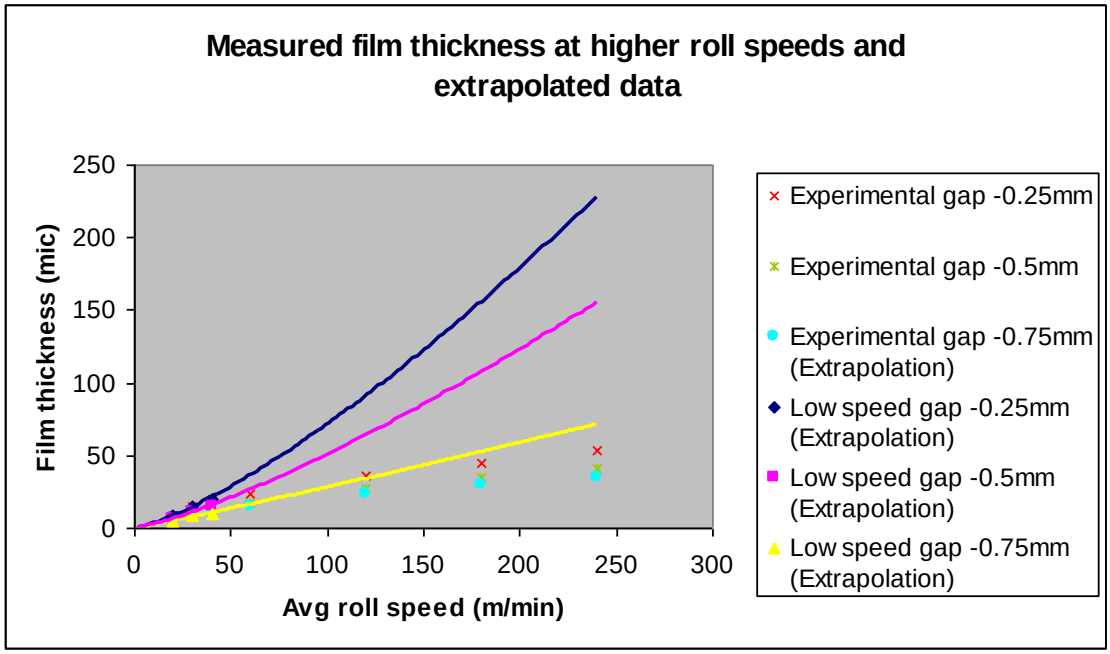

Figure 5-34 Measured film thickness data with extrapolated data from lower roll speed (0.04 Pa.s, 45 Shore A)

From *Figure 5-34*, it becomes clear that actual measured film thicknesses at higher roll speeds are much lower than the extrapolated values. Similarly in *Figure 5-35*, the high speed actual results are compared with Carvalho's predictions.

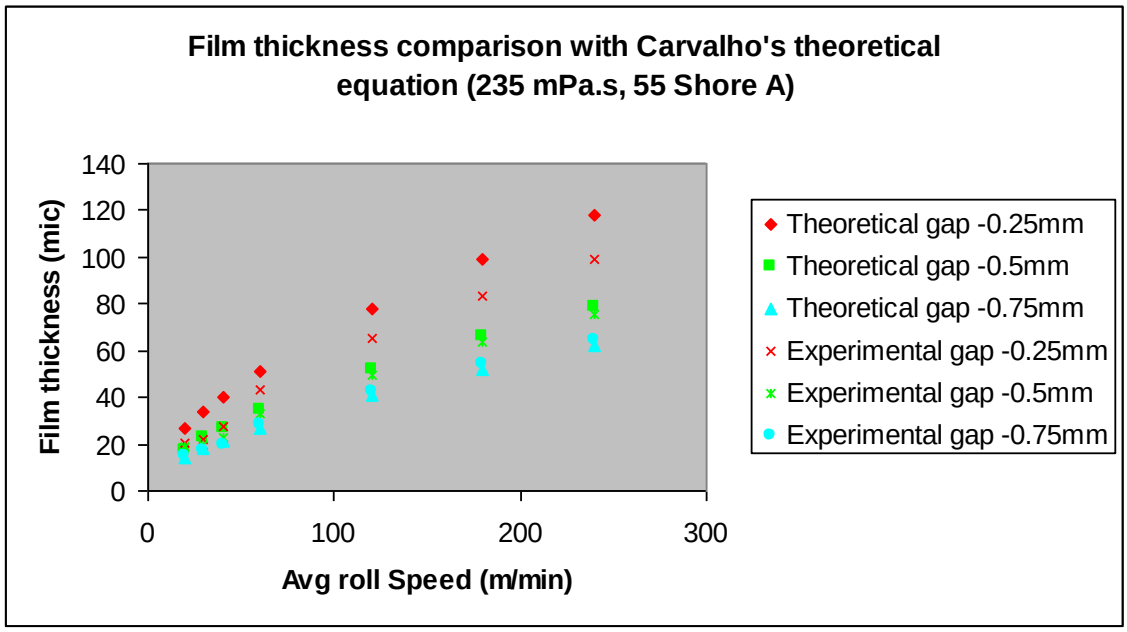

Figure 5-35 Film thickness comparisons with Carvalho's theoretical equation [19]

The theoretical predictions are very close to the measured film thickness for large negative gaps (higher load) conditions. In our study, the film thicknesses were measured with IR guage and the accuracy of measurement is ±1 μm. There are discrepancies at smaller negative gaps; the predictions giving larger film thickness than actual measured data.

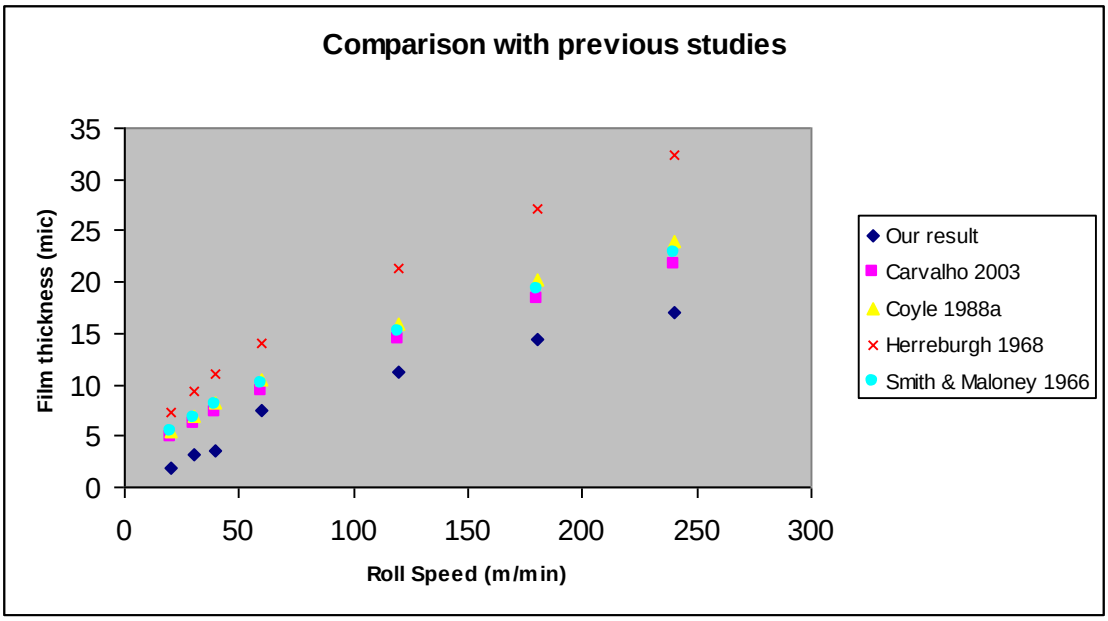

Figure 5-36 Film thickness comparisons with previous theoretical and experimental studies done at lower roll speeds [44, 19, 61, 63]

In the above comparison, Smith and Maloney [63] study was experimental while all other studies were done analytically. The experimental results confirm that the behaviour at high speed is not as predictable theoretically as the films are "ultra thin".

Although there are no direct correlative experimental studies to make a comparison to our studies, O.Cohu et.al [64] work has similar two roll experimental set up with following experimental conditions.

Table 5-16 Operating conditions for O Cohu and A Magnin work [64]

Fluid viscosity (Pa.s)	0.08 – 1.2
Roll Speed (m/s)	0.17 – 1.67
Applied load between rolls (N/m)	1932 –19963
Elastic modulus of the applicator roll cover (MPa)	0.94 – 3.25
Roll radius (mm)	118
Rubber cover thickness (mm)	12 – 25

The maximum roll speed used in the O. Cohu et al study was 1.67 m/s compared to 6 m/s in the current study, but a wider range of fluid viscosities were investigated (See *Table 5-16*).

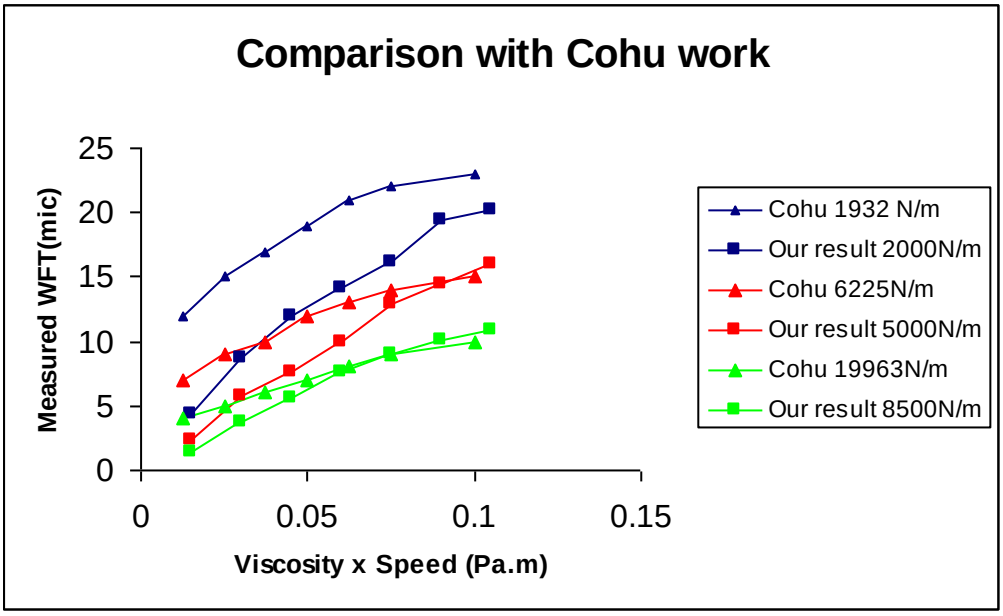

Figure 5-37 Comparison of our results with O.Cohu and A.Magnin [64] study

The main variation between the O. Cohu et al [64] and this study is more at higher roll speed conditions, for all load conditions. As the external load applied between the rolls is higher, at highest roll speeds the variation in the achieved WFT is approximately up to 10 µm. These discrepancies could be attributed to following differences between these two studies:

- Current study explores the previously uninvestigated high speed regime, and the fluid dynamics in this regime are likely to be different compared to those lower speeds.

- The viscoelastic properties associated with the rubber cover materials will be significantly different between the lower speed and higher speed regimes. Although PU material is used as rubber cover in both studies, and O Cohu et.al has given the viscoelastic property details of their studied material (0.94 – 3.25 MPa). The viscoelastic properties of current study are also measured at higher frequencies and results (1.8 – 7.6 MPa) show the discrepancies. The rubber cover thickness in O. Cohu et al study is 25 mm compared to 15 mm in current experimental set up, but both of them are in "thick" rubber cover regime.

- O. Cohu et al study used nip feeding with a third roll. This could offer higher control over feeding step compared to the pressurised pan feeding used in current study, and this could be one of the explanations for differences in measured film thickness.

5.3.2.7 Roller coating studies for non Newtonian model fluids

The three different non Newtonian model fluids with similar shear viscosities were tested on the lab roller coater and the results are as follows,

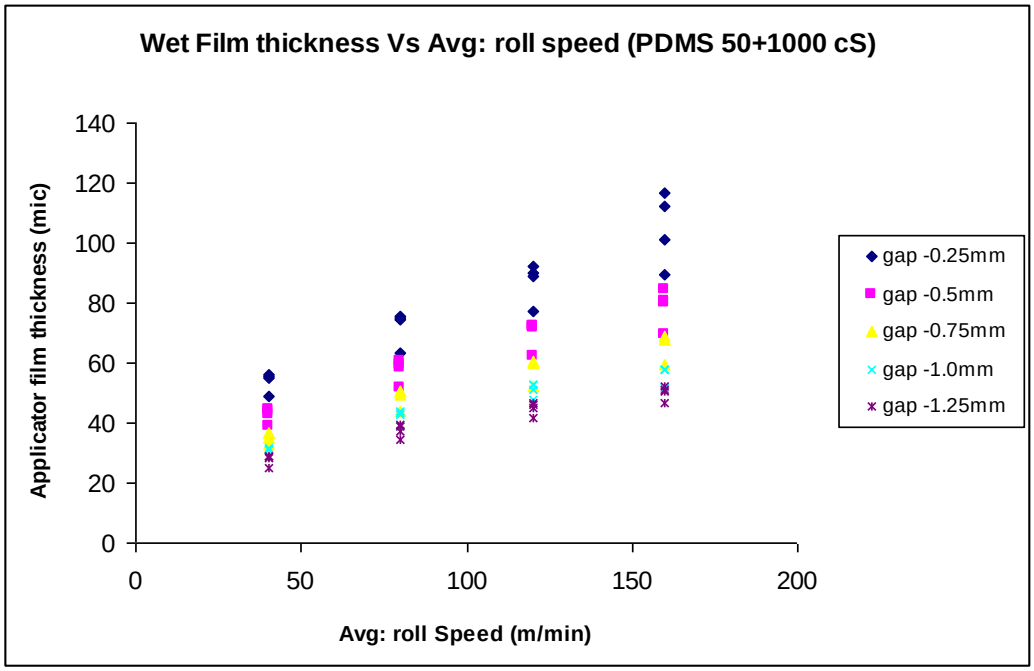

Figure 5-38 Low mole wt PDMS film thickness results

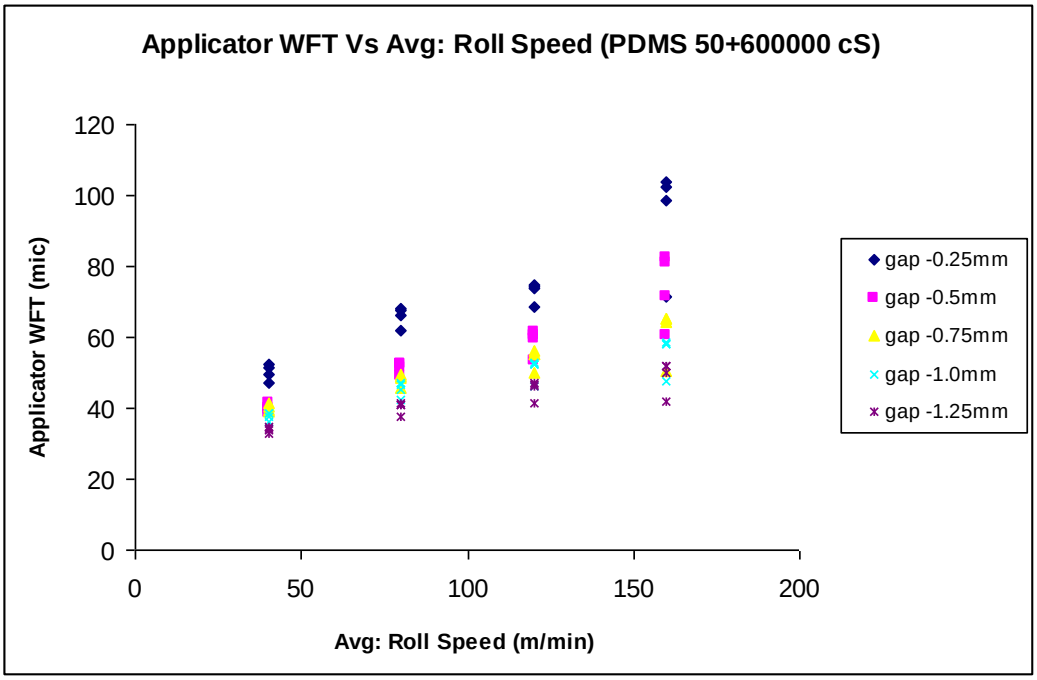

Figure 5-39 Medium mole wt PDMS film thickness results

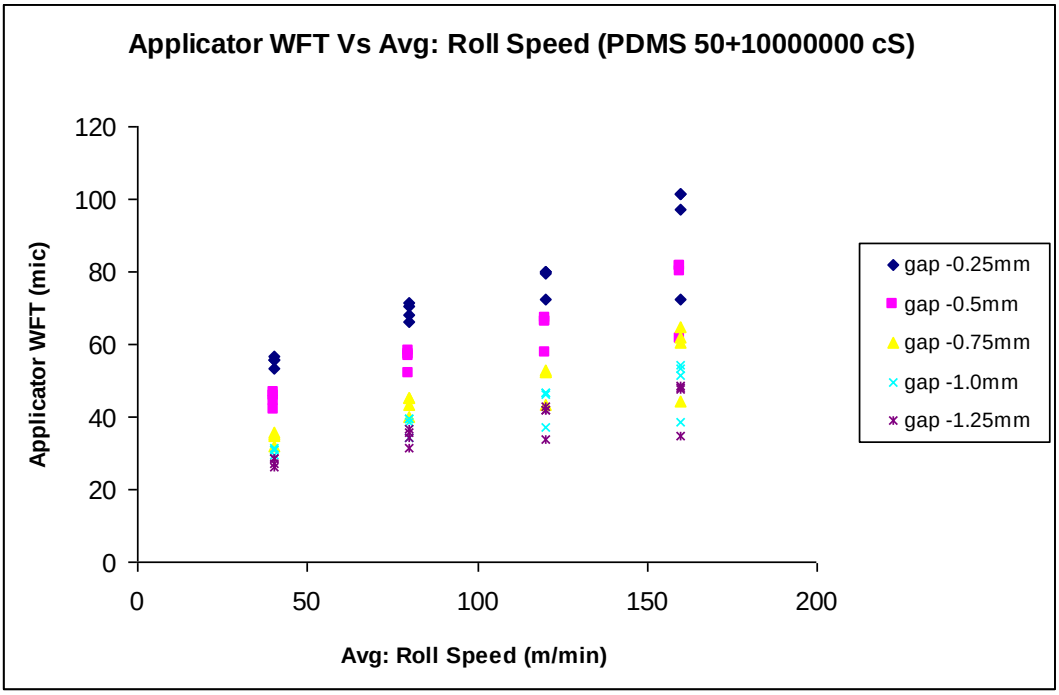

Figure 5-40 High mole wt PDMS film thickness results

The results indicate that the wet film thickness is very similar in case of all the three model fluids, even though the extensional viscosities of them are very dissimilar (See details in *Table 5-9*)

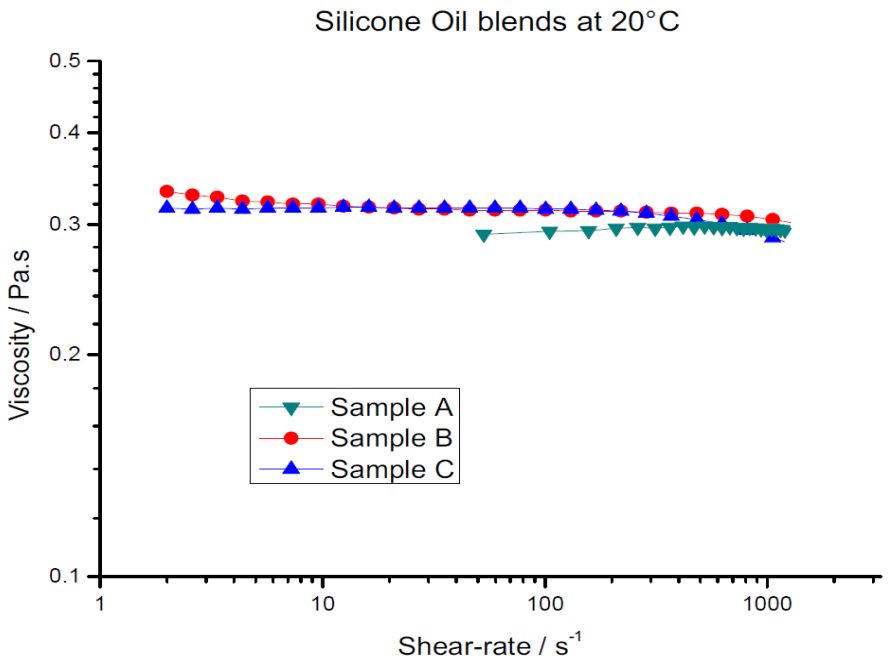

Figure 5-41 PDMS model fluid similar shear viscosities

Here three different model fluids (Sample A,B,C) have similar shear viscosities measured with rotational rheometer as shown in *Figure 5-41*, hence the final metered wet film thickness are also similar. To conclude, the results prove that extensional viscosity of the EB topcoat (Trouton ratio upto 5) will not affect the final coating thickness put down on the strip.

5.3.3 Film thicknesses at unequal roll speeds

In order to exploit the full potential of this coating system, an understanding of the effects of all the operating variables is necessary. One such important variable, the roller speed ratio $r_{s,}$ enables the splitting of the net flux through the nip into two films, one of which can be made extremely thin by varying the speed ratio. Previous experimental works [40, 41] have almost always been carried out at speed ratio equal to 1. Also, theoretical studies usually approach the film splitting analysis in a simple way which does not account for the complexity of the flow. For example, Carvalho and Scriven [18] suggested that the flow in the film split region of deformable roll coating resembles the one encountered when a substrate drags a liquid out of a pool, hence the 2/3 exponential variation with speed ratio.

A critical appraisal of these two flows in film split shows that they are very different, one issuing from a pressure-drag flow and one being purely a drag flow. Nevertheless, Carvalho and Scriven [18] analysed this dual drag flow using Landau and Levich [4] approach and it follows from this analogy that the flux distribution is related simply to the speed ratio as $Q_r/Q_d=r_s^{5/3}$, with Q_r and Q_s being the flux on the rigid and deformable roller respectively and r_s their speed ratio. This 5/3-power law

surprisingly agrees well with experimental data of unsymmetrical rigid roll coating [16] and its full flow analysis [39].

Kang et al. [70], Cohu [64], Jones [120] and Chong [74] are the only workers to report data on unsymmetrical deformable roll coating. Kang et al. [70] measured the flux distribution between the rollers and found it to remain, strangely, equal to 1 at all speed ratios. Cohu [64], on the basis of two sets of data at speed ratio of 1 and 6, however, found a very different experimental result, $Q_r/Q_d=0.83r_s^{1.60}$ which is close to the experimental correlation obtained by Benkreira et al [16] for rigid roll coating who found $Q_1/Q_2=0.87r_s^{1.65}$**.** Note that the constants, 0.83 and 0.87 reflect the effect of gravity in the vertical arrangement of the two rollers used by Benkreira [16] and Cohu [64]. Chong [2] presented data which did not correlate simply in term of the speed ratio; they also show a plateau above speed ratio=1.5. Jones [120] produced the most comprehensive set of data (1000 points) over a range of rubber hardness (30, 45 and 60° shore hardness), thickness of sleeve (7, 10, 12 and 17mm), viscosities (0.014, 0.055, 0.235 and 0.600 Pa.s) and roll speed ratio (0.33, 0.5, 1, 2 and 3) and could correlate all the data as $Q_r/Q_d=r_s^{1.40}$.

From the above descriptions, it is clear that there is a wide discrepancy between previous findings and a need to assess all this work and supplement it with new data. This is precisely the subject of this section. A common feature of all the previous experimental work is that it was carried out at low roller speeds never exceeding 90 m/min at most. The present technological drive is to coat much faster, so data in the higher speed range are necessary. The aim of this study is thus to both assess the flux distribution at low speed and supplement it with data over a wider

speed range reaching much higher speeds using forward configuration. It may be argued that the film-split region of a deformable roll coating is in essence no different from that of rigid roll coating. However, the pool of liquid at the separation region of a deformable roll coating flow is smaller to that present in rigid roll coating. In any case, experimental data supporting this fit are necessary to validate these assumptions.

5.3.3.1 Detailed analysis for dimensionless total flux and flux distribution

Although the correlation gives an overall dependence, was obtained earlier (*section 5.3.2*) the individual factor effects are analysed further in below sections. After the application of dimensional analysis the total flux and flux ratio were expressed in terms of five dimensionless numbers – gap number, elasticity number, speed ratio, capillary number and Reynolds number. The total flux was found to be dependent on average roll speed in all given experimental conditions, as shown in *Figure 5-42* and *5-43*.

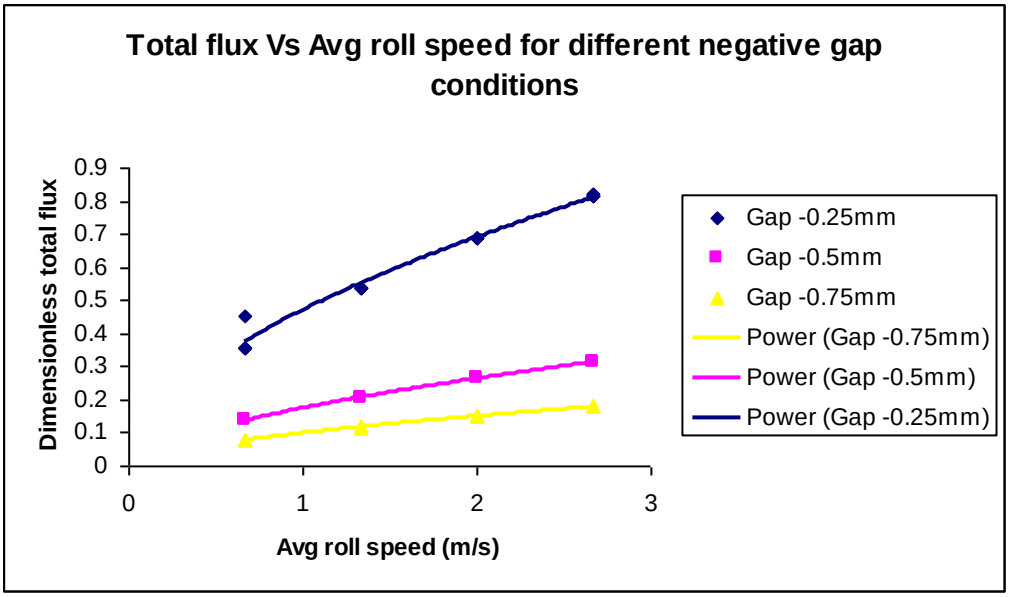

Figure 5-42 Dimensionless total flux relation with varying average roll speed under different negative gap condition (0.19 Pa.s, 55 Shore A)

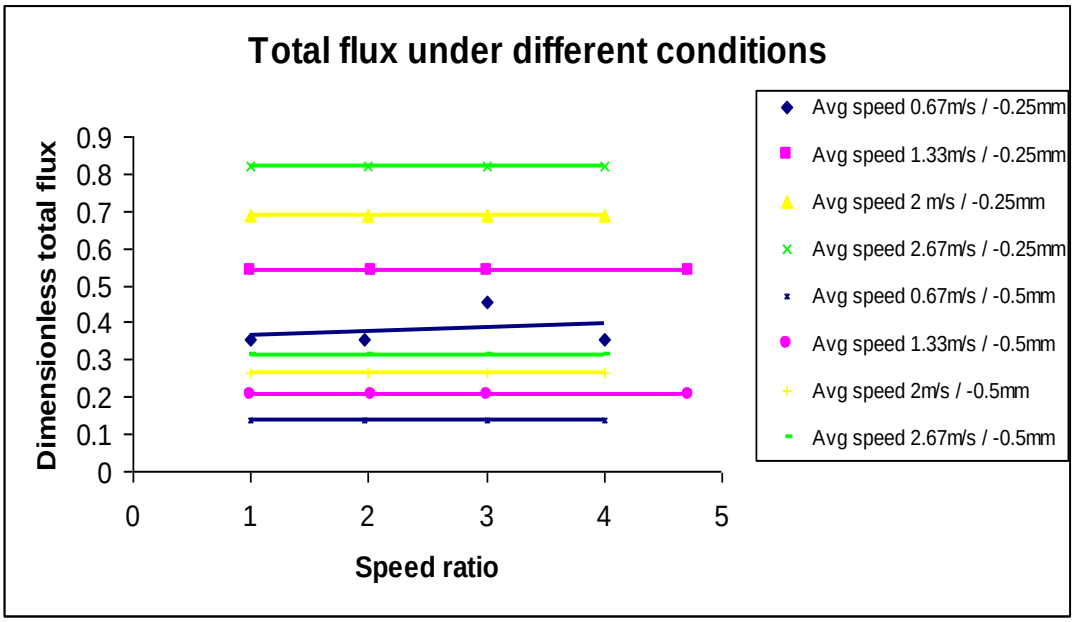

Figure 5-43 Total flux Vs speed ratio, 0.19 Pa.s, b = 15mm, 55 Shore A Hardness

Using the classical dimensional analysis, the flux distribution between the rollers q_1/q_2 can be expressed as,

$$q_1/q_2 = f\ (\mu u/ER,\ u_1/u_2,\ \mu u/\sigma,\ \rho uh/\mu,\ h/R)$$

Here in this study u, which is the average roll speed between the two rolls is kept constant and u_1 and u_2 were varied to introduce a speed ratio. Through various experiments, for a given fluid properties and operating gap between the rolls, the relationship between thickness ratio (h_1/h_2) and roll speed ratio has been established.

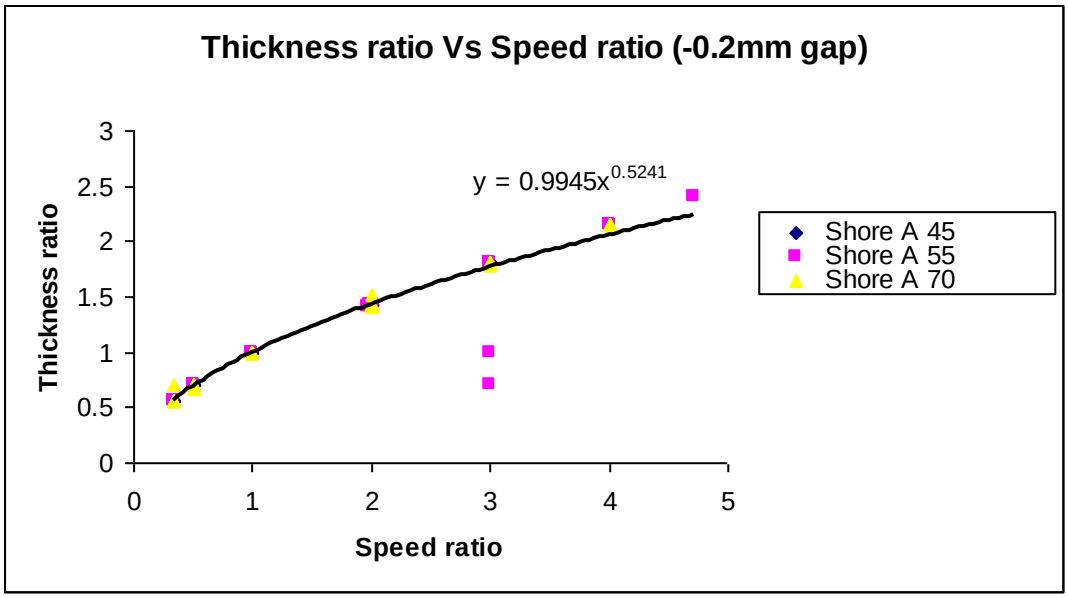

Figure 5-44 Thickness ratio with speed ratio for average speed 0f 0.67 m/s and different viscosities (-0.2 mm gap)

As given *Figure 5-44* at same average roll speed, looked into Newtonian fluids with varying viscosities such as 0.04, 0.1 and 0.19 Pa.s but with same negative gap condition. Building upon this, the average roll speeds are increased upto 2.67 m/s and the trend of thickness ratio found similar to *Figure 5-45*.

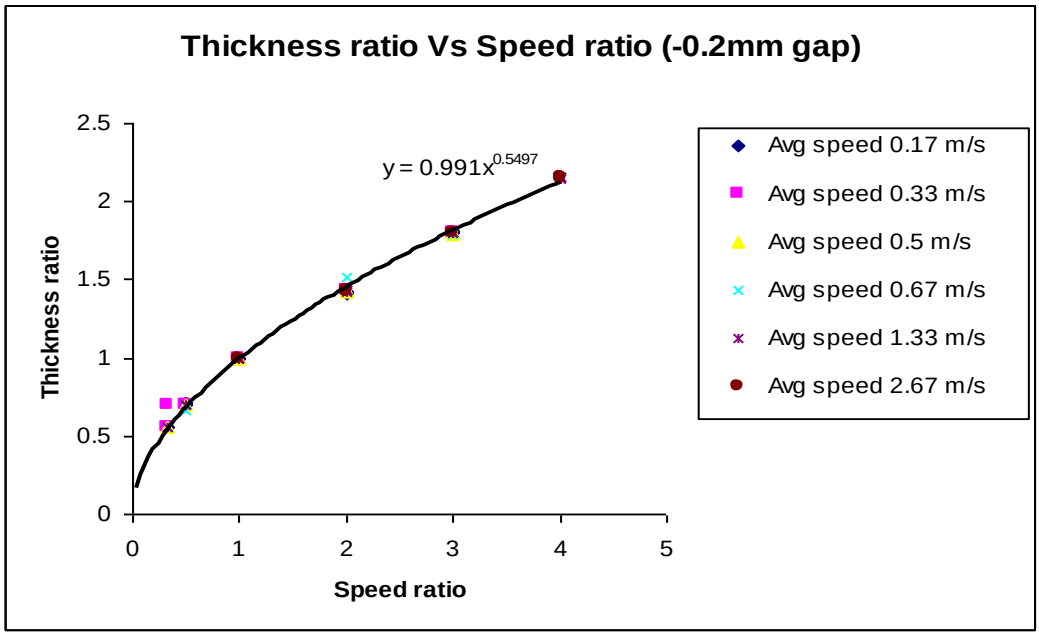

Figure 5-45 Thickness ratio with speed ratio for different average speeds and different viscosities (Shore A 55)

As in the case of rigid roll coating [16], an analysis of the data indicated that the flux ratio q_1/q_2 could be correlated adequately as

$$q_1/q_2 = \alpha\,(u_1/u_2)^{\beta}$$

In the case of deformable roll coating as well, the flux ratio was found to be strongly dependent on the speed ratio u_1/u_2, and the dependence was found to be week with other dimensionless groups. The α value found to be close to unity, as the configuration chosen in this study was not heavily depending on the gravitational forces [16]. Meanwhile the β value found to be consistent around 1.5 as shown in *Figure 5-46* and *Figure 5-47*.

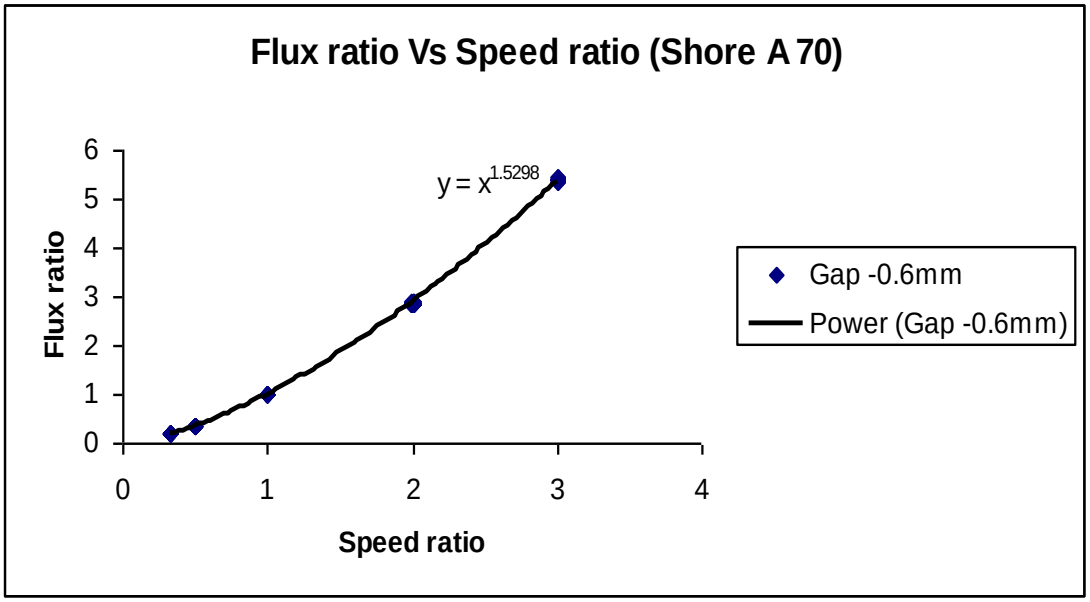

Figure 5-46 Flux ratio with speed ratio with average speed of 0.67m/s (Shore A 70)

As shown in *Figure 5-46*, the α value is 1 in this case and β value was 1.5298, which was found to be similar in all other conditions.

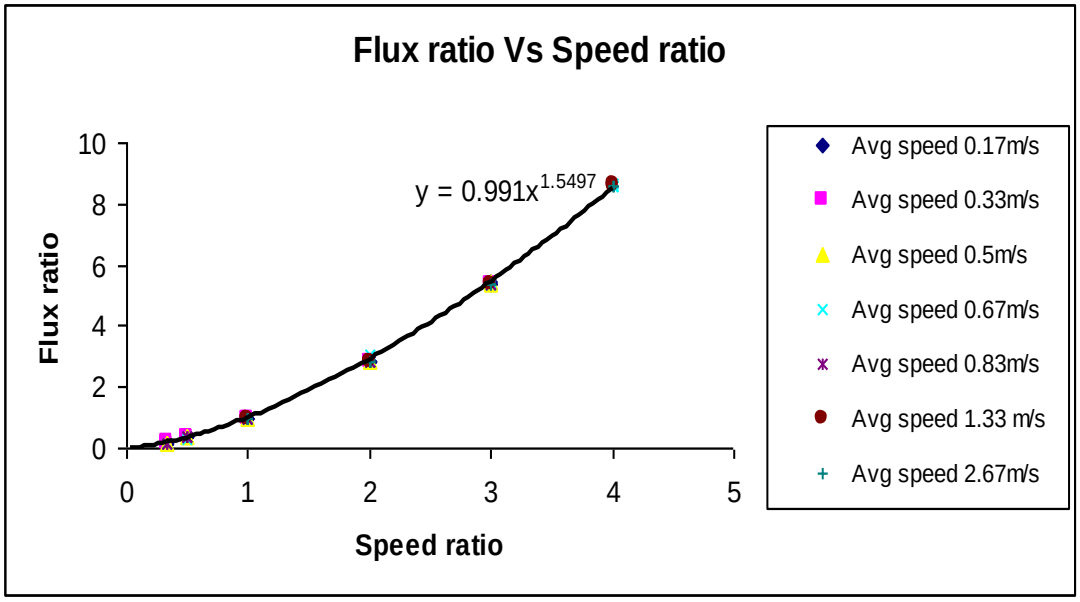

Figure 5-47 Flux ratio with speed ratio for different average roll speeds

Analysing flux ratio for different average speeds as shown in *Figure 5-47*, α, β values found to be similar to that of individual situation (*Figure 5-45*) and it is 0.991 and 1.5497 respectively. This data was further analysed, and as shown in *Figure 5-48* the increased negative roll gap found not to change the flux distribution under same speed ratio conditions.

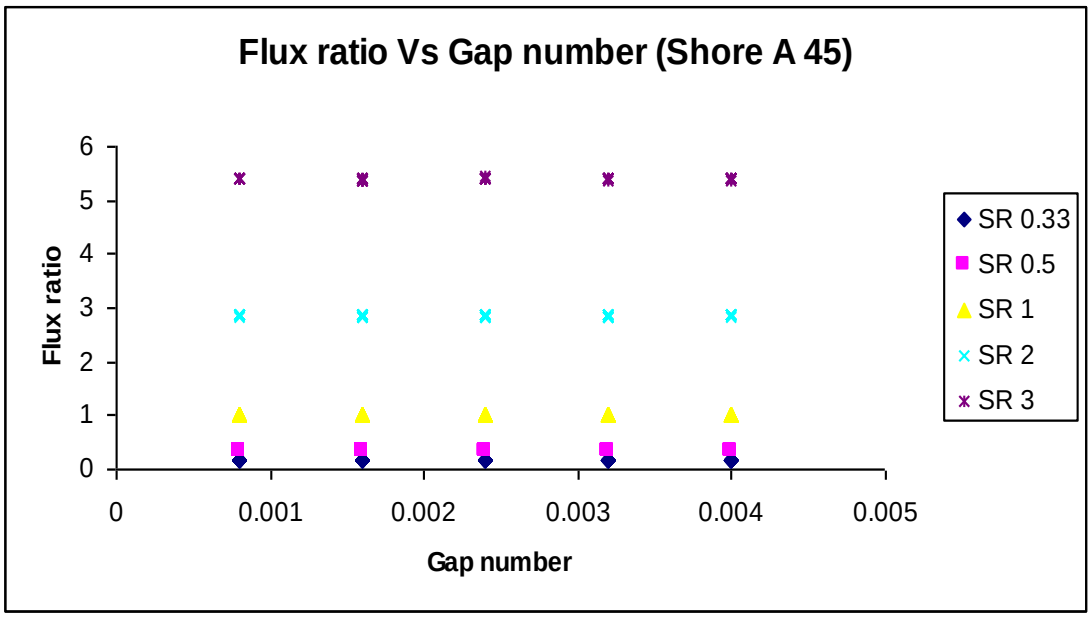

Figure 5-48 Flux ratio with gap number for different speed ratios

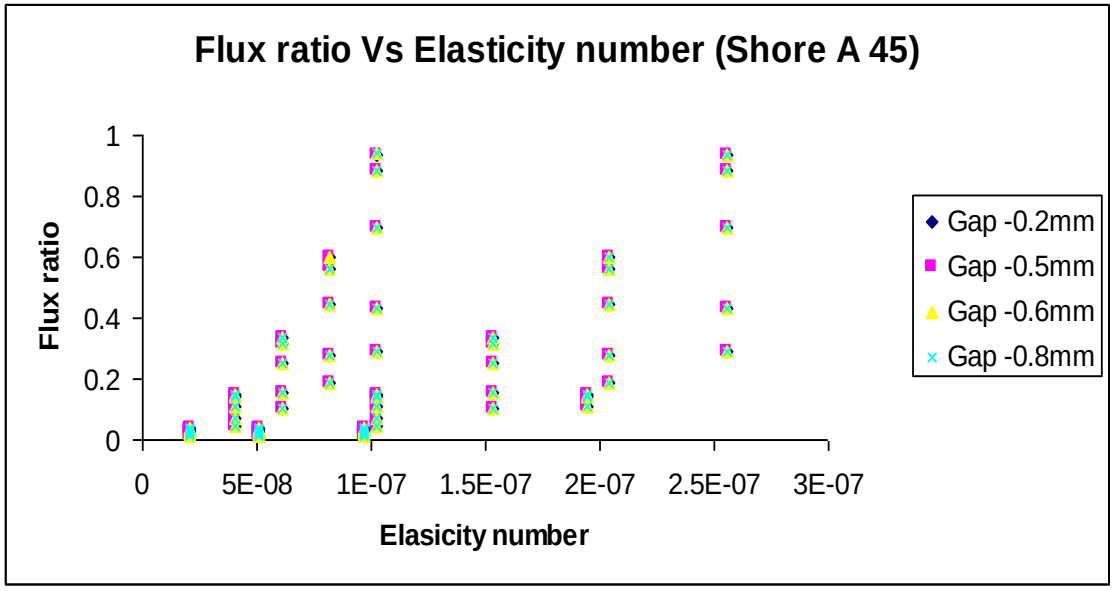

Figure 5-49 Flux ratio with elasticity number for different negative gaps (Gent [119]) calculation modulus used

Further to above, the change in elasticity number was not found to significantly affect the β value and the data found to be spread because of other hidden effects (*Figure 5-49*). As explained in *section 3.10*, the elastic modulus of the rubber cover used for the calculation of elasticity number are measured in four different ways 1) DMTA 2) From Rig measurement 3) Calculation based on Gent [119] equation 4) Measurement from tensile tests. These measuring approaches give different absolute values for elastic modulus as plotted in *Figure 5-50.*

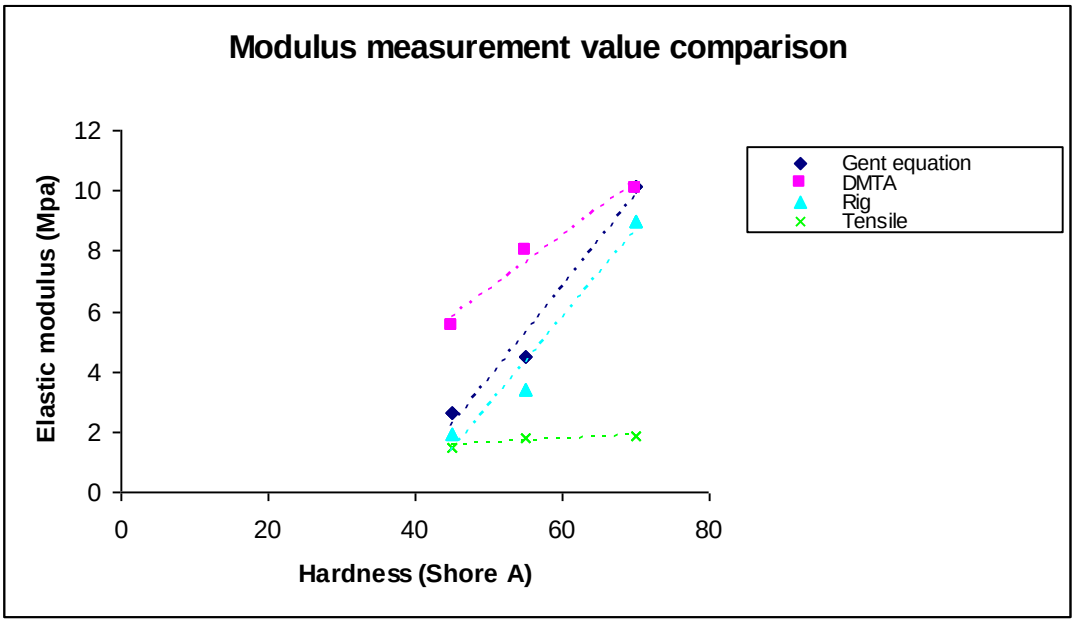

Figure 5-50 Measured and calculated elastic modulus of rubber with different methods

As the elastic modulus of rubber cover varies the elasticity number also varies but its effect with flux ratio found not to change significantly. In all four elastic modulus cases above, the β factor with flux ratio found to be around 1.08.

This concludes that fluid viscosity, roll hardness and roll gap are not significantly affecting the flux distribution phenomena under the range of parameters investigated, while speed ratio found to have the most influence. From our experimental study, the variation in α and β values related to various process parameters in a typical case can be summarised as given in *Table 5-17*,

Table 5-17 Summary of the experimental observations in case of Shore A 70, -0.2 mm gap

Thickness ratio Vs Speed ratio

Avg roll speed (m/s)	α	β
0.17	1	0.5278
0.33	1.0152	0.5039
0.5	1	0.529

0.67	0.993	0.5402
0.83	1.0004	0.5281
1.33	0.991	0.5504
2.67	0.991	0.5497

Flux ratio Vs Speed ratio

Avg roll speed (m/s)	**α**	**β**
0.17	1	1.5278
0.33	1.0152	1.5039
0.5	1	1.529
0.67	0.993	1.5402
0.83	1.0004	1.5281
1.33	0.991	1.5504
2.67	0.991	1.5497

As the configuration of the rolls is parallel, α value remains close to unity, and no effect of gravity. The β value could be approximated to 1.5 in case of whole roll speed regime (upto average speed of 160 m/min). Interesting to note that the detailed calculations in chapter 4 based on lubrication model also predicted β value to be 1.5.

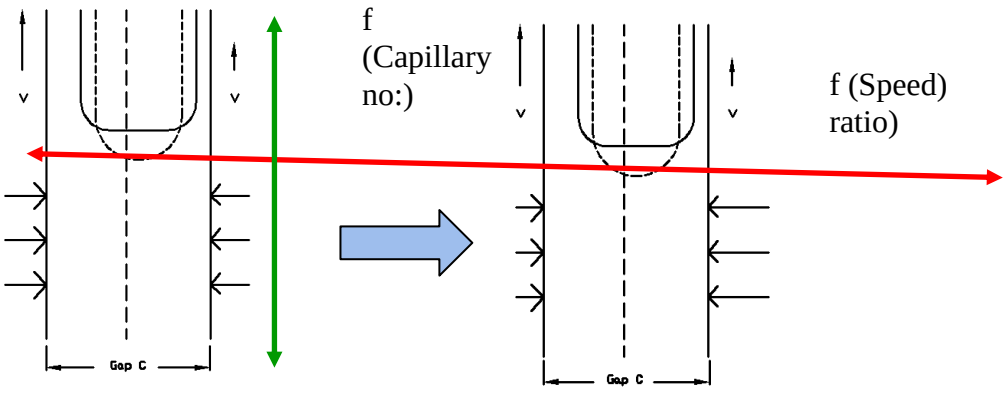

Figure 5-51 Hypothetical model for roll coating flux distribution

At higher roll speed, roll gap found to have a significant effect on flux distribution. The experimental results seem to be fitting well with the proposed hypothetical model (*Figure 5-51*). As the model proposed is representing the roll surfaces in a parallel plate way with a well defined gap between them. The film

meniscus seems to move in parallel direction depending on the roll speed and applied force between the rolls. The height of the origin of the meniscus from the centre of the gap is determined by the capillary number and meniscus seems to come down towards the roll gap centre with higher capillary number.

To summarise the above results,

- In overall analysis from 10 m/min up to 300 m/min roll speeds, the main factors influencing the dimensionless total flux (Q_T) passing through nip in deformable roll coating was found to be elasticity number (factor ~ 0.68) and gap number (factor ~ -1.36), while the influence of speed ratio, capillary number and Reynolds number found negligible. The influence of elasticity number was apparent while using either static or dynamic E values.

- In overall analysis from 10m/min up to 300 m/min, the main factor influencing the flux distribution in deformable roll coating was found to be speed ratio (factor ~ 1.53), while effect of gap number, elasticity number, capillary number and Reynolds number found negligible. The β value in this case is also agreeing to the results from detailed calculations based on lubrication model (As described in chapter 4).

- In low speed regime (average roll speed up to 40 m/min), and high speed (average speed up to 160 m/min) the influences of dimensional numbers found very similar for total flux and flux distribution cases.

- Measured roller coating film thickness for non Newtonian model fluids found to be similar to their Newtonian counter parts (for same high shear viscosity), and hence the correlations for total flux and flux distribution in case of non Newtonian fluids will be similar to Newtonian case.

5.4 Coatings used & their flow stability

As shown in previous research [103, 104, 106, 110, 112, 115], the extensional viscosity of the coating solution significantly affect the instabilities formed at high speeds. Here the three model fluids which replicate EB topcoat in terms of shear viscosity but having different extensional viscosities are investigated. Analyzing these three systems would give relevant information on the relationship between extensional component of viscosity and coating instabilities such as ribbing and misting.

5.4.1 Ribbing instabilities

In roll coating, at low roll speeds the fluid flow is two dimensional and steady; as the roll speed is increased, the two dimensional flow becomes unstable and is replaced by a steady three-dimensional flow which results in regular stripes in the machine direction, an instability known as ribbing (see *Figure 5-52*):

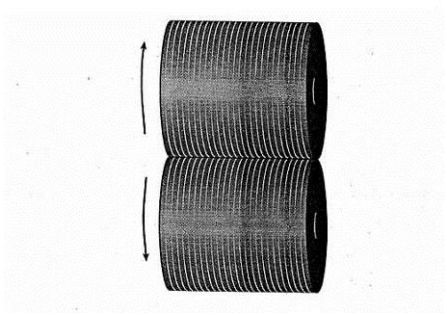

Figure 5-52 Diverging flow after film splitting creates ribbing

This type of instability is common in forward roll coating. If large enough these ribs can be easily seen, they will not level out and will limit the speed of the coating process.

Figure 5-53 Ribbing on steel substrate

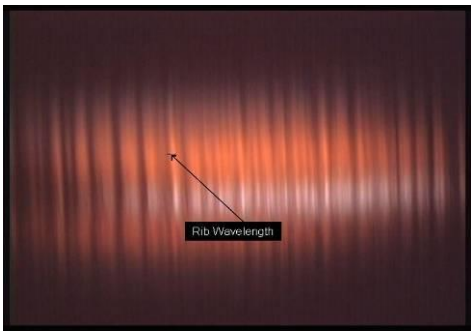

Figure 5-54 Ribbing lines observed in Bradford lab

5.4.1.1 WBPP coating- Newtonian fluid

The water based pre-treatment primer (WBPP) used previously as a Newtonian model fluid was diluted for the study of ribbing. This is done because, previous research showing higher tendency for ribbing of viscous fluids. Its viscosity measured in the Anton Paar Physica MCR 301 is shown in the *Figure 5-55*.

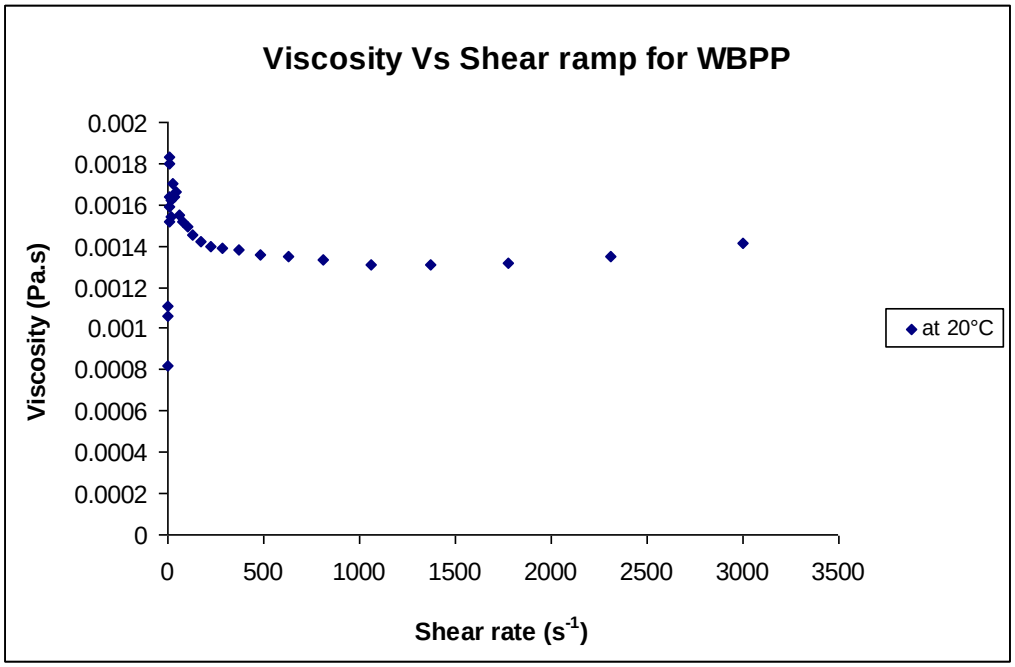

Figure 5-55 Flow curve for WBPP

Here the shear viscosity is found to be very low in the range of 0.014 to 0.016 Pa.s at ambient temperature. The coating is slightly shear thinning at low shear rates and later achieves a Newtonian plateau. These comparatively low values of viscosity indicate that, the contribution of viscosity to ribbing phenomena will be minimal.

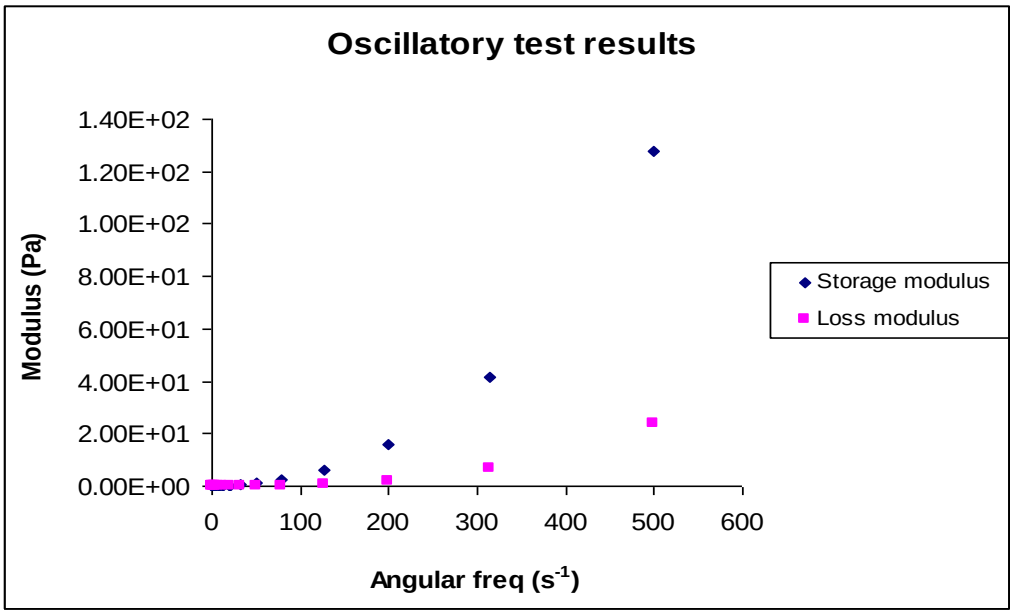

Figure 5-56 Oscillatory study for WBPP

The oscillatory tests done on WBPP show that the storage modulus of the coating is higher at higher angular frequency (lower time scale). This result indicates that the formulation is more gel like when in the feed in pan just before picking up and become viscous only when it is being sheared during coating application.

WBPP wetting concerns and optimisation

This part describes the second important aspect, which is surface tension and it is defined as the tangential force that keeps a fluid together at the air/fluid interface. Clearly it has an important bearing on surface instabilities, the ribbing and other defects that may occur during coating. Surface tension cannot however be

disconnected from the surface energy of the substrate (the balance of the forces represent the extent of wetting) nor can surfactants be considered apart from dynamic surface tension (they require a much longer time than water and other pure liquids to achieve dynamic equilibrium and their effect must be assess in relation to surface energy of the substrate). The essential attribute is that a positive spreading coefficient must result and this requires that the dynamic surface tension of the coating solution be lower than the surface energy of the substrate.

The contact angle was measured using the pendent drop measurement technique, as shown in *Figure 5-57*,

Figure 5-57 Pendent drop measurement system

The contact angle with the WBPP solution was measured to be around 41° (as shown in *Figure 5-58*), and it corresponds to a calculated surface tension of 68 mN/m

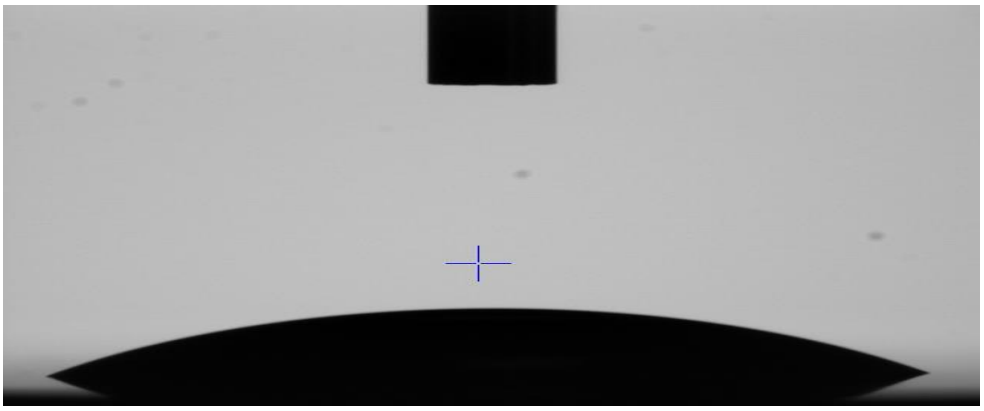

Figure 5-58 Contact angle measurement (~ 41°)

This surface tension value is comparatively higher, and it could be reduced by adding an appropriate wetting agent down to 30 mN/m. There is also a possibility that once the ribs are formed (as shown in *Figure 5-59*), they could level off reaching towards the drying oven. The levelling time in this case is determined by the Orchard equation,

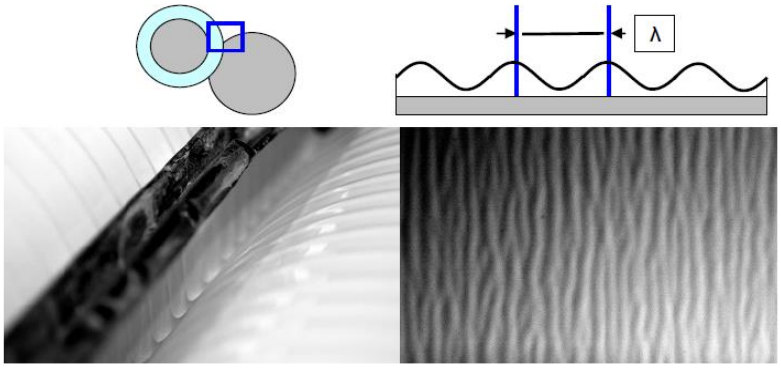

Figure 5-59 Rib formation in roll coating

$$a = a_0 \exp\left(-\frac{16\pi^4 h^3 \gamma t}{3\lambda^4 \eta}\right)$$

Here the amplitude decays exponentially as a function of "h" (wet film thickness) to the third power. Putting the experimental data from our study, the levelling time for ribs are calculated, and it seems to give higher value- reducing the possibility to level them off.

5.4.1.2 Experimental set up – quantification of ribbing

For quantifying and analysing ribs formed under different process conditions, an accurate measurement method is essential to distinguish between rib size, number and frequency. As shown in the *Figure 5-60*, a video camera (JVC RRGB TK 1270 with 3.5X lens) positioned above the top of the deformable roll was used to capture pictures of the rib pattern formed under various process conditions.

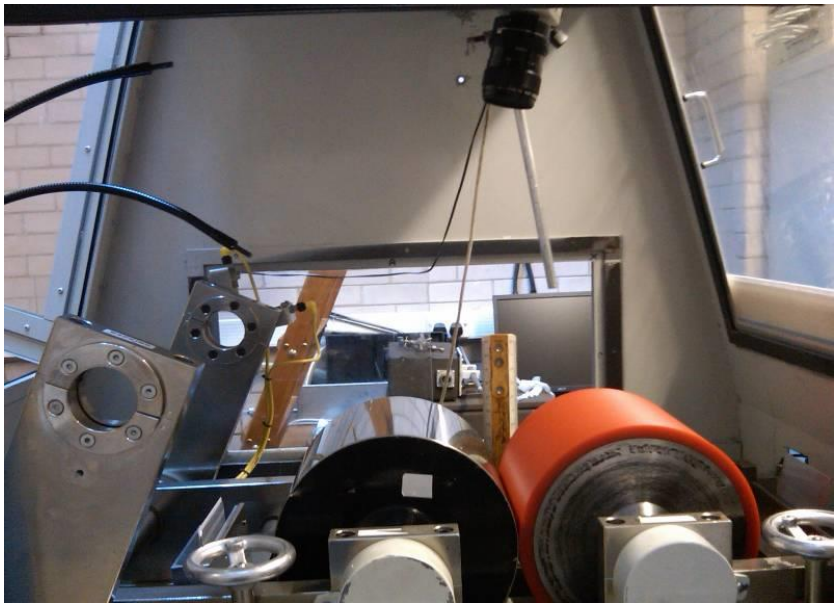

Figure 5-60 Experimental set up for rib measurement

Setting up the gap, the rolls started running at specific speed and once the stable conditions are achieved two photographs under same experimental conditions are taken (details in attached DVD). These photographs are analysed through image analysis software with a reference picture to be able to measure the distance between the ribs (rib wavelength). Ribs on the film were highlighted using a halogen light source, directed onto its surface at an oblique angle. This cast the valleys of the ribs into shadow thereby allowing the average wavelength to be measured from the resulting image.

Initially the smooth rubber roll with 65 Shore A hardness was used in the rig to understand the ribbing phenomena. Here the photographs are taken to analyse the natural ribbing frequency. At the same time, with IR gauge the relevant wet film thickness was measured and recorded. From these results the wet film thickness (WFT) found to increase with roll speed and decrease with increased negative gap between the rolls as shown in *Figure 5-61*.

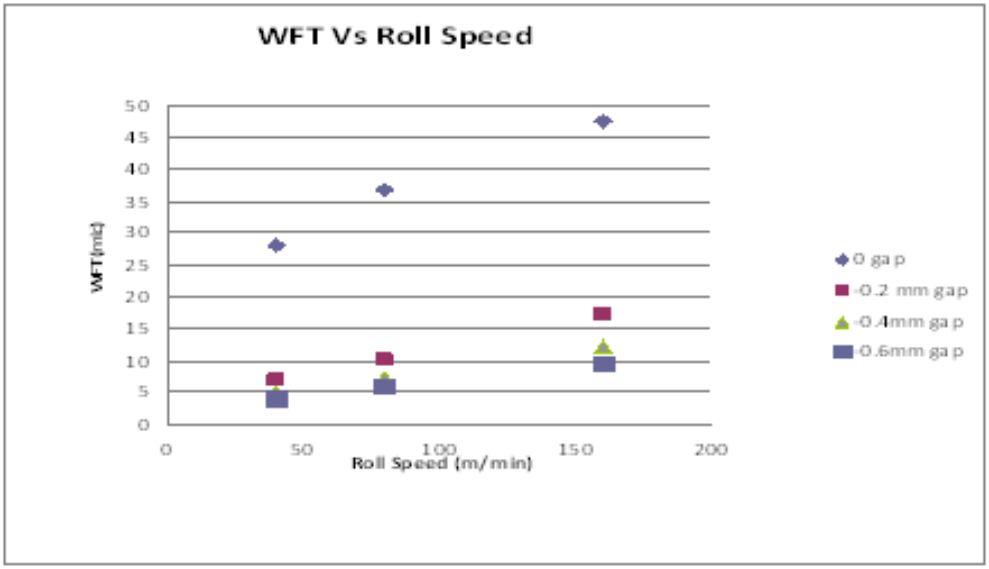

Figure 5-61 Film thicknesses against roll speed for WBPP solution

The film formation is also associated with its natural ribbing frequency, which was measured as mentioned in above section. The results can be summarised as given in *Figure 5-62* below,

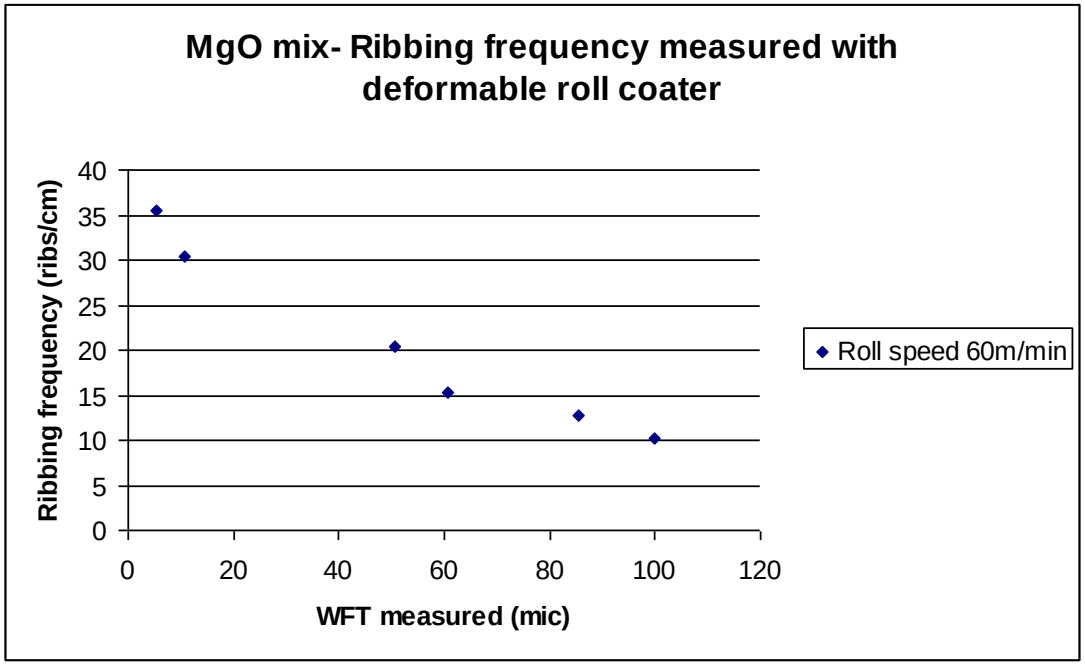

Figure 5-62 Ribbing frequency vs. WFT for smooth roll configuration

Here it is clear that, as the wet film thickness decreases, the natural ribbing frequency increases. This is equivalent to also saying that increasing negative gap (which decreases film thickness) will increase ribbing frequency. For a wet film thickness of 30 µm, the natural ribbing frequency found was 28/cm.

5.4.1.3 Masking ribbing with grooved rollers

Clearly ribbing on coated films is not desirable. There is thus a need to find a method to prevent it and if not possible to mask it without having to change fluid properties, operating speeds and film thickness. In order to mask the ribbing effect, one possibility is to use a roller that has "ribs" or grooves of the same frequency as illustrated below:

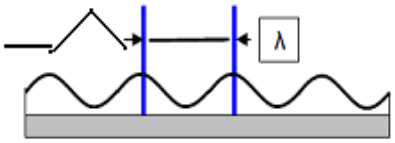

Figure 5-63 Masking effect of ribbing phenomena

Therefore a rubber roll with grooves of 28 grooves/cm was designed. After doing relevant calculations in order to keep the optimum cell volume (to achieve 30 µm metered wet film), the details are as follows. The details of calculation are given in *Appendix III*.

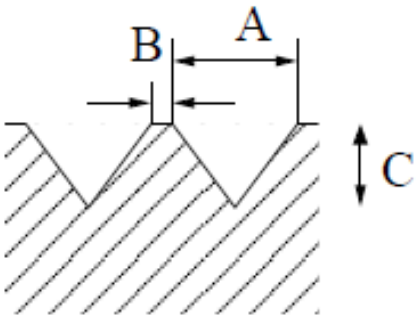

A – Groove width
B – Land width
C – Groove depth

Figure 5-64 Groove geometry dimensional details

1) Grooves/inch ≈ 28 lines/cm

2) Groove depth ≈ 0.0356 cm

3) Volume factor ≈ 0.045165 cm^3/cm^2

The data, a photograph of the film formed, with the grooved roller designed to mask ribbing are shown in *Figure 5-65*. It shows that the concept works very well.

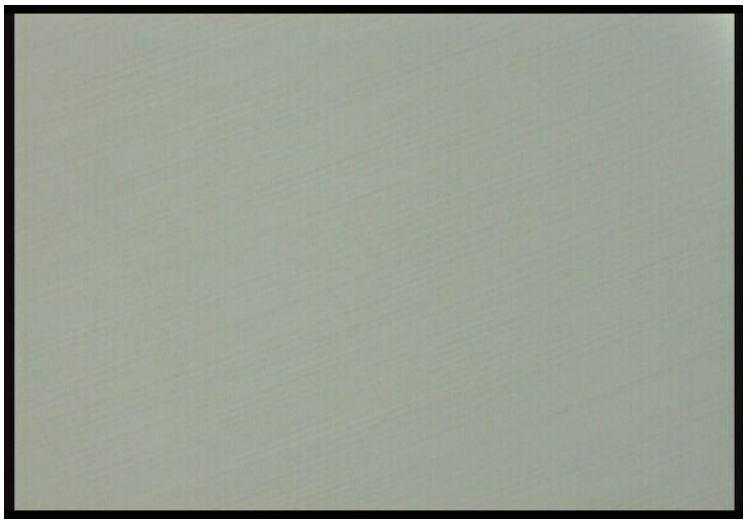

Figure 5-65 Photograph of coated surface with new geometry roll

5.4.2.1 EBR coating- non Newtonian fluid

Here we present our observations of ribbing with the non-Newtonian model fluids; solutions of PDMS of different molecular weight (see *section 5.2.2*). The data given in *Figures 5-66* to *5-67* shows how rib wavelength decreases with increasing negative gap. Also, the initial rib wavelength is seen to decrease with increasing extensional viscosity or using higher molecular weight.

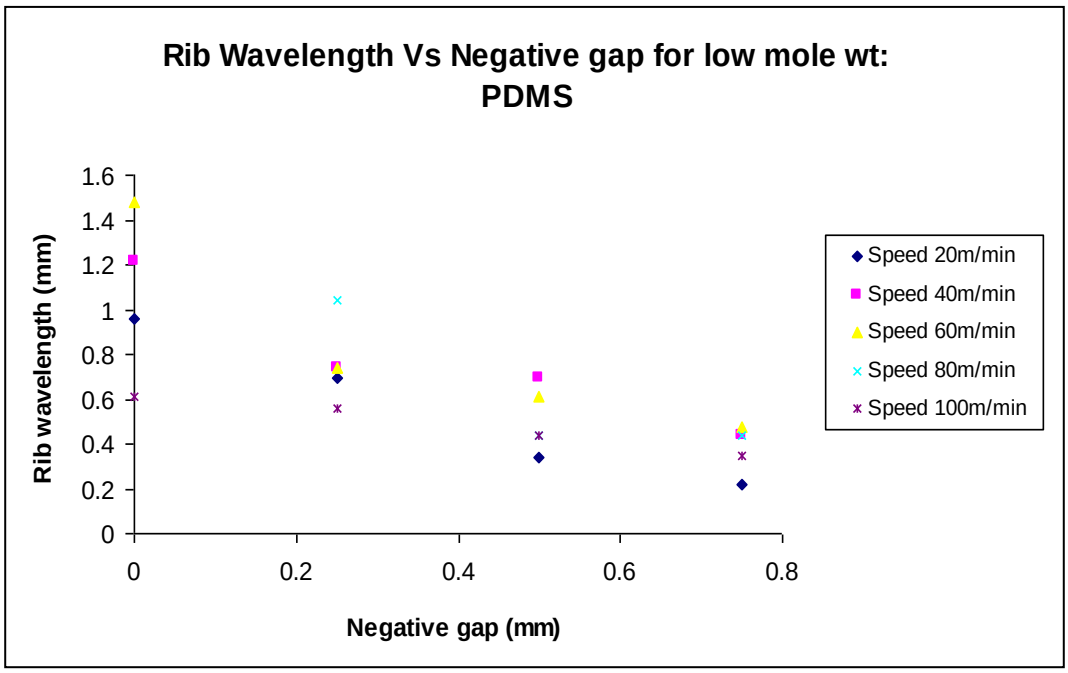

Figure 5-66 Rib wavelength measured for low mole wt: PDMS

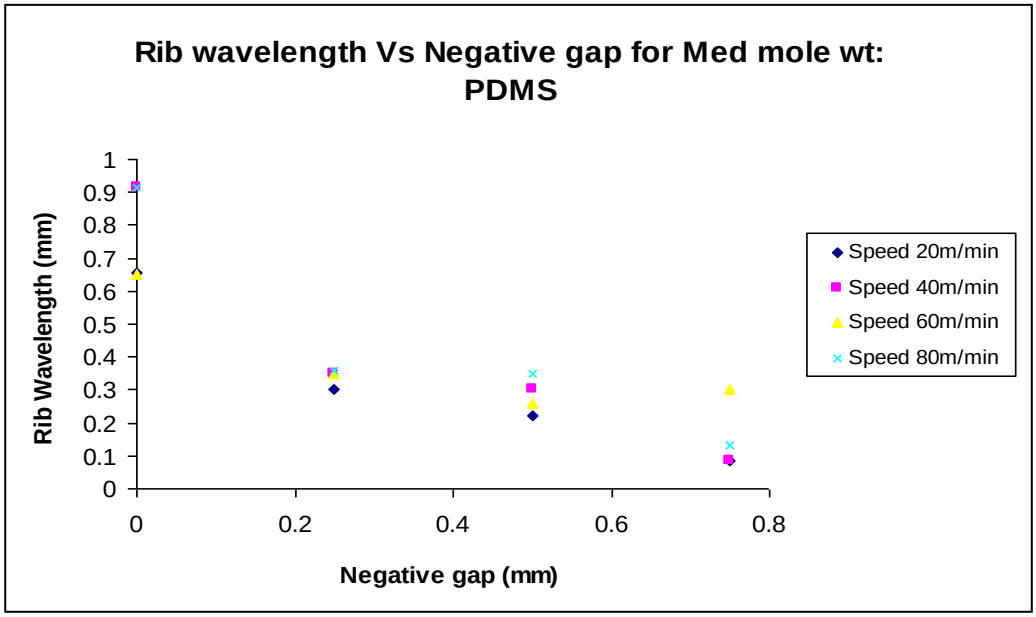

Figure 5-67 Rib wavelength measured for medium mole wt: PDMS

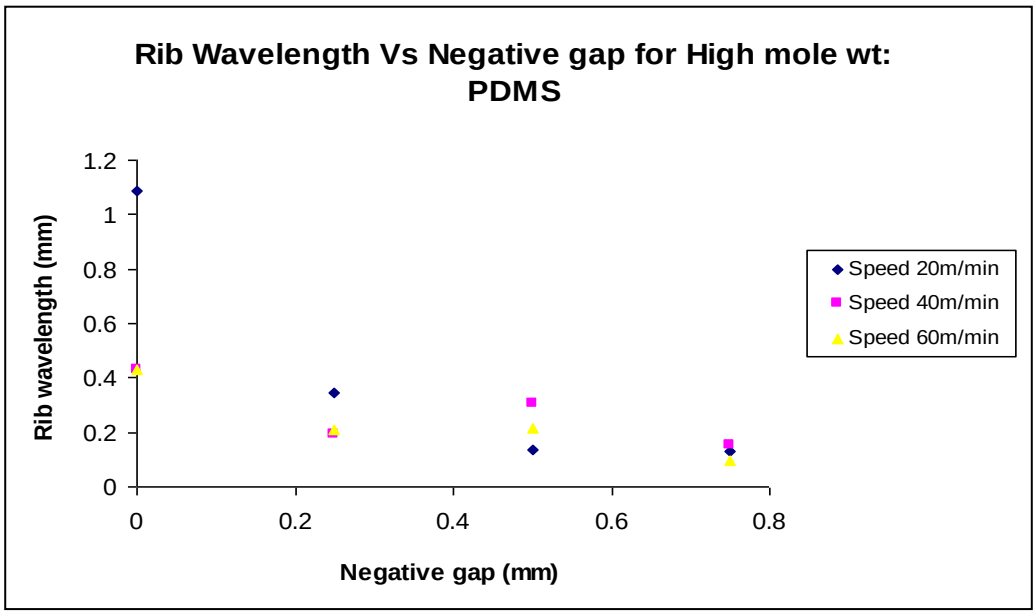

Figure 5-68 Rib wavelength measured for high mole wt: PDMS

An explanation for this phenomenon is that as the molecular weight of the system increases the chain length become longer. These chains act like being hold from both ends and this tend to decrease their width (as represented in *Figure 5-69*). Note that although we did not carry out experiments with the non-Newtonian fluids using

grooved rollers we expect the masking principles to hold. The reasons for not doing the experiments are that would have required the design of new rollers with similar rib frequency. We recommend however that in future work such experiments be done to validate the concept.

.

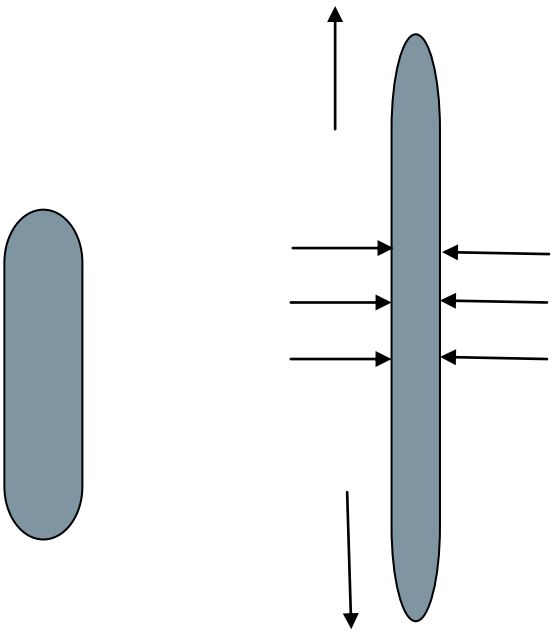

Figure 5-69 Mechanism of ribbing wavelength reduction

5.4.2 Misting instabilities

Forward roll coating is a fundamental coating flow that has attracted much research interest, particularly because it exhibits ribbing instabilities at low speeds. These instabilities are interesting fluid mechanic phenomena and have been the subject of numerous studies, experimental and theoretical as reviewed in the literature survey chapter. When operated with deformable rollers, these instabilities can be masked (very small wave length and amplitude) and this makes forward roll coating a simple and convenient technique of producing very thin films (~ 10 μm) at reasonably economical speed (~ 2-3 m/s). However, when the process is operated at

higher speed (~ 5 m/s), another form of instability appears called misting. This is essentially the ejection of fine fluid droplets formed during film splitting at exit of the nip flow. Misting is a serious limit to high speed coating as it affects the quality of coating coverage as well as creating environmental contamination and safety hazards (see a video of these instabilities in attached DVD).

Misting is a flow instability that occurs after ribbing. As the roll speed is increased beyond the onset of instabilities, the ribs formed are under increased extension; they break into filaments those once ejected form fine droplets as shown in *Figure 5-70*. Clearly non-Newtonian viscoelastic coatings will have a high tendency for forming such instabilities. We observed in our experiments that the speed at which the onset of misting occurs is decreasing with an increase in molecular weight of the coating solutions (see *Figure 5-71*) which indicative of the link with viscoelastic behaviour.

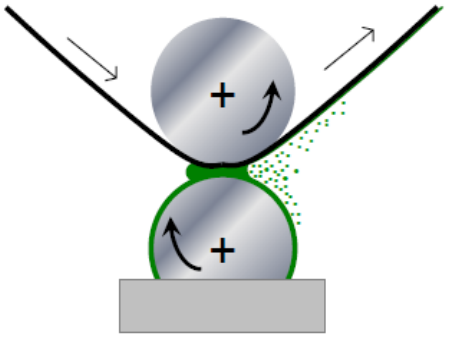

Figure 5-70 Misting phenomena in roller coating [71]

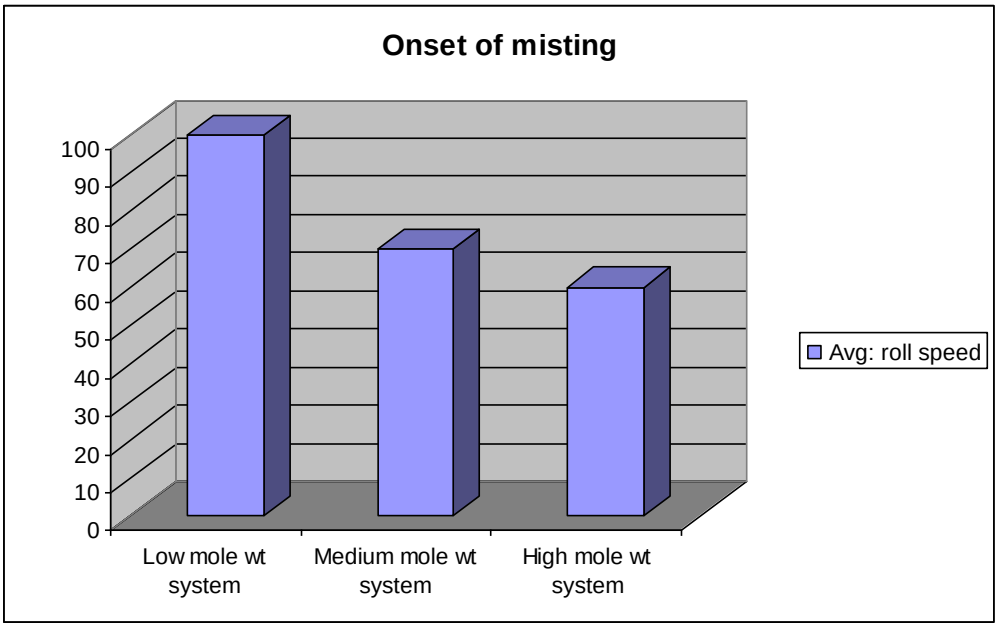

Figure 5-71 Onset of misting with mole wt system

CFD simulation of air entrainment and its link with misting

The numerical simulations were performed with the open source CFD code OpenFOAM [123, 124], which is based on the finite-volume method (FVM), and the interFoam solver is used for the solution of the multiphase flow problem, here air-fluid. The aim is to find the critical conditions that lead to air entrainment. In the simulations, the two-phase flow is described by the equation of continuity and the Navier-Stokes equations in two dimensions and the volume-of-fluid (VOF) method [125] is employed as interface capturing scheme. The two-phase algorithm in interFoam is based on the volume of fluid (VOF) method in which a transport equation is used to determine the relative volume fraction of the two phases (phase fraction) in each computational cell and the physical properties are calculated as weighted averages based on this fraction.

Initially two series of CFD simulations were ran, in order to investigate the effect on the meniscus position. In the first series, the viscosity was varied from 0.05 to 0.2 Pa.s and it was found that the meniscus moved closer to the gap when the viscosity was increased. In the second series, the roll speed was increased, leading to capillary numbers from 1 to 10 and here it was found that the meniscus moved closer to the gap as the capillary number increased. Both these results were in agreement with the results found in the comparing article [39].

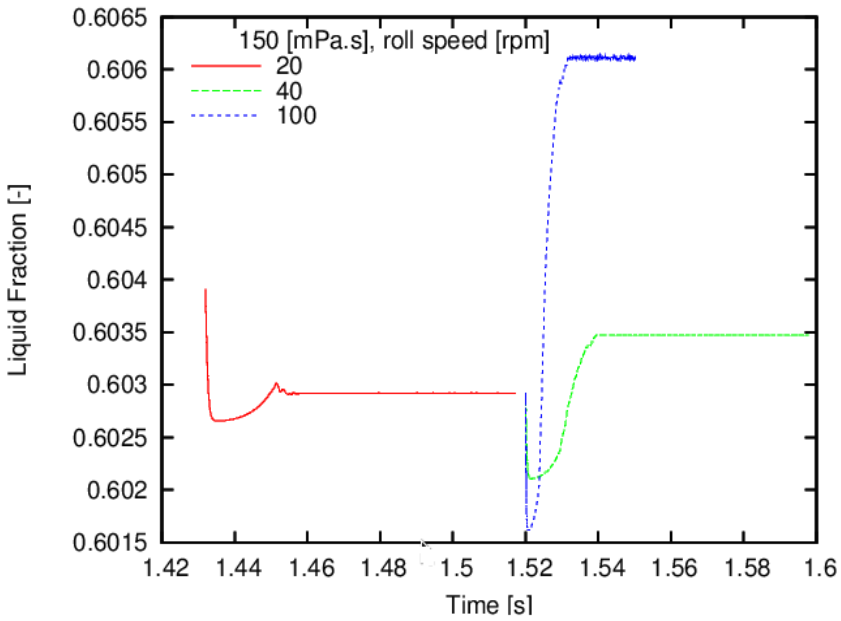

Figure 5-72 Onset of misting with roll speed

After initial verification the misting related high speed roller condition was investigated.As shown in *Figure 5-72*, the liquid fraction remains constant in time at speed 20 and 40 m/min but shows a wide fluctuation at 100 m/min, which is indicative of air entrainment occurring. Interestingly as shown in *Figure 5-71*, the experimental result in case of low molecular weight fluids for the onset of misting is around 100 m/min. For similar operating conditions observing onset of misting at 100 m/min is validating the results of the model. This also suggests that the onset of

misting and air entrainment is closely related phenomena. One mechanism we propose here for the onset of misting is that upon the onset of air entrainment, the air bubbles exit the nip and impart energy to the already elongated ribs which then transform into a mist. This is the first result reporting such a link between air entrainment and misting but further experimental studies are necessary to fully confirm it.

5.5 Pilot line trial

Although it is possible to develop a large amount of knowledge from laboratory-based studies, ultimately a high-speed pilot line facility is essential if high-speed coating and curing technologies are to be developed and validated prior to installation on a commercial production line. An external pilot line facility owned by Polytype Converting SA in Fribourg, Switzerland, was identified which has the capability to process very thin gauged (0.1 mm) steel substrate. Pilot line trials were undertaken in order to assess the feasibility of using this facility to investigate high-speed coating processes for EBR curable products. This section summarises the findings from this important exercise.

5.5.1 Description of the pilot line

- This coating line (diagram and full details in *Appendix V*) comprised of a coating section which can be fitted with a coating head selected from a range of coating methods. Here a deformable roll coating head was used.
- A Infrared oven for drying or curing as required;
- A UV curing station fitted with a FUSION F600 microwave powered system, a wide web arc lamp system from FUSION AETEK and nitrogen inerting;
- A cooling station;

- A Corona station to prevent static electricity to form on the substrate;
- An EB curing station where he accelerating voltage operation can be set within a bandwidth of 125 to 250 kV, with a maximum dose of 1,400 Mrad m/min at 175 kV. Here the reaction chamber is inerted with nitrogen gas.
- A wet & dry laminating station.

To summarise, this pilot line has the capability to conduct line trials with 0.1 mm steel substrate at line speeds of 360 m/min and above. For this line trial, Tata Steel Special Strip Division produced 0.1 mm thick substrate with smooth, mirror-like finish (Ra was evaluated to be 0.087 µm). The 0.1 mm thick cold-rolled steel substrate, made in accordance with EN 10139/10140, steel grade DC04, hardness LC, both sides with a smooth finish, was manufactured by TSSS. Once manufactured the strip was oiled and then slit. A number of the coils had a raised metal edge (or burr) as a consequence of the slitting process. The slit coils were then transported to the IJmuiden Pilot Coating Line (PCL) where they were cleaned, recoiled onto steel cores with diameter of 398 mm and a width of 500 mm and then loaded into specially designed boxes which were purged with nitrogen in order to prevent oxidation of the cleaned steel surface. The boxes were opened less than 24 hours before the line trial and the steel still had a very good visual appearance. The average water contact angle of this material was measured to be 28º. A more detailed check-list of tasks undertaken during the preparation of these line trials can be found in *Appendix V*.

Trial of EBR curable coating system

A commercially available EBR curable paint system for use as a primer on a paper substrate was used. It had a viscosity of 115 mPa.s when heated to 40°C and the

objective was to be able to produce a uniform film of thickness in the range 5-20 μm at line speed of 360 m/min.

The coating configuration used was a 3-roll reverse coating, nip fed set-up and is presented in *Figure 5-73*.

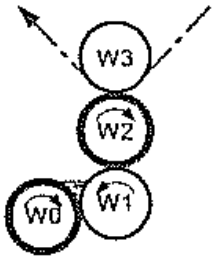

Figure 5-73 Coating head configuration for EB coating (rollers W0 and W2 have a rubber EPDM cover)

The range of conditions tested during this trial is presented in *Table 5-18*. In total 16 groups of settings were investigated, 4 of which were on steel substrate (from 10UW82). The paint was not heated during first 11 trials and it had the viscosity of 420 mPa.s.

5.5.2 Trials with PET and aluminium substrates

The processing conditions were first optimised on PET at a range of speeds (100-400 m/min) in order to adjust the dry film thickness (DFT) and the quality of the coating. During the first set of trial runs EBR cured films with DFT of 7, 14 and 22 μm respectively were achieved at a line speed of 100 m/min. An EB dose of 25 kGy was used to cure the coating during the first trial. As the coating was highly cured (evident due to the obvious shrinkage of the coating as a result of the high degree of crosslinking), the dose was reduced to 10 kGy. Further optimisation of the coater set-up was made during the trials with aluminium foil. Pin-hole type defects were observed on all coated materials and these were attributed to air entrainment

occurring when the rollers plunged into the feed tank. In order to reduce this defect the pick up roller speeds was decreased but this reduced the maximum film thickness that could be applied. Splashing was also observed when applying unheated (higher viscosity – 420 mPa.s) paint at higher at line speeds and with high DFT (20 µm). Therefore this limited processing for a low DFT film of 10 µm.

5.5.3 Trials with steel substrate

The paint was applied onto the steel substrate at a temperature of 40ºC in order to reduce its viscosity from 420 mPa.s to 115 mPa.s. This step reduced the film thickness picked up and eliminated splashing at the coater-head when coating at 400 m/min. Although the concentration of micro bubbles in the paint decreased, they were not totally eliminated. As a consequence of the reduction of the viscosity the negative gap between the rollers W0 and W1 (*Figure 5-70*) had to be reduced in order to allow more paint to go through the nip. As the coating that was applied during this trial was a model EBR coating, no significant performance related testing was performed with this material. The main focus of the testing was to evaluate the dry film thickness (DFT) for the given processing conditions and the quality of the coverage.

Dry film thickness (DFT)

During the trials, the coating weight applied on the strip ranged from 7 to 22 µm by varying the gap between the rollers W0 and W1 and their relative speeds with line speed ranging from 100 to 400 m/min (see *Appendix V*). As the pilot line instrumentation was only able to measure the footprint or contact length between a steel roller and a deformable roller (see zoom on *Figure 5-74*), a study was undertaken in order to find an equivalence between footprint and negative gap. The

footprint measurement was done on the Bradford laboratory roller coater using the technique used in the pilot line. This consisted of sticking a "magic" pressure tape on the deformable roller which left a foot print that could be measured at any given negative gap. The results were compared with a simple geometrical model suggested by Hannah [7]. As one can see in *Figure 5-74* there is very good agreement confirming the validity of the equation for the Bradford set up.

If one compares the negative gaps that were used during the trial (i.e. in the nip between the steel pick up roller and applicator roller or the nip between the applicator roller and the strip) it shows that they are in the order of 0.2 - 0.3 mm which is quite small compared with the experiments that have been done in Bradford [8]. This small negative gap could explain why the wiping of the formulation onto the substrate may not have been 100% efficient in the reverse mode.

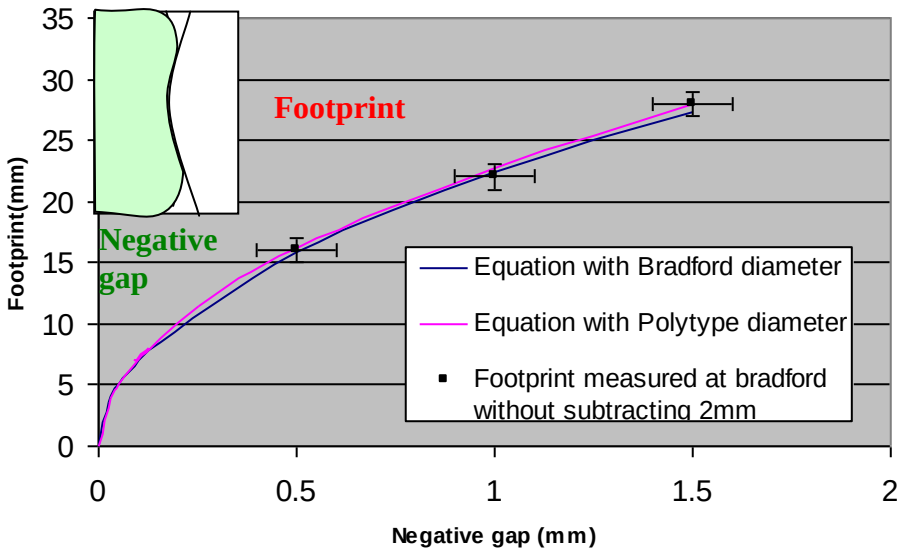

Figure 5-74 Relation between footprint and negative gap in Bradford and correlation with Hannah equation [7] for both pilot line facility and Bradford case (error bar are error of measurement reading 0.1 for negative gap, 1mm in footprint)

As the experiments were done with the coating solutions maintained at two temperatures giving two viscosities conditions (420 and 115 mPas), the gap/footprint between W0 and W1 was changed for each viscosity. From the analysis of the footprint for the first set of data (where the viscosity was 420 mPas) there was an 8 mm footprint (according to the Polytype measurement) between the roller W0 and W1 and a smaller footprint of 5mm between the roller W1 and W2. This indicates that the controlling nip for optimising coating thickness is the nip between the roller W0 and W1.Typical film thickness data collected in the trials are given in *Table 5-18*

Table 5-18 Actual parameter and final wet film thickness on strip in pilot line trial

Line Speed (m/min)	**Foot print (mm)**	**P/Up Speed (m/min)**	**Appl Speed (m/min)**	**Speed ratio**	**Avg: Roll Speed (m/min)**	**Final WFT on strip (mic)**
50	8	5	20	4	12.5	11.1
50	8	5	15	3	10	7.1
50	8	5	25	5	15	15.3
100	8	10	50	5	30	24.5
100	8	10	40	4	25	17.8
100	8	10	30	3	20	11.5
150	8	15	45	3	30	14.5
200	8	20	60	3	40	17.5

Now the above wet film thickness results are compared in *Figure 5-72* with film thickness data obtained from lab roller coating analysis and which were correlated by:

$$WFT_1 = \alpha(\,footpr\,\mathrm{int}/\,gap, vis\cos ity) * \left(\frac{(V_0 + V_1)}{2}\right)^{0.61} * (S)^{0.53} \quad [5.1]$$

Where $\alpha(\,footpr\,\mathrm{int}/\,gap, vis\cos ity)$ constant that depends on footprint or gap and viscosity, S is the speed ratio between the applicator and pick up rollers. As shown in *Figure 5-75* there is a good agreement considering the experimental error that occur

in the measurement of speeds and gaps. Even if these very small (< 5%), they would accumulate.

The first important conclusion of this research is that the laboratory data describe very well actual industrial operation over a wide range of conditions. This is actually to be expected as there is here no real scale-up issue. The films produced in the laboratory were different only in that they were produced over a shorter width and on the rollers rather than on the substrate. This is an important observation for future research, giving confidence in the use of laboratory coaters of the type developed for this research.

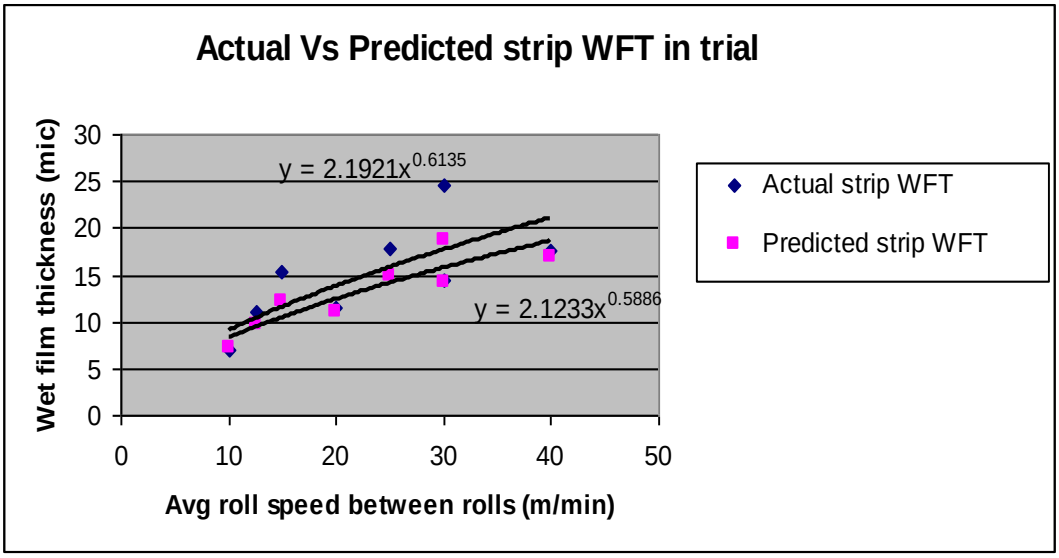

Figure 5-75 Comparison between actual and predicted pilot line trial wet film thickness data

Quality of the coating

Having found a good fit between the film thickness measurements in the laboratory and in the pilot line, we now examine the quality finish of these films in an attempt to assess instabilities that might have arisen in the pilot line trials. The *Figure 5-76* shows the EBR coating have pronounced orange peel effect with increasing speed.

But it has an acceptable visual aspect up to 300 m/min with more pronounced orange peel effect at 400 m/min. However it should be noted that EBR coating used in trial was not designed to make thin paper primer coatings (below 4 µm) and hence the orange peel defect is not a big concern. More relevant, orange peel defects are related to drying issues and a flow problem.

The analysis with Talysurf confirms the worsening of the appearance with speed (via an increase in Ra). In order to understand the reason behind this, it is necessary to investigate the effect of the EBR curing of the coating.

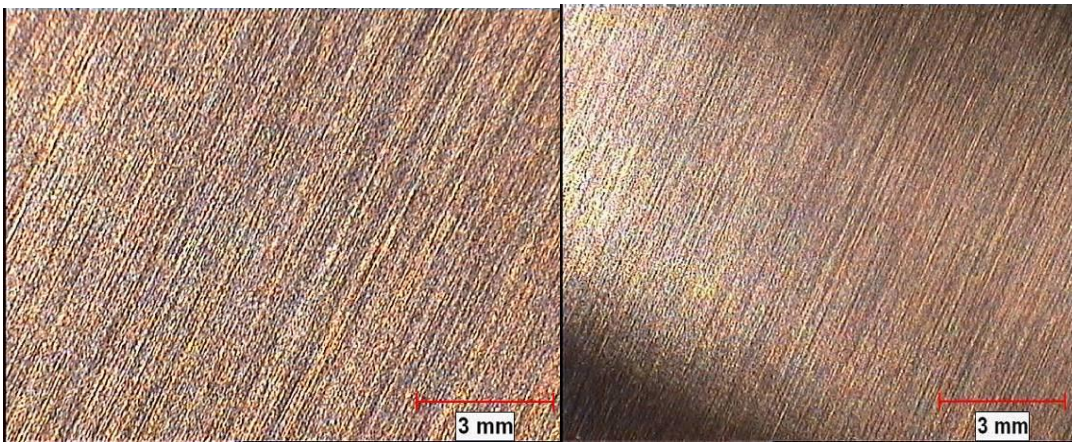

10 UW 83 (100m/min)

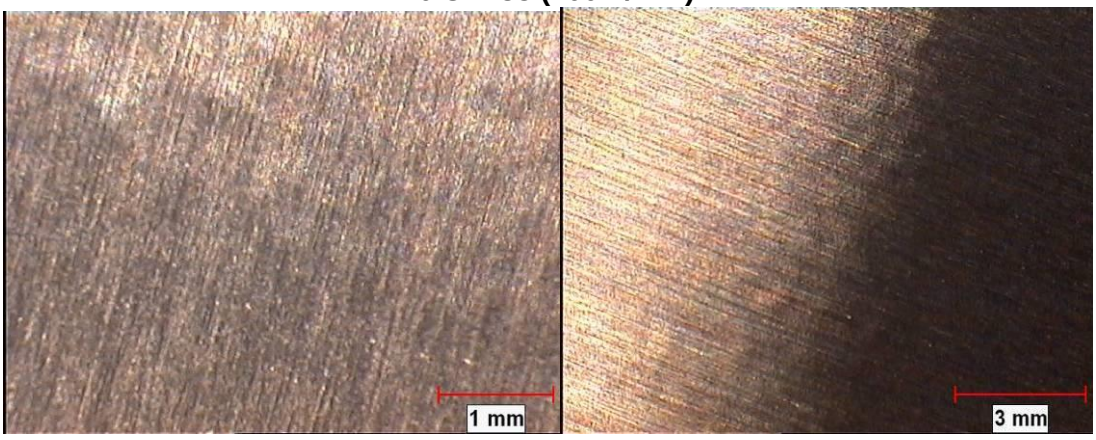

10UW85 (300m/min)

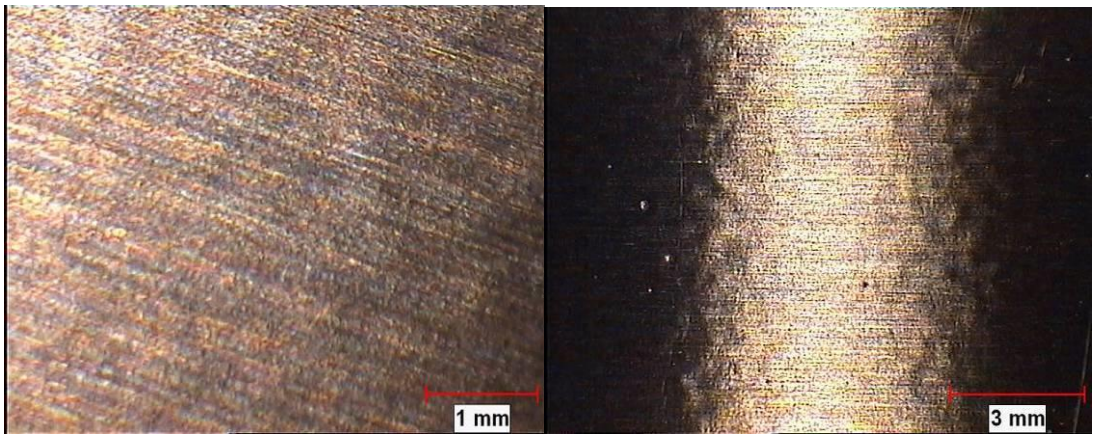

110 UW86 (400m/min)

Figure 5-76 Picture of steel substrate with light in normal direction (left) and grazing light (right)

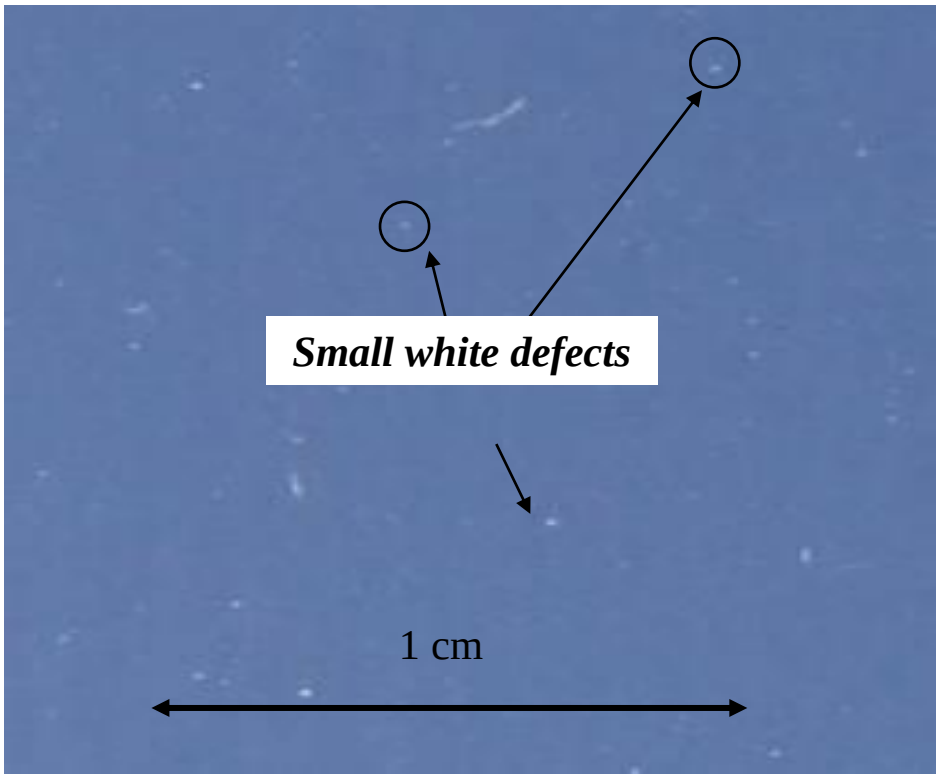

Figure 5-77 Picture of some white defect observed on coated samples

(Picture taken in exterior environment with a clear sky)

Figure 5-77, highlights the presence of small white defects, but SEM analysis did not show any pinholes in the coating. This confirms that the potential bubble that could have been entrapped is not the reason for the above defect. At 400 m/min the substrate started to flap before going to the coating section. This was said to be

linked with a heat up of the roller that induce a slight lost of grip on the steel. Therefore it is necessary to evaluate the potential changes of temperature during any future trials to consider how this temperature can be controlled.

5.6 Conclusions

Table 5-19 gives an overview of the results obtained during the trial and suggestion for further testing on pilot line.

Table 5-19 Summary of the 3 roll deformable roll coating with nip feeding of an EB fluid (non pigmented) onto 0.1 mm gauge smooth CR steel substrate

	Reverse 3 roll deformable roller coating with nip feeding.
Control of WFT 10-20 µm (DFT 10-20 µm) for speed up to 400 m/min	- Good control but only low range of DFT could be generated due to coating configuration used.
Wet film thickness range for speed up to 400m/min	- Stable coating operation only possible for low DFT due to significant bubbling; although this could be specific to the paint system used, better coater set-up may help to avoid this phenomenon
Ease of operation	- No need to increase the temperature to achieve the really low DFT with this configuration. - Easy control of the DFT through changing the relative speeds of the rollers - The footprint measurement between W0 & W1 (as measured by pilot line facility) makes it easy to get an accurate understanding of how changes to this negative gap affect the DFT of the applied coating - Control of general quality of coating and DFT by two independent parameters (pick up roller speed, and applicator up roller speed)
Process stability when increasing for speed up to 400 m/min	Some bubble generation at high speed and high DFT that could be reduced with increased paint temperature

Coverage quality for speed up to 400m/min	- Slight orange peel observed - No significant ribbing observed (masking effect) - Some white defects were seen in the coating but no pinhole defects were observed in the Talysurf and SEM analysis. These defects are confirmed to be not the microbubbles which could have been generated in the coater head during high speed process.
Stability	- Heating of the W2 rubber roller, when coating at high speeds, seems to induce flapping of the substrate in the reverse mode - Slight foaming of the paint - No significant misting observed because of use of lower roll speeds at metering stage.
Curing	- It was possible to cure the coating with the EB oven without any problems.

Chapter 6 : CONCLUSIONS & RECOMMENDATION

6.1 Introduction

This chapter details the conclusions and findings of this research in the light of previous research. These are as follows:

- Comprehensive experimental data was collected and correlated in terms of total flux and flux distribution with previous theoretical and experimental results. The total number of experimental variables was reduced to 5 dimensionless parameters which were elasticity number, speed ratio, gap number, capillary number and Reynolds number and these were correlated as a function for total flux and flux distribution as follows:

  Total flux, low speed regime (below average roll speed 40 m/min- Reynolds number below 4100):

$$\lambda_T = \frac{Q_T}{uR} = \left(\frac{\mu u}{ER}\right)^{0.68}\left(\frac{u_1}{u_2}\right)^{-0.001}\left(\frac{h_d}{R}\right)^{-1.36}\left(\frac{\mu u}{\sigma}\right)^{-0.07}\left(\frac{\rho h_d u}{\mu}\right)^{-0.01}$$

  Total flux, high speed regime (above average roll speed 40 m/min upto 240 m/min- Reynolds number above 4100):

$$\lambda_T = \frac{Q_T}{uR} = \left(\frac{\mu u}{ER}\right)^{0.67}\left(\frac{u_1}{u_2}\right)^{-0.001}\left(\frac{h_d}{R}\right)^{-1.36}\left(\frac{\mu u}{\sigma}\right)^{-0.08}\left(\frac{\rho h_d u}{\mu}\right)^{-0.01}$$

  Flux ratio, low speed regime (below average roll speed 40 m/min- Reynolds number below 4100):

$$\left(\frac{q_1}{q_2}\right)_{h_d} = \left(\frac{\mu u}{ER}\right)^{-0.0003}\left(\frac{u_1}{u_2}\right)^{1.53}\left(\frac{h_d}{R}\right)^{0.001}\left(\frac{\mu u}{\sigma}\right)^{-0.0007}\left(\frac{\rho h_d u}{\mu}\right)^{-0.0002}$$

Flux ratio, high speed regime (above average roll speed 40 m/min upto 240 m/min- Reynolds number above 4100):

$$\left(\frac{q_1}{q_2}\right)_{h_d} = \left(\frac{\mu u}{ER}\right)^{-0.005}\left(\frac{u_1}{u_2}\right)^{1.55}\left(\frac{h_d}{R}\right)^{0.016}\left(\frac{\mu u}{\sigma}\right)^{0.008}\left(\frac{\rho h_d u}{\mu}\right)^{-0.002}$$

- From the above correlations, we observe little or no difference in the correlations for the total flux at low and high speed. The important dimensionless groups are elasticity number and gap number, correlating to the power 0.68 and -1.36 respectively with film thickness number.

- From the above correlations, we observe small differences in the correlations for the flux distribution at low and high speed. The important dimensionless group is speed ratio correlating to the power 1.53-1.55 with film thickness number. A second but minor effect can be seen in the gap number variation. These experimental results also validate the theoretical interpretation of deformable coating which predicted a power of 1.5 after detailed analytical calculations.

- Measured roller coating film thickness for non-Newtonian model fluids found to be similar to their Newtonian counter parts (for same high shear viscosity), and hence the correlations for total flux, flux distribution in case of non Newtonian fluids will be similar to Newtonian case.

- Roller coater related instabilities such as ribbing and misting were studied extensively with the help of high speed visualisation techniques. In the case

of ribbing for Newtonian fluids, an optimised deformable roll with grooves matching the ribbing frequency was used and reduced the visual effect. The ribbing study done on viscous and viscoelastic model fluids showed that the ribbing wavelength decreases with increase in external load applied between the rollers and that the wavelength increases with increase in roller surface speed. At higher roll speeds for same processing conditions ribbing wavelength is higher for a viscoelastic model fluid compared with a purely viscous model fluid.

- In misting, the severity of misting was measured and reported under various high speed deformable conditions and also the effect of elasticity on misting phenomenon was studied. Misting phenomena is significantly higher for a viscoelastic model fluid compared to a purely viscous fluid. Misting severity increases with increase in roll speed. The roll speed at which the onset occurs is delayed with increase in applied external load between the rolls.

- Quality of the film found satisfactory in wet stage, with controllable rib wavelength and no misting at 180 m/min. The rib wavelength was found to be in the range of 1mm, which is less than the critical rib wavelength criteria in dry side used in a related coil coating process study. However this critical rib wavelength should be confirmed for a given coated steel sheet product. There has been no prior theoretical modelling coating of deformable roll at high speeds. We have carried out here CFD simulations with the open source software OpenFoam. The predictions obtained were validated at low speeds against the predictions of Coyle et.al [39] and give confidence in the

predictions. This part of the work was however limited and warrant further efforts.

- Although the deformable roller coating process has been studied extensively, previous data have been limited to speeds lower than 100 m/min. We have provided here the first data at higher speeds up to 300 m/min to guide the design and operation of high speed coating necessary to make certain applications, for example steel coating more economical.

- As well as being limited to low speed, previous data have also been limited to measurements with Newtonian fluids. Here we have presented data for viscoelastic model fluids. These model fluids were developed from a characterisation of industrial viscoelastic coating formulations. These model fluids which we have fully characterised can be used by other researchers to study further features. They can also be used by theoreticians to make predictions relevant to practical applications.

- This research required an appropriate high speed coating rig. An experimental deformable coater rig with the capability of operating up to 400 m/min speed and -1.5 mm gap was constructed and fitted with accurate instrumentation to measure film thickness and view the onset of instabilities, ribbing and misting.

- Previous experimental studies have mainly focussed on coating at fixed load. The rig developed here was designed and instrumented to operate at both fixed load and fixed gap conditions. This has enabled for the first time check data under both conditions and provides the important data at fixed gap

which have been missing from previous work. Such data are important for both guiding design/operation and for checking theoretical modelling predictions.

- Experiments at high speeds are fraught with difficulties as feeding of the nip present problems of fluid being ejected. We have developed and built an experimental roll coater to mitigate this issue by feeding the fluid with a die and using a pressurised pan. Die feeding was found not to be appropriate as the fluid failed to stick to roller surface before coming into the nip at moderate speeds. Pressurised pan feeding, with an optimum fluid level maintained, (which was determined experimentally), was able to deliver the required amount of fluid to the nip and offered the ability to control the wet film thickness (WFT) at higher roll speeds.

- The deformation of the rubber roll cover during high speed deformable coating was identified as an important aspect determining the metered film thickness. Thus it is required in the study of high speed deformable roll coating to characterise rubber deformation and define appropriately to the static and dynamic elastic modulus. We have in this research experimented with various characterisation methods to achieve this.

6.2 Future work

This is the first research on high speed deformable roll coating. In terms of film thickness, it has found essentially no important differences. Onset of instabilities and misting however were found to be different as it may be expected. Further work recommended is:

- Building upon the developed OpenFoam CFD model for roller coating process in order to incorporate 1) Test for higher capillary numbers 2) investigating non-Newtonian fluids 3) Extending model to 3D from current 2D aspect

- Carry out similar test of rheological and rig trial experiments for a water based coating system. This will cover all the major coating formulation type used in coil coating industry, as well as the spectrum of rheologically different model fluid systems. Interpreting the results from these three different systems could enable to develop a simple fluid mechanic model for the deformable roller coating flow at higher speed regime.

- Evaluate the dynamic modulus of different rubber cover materials used in rig study, in order to correlate these values to the static nip pressure in between the rolls under various process conditions.

- Develop a set of non-Newtonian model fluids from the different range of molecular weight PDMS mixture, enabling to understand the misting and air entrainment properties at higher roll speeds. These model fluid systems could enhance the current understanding on the air entrainment phenomena in roller coating case at higher capillary number regime and possibly the effect of extensional viscosity in this condition.

REFERENCE

1) Converting Quarterly Magazine, E. Cohen, Sept edition, 2012

2) Chong, Y H, 'The Onset of Ribbing in Forward-mode Deformable Roll Coating', PhD thesis, University of Leeds, 2004.

3) Benkreira, H., Patel, R., Edwards, M.F., and Wilkinson, W.L. "Classification and analyses of coating flows", J. Non-Newtonian Fluid Mech., Vol. 54, pp.437-447, 1994.

4) Landau, L. and Levich, B.Acta. Phys. URSS 17 pp.42-54, 1942

5) Drufke, R; An introduction to coil coating: Finishing process leads to quality and appearance in metal parts, Metal finishing, vol. 104, no:4, pp 35-37, 2006.

6) Future Prospects for Steel Coating Technology, Nippon Steel Technical Report No.63, October 1994

7) Website: www.Eccacoil.com

8) Pranckh, F R: Elastohydrodynamics in coating flows, PhD thesis, University of Minnesota, 1989.

9) Sollac Technical Brochure, 1998

10) Coyle, D J, Macosko, C W and Scriven, L E: "Film-splitting flows of shear-thinning liquid in forward roll coating", AIChE, 1987, Vol. 33, (5), pp741-746.

11) Modern coating and drying technology, pp 12-13, Editors Edward D. Cohen, Edgar B. Gutoff, Wiley- VCH, 1992.

12) Pitts, E. and Greiller, J., The flow of thin liquid films between rollers, Journal of Fluid Mechanics, 1961, vol. 11, pp 33-50.

13) T.D. Blake, The physics of moving wetting lines, J. Colloid Interf. Sci. 299 (2006) 1-13

14) Spiers, R.P., Subbaraman, C.V., Wilkinson, W.L., 1974. Free coating of a Newtonian liquid onto a vertical surface. Chemical Engineering Science 29, 389-396.

15) Benkreira, H., Cohu, O., 1998a. Angling the wetting line retards air entrainment in premetered coating flows. AIChE Journal 44, 1207-1209

16) Benkreira, H., Edwards, M.F., Wilkinson, W.L., 1981b. Roll coating of purely viscous liquids. Chemical Engineering Science 36, 429-434

17) Benkreira, H., Edwards, M.F., Wilkinson, W.L., 1982a. Flux distribution in forward roll coating: a simple analysis. The Chemical Engineering Journal 25, 211-214

18) Carvalho, M.S., Scriven, L.E., 1997. Deformable roll coating flows: steady state and linear perturbation analysis. Journal of Fluid Mechanics 339, 143-172

19) Carvalho, M.S., 2003. Effect of thickness and viscoelastic properties of roll

cover on deformable roll coating flows. Chemical Engineering Science 58, 4323-4333

20) Blake, T.D., Clarke, A., Ruschak, K.J., 1994. Hydrodynamic assist of dynamic wetting. AIChE Journal 40, 229-242

21) Blake, T.D., Dobson, R.A., Ruschak, K.J., 2004. Wetting at high capillary numbers, Journal of Colloid and Interface Science 279, 198-205

22) Lee, K.-Y., Liu, L.-D., Ta-Jo, L., 1992. Minimum wet thickness in extrusion slot coating. Chemical Engineering Science 47, 1703-1713

23) Carvalho, M.S., Kheshgi, H.S., 2000. Low-flow limit in slot coating: Theory and experiments. AIChE Journal 46, 1907-1917

24) Chang, Y.-R., Chang, H.-M., Lin, C.-F., Liu, T.-J., Wu, P.-Y., 2007. Three minimum wet thickness regions of slot die coating. Journal of Colloid and Interface Science 308, 222-230

25) Romero, O.J., Carvalho, M.S., 2008. Response of slot coating flows to periodic disturbances. Chemical Engineering Science 63, 2161-2173

26) Chin, C.-P., Wu, H.-S., Wang, S.S., 2010. Improved Coating Window for Slot Coating, Industrial & Engineering Chemistry Research 49, 3802-3809

27) Lin, F.-H., Liu, C.-M., Liu, T.-J., Wu, P.-Y., 2007. Experimental study on

tensioned-web slot coating. Polymer Engineering & Science 47, 841-851

28) Ning, C.Y., Tsai, C.C., Liu, T.J., 1996. The effect of polymer additives on extrusion slot coating. Chemical Engineering Science 51, 3289-3297

29) Romero, O.J., Suszynski, W.J., Scriven, L.E., Carvalho, M.S., 2004. Low-flow limit in slot coating of dilute solutions of high molecular weight polymer. Journal of Non- Newtonian Fluid Mechanics 118, 137-156

30) Romero, O.J., Scriven, L.E., Carvalho, M.S., 2006. Slot coating of mildly viscoelastic liquids. Journal of Non-Newtonian Fluid Mechanics 138, 63-75

31) Chu, V., Tsai, M.-Z., Chang, Y.-R., Liu, T.-J., Tiu, C., 2010. Effects of the molecular weight and concentration of poly (vinyl alcohol) on slot die coating. Journal of Applied Polymer Science 116, 654-662

32) Gutoff, E.B., Kendrick, C.E., 1987. Low flow limits of coatability on a slide coater, AIChE Journal 33, 141-145

33) Hens, J., Abbenyen, W.V., 1997. Slide coating, in: S.F.Kistler and P.M.Schweizer, C.H., London (Ed.), Liquid Film Coating, p. 427

34) Blake, T.D., Dobson, R.A., Ruschak, K.J., 2004. Wetting at high capillary numbers, Journal of Colloid and Interface Science 279, 198-205

35) Benkreira, H., Patel, R., 1993. Direct gravure roll coating. Chemical Engineering

Science 48, 2329-2335

36) Kistler, S.F, Schweizer, P.M, Liquid film coating: Scientific principles and their technological implications, Chapman & Hall, 1997

37) Savage, M.D and Gaskell.P. 1990. Meniscus coating. Paper no.81, AIChE Spring National meeting, March, Orlando

38) Reynolds, O. 1886. On the theory of lubrication and its application to Mr. Beauchamp Tower's experiments, including an experimental determination of the viscosity of olive oil. Phil. Trans R. Soc. London Ser. A 177:157-234

39) Coyle, D.J., Macosko, C.W., Scriven, L.E., 1986. Film-splitting flows in forward roll coating. Journal of Fluid Mechanics 171, 183-207

40) Pitts, E., Greiller, J., 1961. The flow of thin liquid films between rollers. Journal of Fluid Mechanics 11, 33-50

41) Greener, J., Middleman, S., 1979. Theoretical and Experimental Studies of the Fluid Dynamics of a Two-Roll Coater. Industrial & Engineering Chemistry Fundamentals 18, 35-41

42) Hintermaier, J.C., and R.E. White. 1965. The splitting of a water film between rotating rolls. TAPPI 48(11): 617-625

43) Sullivan, T.M., and S. Middleman. 1979. Roll coating in the presence of a fixed constraining boundary. Chem. Eng. Commun. 3(6); 469-482

44) Coyle, D.J., 1984. The fluid mechanics of roll coating: steady flows, stability, and rheology. PhD thesis, University of Minnesota, Minneapolis

45) Savage, M.D, 1984, Mathematical model for the onset of ribbing. AIChE J. 30(6): 999-1002

46) Dowson, D, E.H Smith and C.M Taylor. 1980. An experimental study of hydrodynamic film rupture in steadily-loaded, non-conformal contact. J. Mech. Eng. Sci. 22(2): 71-78

47) Coyle et.al, 1987. Film-splitting flows of shear-thinning liquids in forward roll Coating, AIChE J. 33 (5): 741-746

48) Greener, J., Middleman, S., 1975. A theory of roll coating of viscous and viscoelastic fluids. Polym.Eng. Sci. 15(1): 1-10

49) Gaskell PH, Kapur N, Savage MD., 2001, Bead break instability. Phys. Fluid. 13(5): 1243-53

50) Gaskell PH, Innes GE, Savage MD., 1998b, An experimental investigation of meniscus roll coating, J. Fluid mechanics. 355: 17-44

51) Savage MD, 1992, Meniscus instability and ribbing. Ind Coating Res. 2:47-58

52) Coyle, D.J., Macosko, C.W., Scriven, L.E., 1990a. Stability of symmetric film-splitting between counter-rotating cylinders. Journal of Fluid Mechanics 216, 437-458

53) Adachi K, Tamura T, Nakamura R., 1988, Coating flows in a nip region and various critical phenomena. AIChE J. 34(3): 456-64

54) Zevallos, GA, Carvalho, MS, Pasquali, M, Forward roll coating flows of viscoelastic liquids, J Non-Newtonian fluid mech, Vol 130(2-3), 96-109, 2005

55) Dawson, D., and G.R Higginson. 1959. A numerical solution to the elastohydrodynamic problem. J.Mech. Eng. Sci. 1(1): 6-15

56) Johnson, K.L, Contact Mechanics, Cambridge University Press, 1985

57) Dawson, D., and G.R Higginson, 1960. The effect of material properties on the lubrication of elastic rollers. J. Mech. Eng. Sci. 2(3): 188-194

58) Archard, J.F., F.C Gair and W. Hirst, 1961, The elastohydrodynamic lubrication of rollers, Proc. R. Soc. London Ser. A, 262: 51-72

59) Cheng, H.S, 1972, Isothermal elastohydrodynamic theory for the full range of pressure-viscosity coefficient, J. Lubric. Technol. 94: 35-43

60) Archard and Baglin, 1986, Elastohydrodynamic lubrication-improvements in analytic solutions. Proc. Inst. Mech. Eng. 200 (C4): 281-291

61) Herrebrugh, K. 1968. Solving the incompressible and isothermal problem in elastohydrodynamic through an integral equation. J. Lubric. Technol. 90:266

62) Hooke, C. and J.P. O'Donoghue, 1972, Elastohydrodynamic lubrication of soft, highly deformed contacts. J. Mech. Eng. Sci. 14(1): 34-48

63) Smith, J.W., Maloney, J.D. Flow of fluid between rotating rollers, TAPPI Journal, Vol 49(11), 63A-66A, 1966

64) O. Cohu, A. Magnin, Forward roll coating of Newtonian fluids with deformable rolls: an experimental investigation, Chemical engineering science, vol 52, 8, 1997, pp.1339-1347

65) Coyle, D.J. Experimental studies of flows between deformable rollers, AIChE Spring National meeting, New Orleans, Paper 3d, 1988b

66) Bapat, C.N., and R.C. Batra, 1984. Finite plane strain deformation of nonlinear viscoelastic rubber-covered rolls. Int. j. Num. Mech. Eng. 20:1911-1927

67) Carvalho, M.S., Scriven, L.E. Effect of deformable roll cover on roll coating, TAPPI Journal, Vol. 77, No.5, May 1994, pp 201-208

68) Pranckh F.R, Coyle, D.J. Elastohydrodynamic coating systems, Liquid Film Coating, Chapter 12c, 1997, pp 599-635, Chapman and Hall

69) Young, A.E. A theoretical and experimental investigation of deformable roll coating, PhD thesis, University of Leeds, UK, 1997

70) Kang, YT, Lee, KY, Liu, TJ, The effect of polymer additives on the performance of a two roll-coater, Journal of Applied Polymer Science, Vol 43 (6), 1991, pp 1187-1195

71) Carvalho, M.S., Scriven, L.E, Non-linear elastoviscous model of deformable roll cover, Proceedings of 3rd European Coating symposium, 265-272, 1999

72) Malvern, L.E. 1969, The mechanics of continuous medium, Englewood cliffs, NJ: Prentice-Hall

73) Saffman, P.G., and G.I Taylor. 1958, The penetration of a fluid into a porous medium or Hele-Shaw cell containing a more viscous liquid. Proc. R. Soc. London Ser. A 245:312-329

74) Chong, Y H, 'The Onset of Ribbing in Forward-mode Deformable Roll Coating', PhD thesis, University of Leeds, 2004

75) Bixler, N.E. 1982. Stability of a coating flow. PhD. University of Minnesota, Minneapolis

76) Christodoulou, C.N. 1989.Computational physics of slide coating flow. PhD, University of Minnesota, Minneapolis

77) Greener, T Sullivan, B Turner, S Middleman, Ribbing Instability of a Two-Roll Coater: Newtonian Fluids,J. Chem. Eng. Commun., Vol. 5, pp 73-83

78) Savage M.D, Cavitation in lubrication. Part 1. On Boundary Conditions and Cavity-Fluid Interfaces, Journal of Fluid mechanics, vol. 80, pp 743-755, 1977

79) Mill, C.C., and G.R South. 1967, Formation of ribs on rotating rollers. J. Fluid. Mech. 28:523-529

80) Greener, J, 1979, Theoretical and experimental studies of the fluid dynamics of a two- roll coater. Ind. Eng. Chem. Fundam. 18:35-41

81) Pulkrabek, W. W., and J.D. Munter. 1983. Knurl roll design for stable rotogravure coating. Chem. Eng. Dci. 38(8):1309-1314

82) Bauman, T.M., T.M Sullivan and S. Middleman. 1982. Ribbing instability in coating flows: Effect of polymer additives. Chem. Eng. Commun. 14:35-46

83) Glass, J.E. 1978a, Dynamics of roll spatter and tracking. Part 1: Commercial latex trade paints. J. Coatings Technol. 50(640); 53-60

84) J H Lee, S K Han, J S Lee, H W Jung and J C Hyun, Ribbing instability in rigid and deformable forward roll coating flows, Korea-Austrlia Rheology Journal, Vol. 22, No.1, March 2010, pp 75-80

85) Hasegawa T, Sorimachi K, 1993, Wavelength and depth of ribbing in roll coating and its elimination, Vol 39, No. 6, AIChE Journal, pp 935-945

86) Carvahlo, M.S., Scriven, L.E, Multiple states of a viscous free surface flow, International Journal for Numerical Methods in Fluids, 1997, vol. 24, pp 813-

831

87) Chong, Y H, 'The Onset of Ribbing in Forward-mode Deformable Roll Coating', PhD thesis, University of Leeds, 2004

88) Coyle, D.J., 1997. Knife and Roll Coating, in: S.F. Kistler and. P.M. Schweizer, C.H., London (Ed.), Liquid Film Coating, p. 539

89) Burley, R., Kennedy, B.S. 1976. An experimental study of air entrainment at a solid/liquid/gas interface. Chem. Eng. Sci. 31:901-11

90) Blake, T.D., Ruschak, K.J. 1979. A maximum speed of wetting. Nature 282: 489-91

91) Burley, R and Jolly, R.P.S 1984, Entrainment of air into liquids by a high speed continuous solid surface Chem. Engg. Sci. 39, 1357

92) R.P. Spiers, C.V Subbaraman and W.L Wilkinson, Free coating of a Newtonian liquid onto a vertical surface, Chem Eng Sci, 1974, Vol 29, pp 389-396

93) Bolton, B., Middleman, S., 1980. Air entrainment in a roll coating system. Chemical Engineering Science 35, 597-601

94) Innes, G.E, 1993 An experimental and theoretical investigation of viscous lifting in tribology, PhD thesis, University of Leeds

95) P. Bourgin and N. Tahiri, "Generalised Jeffery-hamel flow: Application to high

velocity coating", The mechanics of thin film coating -1995, editors Gaskell P.H, Savage M.D, Summers J.L

96) Benkreira, H: 'Dynamic wetting in metering and pre-metered forward roll coating', Chemical Engineering Science, 2002, Vol. 57, pp3025-3032

97) Roper JA, Attal JF, 1993. Evaluations of coating high-speed runnability using pilot coater data, rheological measurements and computer modelling. Tappi J. 76(5): 55-61

98) Ascanio, G., Carreau, P.J., Brito-De La Fuente, E., Tanguy, P.A., 2004. Forward Deformable Roll Coating at High Speed with Newtonian Fluids. Chemical Engineering Research and Design 82, 390-397

99) Gron J, Sunde, H., and Nikula, E., "Runnabillity aspects in high speed film transfer coating", TAPI Journal, 81(2), 157-165 (1998)

100) R.H Fernando, L.L Xing, J. E Glass Rheology parameters controlling spray atomization and roll misting behaviour of waterborne coatings, Progress in organic coatings 40(2000) 35-38

101) MacPhee, J., 1997a, b, A unified view of the film splitting process, Part I, II, Am. Ink. Maker, 75: 44-56

102) M. S Owens, M Vinjamur, L.E Scriven, C.W Macosko, Misting of Newtonian

liquids in forward roll coating, Ind. Eng. Chem. Res. 2011, 50, 3212-3219

103) Ascanio, G, Carreau, P J, Tanguy: High speed roll coating with complex rheology fluids, Experiment in fluids (2006) 40, pp1-14

104) Willenbacher et al., High shear rheology of paper coating colors – more than just viscosity, Chem.Eng.Tech. **20** (1997), pp 557-563

105) Dirking et al., Elongational flow behaviour of automotive coatings and its relation to atomization and mottling, Prog.Org. Coatings **42** (2001) pp 59-64

106) Varela Lopez et al., Non Newtonian effects on ribbing instability threshold, JNNFM **103** (2002), pp 123-139

107) Pipe et al, High shear rate viscometry, Rheol.Acta **47** (2008), pp 621-642

108) Benthin, S and Munch, M: Influence of rheology on coating processes, Proceedings ECS 1999, pp 355-56

109) Fearnley-Whittingstall, P, Paint Rheology: Surface coating international, 1991, **74**, 10, 360-368

110) J.Edward Glass, The role played by water-soluble polymers in paint performance. J.Oil Col.Chem.Asoc.**58**: 169-177

111) Entov, V M and Hinch, E J: Effect of a spectrum of relaxation times on the capillary thinning of a filament of elastic liquid, J. Non-Newtonian Fluid Mech. (1997), Vol. **72** pp31–53.

112) Results from EngD studentship GU/Corus.

113) Anton Paar Manual, Year 2006.

114) Carvalho, M S et al: 'Ribbing instability in forward deformable roll coating', Proceedings of the 1994 TAAPI Coating Conference, pp99-104, 1994.

115) Bauman, T et al: 'Ribbing instability in coating flows effect of polymer additives', Chem.Engg.Comm. 14, 35-46, 1982.

116) Instruction manual Haake CaBER 1 from Thermo Electron Corporation

117) Savage M.D, Cavitation in lubrication. Part 1. On Boundary Conditions and Cavity-Fluid Interfaces, Journal of Fluid mechanics, Vol. 80, pp 743-755, 1977

118) M Hannah, Contract stress and deformation in a thin elastic layer, Quart. Journ. Mech. And Applied Math., Vol. IV, Pt. 1 (1951)

119) A.N. Gent, (1958), On the relation between indentation hardness and Young's modulus, International Rubber Institute Transactions, 34, pp. 46–57

120) E.R. Jones, The Fluid Mechanics of deformable roll coating, PhD thesis, University of Bradford, 2000

121) NDC wet film thickness gauge website, http://www.ndc.com/thickness-gauge-and-thickness-measurement.aspx

122) G.H. McKinley and A. Tripathi, (2000), J.Rheol., 44, 653-670

123) OpenCFD Ltd. OpenFOAM 1.5 documentation http://www.opencfd.co.uk/openfoamdoc/index.html

124) J.H Ferziger, M. Peric, Computational methods for fluid dynamics, Third rev. ed., Springer, (2002)

125) C.W Hirt, B.D Nichols, Volume of Fluid (VOF) method for dynamics of free boundaries, J. Comput. Phys. 39, 201-221 (1981)

Appendix 1

Operating procedure for deformable roller coater rig

1) Switch on the mains power at the main enclosure

2) Switch on the air supply

3) Press the green reset button back on the panel

4) Enter the 4 digit code “1610” on the touch pad control panel. Then press return

5) Set required gap between the rollers using the two hand wheels on the right hand side of the rig.

6) On the touch pad control panel, select forward or reverse rotation for both rollers.

7) Slide the drip/coating pan under the rollers and raise it using the lever at the front of the rig

8) Switch on the extraction system if required.

9) Pour the coating liquid either into the pan or in the feed tank on the right hand side of the rig.

10) If liquid is to be pumped from the feed tank, the flow rate is controlled by the setting on the touch pad control panel

11) Set the gap at 0.000 mm and null the load cells.

12) Set the negative gap

13) Start the applicator and pick up rollers and set the speeds via the touch pad control panel.

14) After operation, stop the pump (if used) and stop the rotation of the rollers.

15) Set the gap at > 0.5mm.

16) Lower the coating pan and drain the liquid into a suitable vessel.

17) Clean both roller surfaces and wipe any splashes etc.

18) Switch off the air supply

19) Switch off the power at the main enclosure

20) Isolate the supply at the mains (on the wall)

21) Switch off the extractor fan.

Figure A-1 Coating gap control with wedge adjustment system

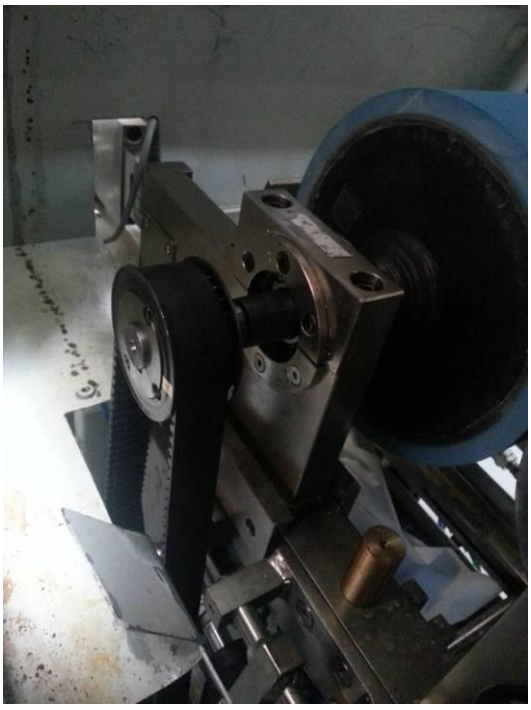

Figure A-2 Coating roll drive with timing belt system

Risk assessment for deformable roller coater rig

University of Bradford **Health & Safety** **Risk Assessments**	Dept: Chemical Engineering Location: Assessor Signature: ..... Date: Review: .....

UNIVERSITY OF BRADFORD

Hazard **List hazards here:**	**Who Might be Harmed?** **List people who are especially at risk from the significant hazards which you have identified**	**Control Measures?** **List existing controls here or note where the information may be found.**	**Further Action required** **List the risks which are not adequately controlled and the action you will take where it is reasonably practicable to do more. You are entitled to take cost into account, unless the risk is high:**
Electrical	Operator People sharing the work place	Ensure all electrical equipment used are ignition proved No electrical work undertaken	Low level of risk
Chemical	Operator	Cleaning of roller should be only done by experienced operator with suitable PPE	Proper safety briefing and only trained operators in room while cleaning.
Chemical/fluid splashes	Operator and those in the work place	Wear safety glasses and protective clothing	Proper safety briefing
Moving rollers	Operator and people in the work place	Easy access and operation mode safety stop from two different positions. Operating person always close to the control panel to be able to control speed, gap, load and other parameters.	Use of an alarm in the rig cabin portion with immediate access and on the body of the operator to be able to operated in stage of any emergency.
Solvent evaporation	Operator and people sharing the work place	Use of extraction system properly and wearing PPE properly	Checking the extraction efficiency regularly
Slipping and tripping	Operator People sharing the work place	Ensure floor areas are clear from unnecessary items Ensure spillage are cleared	Low level of risk

Appendix II

Wet film thickness gauge- Performing a calibration test

We performed calibration procedure to find out the right trim and span values for the Fortex 2 (GC 2801) and Fortex 3 (GC 2840) products.

Our method was:

1) Prior to the commissioning day coat the roller with Fortex 2 (GC 2801) at a known roller speed and gap conditions and perform a scrape test in order to ascertain the coating thickness

2) Set the Span and Trim of the IG710e to 1.0 and 0.0 respectively .On the commissioning day run the roller at the speed in 1) and record the indicated value from the IG710e. The wet film thickness was checked with scraper technique to confirm the results.

3) Repeat 2) for as many different roller speeds as possible but, ideally, not less than 5 different speeds.

4) Repeat 3) to check repeatability and to also obtain more data points.

5) Using Gauge tools XL plot reference values against IG710e indicated values and obtain revised Span and Trim values.

6) Repeat 1-5 for the Fortex 3 tested on the commissioning day.

Performing a calibration test for wet film thickness IR guage

We performed calibration procedure to find out the right trim and span values for Oil products.

Our method was:

1) Prior to trial the roller run at known roller speed and gap conditions and perform a scrape test in order to ascertain the coating thickness three times

2) Set the Span and Trim of IR guage to 1.0 and 0.0 respectively .1) During trial run the roller at the speed from and record the indicated value from guage. The wet film thickness was checked with scraper technique to confirm the results.

3) Repeat 2) for as many different roller speeds as possible but, ideally, not less than 5 different speeds.

4) Repeat 3) to check repeatability and to also obtain more data points.

5) Using Gauge tools XL plot reference values against IG710e indicated values and

obtain revised Span and Trim values.

6) Repeat 1-5 for Oil tested.

Settings

Zero	342	S4	C1	S2	right -1 ON
Span	408	S3	7	Resp Time	4

S1	7	Run	1
Gain	1	In panel	4 ON Normal run ON

Gap (mm)	Speed(m/min)	Wt(g)	Time(s)	WFT(scrapping)	WFT (mic)	IR reading	Correction factor
-0.5	10	3.94	60	3.8539E-06	3.85	5.23	0.73613767
-0.5	40	18.25	20.34	1.3164E-05	13.16	18.74	0.7022412
-0.5	60	35.27	20.14	1.713E-05	17.13	23.36	0.73330479
-0.5	80	49.39	18.06	2.0062E-05	20.06	27.9	0.71899642
-0.5	100	45.06	11.92	2.2185E-05	22.19	31.26	0.70985285

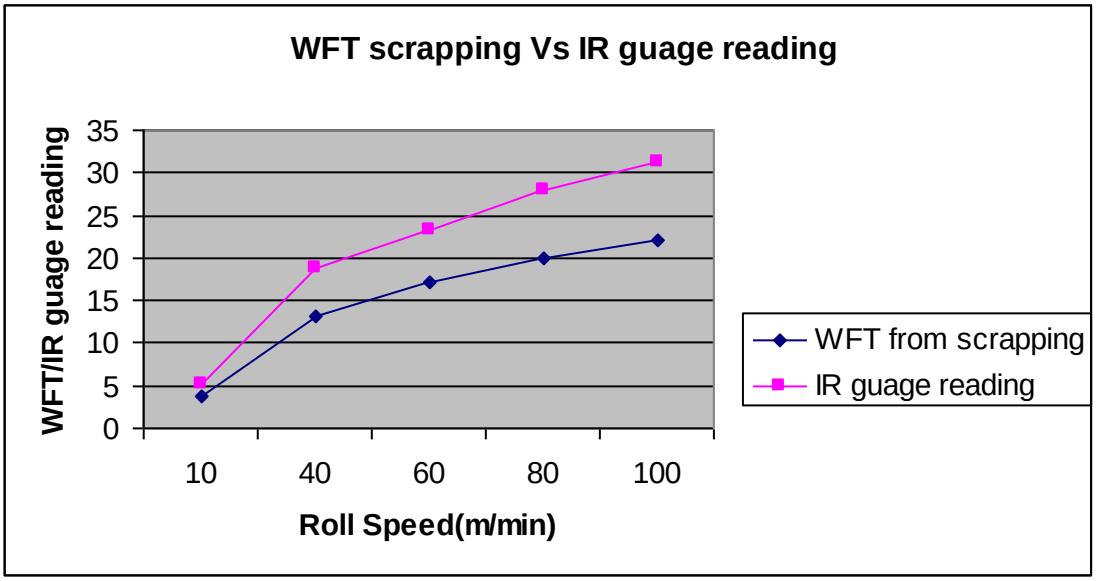

Figure A-3 Film thickness scrapper system (in contact with the roller)

For example, Here the measured values for P/Up roll has been shown with **average std deviation** of **0.3611**

WFT on P/Up roll	**WFT on applicator roll**	**P/Up roll Individual readings 1**	**P/Up roll Individual readings 2**	**P/Up roll Individual readings 3**	**Std Deviation**
27.8	27.77	27.36	27.89	28.12	0.3897435
20.31	31.1	20.18	20.56	20.19	0.2165641
14	31.87	13.99	14.01	14.02	0.0152753
10.52	31.5	10.58	10.36	10.62	0.14
44.55	44.5	44.52	44.4	44.72	0.1616581
30.03	52.2	30.05	30.13	29.92	0.1059874
22.11	53.9	22.11	22.21	22.02	0.0950438

13.66	53.6	13.68	13.63	13.68	0.0288675
56.97	56.97	56.98	56.98	56.96	0.011547
39.65	66.7	39.44	39.4	40.12	0.4046398
28.92	68.55	28.95	28.15	29.65	0.7505553
21.9	68.62	21.69	22.36	21.55	0.4329357
66.6	66.61	66.23	66.98	66.19	0.4450094
47.3	77.33	47.56	47.06	47.52	0.2778489
35.05	79.85	35.63	33.91	35.62	0.9901683
27.56	80.02	27.22	28.26	27.19	0.6092892
19.07	19.02	19.16	18.54	19.53	0.5002333
13.05	21.4	13.09	12.5	13.56	0.5311309
8.12	21.7	8.16	8.04	8.17	0.0723418
5.6	21.77	5.14	6.35	5.16	0.6928925
32.47	32.55	32.45	32.32	32.65	0.1662328
20.8	38.1	20.36	20.96	20.96	0.3464102
14.58	39.4	14.21	14.98	14.55	0.3858756
7.9	39.2	7.9	7.95	7.85	0.05
42.88	42.87	42.58	43.36	42.66	0.4291076
28.46	50.05	28.12	28.95	28.13	0.4763402
19.86	51.47	19.14	20.98	19.45	0.9851057
14.4	57.44	14.4	14.25	14.66	0.2074448
50.9	50.9	50.98	50.88	50.82	0.080829
34.48	59.9	34.56	34.22	34.65	0.2267892
24.63	61.03	24.45	24.89	24.56	0.2289833

18.5	61.15	18.13	19.05	18.16	0.5227173
14.41	14.05	14.25	14.37	14.61	0.183303
9.4	16.72	9.67	9.07	9.54	0.3156475
5.2	17.12	5.28	4.96	5.5	0.2715388
3.11	17.04	2.96	3.51	2.86	0.35
25.96	25.54	24.93	25.81	24.13	0.8403174
15.88	31.18	15.82	16.61	15.22	0.6971609
10.6	32.32	10.45	10.58	10.77	0.1609348
5.2	32.15	5.12	5.32	5.17	0.1040833
34.77	34.4	34.78	34.76	34.77	0.01
22.27	41.55	22.56	21.53	22.73	0.649333
15.03	42.85	15.15	14.75	15.19	0.2433105
10.51	42.85	10.46	10.63	10.44	0.1044031
41.85	41.2	41.25	42.62	41.69	0.6994522
27.32	49.38	27.62	27.22	27.13	0.260832
18.94	51.15	18.49	19.66	18.55	0.6588627
13.85	51.25	13.22	14.76	13.56	0.8090323

Roll speed calibration

Roll speeds are measured with Digital Tacho meter for various speeds and loads as given below,

	M/min	**Measured Speed**		
Gap (mm)	**Set Speed**	**P/up Roll**	**Applicator roll**	**Std deviation**
0	5	4.35	4.77	0.29698485

0	15	14.38	14.56	0.12727922
0	20	19.81	19.77	0.02828427
0	30	29.19	29.55	0.25455844
0	40	40.15	40.22	0.04949747
0	50	50.11	50.69	0.41012193
0	60	60.95	60.19	0.53740115
0	70	70.77	70.18	0.417193
0	90	90.94	90.26	0.48083261
0	120	121.18	120.17	0.71417785
0	150	151.11	150.48	0.44547727
0	180	181.05	180.95	0.07071068
0	240	241.08	241.78	0.49497475
0	300	301.11	300.58	0.37476659
-0.5	5	4.21	4.56	0.24748737
-0.5	15	14.22	14.28	0.04242641
-0.5	20	19.88	19.55	0.23334524
-0.5	30	29.29	29.48	0.13435029
-0.5	40	40.18	39.88	0.21213203
-0.5	50	50.15	50.27	0.08485281
-0.5	60	60.88	60.61	0.19091883
-0.5	70	70.45	70.55	0.07071068
-0.5	90	90.11	90.36	0.1767767
-0.5	120	121.36	121.48	0.08485281
-0.5	150	151.29	151.11	0.12727922

-0.5	180	181.18	180.98	0.14142136
-0.5	240	241.11	241.01	0.07071068
-0.5	300	300.15	300.26	0.07778175
-1	5	4.11	4.48	0.26162951
-1	15	14.35	14.55	0.14142136
-1	20	20.16	20.13	0.0212132
-1	30	29.56	29.65	0.06363961
-1	40	40.08	40.12	0.02828427
-1	50	50.22	50.39	0.12020815
-1	60	60.39	60.29	0.07071068
-1	70	70.55	70.28	0.19091883
-1	90	90.77	90.18	0.417193
-1	120	120.96	120.19	0.54447222
-1	150	151.05	150.55	0.35355339
-1	180	180.36	180.58	0.15556349
-1	240	240.13	240.15	0.01414214
-1	300	300.01	300.21	0.14142136
-1.5	5	4.03	4.11	0.05656854
-1.5	15	14.92	14.91	0.00707107
-1.5	20	20.13	20.19	0.04242641
-1.5	30	30.05	30.64	0.417193
-1.5	40	39.59	40.88	0.91216775
-1.5	50	49.62	50.75	0.79903066
-1.5	60	59.57	60.72	0.8131728

-1.5	70	69.65	70.64	0.70003571
-1.5	90	88.44	90.31	1.32228968
-1.5	120	120.62	121.16	0.38183766
-1.5	150	150.13	151.82	1.19501046
-1.5	180	180.33	180.34	0.00707107
-1.5	240	240.88	240.11	0.54447222
-1.5	300	299.86	300.04	0.12727922

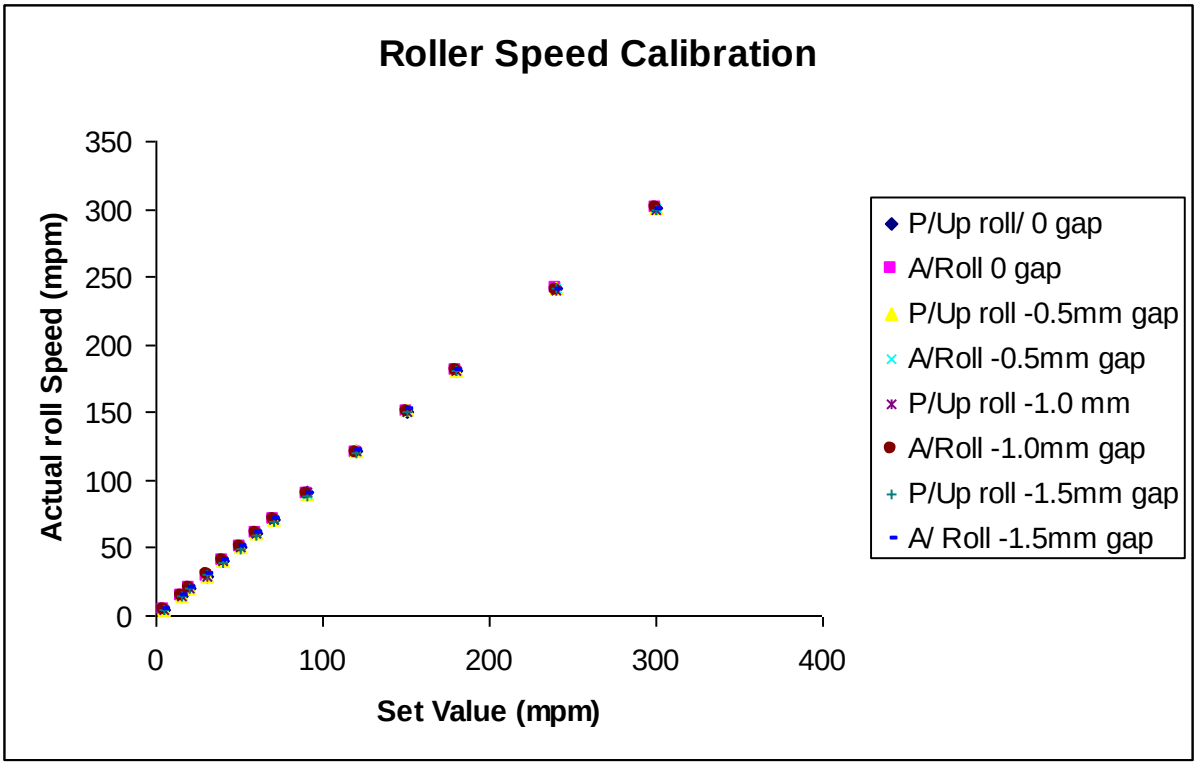

Figure A-4 Roller speed calibration results

Average standard deviation is calculated in readings above as **0.293**

Load cell calibration

Load cells supplied by Applied measurements Ltd., DBBE-250 kg are used to measure the applied load and hydrodynamic loads as a combined load in the coating

nip between the pick up and applicator rollers. Before the installation, initially the load cells are calibrated by placing them under known weights. The spans and zeros of the cells are adjusted until the measured load output is equal to the actual load experienced under the weights. The friction within the linear slides (and other moving parts) are minimised by applying lubrication and it helped for easy movement registering dependable load values. The load values measured is a combination of forces due to the deformation of the rubber and hydrodynamic forces exerted by the liquid. The results of the calibration are given in table below.

Front side		Back side	
Weight (kg)	**Reading (N)**	**Weight (kg)**	**Reading (N)**
6.43	66	6.43	63
11.58	118	11.58	116
15.69	156	15.69	157
23.51	237	23.51	236
51.88	519	51.88	517

Roller speed calibration

A digital tachometer (LT Lutron, DT -2234B) was used to check the roller speeds and values are given below for all three rollers.

SET VALUES(MPM)		ACTUAL TACHOMETER READINGS(RPM)		CALCULATED VALUES(RPM)	
Applicator	**P/UP**	**Applicator**	**P/UP**	**Applicator**	**P/UP**
20	20	48.9	47.5	25.478	25.478
30	20	76.2	47.1	38.217	25.478
40	20	104.2	47.3	50.955	25.478
50	20	131.6	47.8	63.694	25.478
60	20	159.3	47.9	76.433	25.478
80	20	214.6	48.1	101.911	25.478
100	20	269.7	49.2	127.389	25.478
40	40	103.1	101.1	50.955	50.955
60	40	157.9	100.1	76.433	50.955

80	40	213.4	99.8	101.911	50.955
100	40	268.7	100.1	127.389	50.955
120	40	323.6	100	152.866	50.955
140	40	378.6	100.3	178.344	50.955
160	40	433.6	100.2	203.822	50.955
60	60	154.9	152.9	76.433	76.433
80	60	211.8	151.6	101.911	76.433
120	60	321.7	152.3	152.866	76.433
160	60	431.7	150.3	203.822	76.433
180	60	484.5	151.2	229.299	76.433
190	60	509.8	152.2	242.038	76.433
200	60	533.7	153.1	254.777	76.433

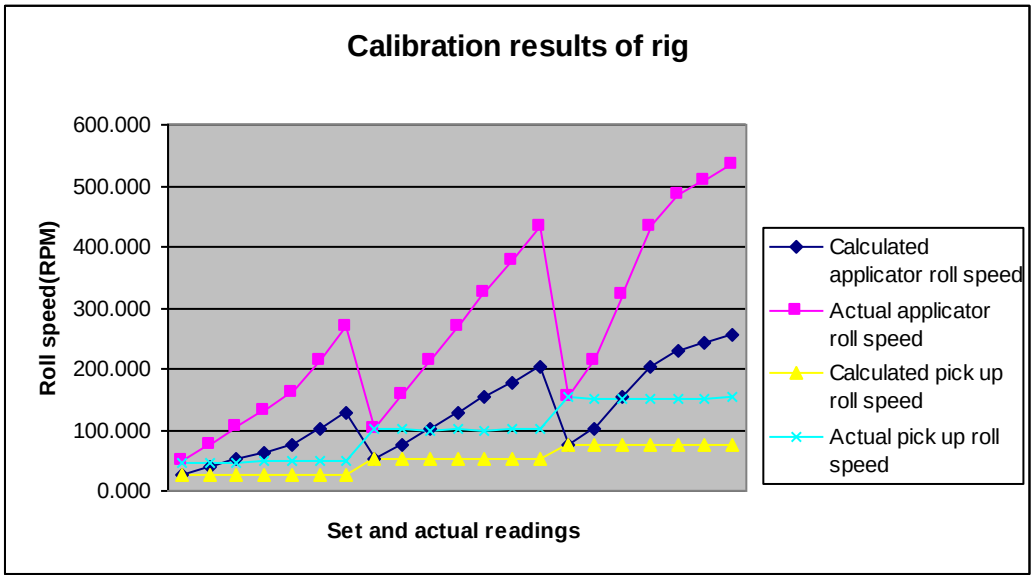

Figure A-5 Actual and set roller speeds in rig

Linear transducer calibration

The linear transducers are used for measuring the coating gaps in an accurate and consistent way. Here this system is calibrated by setting the gap precisely at 1000 µm ± 1 µm and the transducer is normalised. As one of the roller is deformable in nature the gap in negative gap cannot be measured using normal feeler gauges. Here the deformable roller is slowly closed towards the pick up roll (until its slightly touching), until there is no light visible from the top side. This point is taken as the zero gap and accordingly other positive and negative gaps are set in the control panel

for the operating rig. This process of gap calibration is repeated before every new set of coating trials.

Appendix III

Model fluid generation

Required Pa.s	50 mPa.s + 1,000 mPa.s (%)	50 mPa.s + 30,000 mPa.s (%)	50 mPa.s + 100,000 mPa.s (%)	50 mPa.s + 600,000 mPa.s (%)	50 mPa.s + 1,000,000 mPa.s (%)
0	0	0	0	0	0
0.1	18	4	5	3.26	2.77
0.2	37.5	12	9.5	6.31	5.12
0.3	52.5	18	13	8.05	6.63
0.4	63	19.5	15	9.58	7.79
0.5	72.5	22	17	10.87	8.76

1000 mPa.s	Pa.s	Ext	600000 mPa.s	Pa.s	Ext	1000000 mPa.s	Pa.s	Ext
37.5	0.2	1.4175	6.31	0.2	1.3232	6.63	0.3	1.6366
63	0.4	2.0844	8.05	0.3	1.6222	8.76	0.5	2.7115
72.5	0.5	2.7048	9.58	0.4	2.2512			

Modifications for real industrial fluid trial

Experimental rig study with EB paint

As one of the step in the present feasibility study, a short study with actual industrial coating (Supplier A-Confidential) was carried out. The whole purpose of the study was to validate the results obtained with model fluids previously and to highlight any significant differences. The experimental rig modifications undertaken in order to be able use actual industrial coating onto the rig have been explained in following sections.

Figure A-6 Heating and recirculation facility attached to the coating rig

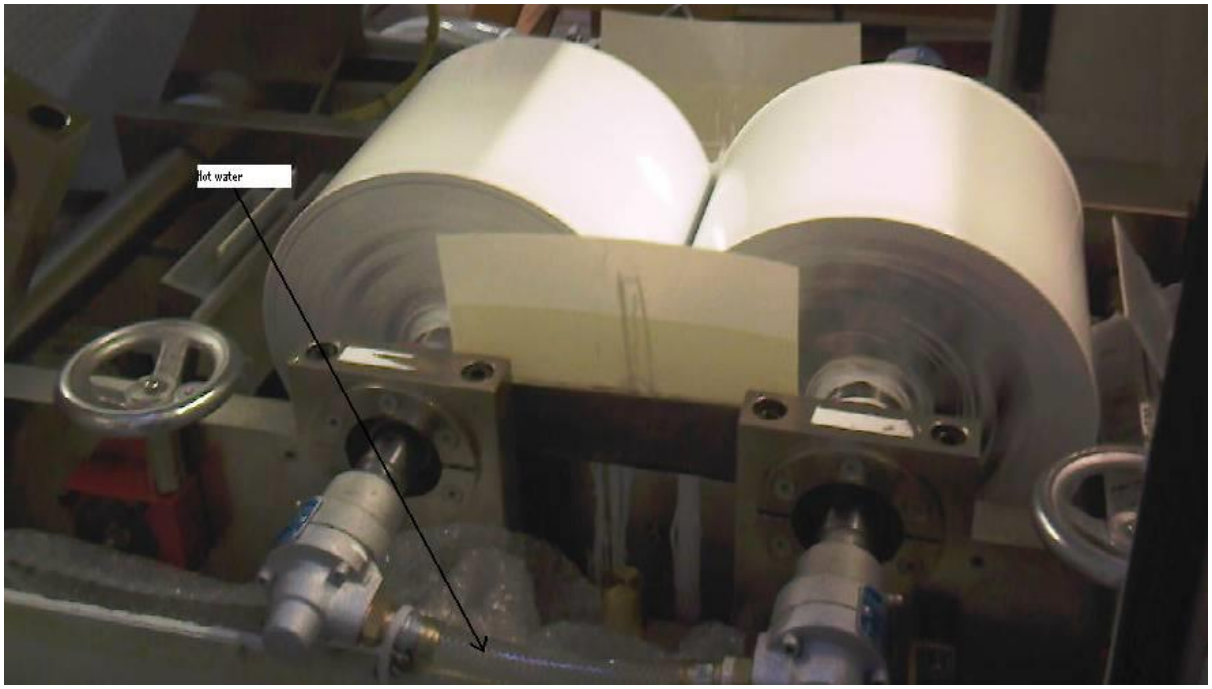

Figure A-7 Deformable roll coating with radiation curable coating in the lab

In order to be able to run the actual paint onto the Bradford experimental rig, the following significant modifications were undertaken:

- Deformable roll and the pick up roll were changed to new ones, which are hollow from inside, giving provision to heat the rolls during operation with hot water circulation.

- The rubber cover of the deformable roll was given a higher hardness (70 Shore A instead of 58 Shore A).

- Use of water bath to control the temperature of the water delivered to the heated roll during circulation process, capable to heat up to 100°C with ± 2 °C accuracy.

- Use of a separate water bath to heat up the paint to the required temperature before the trial.

- Proper electrical insulation around the rig in order to avoid explosion in the event of solvent evaporation from the paint.

- Design and use of proper splash guards minimising the splashing phenomena during high speed operation.

- Use of a non-contact WFT measurement tool in the form of an Infrared gauge (details of it explained in 3.4.2) to measure the WFT at high roll speeds.

- Use of a high speed camera to capture the pictures of the ribbed surface forming at different speeds and gaps between the rolls.

- Use of proper software, allowing accurate analysis of to the rib characteristics for each specific set of conditions.

Experimental procedure

According to the previous rheological measurements, the EB paint needed to be heated up to 55°C, in order to bring down its shear viscosity to 100 mPa.s. This medium viscosity fluid could not give the target WFT at higher roll speeds. In order to achieve this, the pick up steel roller and deformable rolls (which are hollow) were connected to a water bath, which recirculated hot water at 60±5 °C. The set up was allowed to run for 30 min in start up to achieve the uniform temperature of 55±5°C across the width of the rollers. The EB Paint is also heated outside the rig in a separate water bath up to 60±2°C, and poured into the pressurised holding tank. The temperature of the EB paint in the pan is constantly checked with a thermometer and once the fluid temperature goes down 50°C, the trials are stopped, and fresh hot paint is poured into the tray, before any further tests are conducted.

The experimental studies with EB Paint included following studies.

1. Wet film thickness as a function of roll speed and different negative gaps.

2. Ribbing wavelength measurement under various process conditions.

3. Misting study for different conditions.

Appendix IV

Derivation of basic differential equation of fluid mechanics:

- Equation of conservation of mass
- Equation of conservation of momentum

Conservation of mass

"Conserved mass is not lost or destroyed",

Hence for a system,

$$\frac{dM_{sys}}{dt} = 0$$

Now we can use Reynolds Transportation theorem, where we can write equations for controlled volume (cv),

Thus for a CV, $\frac{\partial}{\partial t}\int_{cv} \rho dv$ ------rate of change of mass in cv

Also $\frac{\partial}{\partial t}\int_{cv} \rho dv + \int_{cs} \rho V.n.dA = 0$

↓

Net rate of flow

across the cs

Differential form of the continuity equation

Consider a small fluid element $\partial x \partial y \partial z$

Now first term in above continuity equation for cv,

$\frac{\partial}{\partial t}\int_{cv}\rho dv = \frac{\partial \rho}{\partial t}\partial x\partial y\partial z$ …… (Assumption $\rho = uniform$, as element is very small)

For the second term, rate of mass flow, considering a cube and flow across this geometry

In the x-direction,

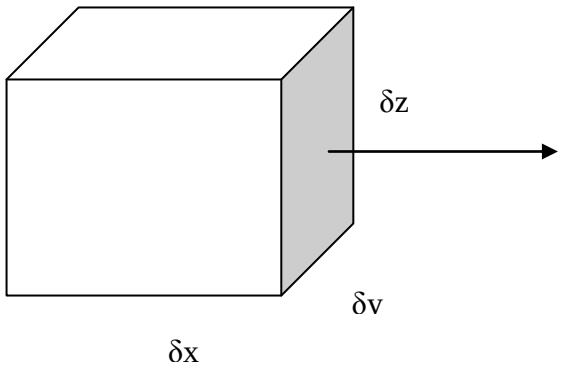

Figure 6-8 Fluid element with direction vectors

Using Taylor expansion series, ρu is the x-component of the mass flow rate coming out of the element would be

$$\left[\rho u + \frac{\partial}{\partial x}(\rho u)\frac{\delta x}{2}\right]\partial y\partial z$$

Now the flux of mass coming in,

$$\left[\rho u - \frac{\partial}{\partial x}(\rho u)\frac{\delta x}{2}\right]\partial y\partial z$$

Now the net rate of mass outflow in the x direction = $\frac{\partial}{\partial x}(\rho u)\partial x\partial y\partial z$

Similarly, we can get in y direction= $\frac{\partial}{\partial y}(\rho v)\partial x\partial y\partial z$

In Z-direction= $\frac{\partial}{\partial z}(\rho w)\partial x\partial y\partial z$

Hence differential equation for conservation of mass =

$$\frac{\partial \rho}{\partial t}+\frac{\partial}{\partial x}(\rho u)+\frac{\partial}{\partial y}(\rho v)+\frac{\partial}{\partial z}(\rho w)=0$$

Or in vector notation, $\frac{\partial \rho}{\partial t}+\nabla.\rho V=0$

We can see for steady flow, $\frac{\partial \rho}{\partial t}=0$, hence divergence of velocity would be zero.

Conservation of momentum

For a system, $F=\frac{d}{dt}\int_{sys} Vdm$

For a C.V, using Reynolds transport theorem

$$\sum F_{cv}=\frac{\partial}{\partial t}\int_{cv} V\rho dv+\int_{CS} V\rho V.n.dA$$

Considering an infinitesimal fluid mass δm : $\delta F=\frac{d}{dt}(Vdm)=dm\frac{dV}{dt}=dm.a$

There are generally, two types of forces that can be considered in fluids,

- Body forces (weight of the element)= $\delta F=m.g$
- Surface forces- Normal and tangential to the surface of the element

Imagine a piece of area in the fluid and we consider an area d A

δF_n

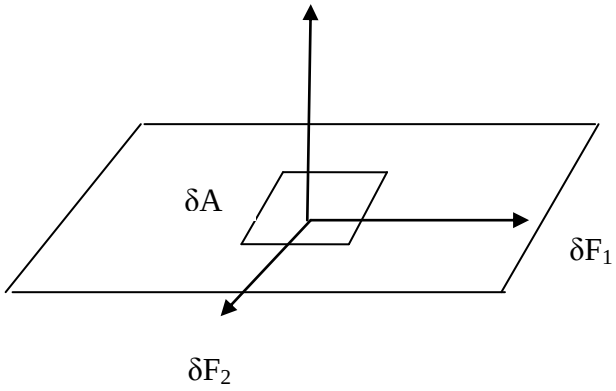

Figure A-9 Piece of area in fluid

δF_n = Normal force to the area d A, while δF_1 and δF_2 are tangential forces to the concerned area and perpendicular to each other.

Now we are interested in stresses,

Normal stress = $\sigma_n = \lim_{\delta A \to 0} \frac{\delta Fn}{\delta A}$

Shearing stresses= $\tau 1 = \lim_{\delta A \to 0} \frac{\delta F_1}{\delta A}$

$\tau 2 = \lim_{\delta A \to 0} \frac{\delta F_2}{\delta A}$

Now we would write these stresses with respect to a co-ordinate system,

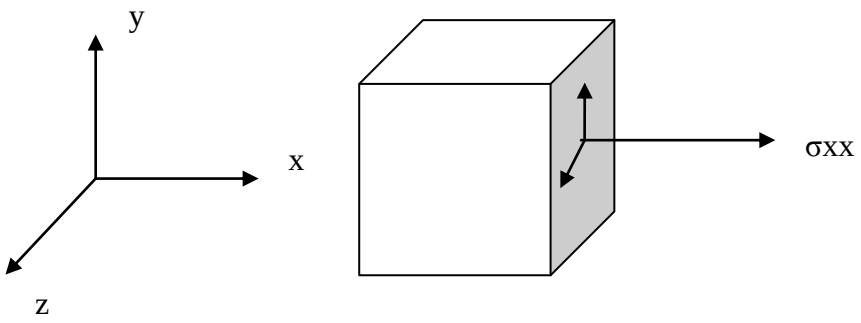

Figure A-10 Co-ordinate system for fluid system

For the plane parallel to y-z

σxx: Normal stress and other directions shear stresses (τ), and using sign convention for stresses involved,

Surface forces in terms of stresses: Normal stresses

$$(\sigma xx - \frac{\partial \sigma xx}{\partial x}\frac{\delta x}{2})\delta y \delta z$$

$$(\sigma xx + \frac{\partial \sigma xx}{\partial x}\frac{\delta x}{2})\delta y \delta z$$

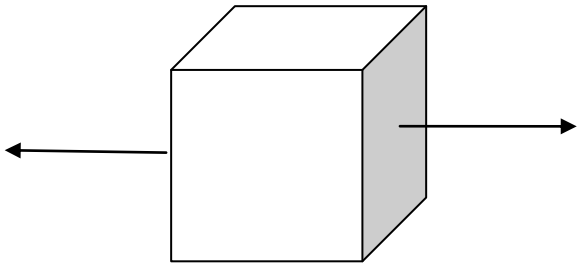

Figure A-11 Normal stresses in fluid element

Now adding on related normal and shear stresses involved,

$$\delta F_{sx} = \left(\frac{\partial \sigma xx}{\partial x} + \frac{\partial \tau_{yx}}{\partial y} + \frac{\partial \tau_{zx}}{\partial z} \right) \delta x \delta y \delta z$$

Similarly for other directions,

$$\delta F_{sy} = \left(\frac{\partial \tau_{xy}}{\partial x} + \frac{\partial \sigma_{yy}}{\partial y} + \frac{\partial \tau_{zy}}{\partial z} \right) \delta x \delta y \delta z$$

$$\delta F_{sz} = \left(\frac{\partial \tau_{xz}}{\partial x} + \frac{\partial \sigma_{zz}}{\partial y} + \frac{\partial \tau_{zz}}{\partial z} \right) \delta x \delta y \delta z$$

Dilution study

The product had to be stirred before use because of possible sedimentation of pigments. As a start of the rheological measurement, the pre-treatment primer A was diluted with deionised water to study the effect this has on high shear viscosity. As the target wet film thickness required to have lower viscosity than the original undiluted solution, the level of dilution in the product was optimised with this study.

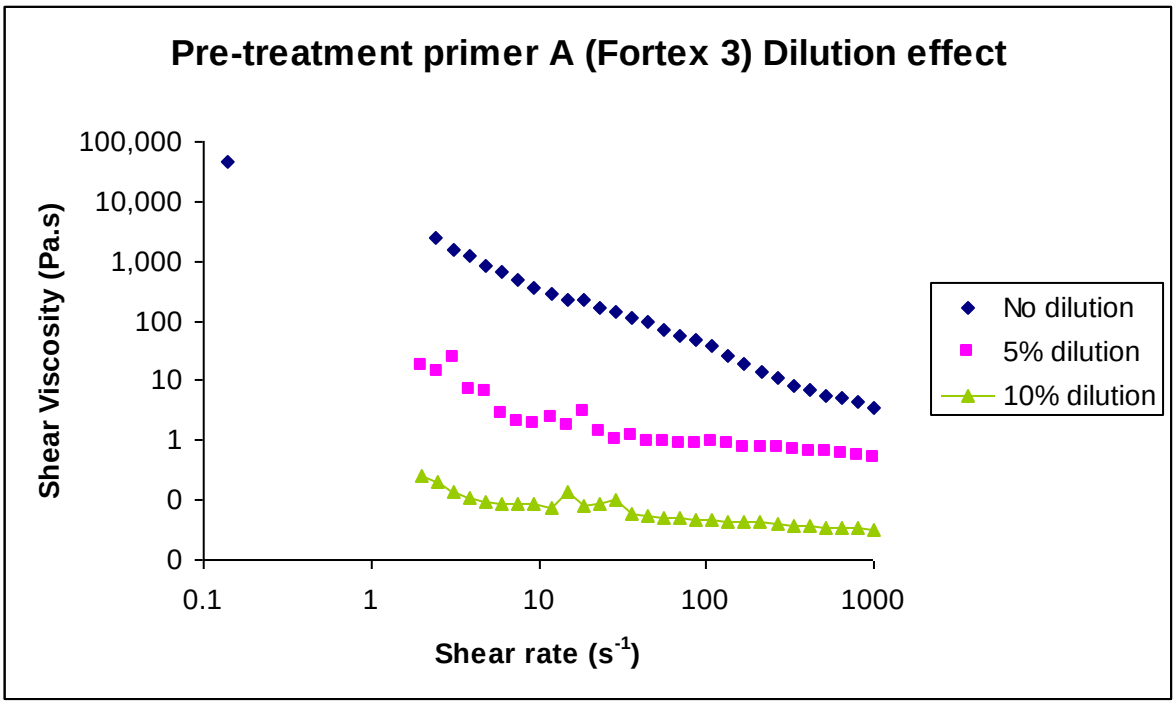

Figure A-12 Effect of dilution on shear viscosity at 20°C

In Fig. 5 the low shear viscosities without dilution were found to be significantly high, but were drastically reduced with addition of DI water. From these measurements, a dilution level of 10% by weight was chosen for the rig study experiments. The solid content by weight for pre-treatment primer A was measured

to be 56±1%. As the curing temperature for the water based system was low (about 75°C), heating the fluid before application was not viable. Also heating the fluid was increasing the viscosity of the fluid by evaporating the water in the system.

Flow curve

Rotational rheometer tests give information about the behaviour at large deformations, similar to the conditions experienced in high speed roller coating. A flow curve is used to measure the flow properties of a material as a function of the shear rate as shown in Fig. A-13

Because the dilution level for the sample was identified, 4 litres of pre-treatment primer A were diluted by 10% weight with DI water and stirred for 10 minutes. The shear viscosity of the new sample was measured using rotational rheometer and the results are shown in Fig.A-13. This 4 litre of solution was used for the Bradford lab roller coater rig trials.

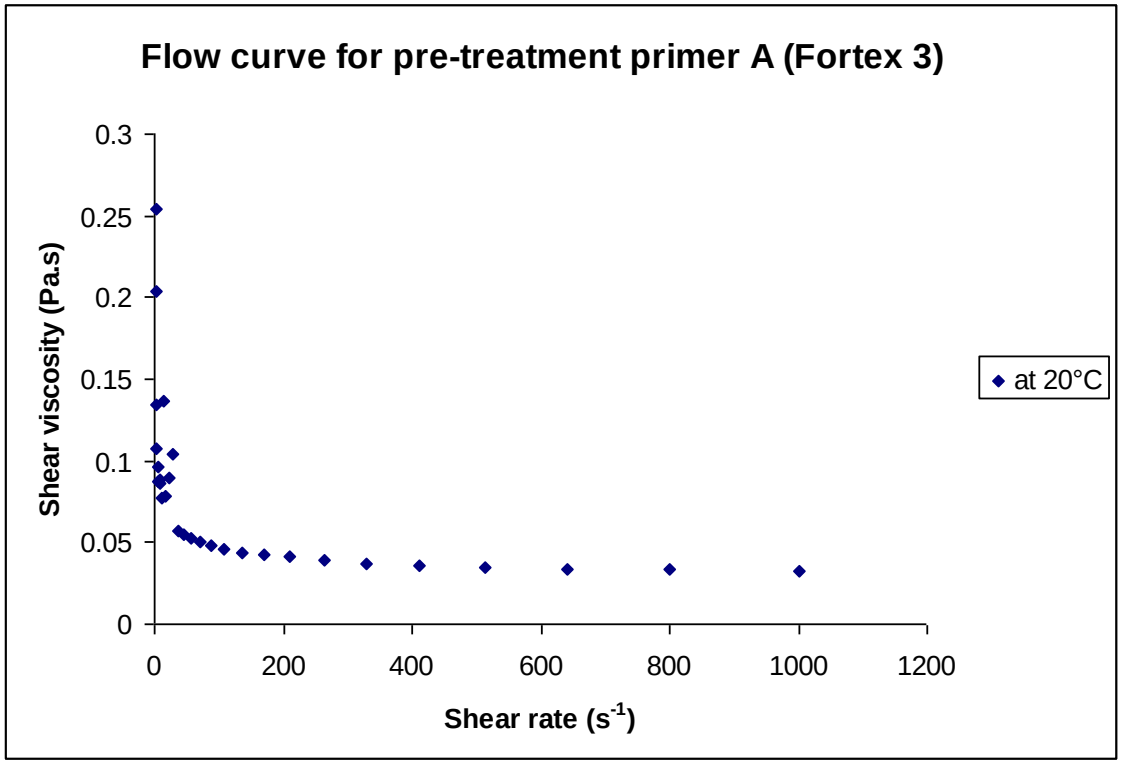

Figure A-13 Flow curve for pre-treatment primer at 20°C [10% by wt dilution]

The high shear rate viscosity was found to be around 35 mPa.s (Newtonian at higher shear rates) at ambient temperature. The pre-treatment primer was found to be shear thinning, as expected, and the plateau in the flow curve is achieved at around 500 s^{-1}, which suggests that an increase in the roller surface speed doesn't change the shear viscosity of the pre-treatment primer A significantly at higher line speeds.

Roller coating rig trial results with pre-treatment primer A (Fortex 3)

WFT study with symmetrical roll speeds

Although in most production lines, pick up and applicator rollers are not moving at the same speed, to start the experimental rig study and get better understanding, a symmetrical roll speed condition were used in the lab assessment. This simple case helps to understand the effect of roll speed on WFT metered under a given load condition between the rolls. As the applicator roll (rubber covered) is pushed against the steel roll the gap between the rolls is negative in its value. As explained in section 2.2, an FTIR gauge was used for the accurate measurement of the wet film thickness on the top of the pick up roll with an accuracy of ±1 µm. Under symmetrical roll speed condition, it was assumed that the WFT on the pick up roll is same as that on the applicator roll.

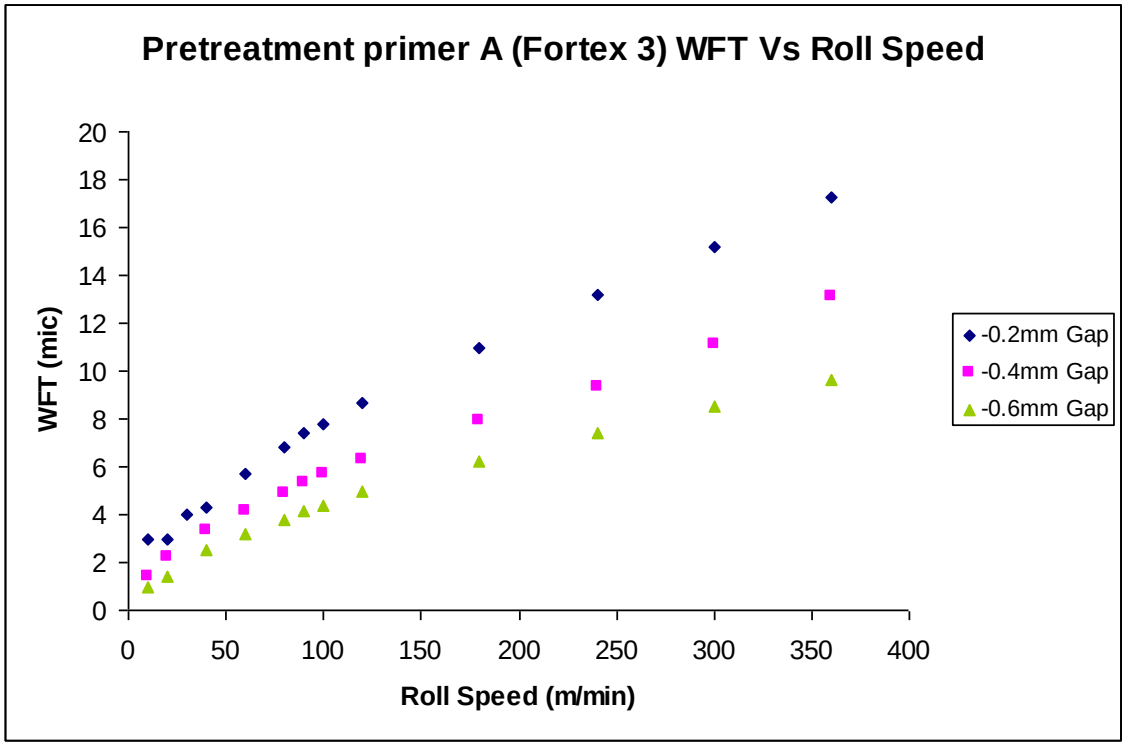

Figure A-14 Wet film thickness relation with roll speed

As shown in Fig. A-14, twelve different roll speeds were studied ranging from 20m/min to 360m/min, along with three different negative gap conditions. From the results of the experiments, at 180m/min, if both pick up and applicator rolls are running at identical speeds, then a WFT ranging from 6 to 11 µm can be achieved by changing the negative gap from -0.6mm to -0.2mm. At speeds above 150m/min, the fluid starts to splash from the edge of the rolls, mainly because of its lower viscosity. Properly designed splash guards help to go to higher roll speeds but it should be mentioned that the splashing phenomena could be controlled in plant conditions because of the longer rolls and superior designed coating pans. Again as shown in Fig. A-14, the WFT was found to increase on increasing roll speed and 9±1 µm is measured at 360m/min (both rolls running at this speed) at largest negative gap of -0.6mm. A target DFT of 9±1 µm could be achieved at 360m/min for symmetrical roll speed condition, if the negative gap chosen between the rolls is -0.2mm.

WFT study with asymmetrical roll speeds

As explained in section 4.1, in production line situation, the pick up and applicator rollers run at different speeds, introducing a speed ratio between them. The applicator roll (rubber covered) comes in contact with the moving steel strip (Fig. A-15) and hence the speed of this roll should be closer to that of the line speed [2]. A high applicator roll speed will potentially minimise friction issues between the applicator roll and the steel substrate by maintaining a good flow of paint in the applicator roller-strip nip region.

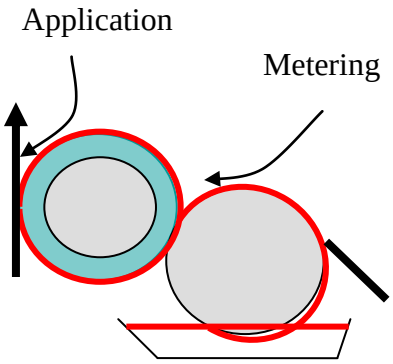

Figure A-15 Wet film thickness relation with roll speed

During our experimental trials, the pick up roll speed was kept constant and the applicator roll speed was increased in order to achieve speed ratios (Applicator roll speed / pick up roll speed) of magnitude ranging from 1 to 4 (Fig. A-16). The main point to note here is that during each of these 4 trials, the pick up roll speed was kept constant. The rubber cover material used for deformable roll coating was made of polyurethane (PU) and had a Shore hardness of 55 Shore A, compared to 53-55 Shore A in the DVL2 line and PU material. These parameters are closely matched, in order for better correlation between the lab and line results.

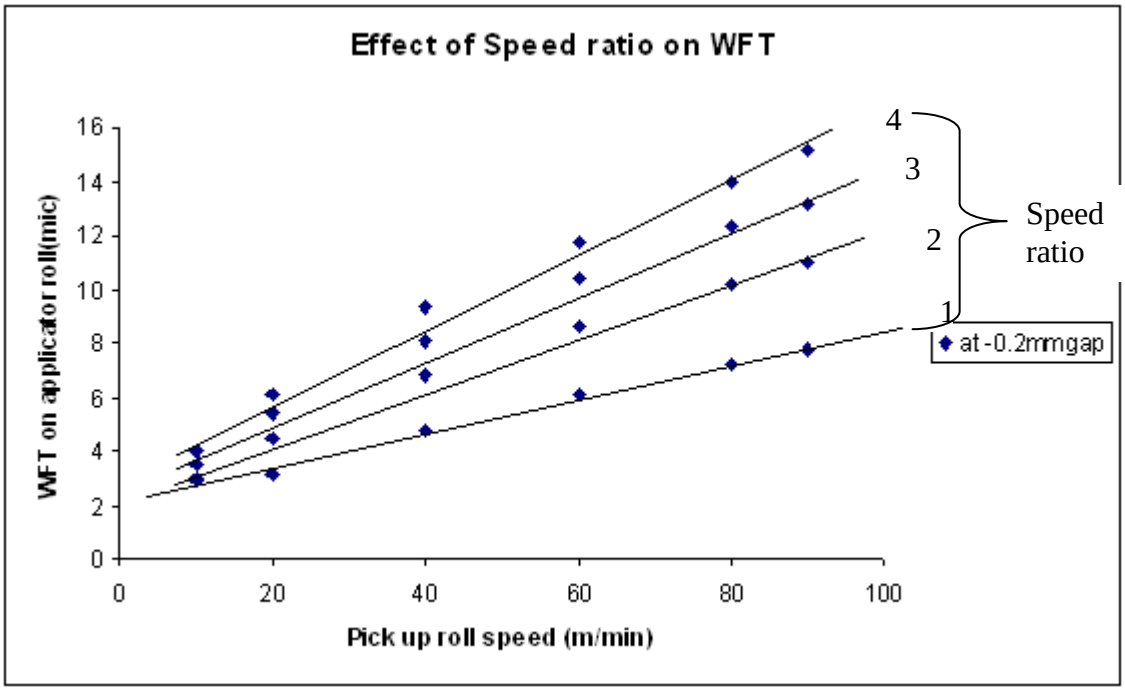

Figure A-16 Effect of speed ratio on applicator roll WFT at -0.2mm gap

As shown in Fig A-16, the increase in speed ratio (in effect, the speed of the applicator roll) is significantly contributing towards an increase in WFT. Similar trends of increase in WFT are also observed at higher load conditions as shown in Fig.A-17 and A-18.

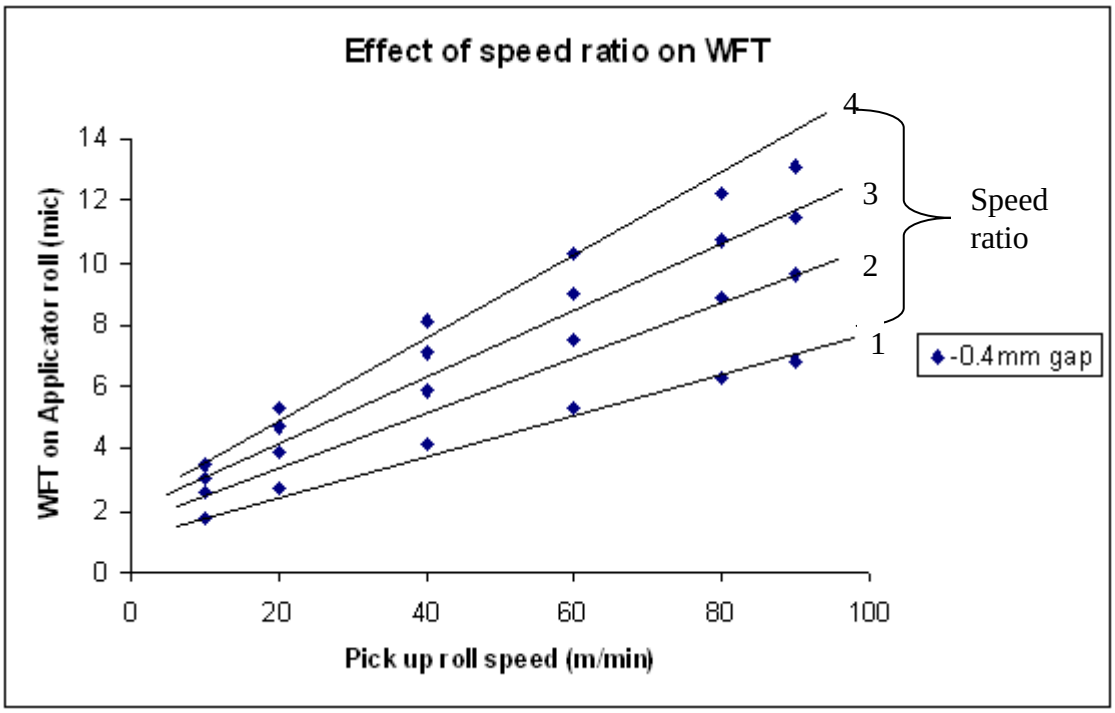

Figure A-17 Effect of speed ratio on applicator roll WFT at -0.4mm gap

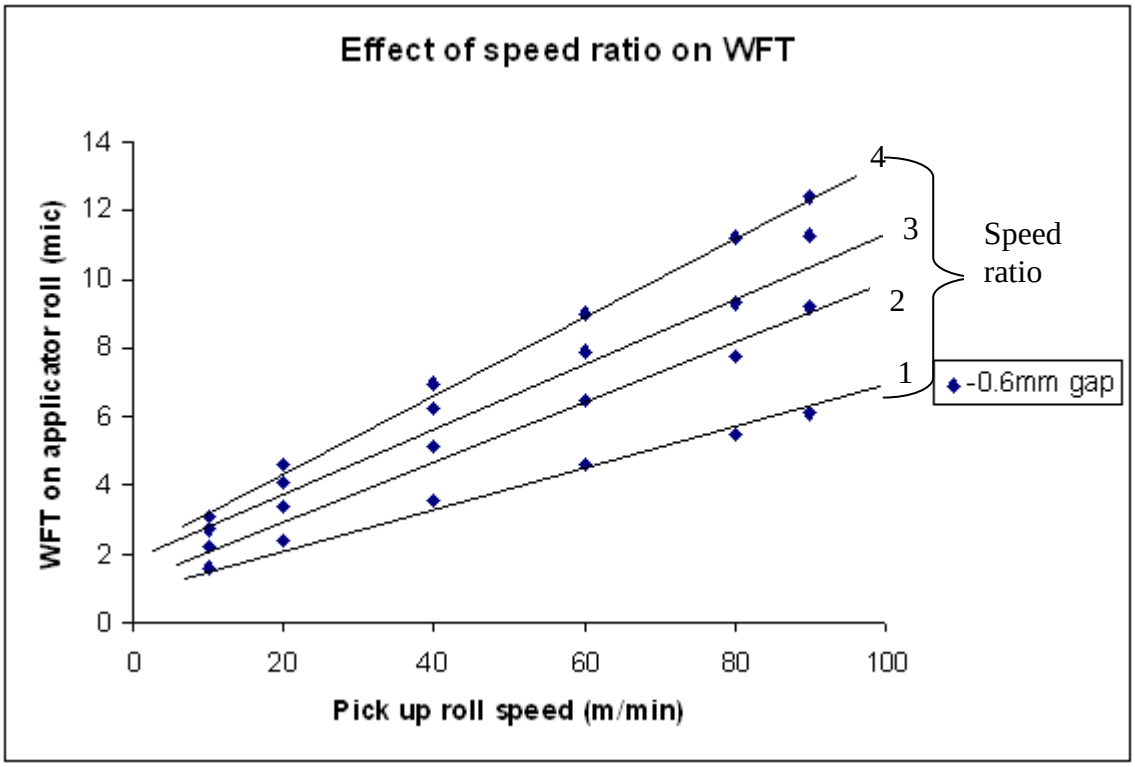

Figure A-18 Effect of speed ratio on applicator roll WFT at -0.6mm gap

In Fig.A-17 and A-18, the trend in increase in applicator WFT, because of the increase in average roll speed, when we increase the speed ratio from 1 to 4.

Study of instabilities at higher speeds

Ribbing

In the experimental study, the rib wavelength (distance between adjacent ribs) was measured. As shown in Fig. A-19, this experiment involves a two roll set up with a video camera (JVC RRGB TK 1270 with 3.5X lens) positioned above the top of the deformable roll to capture pictures of the rib pattern formed under various process conditions.

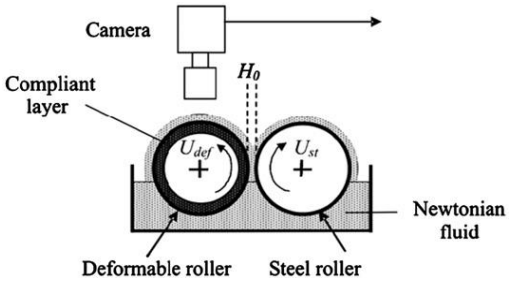

Figure A-19 Experimental set up for ribbing study [2]

The required gap between rollers and the roll speeds are set and, once the stable conditions are achieved, two photographs are taken under the same set up of experimental conditions. Ribs on the film were highlighted using a halogen light source, directed onto its surface at an oblique angle. This cast the valleys of the ribs into shadow thereby allowing the average wavelength to be measured from the resulting image. These photographs were analysed through image analysis software (ImageJ) with use of a reference picture to calibrate the measurement.

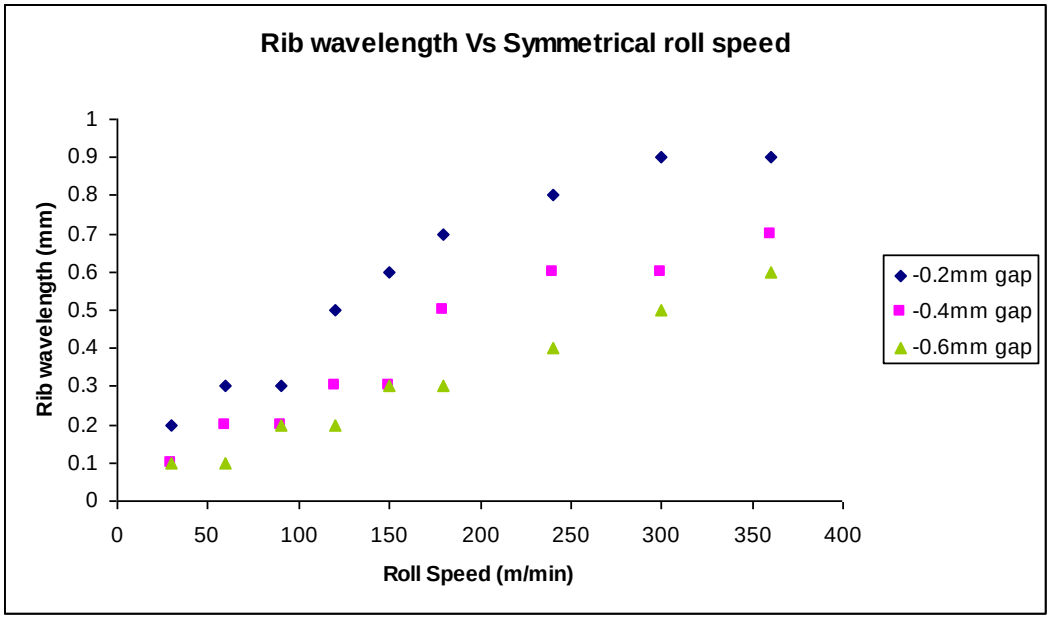

Figure A-20 Rib wavelength against roll speed

As shown in Fig.A-20, rib wavelength was found to increase with increasing roll speed for the pre-treatment primer and to decrease with increasing negative gap between the rollers. The lower the rib wavelength, the faster the rate of levelling. Hence higher negative gap or applied loads between rollers will decrease the rib wavelength and assists in levelling of ribs. This is of relevance to DVL2 as well as CAPL, where the pre-treatment primer is dried within a few seconds after the application, hence will need to level in a very short space of time. Roll speed increases the rib wavelength but at higher negative loads its effect diminishes. All the measured rib wavelengths are below 1mm, which is significantly less than that seen from the PE topcoat systems [1].

Misting

Misting is the phenomena of fine droplets ejecting from the nip region of the two rolls (Fig. A-21), after a critical roll surface speed. The misting phenomena in severe cases can be the limitation of the coating process.

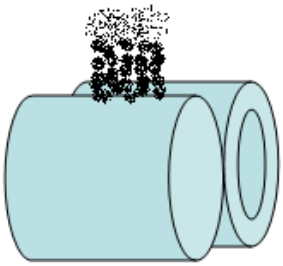

Figure A-21 Misting phenomena

The exact onset of misting phenomena was observed at 240m/min for pre-treatment primer A; the intensity was only significant above 300m/min roll speeds as shown in Fig. A-22.

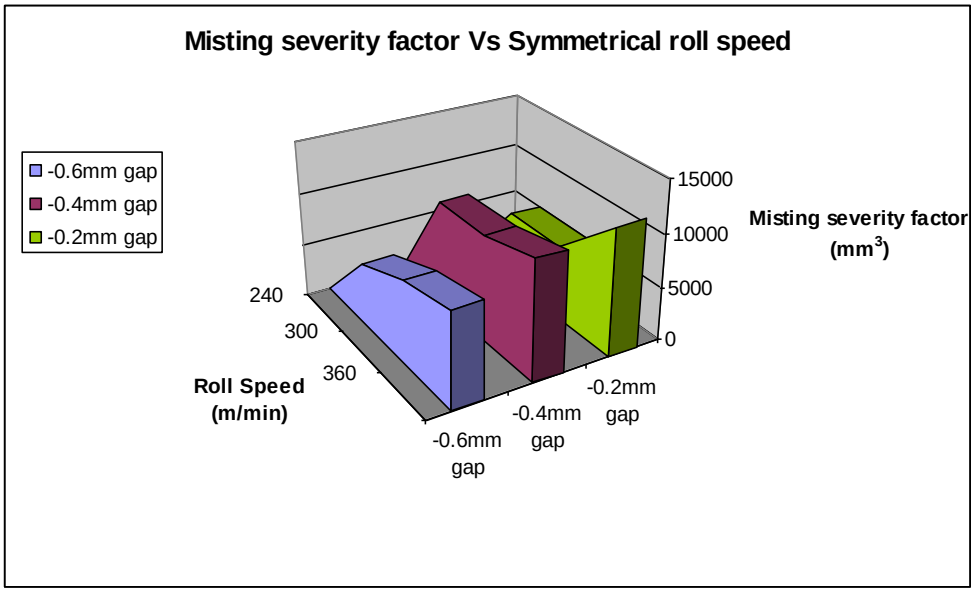

Figure A-22 Misting severity Vs process conditions

In general, the observed misting phenomena can be defined by three different parameters:

1. Misting height (mm)
2. Misting spread across the roll (mm)
3. Misting droplet size (mm)

As these three parameters found equally important at this initial stage of the study, a single term called “misting severity factor” is coined.

Misting severity factor = Misting height (mm) * Misting spread (mm) * Misting droplet size (mm).

All three parameters are found to be significant in the context of the phenomenon, and were therefore measured during the trials (details in Appendix 2). The droplets were collected with a clear glass slide positioned at the top of the rolls. When removed the slide immediately checked under a microscope and the average droplet size was measured. The misting severity factor compared to other high viscous fluid systems (such as solvent based topcoat) is significantly less [1]. The measurements made should be considered more as general indicators than absolute measurements.

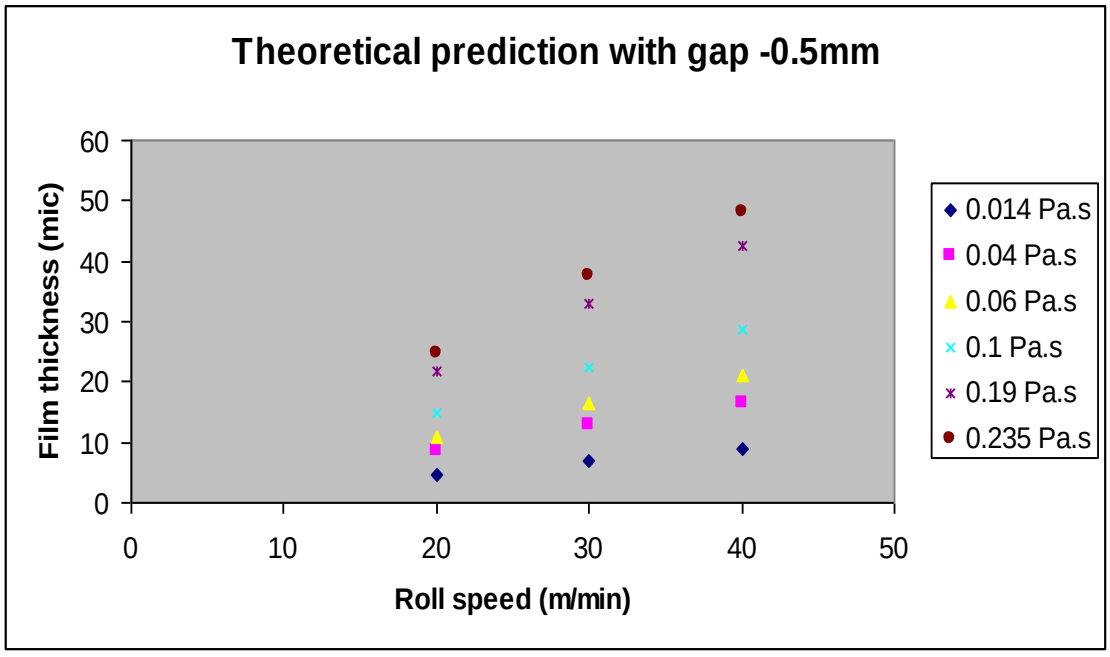

Figure A-23 Film thickness variation with speed at various viscosities and for gap -0.5mm

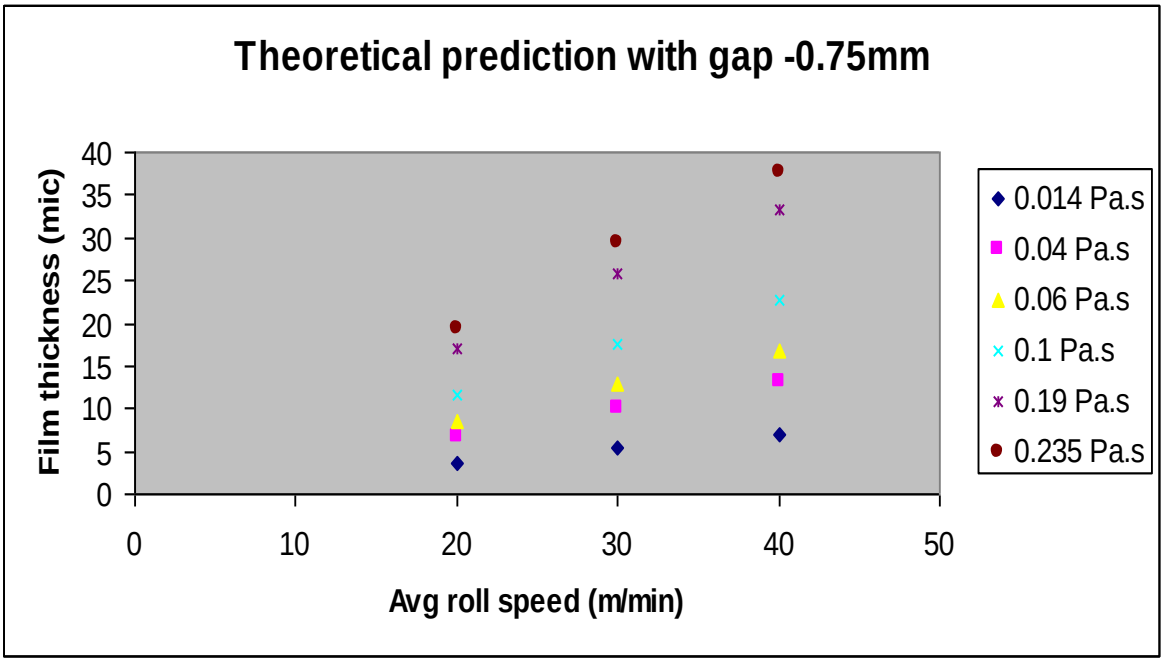

Figure A-24 Film thickness variation with speed at various viscosities and for gap -0.75mm

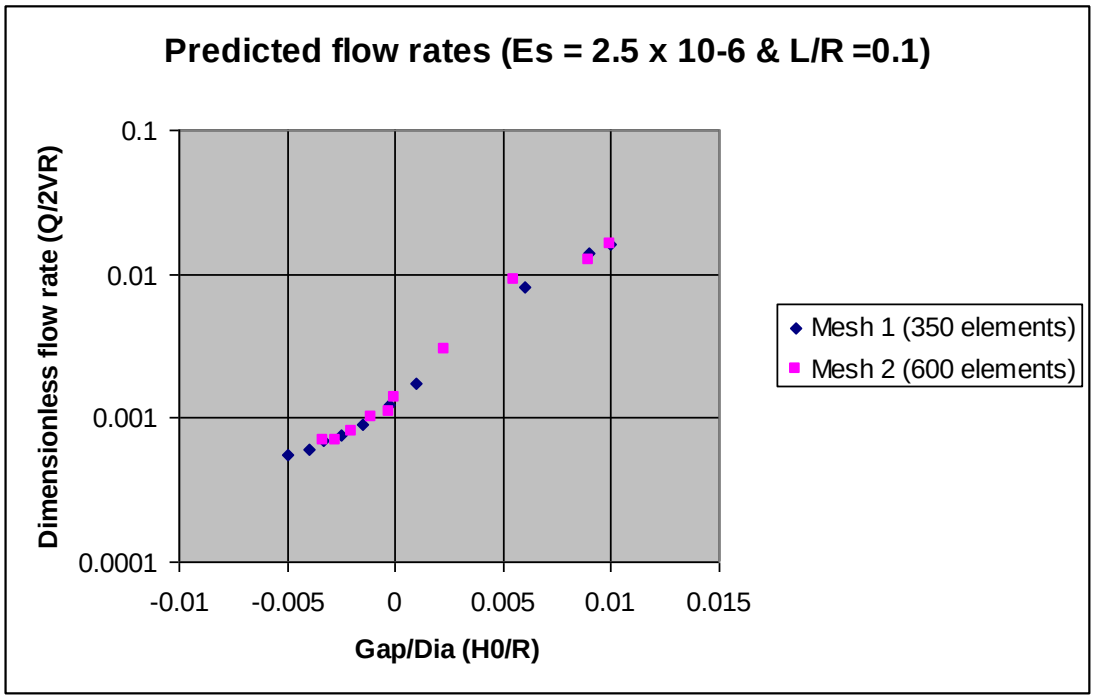

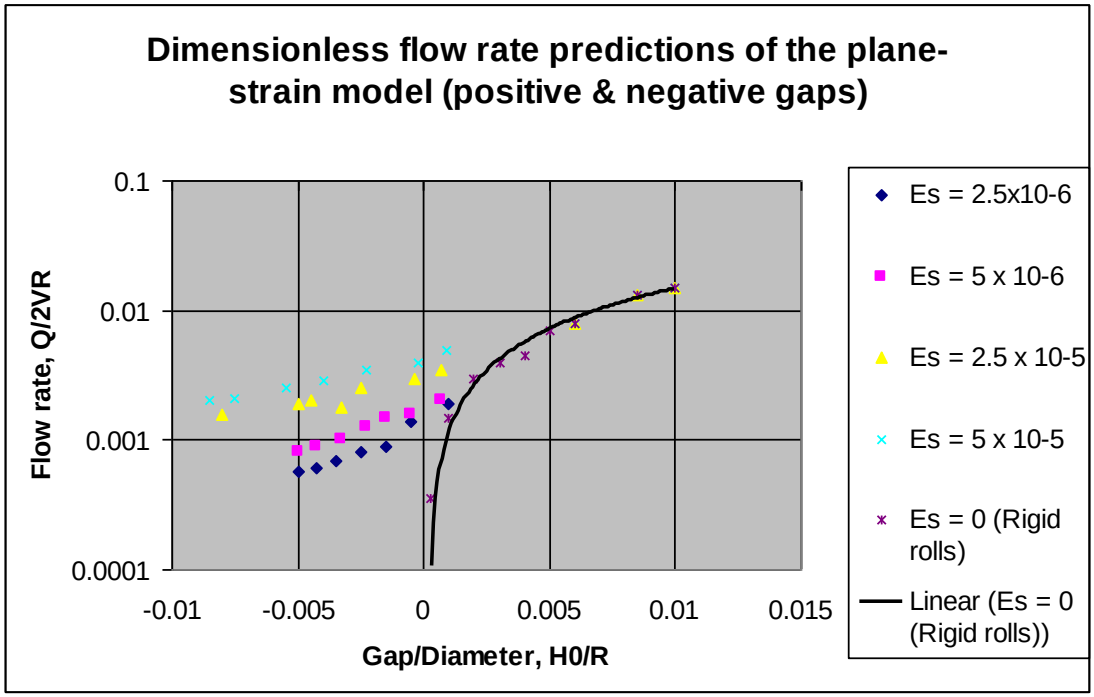
Dimensionless flow rate predictions of the plane-strain model (positive & negative gaps)
Flow rate, Q/2VR
0.1
0.01
0.001
0.0001
-0.01
-0.005
0
0.005
0.01
0.015
Gap/Diameter, H0/R
Es = 2.5x10-6
Es = 5 x 10-6
Es = 2.5 x 10-5
Es = 5 x 10-5
Es = 0 (Rigid rolls)
Linear (Es = 0 (Rigid rolls))

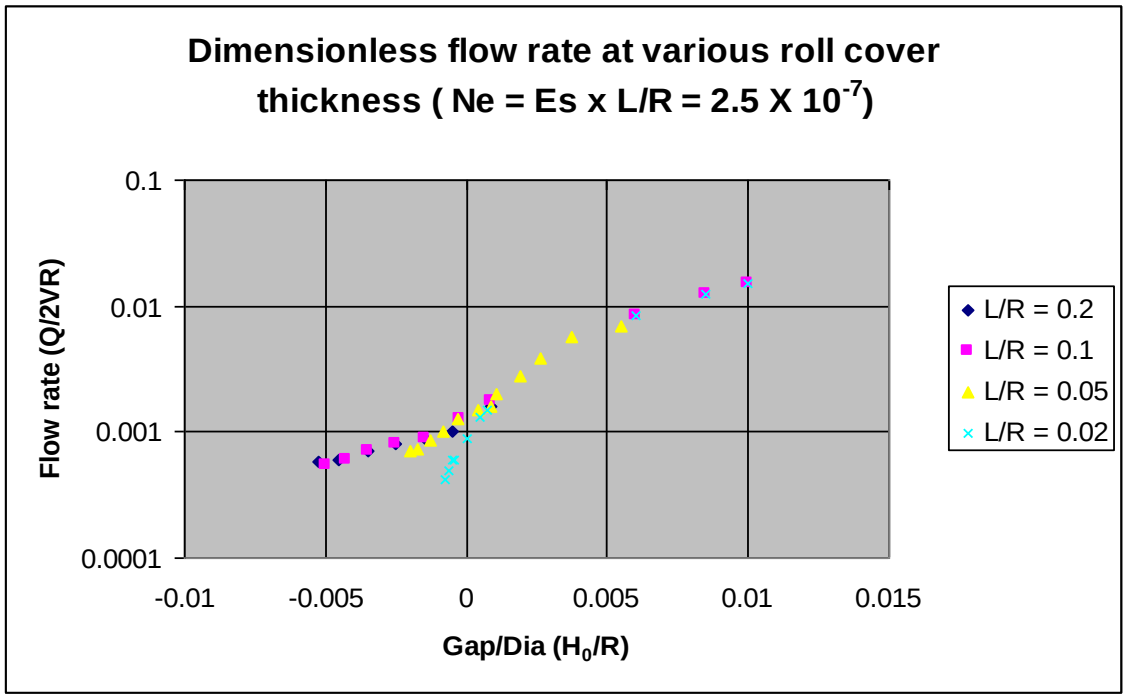
Dimensionless flow rate at various roll cover thickness (Ne = Es x L/R = 2.5 X 10-7)
Flow rate (Q/2VR)
0.1
0.01
0.001
0.0001
-0.01
-0.005
0
0.005
0.01
0.015
Gap/Dia (H0/R)
L/R = 0.2
L/R = 0.1
L/R = 0.05
L/R = 0.02

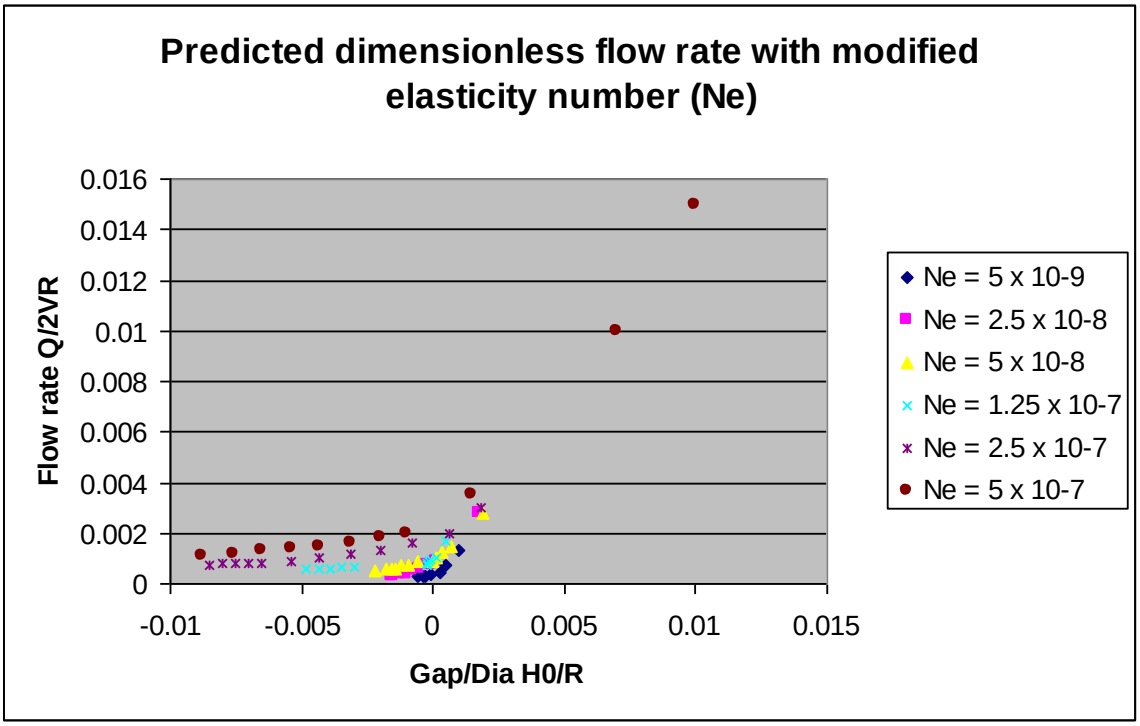
Predicted dimensionless flow rate with modified elasticity number (Ne)
Flow rate Q/2VR
0.016
0.014
0.012
0.01
0.008
0.006
0.004
0.002
0
-0.01
-0.005
0
0.005
0.01
0.015
Gap/Dia H0/R
Ne = 5 x 10-9
Ne = 2.5 x 10-8
Ne = 5 x 10-8
Ne = 1.25 x 10-7
Ne = 2.5 x 10-7
Ne = 5 x 10-7

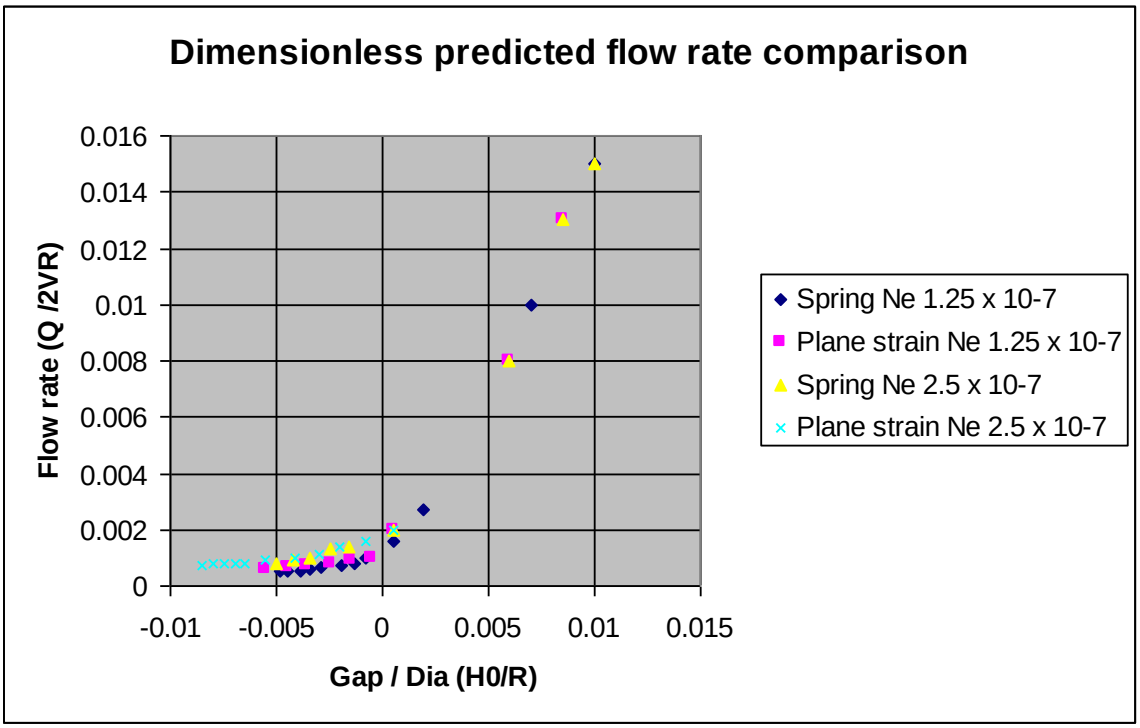
Dimensionless predicted flow rate comparison
Flow rate (Q /2VR)
0.016
0.014
0.012
0.01
0.008
0.006
0.004
0.002
0
-0.01
-0.005
0
0.005
0.01
0.015
Gap / Dia (H0/R)
Spring Ne 1.25 x 10-7
Plane strain Ne 1.25 x 10-7
Spring Ne 2.5 x 10-7
Plane strain Ne 2.5 x 10-7

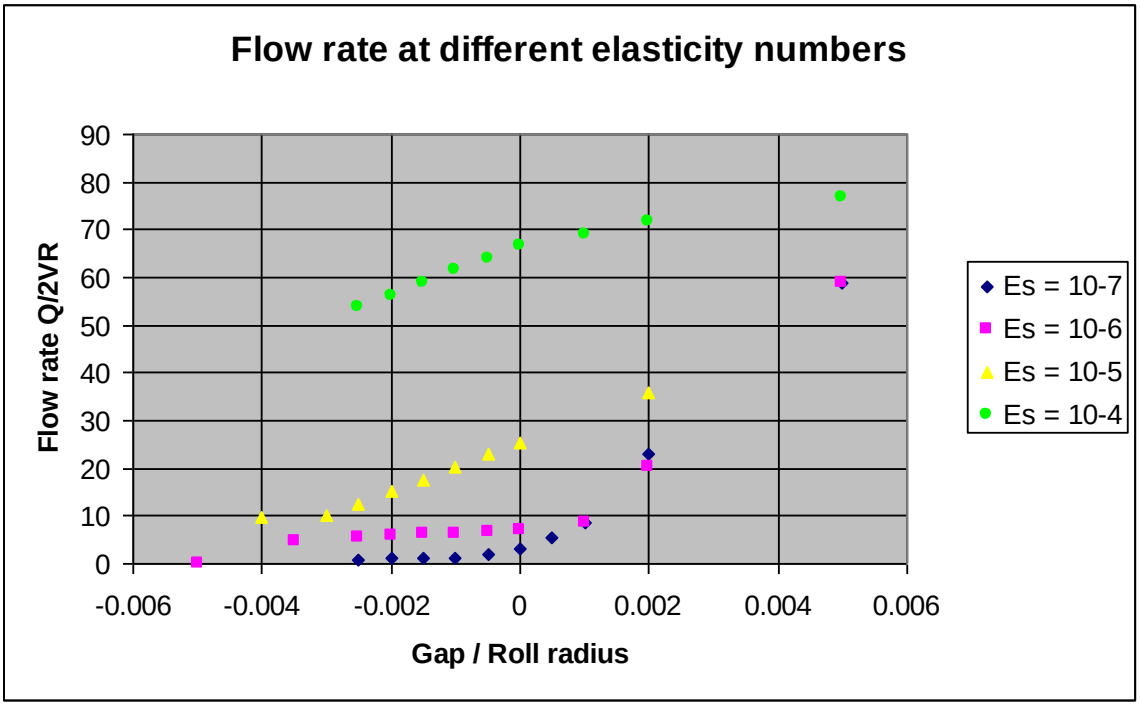

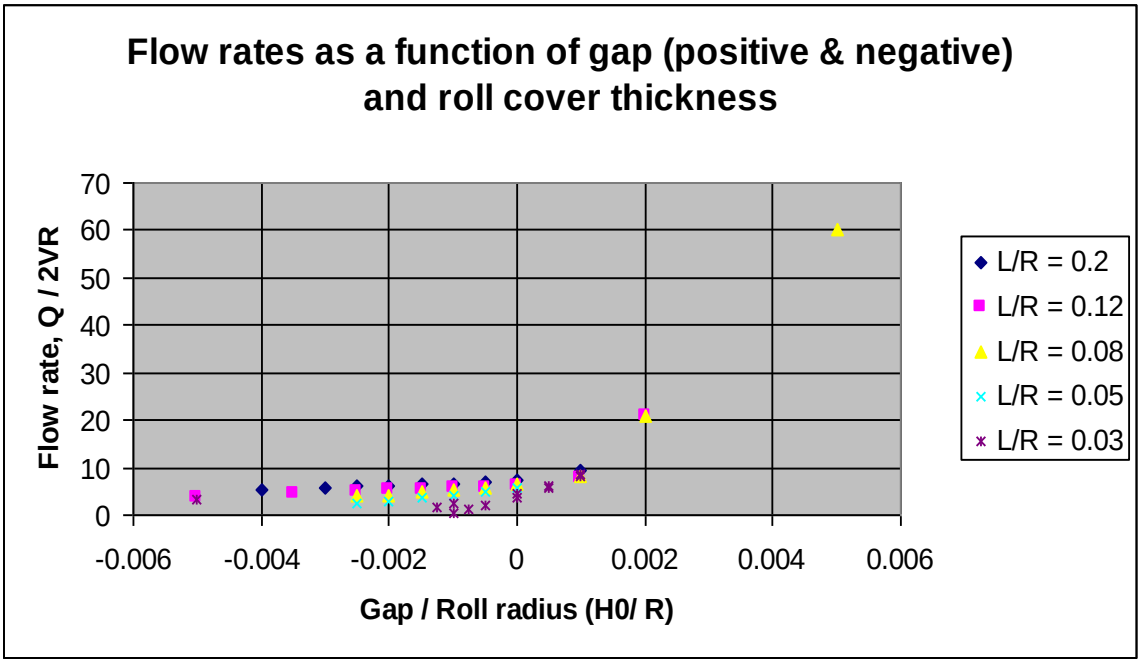

Alternative approach – Study of linear flow rates

As the current study is focusing on metering stage in the fast roller coating process, it could be relevant to explore the linear flow rate approach. Higher roll speeds associate with it different stability and quality issues. In previous sections, we

assumed that roll speeds are equal to the steel substrate line speed to avoid complications. But there could be a provision to introduce a speed ratio between the applicator roll speed and the substrate line speed. The whole roll coating process could be divided into 2 main stages for convenience, as shown in Fig. A-25.

- Metering stage

- Application stage

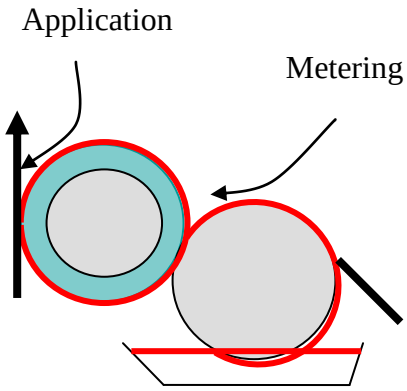

Figure A-25 Schematic diagram of various stages in the deformable roll coating of steel substrate

Initially, we can assume that actual target of this study is to achieve 20 µm wet film thickness (WFT) on the steel strip at 6 m/s line speed. So the linear flow rate of the coating reaching the application zone from the metering zone should be 120 x 10^{-6} m^2/s (20 µm x 6 m/s). The roll speeds to achieve the target linear flow rate for different viscosities at -1.5 mm gap condition for 55 Shore A hardness roll can be calculated as shown in Fig. A-26.

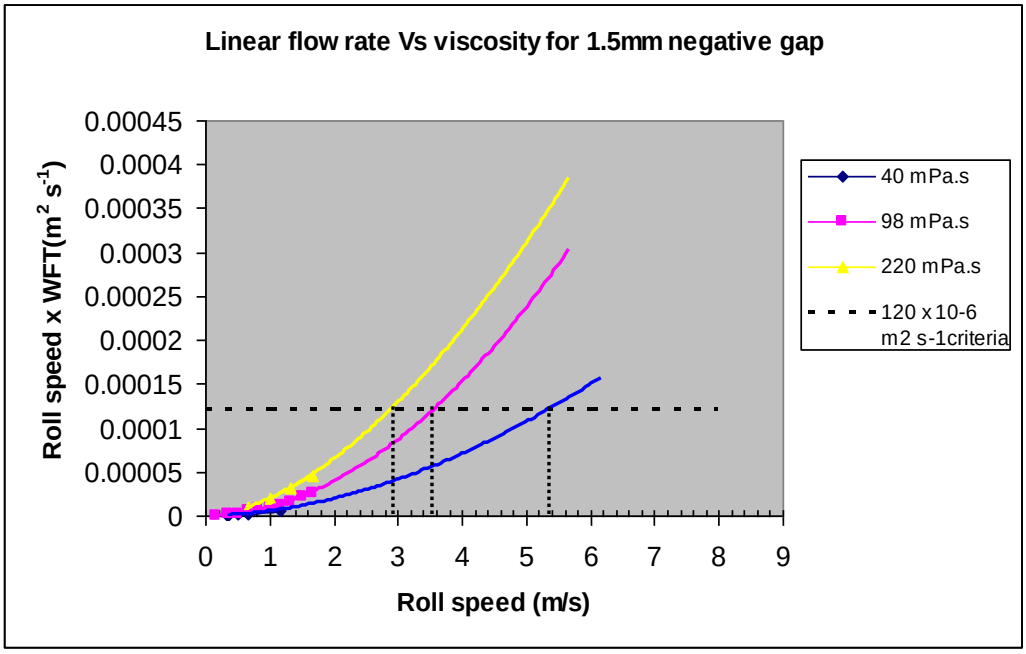

Figure A-26 Linear flow rate criteria for various viscosity fluids

The linear flow rate depends on roll speed and WFT on the rolls. In order to achieve 20 µm WFT running at 6 m/s on a steel substrate, the roll speeds may not have to be as high as 6 m/s. Obviously, the higher viscous fluids are able to achieve linear flow rate at lower speeds, because of higher WFT on the rolls. Our approach could be to achieve the target linear flow rate at maximum roll speed. Because the maximum roll speed will minimise the speed differential and friction issues between the applicator roll and the steel substrate. For example, in the above case the speed ratios between maximum applicator roll speed to achieve the target linear flow rate and target steel foil speed can be calculated as given in Table 5.15.

Table 5.15: Roll speed relation with target linear flow rate for various viscosity fluids

Fluid Shear Viscosity (mPa.s) at 1000 s^{-1} Shear rate	Maximum applicator roll speed (m/min)	WFT on roll at this speed (μm)	Speed ratio between applicator roll speed and foil speed (%)
40	312	23	86.67
100	210	34	58.33
220	174	41	48.33

Here the lowest viscosity fluid at 40 mPa.s running at 312 m/min, is able to achieve the target linear flow rate, would be an ideal choice as the applicator roll speed is closer to the actual line speed of 360 m/min. The stability of the meniscus in the application zone with differential speeds between the applicator roll and steel strip and the amount of pressure the roll needs to apply are unknown in academic world. These solutions could help us to choose the right speed ratio between the strip and applicator roll from the above calculated values. The limitation at the metering stage to go to higher speeds is the film non-uniformity, called ribbing phenomena which starts at a critical capillary number (Ca).

$$Ca = \mu V / \gamma$$

Here μ is the viscosity of fluid in Pa.s and V the average velocity of applicator and pick up roll in m/s, γ is the surface tension of the fluid in N/m [9].

Similarly the target linear flow rate calculations done on a 100 mPa.s fluid at different negative gaps is given in Fig.A-27.

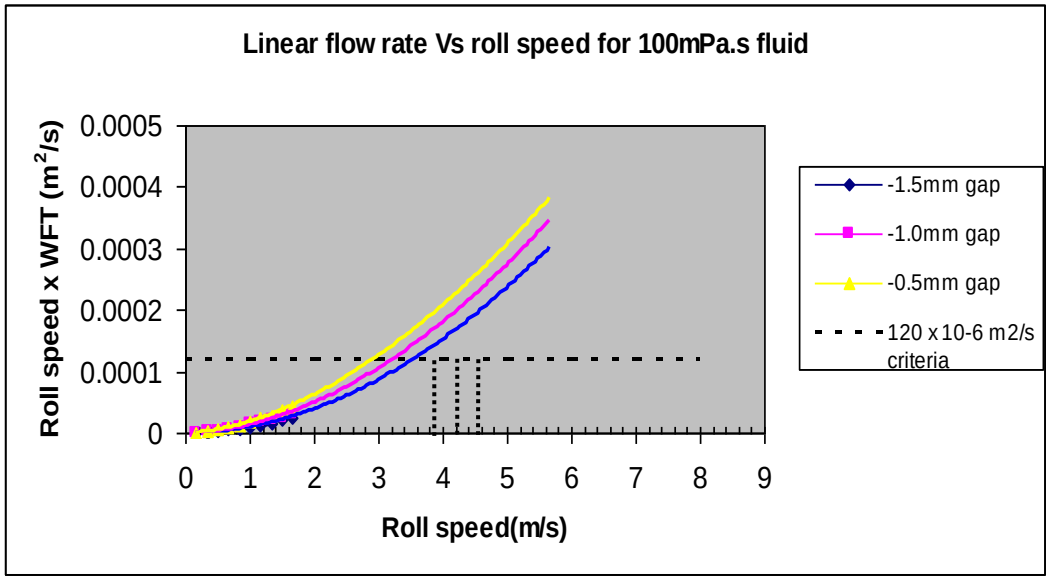

Figure A-27 Effect of negative gap on achieving target linear flow rate

The interpretation from the above calculation is that for a given viscosity fluid (constant heating of paint) the increase in negative gap is allowing to raise the roll speeds from 3 m/s to 3.8 m/s only to achieve the target linear flow rate. Here the lower negative gaps could yield the required linear flow rate at lower roll speeds but other process related issues like splashing and unstable meniscus at nip area need to be investigated in detail.

Film thickness measured- Raw data from the rig study

S.I No	Gap 2h (m)	Applicator speed (m/min)	P/Up speed (m/min)	Viscosity (Pa.s)	Hardness	Applicator thickness (mic)	Pick up Thickness (mic)
1	0.0002	15	5	0.04	70	2.82	1.56
2	0.0002	13.33	6.67	0.04	70	2.76	1.95
3	0.0002	10	10	0.04	70	2.49	2.49
4	0.0002	6.67	13.33	0.04	70	1.95	2.76
5	0.0002	5	15	0.04	70	1.56	2.82
6	0.0002	30	10	0.04	70	4.26	2.37
7	0.0002	26.67	13.33	0.04	70	4.2	2.94

8	0.0002	20	20	0.04	70	3.78	3.78
9	0.0002	13.33	26.67	0.04	70	2.94	4.2
10	0.0002	10	30	0.04	70	2.37	4.26
11	0.0002	45	15	0.04	70	5.43	3.03
12	0.0002	40	20	0.04	70	5.37	3.75
13	0.0002	30	30	0.04	70	4.83	4.83
14	0.0002	20	40	0.04	70	3.75	5.37
15	0.0002	15	45	0.04	70	3.03	5.43
16	0.0002	60	20	0.04	70	6.45	3.57
17	0.0002	53.33	26.67	0.04	70	6.36	4.47
18	0.0002	40	40	0.04	70	5.73	5.73
19	0.0002	26.67	53.33	0.04	70	4.47	6.36
20	0.0002	20	60	0.04	70	3.57	6.45
21	0.0002	75	25	0.04	70	7.38	4.11
22	0.0002	66.67	33.33	0.04	70	7.29	5.1
23	0.0002	50	50	0.04	70	6.57	6.57
24	0.0002	33.33	66.67	0.04	70	5.1	7.29
25	0.0004	15	5	0.04	70	2.16	1.2
26	0.0004	13.33	6.67	0.04	70	2.13	1.5
27	0.0004	10	10	0.04	70	1.92	1.92
28	0.0004	6.67	13.33	0.04	70	1.5	2.13
29	0.0004	5	15	0.04	70	1.2	2.16
30	0.0004	30	10	0.04	70	3.27	1.8
31	0.0004	26.67	13.33	0.04	70	3.21	2.25
32	0.0004	20	20	0.04	70	2.91	2.91
33	0.0004	13.33	26.67	0.04	70	2.25	3.21
34	0.0004	10	30	0.04	70	1.8	3.27
35	0.0004	45	15	0.04	70	4.14	2.31
36	0.0004	40	20	0.04	70	4.11	2.88
37	0.0004	30	30	0.04	70	3.69	3.69
38	0.0004	20	40	0.04	70	2.88	4.11
39	0.0004	15	45	0.04	70	2.31	4.14
40	0.0004	60	20	0.04	70	4.95	2.73
41	0.0004	53.33	26.67	0.04	70	4.89	3.42
42	0.0004	40	40	0.04	70	4.38	4.38
43	0.0004	26.67	53.33	0.04	70	3.42	4.89
44	0.0004	20	60	0.04	70	2.73	4.95
45	0.0004	75	25	0.04	70	5.64	3.15
46	0.0004	66.67	33.33	0.04	70	5.58	3.9
47	0.0004	50	50	0.04	70	5.01	5.01
48	0.0004	33.33	66.67	0.04	70	3.9	5.58
49	0.0006	15	5	0.04	70	1.83	1.02
50	0.0006	13.33	6.67	0.04	70	1.83	1.26
51	0.0006	10	10	0.04	70	1.62	1.62
52	0.0006	6.67	13.33	0.04	70	1.26	1.83
53	0.0006	5	15	0.04	70	1.02	1.83
54	0.0006	30	10	0.04	70	2.79	1.56
55	0.0006	26.67	13.33	0.04	70	2.76	1.92
56	0.0006	20	20	0.04	70	2.49	2.49
57	0.0006	13.33	26.67	0.04	70	1.92	2.76
58	0.0006	10	30	0.04	70	1.56	2.79
59	0.0006	45	15	0.04	70	3.54	1.98

60	0.0006	40	20	0.04	70	3.51	2.46
61	0.0006	30	30	0.04	70	3.15	3.15
62	0.0006	20	40	0.04	70	2.46	3.51
63	0.0006	15	45	0.04	70	1.98	3.54
64	0.0006	60	20	0.04	70	4.23	2.34
65	0.0006	53.33	26.67	0.04	70	4.17	2.91
66	0.0006	40	40	0.04	70	3.75	3.75
67	0.0006	26.67	53.33	0.04	70	2.91	4.17
68	0.0006	20	60	0.04	70	2.34	4.23
69	0.0006	75	25	0.04	70	4.83	2.67
70	0.0006	66.67	33.33	0.04	70	4.77	3.33
71	0.0006	50	50	0.04	70	4.29	4.29
72	0.0006	33.33	66.67	0.04	70	3.33	4.77
73	0.0006	25	75	0.04	70	2.67	4.83
74	0.0008	15	5	0.04	70	1.65	0.9
75	0.0008	13.33	6.67	0.04	70	1.62	1.14
76	0.0008	10	10	0.04	70	1.47	1.47
77	0.0008	6.67	13.33	0.04	70	1.14	1.62
78	0.0008	5	15	0.04	70	0.9	1.65
79	0.0008	30	10	0.04	70	2.49	1.38
80	0.0008	26.67	13.33	0.04	70	2.46	1.71
81	0.0008	20	20	0.04	70	2.22	2.22
82	0.0008	13.33	26.67	0.04	70	1.71	2.46
83	0.0008	10	30	0.04	70	1.38	2.49
84	0.0008	45	15	0.04	70	3.18	1.77
85	0.0008	40	20	0.04	70	3.15	2.19
86	0.0008	30	30	0.04	70	2.82	2.82
87	0.0008	20	40	0.04	70	2.19	3.15
88	0.0008	15	45	0.04	70	1.77	3.18
89	0.0008	60	20	0.04	70	3.78	2.1
90	0.0008	53.33	26.67	0.04	70	3.72	2.61
91	0.0008	40	40	0.04	70	3.36	3.36
92	0.0008	26.67	53.33	0.04	70	2.61	3.72
93	0.0008	20	60	0.04	70	2.1	3.78
94	0.0008	75	25	0.04	70	4.32	2.4
95	0.0008	66.67	33.33	0.04	70	4.26	2.97
96	0.0008	50	50	0.04	70	3.84	3.84
97	0.0008	33.33	66.67	0.04	70	2.97	4.26
98	0.0008	25	75	0.04	70	2.4	4.32
99	0.001	15	5	0.04	70	1.5	0.84
100	0.001	13.33	6.67	0.04	70	1.5	1.05
101	0.001	10	10	0.04	70	1.35	1.35
102	0.001	6.67	13.33	0.04	70	1.05	1.5
103	0.001	5	15	0.04	70	0.84	1.5
104	0.001	30	10	0.04	70	2.28	1.26
105	0.001	26.67	13.33	0.04	70	2.25	1.59
106	0.001	20	20	0.04	70	2.04	2.04
107	0.001	13.33	26.67	0.04	70	1.59	2.25
108	0.001	10	30	0.04	70	1.26	2.28
109	0.001	45	15	0.04	70	2.91	1.62
110	0.001	40	20	0.04	70	2.88	2.01
111	0.001	30	30	0.04	70	2.58	2.58

112	0.001	20	40	0.04	70	2.01	2.88
113	0.001	15	45	0.04	70	1.62	2.91
114	0.001	60	20	0.04	70	3.48	1.92
115	0.001	53.33	26.67	0.04	70	3.42	2.4
116	0.001	40	40	0.04	70	3.09	3.09
117	0.001	26.67	53.33	0.04	70	2.4	3.42
118	0.001	20	60	0.04	70	1.92	3.48
119	0.001	75	25	0.04	70	3.96	2.19
120	0.001	66.67	33.33	0.04	70	3.9	2.73
121	0.001	50	50	0.04	70	3.51	3.51
122	0.001	33.33	66.67	0.04	70	2.73	3.9
123	0.001	25	75	0.04	70	2.19	3.96
124	0.0002	15	5	0.04	55	4.68	2.58
125	0.0002	13.33	6.67	0.04	55	4.59	3.24
126	0.0002	10	10	0.04	55	4.14	4.14
127	0.0002	6.67	13.33	0.04	55	3.24	4.59
128	0.0002	5	15	0.04	55	2.58	4.68
129	0.0002	30	10	0.04	55	7.08	3.93
130	0.0002	26.67	13.33	0.04	55	6.99	4.89
131	0.0002	20	20	0.04	55	6.3	6.3
132	0.0002	13.33	26.67	0.04	55	4.89	6.99
133	0.0002	10	30	0.04	55	3.93	7.08
134	0.0002	45	15	0.04	55	9.03	5.01
135	0.0002	40	20	0.04	55	8.91	6.24
136	0.0002	30	30	0.04	55	8.01	8.01
137	0.0002	20	40	0.04	55	6.24	8.91
138	0.0002	15	45	0.04	55	5.01	9.03
139	0.0002	60	20	0.04	55	10.71	5.97
140	0.0002	53.33	26.67	0.04	55	10.59	7.41
141	0.0002	40	40	0.04	55	9.54	9.54
142	0.0002	26.67	53.33	0.04	55	7.41	10.59
143	0.0002	20	60	0.04	55	5.97	10.71
144	0.0002	75	25	0.04	55	12.24	6.81
145	0.0002	66.67	33.33	0.04	55	12.09	8.46
146	0.0002	50	50	0.04	55	10.89	10.89
147	0.0002	33.33	66.67	0.04	55	8.46	12.09
148	0.0002	25	75	0.04	55	6.81	12.24
149	0.0004	15	5	0.04	55	3.57	1.98
150	0.0004	13.33	6.67	0.04	55	3.54	2.46
151	0.0004	10	10	0.04	55	3.18	3.18
152	0.0004	6.67	13.33	0.04	55	2.46	3.54
153	0.0004	5	15	0.04	55	1.98	3.57
154	0.0004	30	10	0.04	55	5.4	3
155	0.0004	26.67	13.33	0.04	55	5.34	3.72
156	0.0004	20	20	0.04	55	4.8	4.8
157	0.0004	13.33	26.67	0.04	55	3.72	5.34
158	0.0004	10	30	0.04	55	3	5.4
159	0.0004	45	15	0.04	55	6.9	3.84
160	0.0004	40	20	0.04	55	6.81	4.77
161	0.0004	30	30	0.04	55	6.15	6.15
162	0.0004	20	40	0.04	55	4.77	6.81
163	0.0004	15	45	0.04	55	3.84	6.9

164	0.0004	60	20	0.04	55	8.19	4.56
165	0.0004	53.33	26.67	0.04	55	8.1	5.67
166	0.0004	40	40	0.04	55	7.29	7.29
167	0.0004	26.67	53.33	0.04	55	5.67	8.1
168	0.0004	20	60	0.04	55	4.56	8.19
169	0.0004	75	25	0.04	55	9.39	5.22
170	0.0004	66.67	33.33	0.04	55	9.27	6.48
171	0.0004	50	50	0.04	55	8.34	8.34
172	0.0004	33.33	66.67	0.04	55	6.48	9.27
173	0.0004	25	75	0.04	55	5.22	9.39
174	0.0006	15	5	0.04	55	3.06	1.71
175	0.0006	13.33	6.67	0.04	55	3	2.13
176	0.0006	10	10	0.04	55	2.7	2.7
177	0.0006	6.67	13.33	0.04	55	2.13	3
178	0.0006	5	15	0.04	55	1.71	3.06
179	0.0006	30	10	0.04	55	4.62	2.58
180	0.0006	26.67	13.33	0.04	55	4.56	3.18
181	0.0006	20	20	0.04	55	4.11	4.11
182	0.0006	13.33	26.67	0.04	55	3.18	4.56
183	0.0006	10	30	0.04	55	2.58	4.62
184	0.0006	45	15	0.04	55	5.91	3.27
185	0.0006	40	20	0.04	55	5.82	4.08
186	0.0006	30	30	0.04	55	5.25	5.25
187	0.0006	20	40	0.04	55	4.08	5.82
188	0.0006	15	45	0.04	55	3.27	5.91
189	0.0006	60	20	0.04	55	7.02	3.9
190	0.0006	53.33	26.67	0.04	55	6.93	4.86
191	0.0006	40	40	0.04	55	6.24	6.24
192	0.0006	26.67	53.33	0.04	55	4.86	6.93
193	0.0006	20	60	0.04	55	3.9	7.02
194	0.0006	75	25	0.04	55	8.01	4.47
195	0.0006	66.67	33.33	0.04	55	7.92	5.55
196	0.0006	50	50	0.04	55	7.14	7.14
197	0.0006	33.33	66.67	0.04	55	5.55	7.92
198	0.0006	25	75	0.04	55	4.47	8.01
199	0.0008	15	5	0.04	55	2.73	1.53
200	0.0008	13.33	6.67	0.04	55	2.7	1.89
201	0.0008	10	10	0.04	55	2.43	2.43
202	0.0008	6.67	13.33	0.04	55	1.89	2.7
203	0.0008	5	15	0.04	55	1.53	2.73
204	0.0008	30	10	0.04	55	4.14	2.31
205	0.0008	26.67	13.33	0.04	55	4.08	2.85
206	0.0008	20	20	0.04	55	3.69	3.69
207	0.0008	13.33	26.67	0.04	55	2.85	4.08
208	0.0008	10	30	0.04	55	2.31	4.14
209	0.0008	45	15	0.04	55	5.28	2.94
210	0.0008	40	20	0.04	55	5.22	3.66
211	0.0008	30	30	0.04	55	4.71	4.71
212	0.0008	20	40	0.04	55	3.66	5.22
213	0.0008	15	45	0.04	55	2.94	5.28
214	0.0008	60	20	0.04	55	6.27	3.48
215	0.0008	53.33	26.67	0.04	55	6.21	4.35

216	0.0008	40	40	0.04	55	5.58	5.58
217	0.0008	26.67	53.33	0.04	55	4.35	6.21
218	0.0008	20	60	0.04	55	3.48	6.27
219	0.0008	75	25	0.04	55	7.17	3.99
220	0.0008	66.67	33.33	0.04	55	7.08	4.95
221	0.0008	50	50	0.04	55	6.39	6.39
222	0.0008	33.33	66.67	0.04	55	4.95	7.08
223	0.0008	25	75	0.04	55	3.99	7.17
224	0.001	15	5	0.04	55	2.52	1.38
225	0.001	13.33	6.67	0.04	55	2.46	1.74
226	0.001	10	10	0.04	55	2.22	2.22
227	0.001	6.67	13.33	0.04	55	1.74	2.46
228	0.001	5	15	0.04	55	1.38	2.52
229	0.001	30	10	0.04	55	3.81	2.1
230	0.001	26.67	13.33	0.04	55	3.75	2.61
231	0.001	20	20	0.04	55	3.39	3.39
232	0.001	13.33	26.67	0.04	55	2.61	3.75
233	0.001	10	30	0.04	55	2.1	3.81
234	0.001	45	15	0.04	55	4.86	2.7
235	0.001	40	20	0.04	55	4.8	3.36
236	0.001	30	30	0.04	55	4.32	4.32
237	0.001	20	40	0.04	55	3.36	4.8
238	0.001	15	45	0.04	55	2.7	4.86
239	0.001	60	20	0.04	55	5.76	3.21
240	0.001	53.33	26.67	0.04	55	5.7	3.99
241	0.001	40	40	0.04	55	5.13	5.13
242	0.001	26.67	53.33	0.04	55	3.99	5.7
243	0.001	20	60	0.04	55	3.21	5.76
244	0.001	75	25	0.04	55	6.57	3.66
245	0.001	66.67	33.33	0.04	55	6.51	4.56
246	0.001	50	50	0.04	55	5.85	5.85
247	0.001	33.33	66.67	0.04	55	4.56	6.51
248	0.001	25	75	0.04	55	3.66	6.57
249	0.0002	15	5	0.04	45	6.54	3.63
250	0.0002	13.33	6.67	0.04	45	6.48	4.53
251	0.0002	10	10	0.04	45	5.82	5.82
252	0.0002	6.67	13.33	0.04	45	4.53	6.48
253	0.0002	5	15	0.04	45	3.63	6.54
254	0.0002	30	10	0.04	45	9.93	5.52
255	0.0002	26.67	13.33	0.04	45	9.78	6.84
256	0.0002	20	20	0.04	45	8.82	8.82
257	0.0002	13.33	26.67	0.04	45	6.84	9.78
258	0.0002	10	30	0.04	45	5.52	9.93
259	0.0002	45	15	0.04	45	12.66	7.02
260	0.0002	40	20	0.04	45	12.51	8.76
261	0.0002	30	30	0.04	45	11.25	11.25
262	0.0002	20	40	0.04	45	8.76	12.51
263	0.0002	15	45	0.04	45	7.02	12.66
264	0.0002	60	20	0.04	45	15.03	8.34
265	0.0002	53.33	26.67	0.04	45	14.85	10.41
266	0.0002	40	40	0.04	45	13.35	13.35
267	0.0002	26.67	53.33	0.04	45	10.41	14.85

268	0.0002	20	60	0.04	45	8.34	15.03
269	0.0002	75	25	0.04	45	17.19	9.54
270	0.0002	66.67	33.33	0.04	45	16.98	11.88
271	0.0002	50	50	0.04	45	15.27	15.27
272	0.0002	33.33	66.67	0.04	45	11.88	16.98
273	0.0002	25	75	0.04	45	9.54	17.19
274	0.0004	15	5	0.04	45	5.01	2.79
275	0.0004	13.33	6.67	0.04	45	4.95	3.48
276	0.0004	10	10	0.04	45	4.44	4.44
277	0.0004	6.67	13.33	0.04	45	3.48	4.95
278	0.0004	5	15	0.04	45	2.79	5.01
279	0.0004	30	10	0.04	45	7.59	4.23
280	0.0004	26.67	13.33	0.04	45	7.5	5.25
281	0.0004	20	20	0.04	45	6.75	6.75
282	0.0004	13.33	26.67	0.04	45	5.25	7.5
283	0.0004	10	30	0.04	45	4.23	7.59
284	0.0004	45	15	0.04	45	9.69	5.37
285	0.0004	40	20	0.04	45	9.57	6.69
286	0.0004	30	30	0.04	45	8.61	8.61
287	0.0004	20	40	0.04	45	6.69	9.57
288	0.0004	15	45	0.04	45	5.37	9.69
289	0.0004	60	20	0.04	45	11.52	6.39
290	0.0004	53.33	26.67	0.04	45	11.37	7.95
291	0.0004	40	40	0.04	45	10.23	10.23
292	0.0004	26.67	53.33	0.04	45	7.95	11.37
293	0.0004	20	60	0.04	45	6.39	11.52
294	0.0004	75	25	0.04	45	13.14	7.32
295	0.0004	66.67	33.33	0.04	45	12.99	9.09
296	0.0004	50	50	0.04	45	11.7	11.7
297	0.0004	33.33	66.67	0.04	45	9.09	12.99
298	0.0004	25	75	0.04	45	7.32	13.14
299	0.0006	15	5	0.04	45	4.29	2.37
300	0.0006	13.33	6.67	0.04	45	4.23	2.97
301	0.0006	10	10	0.04	45	3.81	3.81
302	0.0006	6.67	13.33	0.04	45	2.97	4.23
303	0.0006	5	15	0.04	45	2.37	4.29
304	0.0006	30	10	0.04	45	6.48	3.6
305	0.0006	26.67	13.33	0.04	45	6.42	4.47
306	0.0006	20	20	0.04	45	5.76	5.76
307	0.0006	13.33	26.67	0.04	45	4.47	6.42
308	0.0006	10	30	0.04	45	3.6	6.48
309	0.0006	45	15	0.04	45	8.28	4.59
310	0.0006	40	20	0.04	45	8.19	5.73
311	0.0006	30	30	0.04	45	7.35	7.35
312	0.0006	20	40	0.04	45	5.73	8.19
313	0.0006	15	45	0.04	45	4.59	8.28
314	0.0006	60	20	0.04	45	9.84	5.46
315	0.0006	53.33	26.67	0.04	45	9.72	6.81
316	0.0006	40	40	0.04	45	8.76	8.76
317	0.0006	26.67	53.33	0.04	45	6.81	9.72
318	0.0006	20	60	0.04	45	5.46	9.84
319	0.0006	75	25	0.04	45	11.25	6.24

320	0.0006	66.67	33.33	0.04	45	11.1	7.77
321	0.0006	50	50	0.04	45	9.99	9.99
322	0.0006	33.33	66.67	0.04	45	7.77	11.1
323	0.0006	25	75	0.04	45	6.24	11.25
324	0.0008	15	5	0.04	45	3.84	2.13
325	0.0008	13.33	6.67	0.04	45	3.78	2.67
326	0.0008	10	10	0.04	45	3.42	3.42
327	0.0008	6.67	13.33	0.04	45	2.67	3.78
328	0.0008	5	15	0.04	45	2.13	3.84
329	0.0008	30	10	0.04	45	5.82	3.24
330	0.0008	26.67	13.33	0.04	45	5.73	4.02
331	0.0008	20	20	0.04	45	5.16	5.16
332	0.0008	13.33	26.67	0.04	45	4.02	5.73
333	0.0008	10	30	0.04	45	3.24	5.82
334	0.0008	45	15	0.04	45	7.41	4.11
335	0.0008	40	20	0.04	45	7.32	5.13
336	0.0008	30	30	0.04	45	6.6	6.6
337	0.0008	20	40	0.04	45	5.13	7.32
338	0.0008	15	45	0.04	45	4.11	7.41
339	0.0008	53.33	26.67	0.04	45	8.7	6.09
340	0.0008	40	40	0.04	45	7.83	7.83
341	0.0008	26.67	53.33	0.04	45	6.09	8.7
342	0.0008	20	60	0.04	45	4.89	8.79
343	0.0008	75	25	0.04	45	10.08	5.58
344	0.0008	66.67	33.33	0.04	45	9.93	6.96
345	0.0008	50	50	0.04	45	8.94	8.94
346	0.0008	33.33	66.67	0.04	45	6.96	9.93
347	0.0008	25	75	0.04	45	5.58	10.08
348	0.001	15	5	0.04	45	3.51	1.95
349	0.001	13.33	6.67	0.04	45	3.48	2.43
350	0.001	10	10	0.04	45	3.12	3.12
351	0.001	6.67	13.33	0.04	45	2.43	3.48
352	0.001	5	15	0.04	45	1.95	3.51
353	0.001	30	10	0.04	45	5.34	2.97
354	0.001	26.67	13.33	0.04	45	5.28	3.69
355	0.001	20	20	0.04	45	4.74	4.74
356	0.001	13.33	26.67	0.04	45	3.69	5.28
357	0.001	10	30	0.04	45	2.97	5.34
358	0.001	45	15	0.04	45	6.81	3.78
359	0.001	40	20	0.04	45	6.72	4.71
360	0.001	30	30	0.04	45	6.03	6.03
361	0.001	20	40	0.04	45	4.71	6.72
362	0.001	15	45	0.04	45	3.78	6.81
363	0.001	60	20	0.04	45	8.07	4.5
364	0.001	53.33	26.67	0.04	45	7.98	5.58
365	0.001	40	40	0.04	45	7.17	7.17
366	0.001	26.67	53.33	0.04	45	5.58	7.98
367	0.001	20	60	0.04	45	4.5	8.07
368	0.001	75	25	0.04	45	9.24	5.13
369	0.001	66.67	33.33	0.04	45	9.12	6.39
370	0.001	50	50	0.04	45	8.22	8.22
371	0.001	33.33	66.67	0.04	45	6.39	9.12

372	0.001	25	75	0.04	45	5.13	9.24
373	0.0002	15	5	0.1	55	8.1	4.5
374	0.0002	13.33	6.67	0.1	55	7.98	5.61
375	0.0002	10	10	0.1	55	7.2	7.2
376	0.0002	6.67	13.33	0.1	55	5.61	7.98
377	0.0002	5	15	0.1	55	4.5	8.1
378	0.0002	30	10	0.1	55	12.24	6.81
379	0.0002	26.67	13.33	0.1	55	12.12	8.46
380	0.0002	20	20	0.1	55	10.89	10.89
381	0.0002	13.33	26.67	0.1	55	8.46	12.12
382	0.0002	10	30	0.1	55	6.81	12.24
383	0.0002	45	15	0.1	55	15.63	8.67
384	0.0002	40	20	0.1	55	15.45	10.8
385	0.0002	30	30	0.1	55	13.89	13.89
386	0.0002	20	40	0.1	55	10.8	15.45
387	0.0002	15	45	0.1	55	8.67	15.63
388	0.0002	60	20	0.1	55	18.57	10.32
389	0.0002	53.33	26.67	0.1	55	18.33	12.84
390	0.0002	40	40	0.1	55	16.5	16.5
391	0.0002	26.67	53.33	0.1	55	12.84	18.33
392	0.0002	20	60	0.1	55	10.32	18.57
393	0.0002	75	25	0.1	55	21.24	11.79
394	0.0002	66.67	33.33	0.1	55	20.97	14.67
395	0.0002	50	50	0.1	55	18.87	18.87
396	0.0002	33.33	66.67	0.1	55	14.67	20.97
397	0.0002	25	75	0.1	55	11.79	21.24
398	0.0004	15	5	0.1	55	6.18	3.45
399	0.0004	13.33	6.67	0.1	55	6.12	4.29
400	0.0004	10	10	0.1	55	5.49	5.49
401	0.0004	6.67	13.33	0.1	55	4.29	6.12
402	0.0004	5	15	0.1	55	3.45	6.18
403	0.0004	30	10	0.1	55	9.39	5.22
404	0.0004	26.67	13.33	0.1	55	9.27	6.48
405	0.0004	20	20	0.1	55	8.34	8.34
406	0.0004	13.33	26.67	0.1	55	6.48	9.27
407	0.0004	10	30	0.1	55	5.22	9.39
408	0.0004	45	15	0.1	55	11.97	6.63
409	0.0004	40	20	0.1	55	11.82	8.28
410	0.0004	30	30	0.1	55	10.62	10.62
411	0.0004	20	40	0.1	55	8.28	11.82
412	0.0004	15	45	0.1	55	6.63	11.97
413	0.0004	60	20	0.1	55	14.22	7.89
414	0.0004	53.33	26.67	0.1	55	14.04	9.84
415	0.0004	40	40	0.1	55	12.63	12.63
416	0.0004	26.67	53.33	0.1	55	9.84	14.04
417	0.0004	20	60	0.1	55	7.89	14.22
418	0.0004	75	25	0.1	55	16.26	9.03
419	0.0004	66.67	33.33	0.1	55	16.05	11.22
420	0.0004	50	50	0.1	55	14.43	14.43
421	0.0004	33.33	66.67	0.1	55	11.22	16.05
422	0.0004	25	75	0.1	55	9.03	16.26
423	0.0006	15	5	0.1	55	5.28	2.94

424	0.0006	13.33	6.67	0.1	55	5.22	3.66
425	0.0006	10	10	0.1	55	4.71	4.71
426	0.0006	6.67	13.33	0.1	55	3.66	5.22
427	0.0006	5	15	0.1	55	2.94	5.28
428	0.0006	30	10	0.1	55	8.01	4.47
429	0.0006	26.67	13.33	0.1	55	7.92	5.52
430	0.0006	20	20	0.1	55	7.14	7.14
431	0.0006	13.33	26.67	0.1	55	5.52	7.92
432	0.0006	10	30	0.1	55	4.47	8.01
433	0.0006	45	15	0.1	55	10.23	5.67
434	0.0006	40	20	0.1	55	10.11	7.08
435	0.0006	30	30	0.1	55	9.09	9.09
436	0.0006	20	40	0.1	55	7.08	10.11
437	0.0006	15	45	0.1	55	5.67	10.23
438	0.0006	60	20	0.1	55	12.15	6.75
439	0.0006	53.33	26.67	0.1	55	12	8.4
440	0.0006	40	40	0.1	55	10.8	10.8
441	0.0006	26.67	53.33	0.1	55	8.4	12
442	0.0006	20	60	0.1	55	6.75	12.15
443	0.0006	75	25	0.1	55	13.89	7.71
444	0.0006	66.67	33.33	0.1	55	13.74	9.6
445	0.0006	50	50	0.1	55	12.36	12.36
446	0.0006	33.33	66.67	0.1	55	9.6	13.74
447	0.0006	25	75	0.1	55	7.71	13.89
448	0.0008	15	5	0.1	55	4.74	2.64
449	0.0008	13.33	6.67	0.1	55	4.68	3.3
450	0.0008	10	10	0.1	55	4.2	4.2
451	0.0008	6.67	13.33	0.1	55	3.3	4.68
452	0.0008	5	15	0.1	55	2.64	4.74
453	0.0008	30	10	0.1	55	7.17	3.99
454	0.0008	26.67	13.33	0.1	55	7.08	4.95
455	0.0008	20	20	0.1	55	6.39	6.39
456	0.0008	13.33	26.67	0.1	55	4.95	7.08
457	0.0008	10	30	0.1	55	3.99	7.17
458	0.0008	45	15	0.1	55	9.15	5.07
459	0.0008	40	20	0.1	55	9.03	6.33
460	0.0008	30	30	0.1	55	8.13	8.13
461	0.0008	20	40	0.1	55	6.33	9.03
462	0.0008	15	45	0.1	55	5.07	9.15
463	0.0008	60	20	0.1	55	10.89	6.03
464	0.0008	53.33	26.67	0.1	55	10.74	7.53
465	0.0008	40	40	0.1	55	9.66	9.66
466	0.0008	26.67	53.33	0.1	55	7.53	10.74
467	0.0008	20	60	0.1	55	6.03	10.89
468	0.0008	75	25	0.1	55	12.45	6.9
469	0.0008	66.67	33.33	0.1	55	12.27	8.58
470	0.0008	50	50	0.1	55	11.04	11.04
471	0.0008	33.33	66.67	0.1	55	8.58	12.27
472	0.0008	25	75	0.1	55	6.9	12.45
473	0.001	15	5	0.1	55	4.35	2.4
474	0.001	13.33	6.67	0.1	55	4.29	3
475	0.001	10	10	0.1	55	3.87	3.87

476	0.001	6.67	13.33	0.1	55	3	4.29
477	0.001	5	15	0.1	55	2.4	4.35
478	0.001	30	10	0.1	55	6.57	3.66
479	0.001	26.67	13.33	0.1	55	6.51	4.53
480	0.001	20	20	0.1	55	5.85	5.85
481	0.001	13.33	26.67	0.1	55	4.53	6.51
482	0.001	10	30	0.1	55	3.66	6.57
483	0.001	45	15	0.1	55	8.4	4.68
484	0.001	40	20	0.1	55	8.28	5.82
485	0.001	30	30	0.1	55	7.47	7.47
486	0.001	20	40	0.1	55	5.82	8.28
487	0.001	15	45	0.1	55	4.68	8.4
488	0.001	60	20	0.1	55	9.99	5.55
489	0.001	53.33	26.67	0.1	55	9.87	6.9
490	0.001	40	40	0.1	55	8.88	8.88
491	0.001	26.67	53.33	0.1	55	6.9	9.87
492	0.001	20	60	0.1	55	5.55	9.99
493	0.001	75	25	0.1	55	11.4	6.33
494	0.001	66.67	33.33	0.1	55	11.28	7.89
495	0.001	50	50	0.1	55	10.14	10.14
496	0.001	33.33	66.67	0.1	55	7.89	11.28
497	0.001	25	75	0.1	55	6.33	11.4
498	0.0002	15	5	0.1	70	4.86	2.7
499	0.0002	13.33	6.67	0.1	70	4.8	3.39
500	0.0002	10	10	0.1	70	4.32	4.32
501	0.0002	6.67	13.33	0.1	70	3.39	4.8
502	0.0002	5	15	0.1	70	2.7	4.86
503	0.0002	30	10	0.1	70	7.38	4.11
504	0.0002	26.67	13.33	0.1	70	7.29	5.1
505	0.0002	20	20	0.1	70	6.57	6.57
506	0.0002	13.33	26.67	0.1	70	5.1	7.29
507	0.0002	10	30	0.1	70	4.11	7.38
508	0.0002	45	15	0.1	70	9.42	5.22
509	0.0002	40	20	0.1	70	9.3	6.51
510	0.0002	30	30	0.1	70	8.37	8.37
511	0.0002	20	40	0.1	70	6.51	9.3
512	0.0002	15	45	0.1	70	5.22	9.42
513	0.0002	60	20	0.1	70	11.19	6.21
514	0.0002	53.33	26.67	0.1	70	11.04	7.29
515	0.0002	40	40	0.1	70	9.93	9.93
516	0.0002	26.67	53.33	0.1	70	7.29	11.04
517	0.0002	20	60	0.1	70	6.21	11.19
518	0.0002	75	25	0.1	70	12.78	7.11
519	0.0002	66.67	33.33	0.1	70	12.63	8.82
520	0.0002	50	50	0.1	70	11.37	11.37
521	0.0002	33.33	66.67	0.1	70	8.82	12.63
522	0.0002	25	75	0.1	70	7.11	12.78
523	0.0004	15	5	0.1	70	3.72	2.07
524	0.0004	13.33	6.67	0.1	70	3.69	2.58
525	0.0004	10	10	0.1	70	3.3	3.3
526	0.0004	6.67	13.33	0.1	70	2.58	3.69
527	0.0004	5	15	0.1	70	2.07	3.72

528	0.0004	30	10	0.1	70	5.64	3.15
529	0.0004	26.67	13.33	0.1	70	5.58	3.9
530	0.0004	20	20	0.1	70	5.01	5.01
531	0.0004	13.33	26.67	0.1	70	3.9	5.58
532	0.0004	10	30	0.1	70	3.15	5.64
533	0.0004	45	15	0.1	70	7.2	3.99
534	0.0004	40	20	0.1	70	7.11	4.98
535	0.0004	30	30	0.1	70	6.39	6.39
536	0.0004	20	40	0.1	70	4.98	7.11
537	0.0004	15	45	0.1	70	3.99	7.2
538	0.0004	60	20	0.1	70	8.55	4.74
539	0.0004	53.33	26.67	0.1	70	8.46	5.91
540	0.0004	40	40	0.1	70	7.62	7.62
541	0.0004	26.67	53.33	0.1	70	5.91	8.46
542	0.0004	20	60	0.1	70	4.74	8.55
543	0.0004	75	25	0.1	70	9.78	5.43
544	0.0004	66.67	33.33	0.1	70	9.66	6.75
545	0.0004	50	50	0.1	70	8.7	8.7
546	0.0004	33.33	66.67	0.1	70	6.75	9.66
547	0.0004	25	75	0.1	70	5.43	9.78
548	0.0006	15	5	0.1	70	3.18	1.77
549	0.0006	13.33	6.67	0.1	70	3.15	2.22
550	0.0006	10	10	0.1	70	2.82	2.82
551	0.0006	6.67	13.33	0.1	70	2.22	3.15
552	0.0006	5	15	0.1	70	1.77	3.18
553	0.0006	30	10	0.1	70	4.83	2.67
554	0.0006	26.67	13.33	0.1	70	4.77	3.33
555	0.0006	20	20	0.1	70	4.29	4.29
556	0.0006	13.33	26.67	0.1	70	3.33	4.77
557	0.0006	10	30	0.1	70	2.67	4.83
558	0.0006	45	15	0.1	70	6.15	3.42
559	0.0006	40	20	0.1	70	6.09	4.26
560	0.0006	30	30	0.1	70	5.46	5.46
561	0.0006	20	40	0.1	70	4.26	6.09
562	0.0006	15	45	0.1	70	3.42	6.15
563	0.0006	60	20	0.1	70	7.32	4.05
564	0.0006	53.33	26.67	0.1	70	7.23	5.07
565	0.0006	40	40	0.1	70	6.51	6.51
566	0.0006	26.67	53.33	0.1	70	5.07	7.23
567	0.0006	20	60	0.1	70	4.05	7.32
568	0.0006	75	25	0.1	70	8.37	4.65
569	0.0006	66.67	33.33	0.1	70	8.25	5.73
570	0.0006	50	50	0.1	70	7.44	7.44
571	0.0006	33.33	66.67	0.1	70	5.73	8.25
572	0.0006	25	75	0.1	70	4.65	8.37
573	0.0008	15	5	0.1	70	2.85	1.59
574	0.0008	13.33	6.67	0.1	70	2.82	1.98
575	0.0008	10	10	0.1	70	2.52	2.52
576	0.0008	6.67	13.33	0.1	70	1.98	2.82
577	0.0008	5	15	0.1	70	1.59	2.85
578	0.0008	30	10	0.1	70	4.32	2.4
579	0.0008	26.67	13.33	0.1	70	4.26	2.97

580	0.0008	20	20	0.1	70	3.84	3.84
581	0.0008	13.33	26.67	0.1	70	2.97	4.26
582	0.0008	10	30	0.1	70	2.4	4.32
583	0.0008	45	15	0.1	70	5.52	3.06
584	0.0008	40	20	0.1	70	5.43	3.81
585	0.0008	30	30	0.1	70	4.89	4.89
586	0.0008	20	40	0.1	70	3.81	5.43
587	0.0008	15	45	0.1	70	3.06	5.52
588	0.0008	60	20	0.1	70	6.54	3.63
589	0.0008	53.33	26.67	0.1	70	6.48	4.53
590	0.0008	40	40	0.1	70	5.82	5.82
591	0.0008	26.67	53.33	0.1	70	4.53	6.48
592	0.0008	20	60	0.1	70	3.63	6.54
593	0.0008	75	25	0.1	70	7.5	4.17
594	0.0008	66.67	33.33	0.1	70	7.38	5.16
595	0.0008	50	50	0.1	70	6.66	6.66
596	0.0008	33.33	66.67	0.1	70	5.16	7.38
597	0.0008	25	75	0.1	70	4.17	7.5
598	0.001	15	5	0.1	70	2.61	1.44
599	0.001	13.33	6.67	0.1	70	2.58	1.8
600	0.001	10	10	0.1	70	2.31	2.31
601	0.001	6.67	13.33	0.1	70	1.8	2.58
602	0.001	5	15	0.1	70	1.44	2.61
603	0.001	30	10	0.1	70	3.96	2.19
604	0.001	26.67	13.33	0.1	70	3.93	2.73
605	0.001	20	20	0.1	70	3.51	3.51
606	0.001	13.33	26.67	0.1	70	2.73	3.93
607	0.001	10	30	0.1	70	2.19	3.96
608	0.001	45	15	0.1	70	5.04	2.82
609	0.001	40	20	0.1	70	4.98	3.48
610	0.001	30	30	0.1	70	4.5	4.5
611	0.001	20	40	0.1	70	3.48	4.98
612	0.001	15	45	0.1	70	2.82	5.04
613	0.001	60	20	0.1	70	6	3.33
614	0.001	53.33	26.67	0.1	70	5.94	3.93
615	0.001	40	40	0.1	70	5.34	5.34
616	0.001	26.67	53.33	0.1	70	3.93	5.94
617	0.001	20	60	0.1	70	3.33	6
618	0.001	75	25	0.1	70	6.87	3.81
619	0.001	66.67	33.33	0.1	70	6.78	4.74
620	0.001	50	50	0.1	70	6.09	6.09
621	0.001	33.33	66.67	0.1	70	4.74	6.78
622	0.001	25	75	0.1	70	3.81	6.87
623	0.0002	15	5	0.1	45	11.34	6.3
624	0.0002	13.33	6.67	0.1	45	11.22	7.86
625	0.0002	10	10	0.1	45	10.08	10.08
626	0.0002	6.67	13.33	0.1	45	7.86	11.22
627	0.0002	5	15	0.1	45	6.3	11.34
628	0.0002	30	10	0.1	45	17.19	9.54
629	0.0002	26.67	13.33	0.1	45	16.98	11.85
630	0.0002	20	20	0.1	45	15.27	15.27
631	0.0002	13.33	26.67	0.1	45	11.85	16.98

632	0.0002	10	30	0.1	45	9.54	17.19
633	0.0002	45	15	0.1	45	21.93	12.18
634	0.0002	40	20	0.1	45	21.66	15.15
635	0.0002	30	30	0.1	45	19.5	19.5
636	0.0002	20	40	0.1	45	15.15	21.66
637	0.0002	15	45	0.1	45	12.18	21.93
638	0.0002	60	20	0.1	45	26.04	14.46
639	0.0002	53.33	26.67	0.1	45	25.74	18.03
640	0.0002	40	40	0.1	45	23.16	23.16
641	0.0002	26.67	53.33	0.1	45	18.03	25.74
642	0.0002	20	60	0.1	45	14.46	26.04
643	0.0002	75	25	0.1	45	29.79	16.56
644	0.0002	66.67	33.33	0.1	45	29.43	20.58
645	0.0002	50	50	0.1	45	26.49	26.49
646	0.0002	33.33	66.67	0.1	45	20.58	29.43
647	0.0002	25	75	0.1	45	16.56	29.79
648	0.0004	15	5	0.1	45	8.67	4.83
649	0.0004	13.33	6.67	0.1	45	8.55	6.03
650	0.0004	10	10	0.1	45	7.71	7.71
651	0.0004	6.67	13.33	0.1	45	6.03	8.58
652	0.0004	5	15	0.1	45	4.83	8.67
653	0.0004	30	10	0.1	45	13.14	7.32
654	0.0004	26.67	13.33	0.1	45	12.99	9.09
655	0.0004	20	20	0.1	45	11.7	11.7
656	0.0004	13.33	26.67	0.1	45	9.09	12.99
657	0.0004	10	30	0.1	45	7.32	13.14
658	0.0004	45	15	0.1	45	16.77	9.33
659	0.0004	40	20	0.1	45	16.56	11.61
660	0.0004	30	30	0.1	45	14.91	14.91
661	0.0004	20	40	0.1	45	11.61	16.56
662	0.0004	15	45	0.1	45	9.33	16.77
663	0.0004	60	20	0.1	45	19.95	11.07
664	0.0004	53.33	26.67	0.1	45	19.68	13.8
665	0.0004	40	40	0.1	45	17.73	17.73
666	0.0004	26.67	53.33	0.1	45	13.8	19.68
667	0.0004	20	60	0.1	45	11.07	19.95
668	0.0004	75	25	0.1	45	22.8	12.66
669	0.0004	66.67	33.33	0.1	45	22.53	15.75
670	0.0004	50	50	0.1	45	20.25	20.25
671	0.0004	33.33	66.67	0.1	45	15.75	22.53
672	0.0004	25	75	0.1	45	12.66	22.8
673	0.0006	15	5	0.1	45	7.41	4.11
674	0.0006	13.33	6.67	0.1	45	7.32	5.16
675	0.0006	10	10	0.1	45	6.6	6.6
676	0.0006	6.67	13.33	0.1	45	5.16	7.32
677	0.0006	5	15	0.1	45	4.11	7.41
678	0.0006	30	10	0.1	45	11.25	6.24
679	0.0006	26.67	13.33	0.1	45	11.1	7.77
680	0.0006	20	20	0.1	45	9.99	9.99
681	0.0006	13.33	26.67	0.1	45	7.77	11.1
682	0.0006	10	30	0.1	45	6.24	11.25
683	0.0006	45	15	0.1	45	14.34	7.98

684	0.0006	40	20	0.1	45	14.16	9.93
685	0.0006	30	30	0.1	45	12.75	12.75
686	0.0006	20	40	0.1	45	9.93	14.16
687	0.0006	15	45	0.1	45	7.98	14.34
688	0.0006	60	20	0.1	45	17.04	9.48
689	0.0006	53.33	26.67	0.1	45	16.83	11.79
690	0.0006	40	40	0.1	45	15.15	15.15
691	0.0006	26.67	53.33	0.1	45	11.79	16.83
692	0.0006	20	60	0.1	45	9.48	17.04
693	0.0006	75	25	0.1	45	19.5	10.83
694	0.0006	66.67	33.33	0.1	45	19.26	13.47
695	0.0006	50	50	0.1	45	17.34	17.34
696	0.0006	33.33	66.67	0.1	45	13.47	19.26
697	0.0006	25	75	0.1	45	10.83	19.5
698	0.0008	15	5	0.1	45	6.63	3.69
699	0.0008	13.33	6.67	0.1	45	6.57	4.62
700	0.0008	10	10	0.1	45	5.91	5.91
701	0.0008	6.67	13.33	0.1	45	4.62	6.57
702	0.0008	5	15	0.1	45	3.69	6.63
703	0.0008	30	10	0.1	45	10.08	5.58
704	0.0008	26.67	13.33	0.1	45	9.93	6.96
705	0.0008	20	20	0.1	45	8.94	8.94
706	0.0008	13.33	26.67	0.1	45	6.96	9.93
707	0.0008	10	30	0.1	45	5.58	10.08
708	0.0008	45	15	0.1	45	12.84	7.14
709	0.0008	40	20	0.1	45	12.69	8.88
710	0.0008	30	30	0.1	45	11.4	11.4
711	0.0008	20	40	0.1	45	8.88	12.69
712	0.0008	15	45	0.1	45	7.14	12.84
713	0.0008	60	20	0.1	45	15.27	8.49
714	0.0008	53.33	26.67	0.1	45	15.06	10.56
715	0.0008	40	40	0.1	45	13.56	13.56
716	0.0008	26.67	53.33	0.1	45	10.56	15.06
717	0.0008	20	60	0.1	45	8.49	15.27
718	0.0008	75	25	0.1	45	17.43	9.69
719	0.0008	66.67	33.33	0.1	45	17.22	12.06
720	0.0008	50	50	0.1	45	15.51	15.51
721	0.0008	33.33	66.67	0.1	45	12.06	17.22
722	0.0008	25	75	0.1	45	9.69	17.43
723	0.001	15	5	0.1	45	6.09	3.39
724	0.001	13.33	6.67	0.1	45	6	4.23
725	0.001	10	10	0.1	45	5.43	5.43
726	0.001	6.67	13.33	0.1	45	4.23	6
727	0.001	5	15	0.1	45	3.39	6.09
728	0.001	30	10	0.1	45	9.24	5.13
729	0.001	26.67	13.33	0.1	45	9.12	6.36
730	0.001	20	20	0.1	45	8.22	8.22
731	0.001	13.33	26.67	0.1	45	6.36	9.12
732	0.001	10	30	0.1	45	5.13	9.24
733	0.001	45	15	0.1	45	11.79	6.54
734	0.001	40	20	0.1	45	11.64	8.13
735	0.001	30	30	0.1	45	10.47	10.47

736	0.001	20	40	0.1	45	8.13	11.64
737	0.001	15	45	0.1	45	6.54	11.79
738	0.001	60	20	0.1	45	14.01	7.77
739	0.001	53.33	26.67	0.1	45	13.83	9.69
740	0.001	40	40	0.1	45	12.45	12.45
741	0.001	26.67	53.33	0.1	45	9.69	13.83
742	0.001	20	60	0.1	45	7.77	14.01
743	0.001	75	25	0.1	45	15.99	8.88
744	0.001	66.67	33.33	0.1	45	15.81	11.07
745	0.001	50	50	0.1	45	14.22	14.22
746	0.001	33.33	66.67	0.1	45	11.07	15.81
747	0.001	25	75	0.1	45	8.88	15.99
748	0.0002	15	5	0.19	70	7.14	3.96
749	0.0002	13.33	6.67	0.19	70	7.05	4.95
750	0.0002	10	10	0.19	70	6.36	6.36
751	0.0002	6.67	13.33	0.19	70	4.95	7.05
752	0.0002	5	15	0.19	70	3.96	7.14
753	0.0002	30	10	0.19	70	10.83	6.03
754	0.0002	26.67	13.33	0.19	70	10.71	7.47
755	0.0002	20	20	0.19	70	9.63	9.63
756	0.0002	13.33	26.67	0.19	70	17.43	24.96
757	0.0002	10	30	0.19	70	7.47	10.71
758	0.0002	45	15	0.19	70	13.83	7.68
759	0.0002	40	20	0.19	70	13.65	9.57
760	0.0002	30	30	0.19	70	12.3	12.3
761	0.0002	20	40	0.19	70	9.57	13.65
762	0.0002	15	45	0.19	70	7.68	13.83
763	0.0002	60	20	0.19	70	16.44	9.12
764	0.0002	53.33	26.67	0.19	70	16.23	11.37
765	0.0002	40	40	0.19	70	14.61	14.61
766	0.0002	26.67	53.33	0.19	70	11.37	16.23
767	0.0002	20	60	0.19	70	9.12	16.44
768	0.0002	75	25	0.19	70	18.78	10.44
769	0.0002	66.67	33.33	0.19	70	18.57	12.99
770	0.0002	50	50	0.19	70	16.71	16.71
771	0.0002	33.33	66.67	0.19	70	12.99	18.57
772	0.0002	25	75	0.19	70	10.44	18.78
773	0.0004	15	5	0.19	70	5.46	3.03
774	0.0004	13.33	6.67	0.19	70	5.4	3.81
775	0.0004	10	10	0.19	70	4.86	4.86
776	0.0004	6.67	13.33	0.19	70	3.81	5.4
777	0.0004	5	15	0.19	70	3.03	5.46
778	0.0004	30	10	0.19	70	8.31	4.62
779	0.0004	26.67	13.33	0.19	70	8.19	5.73
780	0.0004	20	20	0.19	70	7.38	7.38
781	0.0004	13.33	26.67	0.19	70	5.73	8.19
782	0.0004	10	30	0.19	70	4.62	8.31
783	0.0004	45	15	0.19	70	10.59	5.88
784	0.0004	40	20	0.19	70	10.44	7.32
785	0.0004	30	30	0.19	70	9.42	9.42
786	0.0004	20	40	0.19	70	7.32	10.44
787	0.0004	15	45	0.19	70	5.88	10.59

788	0.0004	60	20	0.19	70	12.57	6.99
789	0.0004	53.33	26.67	0.19	70	12.42	8.7
790	0.0004	40	40	0.19	70	11.19	11.19
791	0.0004	26.67	53.33	0.19	70	8.7	12.42
792	0.0004	20	60	0.19	70	6.99	12.57
793	0.0004	75	25	0.19	70	14.37	7.98
794	0.0004	66.67	33.33	0.19	70	14.19	9.93
795	0.0004	50	50	0.19	70	12.78	12.78
796	0.0004	33.33	66.67	0.19	70	9.93	14.19
797	0.0004	25	75	0.19	70	7.98	14.37
798	0.0006	15	5	0.19	70	4.68	2.61
799	0.0006	13.33	6.67	0.19	70	4.62	3.24
800	0.0006	10	10	0.19	70	4.17	4.17
801	0.0006	6.67	13.33	0.19	70	3.24	4.62
802	0.0006	5	15	0.19	70	2.61	4.68
803	0.0006	30	10	0.19	70	7.08	3.93
804	0.0006	26.67	13.33	0.19	70	7.02	4.89
805	0.0006	20	20	0.19	70	6.3	6.3
806	0.0006	13.33	26.67	0.19	70	4.89	7.02
807	0.0006	10	30	0.19	70	3.93	7.08
808	0.0006	45	15	0.19	70	9.06	5.04
809	0.0006	40	20	0.19	70	8.94	6.27
810	0.0006	30	30	0.19	70	8.04	8.04
811	0.0006	20	40	0.19	70	6.27	8.94
812	0.0006	15	45	0.19	70	5.04	9.06
813	0.0006	60	20	0.19	70	10.74	5.97
814	0.0006	53.33	26.67	0.19	70	10.62	7.44
815	0.0006	40	40	0.19	70	9.57	9.57
816	0.0006	26.67	53.33	0.19	70	7.44	10.62
817	0.0006	20	60	0.19	70	5.97	10.74
818	0.0006	75	25	0.19	70	12.3	6.84
819	0.0006	66.67	33.33	0.19	70	12.15	8.49
820	0.0006	50	50	0.19	70	10.92	10.92
821	0.0006	33.33	66.67	0.19	70	8.49	12.15
822	0.0006	25	75	0.19	70	6.84	12.3
823	0.0008	15	5	0.19	70	4.2	2.34
824	0.0008	13.33	6.67	0.19	70	4.14	2.91
825	0.0008	10	10	0.19	70	3.72	3.72
826	0.0008	6.67	13.33	0.19	70	2.91	4.14
827	0.0008	5	15	0.19	70	2.34	4.2
828	0.0008	30	10	0.19	70	6.36	3.54
829	0.0008	26.67	13.33	0.19	70	6.27	4.38
830	0.0008	20	20	0.19	70	5.64	5.64
831	0.0008	13.33	26.67	0.19	70	4.38	6.27
832	0.0008	10	30	0.19	70	3.54	6.36
833	0.0008	45	15	0.19	70	8.1	4.5
834	0.0008	40	20	0.19	70	8.01	5.61
835	0.0008	30	30	0.19	70	7.2	7.2
836	0.0008	20	40	0.19	70	5.61	8.01
837	0.0008	15	45	0.19	70	4.5	8.1
838	0.0008	60	20	0.19	70	9.63	5.34
839	0.0008	53.33	26.67	0.19	70	9.51	6.66

840	0.0008	40	40	0.19	70	8.55	8.55
841	0.0008	26.67	53.33	0.19	70	6.66	9.51
842	0.0008	20	60	0.19	70	5.34	9.63
843	0.0008	75	25	0.19	70	11.01	6.12
844	0.0008	66.67	33.33	0.19	70	10.86	7.59
845	0.0008	50	50	0.19	70	9.78	9.78
846	0.0008	33.33	66.67	0.19	70	7.59	10.86
847	0.0008	25	75	0.19	70	6.12	11.01
848	0.001	15	5	0.19	70	3.84	2.13
849	0.001	13.33	6.67	0.19	70	3.78	2.67
850	0.001	10	10	0.19	70	3.42	3.42
851	0.001	6.67	13.33	0.19	70	2.67	3.78
852	0.001	5	15	0.19	70	2.13	3.84
853	0.001	30	10	0.19	70	5.82	3.24
854	0.001	26.67	13.33	0.19	70	5.76	4.02
855	0.001	20	20	0.19	70	5.19	5.19
856	0.001	13.33	26.67	0.19	70	4.02	5.76
857	0.001	10	30	0.19	70	3.24	5.82
858	0.001	45	15	0.19	70	7.44	4.14
859	0.001	40	20	0.19	70	7.35	5.13
860	0.001	30	30	0.19	70	6.6	6.6
861	0.001	20	40	0.19	70	5.13	7.35
862	0.001	15	45	0.19	70	4.14	7.44
863	0.001	60	20	0.19	70	8.82	4.92
864	0.001	53.33	26.67	0.19	70	8.73	6.12
865	0.001	40	40	0.19	70	7.86	7.86
866	0.001	26.67	53.33	0.19	70	6.12	8.73
867	0.001	20	60	0.19	70	4.92	8.82
868	0.001	75	25	0.19	70	10.08	5.61
869	0.001	66.67	33.33	0.19	70	9.96	6.96
870	0.001	50	50	0.19	70	8.97	8.97
871	0.001	33.33	66.67	0.19	70	6.96	9.96
872	0.001	25	75	0.19	70	5.61	10.08
873	0.0002	15	5	0.19	55	11.88	6.6
874	0.0002	13.33	6.67	0.19	55	11.73	8.25
875	0.0002	10	10	0.19	55	10.56	10.56
876	0.0002	6.67	13.33	0.19	55	8.25	11.73
877	0.0002	5	15	0.19	55	6.6	11.88
878	0.0002	30	10	0.19	55	18	10.02
879	0.0002	26.67	13.33	0.19	55	17.79	12.42
880	0.0002	20	20	0.19	55	16.02	16.02
881	0.0004	15	5	0.19	55	9.09	5.04
882	0.0004	13.33	6.67	0.19	55	8.97	6.3
883	0.0004	10	10	0.19	55	8.07	8.07
884	0.0004	6.67	13.33	0.19	55	6.3	8.97
885	0.0004	5	15	0.19	55	5.04	9.09
886	0.0004	30	10	0.19	55	13.77	7.65
887	0.0004	26.67	13.33	0.19	55	13.62	9.51
888	0.0004	20	20	0.19	55	12.24	12.24
889	0.0006	15	5	0.19	55	7.77	4.32
890	0.0006	13.33	6.67	0.19	55	7.68	5.4
891	0.0006	10	10	0.19	55	6.9	6.9

892	0.0006	6.67	13.33	0.19	55	5.4	7.68
893	0.0006	5	15	0.19	55	4.32	7.77
894	0.0006	30	10	0.19	55	11.79	6.54
895	0.0006	26.67	13.33	0.19	55	11.64	8.13
896	0.0006	20	20	0.19	55	10.47	10.47
897	0.0008	15	5	0.19	55	6.96	3.87
898	0.0008	13.33	6.67	0.19	55	6.87	4.83
899	0.0008	10	10	0.19	55	6.18	6.18
900	0.0008	6.67	13.33	0.19	55	4.83	6.87
901	0.0008	5	15	0.19	55	3.87	6.96
902	0.0008	30	10	0.19	55	10.56	5.85
903	0.0008	26.67	13.33	0.19	55	10.41	7.29
904	0.0008	20	20	0.19	55	9.39	9.39
905	0.001	15	5	0.19	55	6.39	3.54
906	0.001	13.33	6.67	0.19	55	6.3	4.44
907	0.001	10	10	0.19	55	5.67	5.67
908	0.001	6.67	13.33	0.19	55	4.44	6.3
909	0.001	5	15	0.19	55	3.54	6.39
910	0.001	30	10	0.19	55	9.69	5.37
911	0.001	26.67	13.33	0.19	55	9.57	6.69
912	0.001	20	20	0.19	55	8.61	8.61
913	0.0002	15	5	0.19	45	16.68	9.27
914	0.0002	13.33	6.67	0.19	45	16.44	11.58
915	0.0002	10	10	0.19	45	14.82	14.82
916	0.0002	6.67	13.33	0.19	45	11.58	16.44
917	0.0002	5	15	0.19	45	9.27	16.68
918	0.0002	30	10	0.19	45	25.26	14.04
919	0.0002	26.67	13.33	0.19	45	24.96	17.43
920	0.0002	20	20	0.19	45	22.47	22.47
921	0.0004	15	5	0.19	45	12.75	7.08
922	0.0004	13.33	6.67	0.19	45	12.6	8.85
923	0.0004	10	10	0.19	45	11.34	11.34
924	0.0004	6.67	13.33	0.19	45	8.85	12.6
925	0.0004	5	15	0.19	45	7.08	12.75
926	0.0004	30	10	0.19	45	19.32	10.74
927	0.0004	26.67	13.33	0.19	45	19.11	13.35
928	0.0004	20	20	0.19	45	17.19	17.19
929	0.0006	15	5	0.19	45	10.92	6.06
930	0.0006	13.33	6.67	0.19	45	10.77	7.56
931	0.0006	10	10	0.19	45	9.69	9.69
932	0.0006	6.67	13.33	0.19	45	7.56	10.77
933	0.0006	5	15	0.19	45	6.06	10.92
934	0.0006	30	10	0.19	45	16.53	9.18
935	0.0006	26.67	13.33	0.19	45	16.32	11.4
936	0.0006	20	20	0.19	45	14.7	14.7
937	0.0008	15	5	0.19	45	9.75	5.43
938	0.0008	13.33	6.67	0.19	45	9.63	6.78
939	0.0008	10	10	0.19	45	8.67	8.67
940	0.0008	6.67	13.33	0.19	45	6.78	9.63
941	0.0008	5	15	0.19	45	5.43	9.75
942	0.0008	30	10	0.19	45	14.79	8.22
943	0.0008	26.67	13.33	0.19	45	14.61	10.2

944	0.0008	20	20	0.19	45	13.14	13.14
945	0.001	15	5	0.19	45	8.97	4.98
946	0.001	13.33	6.67	0.19	45	8.85	6.21
947	0.001	10	10	0.19	45	7.95	7.95
948	0.001	6.67	13.33	0.19	45	6.21	8.85
949	0.001	5	15	0.19	45	4.98	8.97
950	0.001	30	10	0.19	45	13.56	7.53
951	0.001	26.67	13.33	0.19	45	13.41	9.36
952	0.001	20	20	0.19	45	12.06	12.06
953	0.00025	40	40	0.19	55	22.26	22.26
954	0.00025	53	27	0.19	55	24.72	17.46
955	0.00025	60	20	0.19	55	28.41	28.41
956	0.00025	64	16	0.19	55	24.93	11.58
957	0.00025	80	80	0.19	55	33.75	33.75
958	0.00025	107	53	0.19	55	37.53	26.13
959	0.00025	120	40	0.19	55	37.95	21.09
960	0.00025	132	28	0.19	55	37.59	15.66
961	0.00025	120	120	0.19	55	43.05	43.05
962	0.00025	160	80	0.19	55	47.82	33.48
963	0.00025	180	60	0.19	55	48.42	26.91
964	0.00025	192	48	0.19	55	48.21	22.38
965	0.00025	160	160	0.19	55	51.15	51.15
966	0.00025	213	107	0.19	55	56.82	39.87
967	0.00025	240	80	0.19	55	57.54	31.98
968	0.00025	256	64	0.19	55	57.3	26.61
969	0.0005	40	40	0.19	55	17.04	17.04
970	0.0005	53	27	0.19	55	18.9	13.38
971	0.0005	60	20	0.19	55	19.17	10.65
972	0.0005	64	16	0.19	55	19.08	8.85
973	0.0005	80	80	0.19	55	25.83	25.83
974	0.0005	107	53	0.19	55	28.71	20.01
975	0.0005	120	40	0.19	55	29.04	16.14
976	0.0005	132	28	0.19	55	28.68	11.97
977	0.0005	120	120	0.19	55	32.94	32.94
978	0.0005	160	80	0.19	55	36.6	25.62
979	0.0005	180	60	0.19	55	37.05	20.58
980	0.0005	192	48	0.19	55	36.9	17.13
981	0.0005	160	160	0.19	55	39.15	39.15
982	0.0005	213	107	0.19	55	43.47	30.51
983	0.0005	240	80	0.19	55	44.04	24.45
984	0.0005	256	64	0.19	55	43.83	20.34
985	0.00075	40	40	0.19	55	14.58	14.58
986	0.00075	53	27	0.19	55	16.17	11.43
987	0.00075	60	20	0.19	55	16.38	9.12
988	0.00075	64	16	0.19	55	16.32	7.59
989	0.00075	80	80	0.19	55	22.08	22.08
990	0.00075	107	53	0.19	55	24.54	17.1
991	0.00075	120	40	0.19	55	24.84	13.8
992	0.00075	132	28	0.19	55	24.6	10.23
993	0.00075	120	120	0.19	55	28.17	28.17
994	0.00075	160	80	0.19	55	31.29	21.9
995	0.00075	180	60	0.19	55	31.68	17.61

996	0.00075	192	48	0.19	55	31.56	14.64
997	0.00075	160	160	0.19	55	33.48	33.48
998	0.00075	213	107	0.19	55	37.17	26.1
999	0.00075	240	80	0.19	55	37.65	20.91
1000	0.00075	256	64	0.19	55	37.5	17.4
1001	0.00025	40	40	0.19	55	22.26	22.26
1002	0.00025	54	27	0.19	55	24.93	17.46
1003	0.00025	60	20	0.19	55	25.05	13.92
1004	0.00025	64	16	0.19	55	24.93	11.58
1005	0.00025	80	80	0.19	55	33.75	33.75
1006	0.00025	107	54	0.19	55	37.62	26.46
1007	0.00025	120	40	0.19	55	37.95	21.09
1008	0.00025	128	32	0.19	55	37.8	17.55
1009	0.00025	160	160	0.19	55	51.15	51.15
1010	0.00025	216	108	0.19	55	57.27	40.08
1011	0.00025	240	80	0.19	55	57.54	31.98
1012	0.00025	256	64	0.19	55	57.3	26.61
1013	0.0005	40	40	0.19	55	17.04	17.04
1014	0.0005	54	27	0.19	55	19.08	13.35
1015	0.0005	60	20	0.19	55	19.17	10.65
1016	0.0005	64	16	0.19	55	19.08	8.85
1017	0.0005	80	80	0.19	55	25.83	25.83
1018	0.0005	107	54	0.19	55	28.77	20.25
1019	0.0005	120	40	0.19	55	29.04	16.14
1020	0.0005	128	32	0.19	55	28.92	13.44
1021	0.0005	160	160	0.19	55	39.15	39.15
1022	0.0005	216	108	0.19	55	43.83	30.66
1023	0.0005	240	80	0.19	55	44.04	24.45
1024	0.0005	256	64	0.19	55	43.83	20.34
1025	0.00075	40	40	0.19	55	14.58	14.58
1026	0.00075	54	27	0.19	55	16.32	11.43
1027	0.00075	60	20	0.19	55	16.38	9.12
1028	0.00075	64	16	0.19	55	16.32	7.59
1029	0.00075	80	80	0.19	55	22.08	22.08
1030	0.00075	107	54	0.19	55	24.6	17.31
1031	0.00075	120	40	0.19	55	24.84	13.8
1032	0.00075	128	32	0.19	55	24.72	11.49
1033	0.00075	160	160	0.19	55	33.48	33.48
1034	0.00075	216	108	0.19	55	37.47	26.22
1035	0.00075	240	80	0.19	55	37.65	20.91
1036	0.00075	256	64	0.19	55	37.5	17.4
1037	0.0005	60	60	0.1	55	14.79	14.79
1038	0.0005	80	40	0.1	55	16.44	11.49
1039	0.0005	90	30	0.1	55	16.62	9.24
1040	0.0005	96	24	0.1	55	16.56	7.68
1041	0.0005	120	120	0.1	55	22.41	22.41
1042	0.0005	160	80	0.1	55	24.9	17.43
1043	0.0005	180	60	0.1	55	25.2	14.01
1044	0.0005	192	48	0.1	55	25.11	11.64
1045	0.0005	180	180	0.1	55	28.59	28.59
1046	0.001	60	60	0.1	55	11.31	11.31
1047	0.001	80	40	0.1	55	12.57	8.79

1048	0.001	90	30	0.1	55	12.72	7.08
1049	0.001	96	24	0.1	55	12.66	5.88
1050	0.001	80	80	0.1	55	13.44	13.44
1051	0.001	100	100	0.1	55	15.36	15.36
1052	0.001	240	120	0.1	55	24.3	17.01
1053	0.001	270	90	0.1	55	24.6	13.68
1054	0.001	120	120	0.1	55	17.16	17.16
1055	0.001	160	80	0.1	55	19.05	13.35
1056	0.001	180	60	0.1	55	19.29	10.71
1057	0.001	192	48	0.1	55	19.2	8.91
1058	0.001	180	180	0.1	55	21.87	21.87
1059	0.00025	40	40	0.1	55	15.15	15.15
1060	0.00025	60	20	0.1	55	17.04	9.48
1061	0.00025	54	27	0.1	55	16.95	11.88
1062	0.00025	64	16	0.1	55	16.98	7.89
1063	0.00025	80	80	0.1	55	22.95	22.95
1064	0.00025	120	40	0.1	55	25.83	14.34
1065	0.00025	108	54	0.1	55	25.71	18
1066	0.00025	128	32	0.1	55	25.71	11.94
1067	0.00025	160	160	0.1	55	34.8	34.8
1068	0.00025	240	80	0.1	55	39.15	21.75
1069	0.00025	216	108	0.1	55	38.97	27.27
1070	0.00025	256	64	0.1	55	38.97	18.09
1071	0.00025	320	320	0.1	55	52.74	52.74
1072	0.0005	40	40	0.1	55	11.58	11.58
1073	0.0005	60	20	0.1	55	13.05	7.26
1074	0.0005	54	27	0.1	55	12.99	9.09
1075	0.0005	64	16	0.1	55	12.99	6.03
1076	0.0005	80	80	0.1	55	17.58	17.58
1077	0.0005	120	40	0.1	55	19.77	10.98
1078	0.0005	108	54	0.1	55	19.68	13.77
1079	0.0005	128	32	0.1	55	19.68	9.15
1080	0.0005	160	160	0.1	55	26.64	26.64
1081	0.0005	240	80	0.1	55	29.97	16.65
1082	0.0005	216	108	0.1	55	29.82	20.88
1083	0.0005	256	64	0.1	55	29.82	13.86
1084	0.00075	40	40	0.1	55	9.9	9.9
1085	0.00075	60	20	0.1	55	11.16	6.21
1086	0.00075	54	27	0.1	55	11.1	7.77
1087	0.00075	64	16	0.1	55	11.1	5.16
1088	0.00075	80	80	0.1	55	15.03	15.03
1089	0.00075	120	40	0.1	55	16.89	9.39
1090	0.00075	108	54	0.1	55	16.83	11.76
1091	0.00075	128	32	0.1	55	16.83	7.8
1092	0.00075	160	160	0.1	55	22.77	22.77
1093	0.00075	240	80	0.1	55	25.62	14.22
1094	0.00075	216	108	0.1	55	25.5	17.85
1095	0.00075	256	64	0.1	55	25.5	11.85
1096	0.00025	40	40	0.1	55	15.15	15.15
1097	0.00025	60	20	0.1	55	17.04	9.48
1098	0.00025	54	27	0.1	55	16.95	11.88
1099	0.00025	64	16	0.1	55	16.98	7.89

1100	0.00025	80	80	0.1	55	22.95	22.95
1101	0.00025	120	40	0.1	55	25.83	14.34
1102	0.00025	108	54	0.1	55	25.71	18
1103	0.00025	128	32	0.1	55	25.71	11.94
1104	0.00025	160	160	0.1	55	34.8	34.8
1105	0.00025	240	80	0.1	55	39.15	21.75
1106	0.00025	216	108	0.1	55	38.97	27.27
1107	0.00025	256	64	0.1	55	38.97	18.09
1108	0.00025	320	320	0.1	55	52.74	52.74
1109	0.0005	40	40	0.1	55	11.58	11.58
1110	0.0005	60	20	0.1	55	13.05	7.26
1111	0.0005	54	27	0.1	55	12.99	9.09
1112	0.0005	64	16	0.1	55	12.99	6.03
1113	0.0005	80	80	0.1	55	17.58	17.58
1114	0.0005	120	40	0.1	55	19.77	10.98
1115	0.0005	108	54	0.1	55	19.68	13.77
1116	0.0005	128	32	0.1	55	19.68	9.15
1117	0.0005	160	160	0.1	55	26.64	26.64
1118	0.0005	240	80	0.1	55	29.97	16.65
1119	0.0005	216	108	0.1	55	29.82	20.88
1120	0.0005	256	64	0.1	55	29.82	13.86
1121	0.00075	40	40	0.1	55	9.9	9.9
1122	0.00075	60	20	0.1	55	11.16	6.21
1123	0.00075	54	27	0.1	55	11.1	7.77
1124	0.00075	64	16	0.1	55	11.1	5.16
1125	0.00075	80	80	0.1	55	15.03	15.03
1126	0.00075	120	40	0.1	55	16.89	9.39
1127	0.00075	108	54	0.1	55	16.83	11.76
1128	0.00075	128	32	0.1	55	16.83	7.8
1129	0.00075	160	160	0.1	55	22.77	22.77
1130	0.00075	240	80	0.1	55	25.62	14.22
1131	0.00075	216	108	0.1	55	25.5	17.85
1132	0.00075	256	64	0.1	55	25.5	11.85
1133	0.00025	40	40	0.04	55	8.73	8.73
1134	0.00025	53	27	0.04	55	9.69	6.87
1135	0.00025	60	20	0.04	55	9.84	5.46
1136	0.00025	64	16	0.04	55	9.78	4.56
1137	0.00025	80	80	0.04	55	13.26	13.26
1138	0.00025	107	53	0.04	55	14.73	10.26
1139	0.00025	120	40	0.04	55	14.91	8.28
1140	0.00025	132	28	0.04	55	14.76	6.15
1141	0.00025	120	120	0.04	55	16.89	16.89
1142	0.00025	160	80	0.04	55	18.78	13.14
1143	0.00025	180	60	0.04	55	13.14	18.78
1144	0.00025	192	48	0.04	55	18.93	8.79
1145	0.00025	160	160	0.04	55	20.07	20.07
1146	0.00025	213	107	0.04	55	22.32	15.66
1147	0.00025	240	80	0.04	55	22.59	12.54
1148	0.00025	256	64	0.04	55	22.5	10.44
1149	0.0005	40	40	0.04	55	6.69	6.69
1150	0.0005	53	27	0.04	55	7.41	5.25
1151	0.0005	60	20	0.04	55	7.53	4.17

1152	0.0005	64	16	0.04	55	7.5	3.48
1153	0.0005	80	80	0.04	55	10.14	10.14
1154	0.0005	107	53	0.04	55	11.28	7.86
1155	0.0005	120	40	0.04	55	11.4	6.33
1156	0.0005	132	28	0.04	55	11.28	4.71
1157	0.0005	120	120	0.04	55	12.93	12.93
1158	0.0005	160	80	0.04	55	14.37	10.05
1159	0.0005	180	60	0.04	55	14.55	8.07
1160	0.0005	192	48	0.04	55	14.49	6.72
1161	0.0005	160	160	0.04	55	15.36	15.36
1162	0.0005	213	107	0.04	55	17.07	11.97
1163	0.0005	240	80	0.04	55	17.28	9.6
1164	0.0005	256	64	0.04	55	17.22	7.98
1165	0.00075	40	40	0.04	55	5.73	5.73
1166	0.00075	53	27	0.04	55	6.36	4.5
1167	0.00075	60	20	0.04	55	6.45	3.57
1168	0.00075	64	16	0.04	55	6.42	2.97
1169	0.00075	80	80	0.04	55	8.67	8.67
1170	0.00075	107	53	0.04	55	9.63	6.72
1171	0.00075	120	40	0.04	55	9.75	5.43
1172	0.00075	132	28	0.04	55	9.66	4.02
1173	0.00075	120	120	0.04	55	11.07	11.07
1174	0.00075	160	80	0.04	55	12.3	8.61
1175	0.00075	180	60	0.04	55	12.45	6.9
1176	0.00075	192	48	0.04	55	12.39	5.76
1177	0.00075	160	160	0.04	55	13.14	13.14
1178	0.00075	213	107	0.04	55	14.61	10.23
1179	0.00075	240	80	0.04	55	14.79	8.22
1180	0.00075	256	64	0.04	55	14.73	6.84
1181	0.00025	40	40	0.04	70	5.25	5.25
1182	0.00025	54	27	0.04	70	5.88	4.11
1183	0.00025	60	20	0.04	70	5.91	3.3
1184	0.00025	64	16	0.04	70	5.88	2.73
1185	0.00025	80	80	0.04	70	7.98	7.98
1186	0.00025	108	54	0.04	70	8.94	6.24
1187	0.00025	120	40	0.04	70	8.97	4.98
1188	0.00025	128	32	0.04	70	8.94	4.14
1189	0.00025	160	160	0.04	70	12.09	12.09
1190	0.00025	216	108	0.04	70	13.53	9.48
1191	0.00025	240	80	0.04	70	13.59	7.56
1192	0.00025	256	64	0.04	70	13.53	6.3
1193	0.0005	40	40	0.04	70	4.02	4.02
1194	0.0005	54	27	0.04	70	4.5	3.15
1195	0.0005	60	20	0.04	70	4.53	2.52
1196	0.0005	64	16	0.04	70	4.5	2.1
1197	0.0005	80	80	0.04	70	6.09	6.09
1198	0.0005	108	54	0.04	70	6.84	4.77
1199	0.0005	120	40	0.04	70	6.87	3.81
1200	0.0005	128	32	0.04	70	6.84	3.18
1201	0.0005	160	160	0.04	70	9.24	9.24
1202	0.0005	216	108	0.04	70	10.35	7.26
1203	0.0005	240	80	0.04	70	10.41	5.79

1204	0.0005	256	64	0.04	70	10.35	4.8
1205	0.00075	40	40	0.04	70	3.45	3.45
1206	0.00075	54	27	0.04	70	3.84	2.7
1207	0.00075	60	20	0.04	70	3.87	2.16
1208	0.00075	64	16	0.04	70	3.87	1.8
1209	0.00075	80	80	0.04	70	5.22	5.22
1210	0.00075	108	54	0.04	70	5.85	4.08
1211	0.00075	120	40	0.04	70	5.88	3.27
1212	0.00075	128	32	0.04	70	5.85	2.7
1213	0.00075	160	160	0.04	70	7.92	7.92
1214	0.00075	216	108	0.04	70	8.85	6.21
1215	0.00075	240	80	0.04	70	8.91	4.95
1216	0.00075	256	64	0.04	70	8.85	4.11
1217	0.00025	40	40	0.1	70	9.12	9.12
1218	0.00025	54	27	0.1	70	10.2	7.14
1219	0.00025	60	20	0.1	70	10.26	5.7
1220	0.00025	64	16	0.1	70	10.2	4.74
1221	0.00025	80	80	0.1	70	13.83	13.83
1222	0.00025	108	54	0.1	70	15.48	10.83
1223	0.00025	120	40	0.1	70	15.54	8.64
1224	0.00025	128	32	0.1	70	15.48	7.2
1225	0.00025	160	160	0.1	70	20.94	20.94
1226	0.00025	216	108	0.1	70	23.46	16.41
1227	0.00025	240	80	0.1	70	23.58	13.08
1228	0.00025	256	64	0.1	70	23.46	10.89
1229	0.0005	40	40	0.1	70	6.99	6.99
1230	0.0005	54	27	0.1	70	7.8	5.46
1231	0.0005	60	20	0.1	70	7.86	4.35
1232	0.0005	64	16	0.1	70	7.83	3.63
1233	0.0005	80	80	0.1	70	10.59	10.59
1234	0.0005	108	54	0.1	70	11.85	8.28
1235	0.0005	120	40	0.1	70	11.91	6.6
1236	0.0005	128	32	0.1	70	11.85	5.49
1237	0.0005	160	160	0.1	70	16.02	16.02
1238	0.0005	216	108	0.1	70	17.94	12.57
1239	0.0005	240	80	0.1	70	18.03	10.02
1240	0.0005	256	64	0.1	70	17.94	8.34
1241	0.00075	40	40	0.1	70	5.97	5.97
1242	0.00075	54	27	0.1	70	6.69	4.68
1243	0.00075	60	20	0.1	70	6.72	3.72
1244	0.00075	64	16	0.1	70	6.69	3.09
1245	0.00075	80	80	0.1	70	9.03	9.03
1246	0.00075	108	54	0.1	70	10.11	7.08
1247	0.00075	120	40	0.1	70	10.17	5.64
1248	0.00075	128	32	0.1	70	10.14	4.71
1249	0.00075	160	160	0.1	70	13.71	13.71
1250	0.00075	216	108	0.1	70	15.36	10.74
1251	0.00075	240	80	0.1	70	15.42	8.58
1252	0.00075	256	64	0.1	70	15.36	7.14
1253	0.00025	40	40	0.19	70	13.41	13.41
1254	0.00025	54	27	0.19	70	15	10.5
1255	0.00025	60	20	0.19	70	15.09	8.37

1256	0.00025	64	16	0.19	70	15	6.96
1257	0.00025	80	80	0.19	70	20.31	20.31
1258	0.00025	108	54	0.19	70	22.74	15.93
1259	0.00025	120	40	0.19	70	22.86	12.69
1260	0.00025	128	32	0.19	70	22.74	10.56
1261	0.00025	160	160	0.19	70	30.78	30.78
1262	0.00025	216	108	0.19	70	34.47	24.12
1263	0.00025	240	80	0.19	70	34.65	19.23
1264	0.00025	256	64	0.19	70	34.47	16.02
1265	0.0005	40	40	0.19	70	10.26	10.26
1266	0.0005	54	27	0.19	70	11.49	8.04
1267	0.0005	60	20	0.19	70	11.55	6.42
1268	0.0005	64	16	0.19	70	11.49	5.34
1269	0.0005	80	80	0.19	70	15.54	15.54
1270	0.0005	108	54	0.19	70	17.4	12.18
1271	0.0005	120	40	0.19	70	17.49	9.72
1272	0.0005	128	32	0.19	70	17.4	8.07
1273	0.0005	160	160	0.19	70	23.55	23.55
1274	0.0005	216	108	0.19	70	26.37	18.45
1275	0.0005	240	80	0.19	70	26.52	14.73
1276	0.0005	256	64	0.19	70	26.4	12.24
1277	0.00075	40	40	0.19	70	10.26	10.26
1278	0.00075	54	27	0.19	70	11.49	8.04
1279	0.00075	60	20	0.19	70	11.55	6.42
1280	0.00075	64	16	0.19	70	11.49	5.34
1281	0.00075	80	80	0.19	70	13.29	13.29
1282	0.00075	108	54	0.19	70	14.88	10.41
1283	0.00075	120	40	0.19	70	14.94	8.31
1284	0.00075	128	32	0.19	70	14.88	6.9
1285	0.00075	160	160	0.19	70	20.16	20.16
1286	0.00075	216	108	0.19	70	22.56	15.78
1287	0.00075	240	80	0.19	70	22.68	12.6
1288	0.00075	256	64	0.19	70	22.56	10.47

Density	Avg Velocity	Characteristic length	Viscosity	Reynolds number
1000	0.17	0.392	0.04	1666
1000	0.33	0.392	0.04	3234
1000	0.5	0.392	0.04	4900
1000	0.67	0.392	0.04	6566
1000	0.83	0.392	0.04	8134
1000	1.33	0.392	0.04	13034
1000	2	0.392	0.04	19600
1000	2.67	0.392	0.04	26166
1000	3	0.392	0.04	29400
1000	0.17	0.392	0.1	666.4
1000	0.33	0.392	0.1	1293.6
1000	0.5	0.392	0.1	1960
1000	0.67	0.392	0.1	2626.4

1000	0.83	0.392	0.1	3253.6
1000	1.33	0.392	0.1	5213.6
1000	2	0.392	0.1	7840
1000	2.67	0.392	0.1	10466.4
1000	3	0.392	0.1	11760
1000	0.17	0.392	0.19	350.7368
1000	0.33	0.392	0.19	680.8421
1000	0.5	0.392	0.19	1031.579
1000	0.67	0.392	0.19	1382.316
1000	0.83	0.392	0.19	1712.421
1000	1.33	0.392	0.19	2744
1000	2	0.392	0.19	4126.316
1000	2.67	0.392	0.19	5508.632
1000	3	0.392	0.19	6189.474

Appendix V Diagrams of Techma pilot lines

A1.1: Diagrams of Techma I

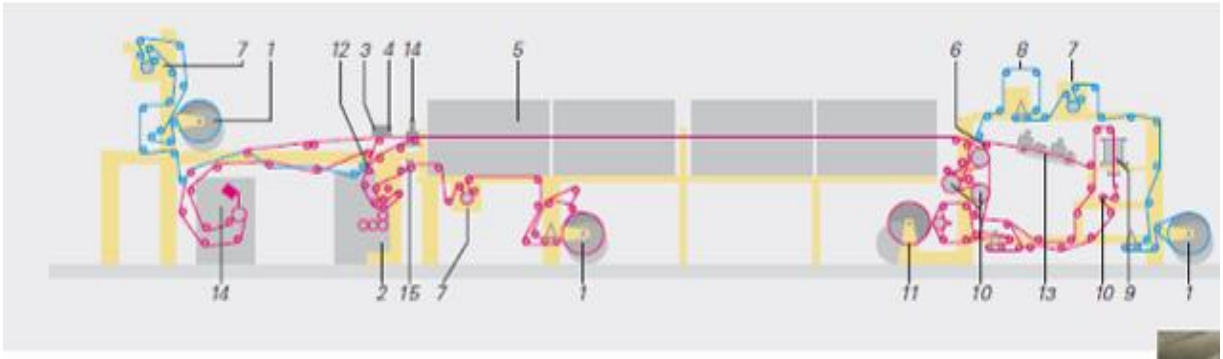

1. Unwinder
2. Coating unit
3. Infrared lamp (short wave)
4. Infrared lamp (medium wave)
5. Air floatation dryer
6. Dry laminating station
7. Corona station
8. Edge guide unit
9. Remoisturising station
10. Cooling station
11. Rewinder
12. Wet laminating station
13. Ultra-Violet curing station (UV)
14. Curtain coater
15. Web cleaning station

A 1.2: Diagrams of Techma II

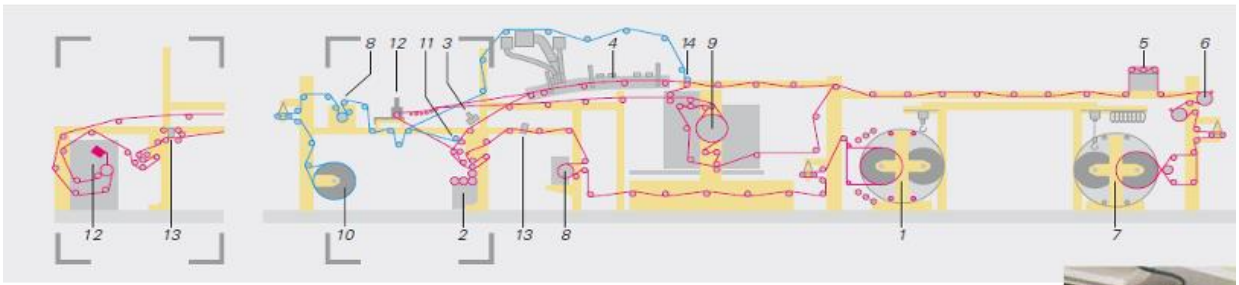

1. Automatic unwinder
2. Coating unit
3. Infrared lamp (short wave)
4. Ultra-Violet curing station (UV)
5. Edge guide unit
6. Cooling station
7. Automatic rewinder
8. Corona station
9. Electron Beam curing station (EB)
10. Lamination unwinder
11. Wet laminating station
12. Curtain coater
13. Web cleaning station
14. Laminating station

QA (10UW??)	71		72	73	74	75		76	77	78	79	80	81	82	83	84	85	86
Web																		
Material	PET	PET		PET	PET	PET	PET		PET	Al	Al	Al	Al	Al	Steel	steel	Steel	Steel
Line speed	100		100	100	100	100		200	200	100	200	300	400	100	100	200	300	400
coronna treatment	No	No		No	No	No	No		No	No	No	No	No	No	No	No	No	No
unwind Tension (N)	100		100	100	100	100		100	100	80	80	80	80	80	80	80	80	80
Enhanced coater (N)	110		110	110	110	110		110	110	220	220	220	220	220	220	220	220	220
coater-EB-cooling roll (N)	115		115	115	115	115		115	115	275	275	275	275	275	275	275	275	275
Rewind Tension	120		120	120	120	120		120	120	300	300	300	300	300	300	300	300	300
Rewind end	80		80	80	80	80		80	80	250	250	250	250	250	250	250	250	250
Coating																		
Forward or reverse	Rev.	Rev.		Rev.	Rev.	Rev.	Rev.		Rev.	Rev.	Rev.	Rev.	Rev.	Rev.	Rev.	Rev.	Reverse	Reverse
speed roll 0(m/min)	10		10	10	10	10		10	10	10	10	10	10	10	10	10	10	10
speed roll 1(%)	50		70	30	38	67		30	50	38	30	27	25	38	45	38	36	30
Speed roll 2 (%)	120		120	120	120	120		120	120	120	120	120	120	120	120	120	120	120
Speed roll 3 (%)	100		100	100	100	100		100	100	100	100	100	100	100	100	100	100	100
Nip roll 0/1(mm)	8		8	8	8	8		8	8	8	8	8	8	4	4	4	4	4
Nip rolls 1/2 (mm)	5		5	5	5	5		5	5	5	5	5	5	5	5	5	5	5
Nip rolls 2/3 (mm)	8		8	8	8	8		8	8	8	8	8	8	8	8	8	8	8
Temperature roll (1&3)	22		22	22	22	22		22	22	22	22	22	22	40	40	40	40	40
Viscosity (mPa.s)	420		420	420	420	420		420	420	420	420	420	420	115	115	115(38'C)	115(38'C)	115(38'C)
Temperature coating	RT	RT		RT	RT	RT	RT		RT	RT	RT	RT	RT	40	40	41	42	43
Drying- EB curing																		
dose	19.2		19.2	19.2	10	10		10	10	9.1	9.5	9.5	9.5	9.1	9.1	9.5	9.5	9.9
unwind Tension (N)	150		150	150	150	150		150	150	150	150	150	150	150	150	150	150	
I	112		112	112	53	53		115	115	54	115	115	115	53	53	114	114	236
O2-Concentration	31		31	31	17	17		20	20	19	22	22	22	18	18	22	22	55
Results																		
coating weight off line (g/m2)	14.6		22.2	7.1	9.8	20.1		10.2	20.2	10.1	9.7	9	9.4	6	8.1	9.7	10.8	9